# UNIVERSITY OF LONDON THESIS

Degree PhD Year 2006 Name of Author THILAKAWARDHANA Shanaka Bihar

# POTENTIAL NEUROTOXICITY OF APOLIPOPROTEIN E4 BY DYSREGULATION OF NITRIC OXIDE BIOSYNTHESIS IN HUMAN BRAIN-DERIVED CELL LINES

by

**Shanaka Bihan Thilakawardhana**

A thesis submitted in partial fulfilment of the requirements for the degree of:

*Doctor of Philosophy*

Royal Free & University College Medical School,
University of London

2005





ProQuest LLC
789 East Eisenhower Parkway
P.O. Box 1346
Ann Arbor, MI 48106-1346

# ABSTRACT

## POTENTIAL NEUROTOXICITY OF APOLIPOPROTEIN E4 BY DYSREGULATION OF NITRIC OXIDE BIOSYNTHESIS IN HUMAN BRAIN-DERIVED CELL-LINES

*by Shanaka Bihan Thilakawardhana*

Alzheimer's disease (AD) is the most common neurodegenerative disease. Clinical features and disease pathology are well characterised, despite the incomplete understanding of its pathophysiology and molecular basis. Genetic mutations and key proteins have also been identified. Genetic linkage analysis has identified the circulating plasma lipoprotein, apolipoprotein e (apoE), as a significant contributor to AD susceptibility, specifically the ε4 allele, in a dose dependent manner. The mechanism by which this dysfunctional apoE isoform mediates this effect has not been fully elucidated. One possibility, demonstrated previously in peripheral tissue cell lines, is by altering nitric oxide synthase (NOS) via receptor-dependent signalling pathways.

Initially, a panel of human neuronal and astrocytic cell-lines was investigated by quantitative real-time polymerase chain reaction (PCR). Expression of specific apoE receptors and NO biosynthesis pathway components highlighted SH-SY5Y neuroblastoma cells as a suitable model for investigation, while additional lines were identified for future study. Different assay methods were utilised to investigate the hypothesis that: **"exposure of neuronal cells to apoE modulates NO release, with apoE4 causing inappropriate synthesis compared to wild-type apoE3"**. Test apoE was secreted by recombinant CHO cells and was quantified following development of an ELISA. A direct fluorimetric method to measure NO release proved unreliable. Instead, the concentration of cyclic-GMP, a NO secondary messenger, was measured using both colorimetric and radioactive assays. Radioimmunoassay indicated apoE4 exposure down-regulated NO release relative to apoE3; however, results were not conclusive. Following this, the effect of apoE on intracellular signalling pathways was studied by phosphospecific immunoassay, with respect to protein kinase B (Akt), the apoER2 receptor, and the NOS3 enzyme. No change was observed in NOS3 phosphorylation, even after 6 h, but peak phosphorylation of apoER2 and Akt were observed 5 min post-exposure to apoE, with apoE4 having an enhanced effect.

This study reveals that apoE does modify signalling events within brain derived cell-lines, with a minor effect on NO biosynthesis itself. More sensitive assay methods, or possibly a different target cell-line, may have revealed a more significant response. However, the ability of apoE to mediate such events within the brain is a notable observation and physiologically could have a significant impact on AD progression.

# TABLE OF CONTENTS

# LIST OF FIGURES

**CHAPTER 1**



**CHAPTER 2**



**CHAPTER 3**



**CHAPTER 4**

**CHAPTER 5**

# LIST OF TABLES

# DEDICATION

I wish to dedicate this thesis to my loving wife, Fi, and to my parents, Ammi and Thaththi.
I am forever grateful for all the love, support, and continued encouragement you have given me.

# ACKNOWLEDGEMENTS

I would like to begin by expressing my immense gratitude to Professor Jim Owen for his continued supervision, guidance, and patience during the entire course of my PhD, and the critical reviewing of this manuscript. Also, a huge thank you to Dr Colin Dingwall for always showing me the alternate perspective, which has proven invaluable. I really would not be at this point without either of your contributions.

I am very grateful to all the colleagues that I have known during my years at the Royal Free. I would especially like to thank Dr Anna Manzano, Dr Aris Tagalakis, Dr Zahra Mohri, Dr Bhim Odedra, and Dr Galia Sperber. Your support has meant so much to me, and I feel privileged to have worked alongside all of you; even more so to have you as my friends.

I would like to acknowledge the assistance provided by Dr Paul Murdock and Dr David Everett at GlaxoSmithKline, and Professor John Garthwaite and Dr Elaine Mo at the Wolfson Institute of Biomedical Research. Their technical expertise was critical to this project, and I am extremely indebted to you all for your help.

The joint financial support of GlaxoSmithKline and the British Biotechnology and Biological Sciences Research Council, is also acknowledged and greatly appreciated.

Finally, I would like to thank my wife, Fiona. Your support and encouragement have brought me this far, and made me believe that I can keep aiming higher.

*Shanaka Thilakawardhana, December 2005*

# ABBREVIATIONS

AC ..... Adenylate cyclase
ACh ..... Acetylcholine
AChE ..... Acetylcholine esterase
AD ..... Alzheimer's disease
AMPA ..... Alpha-amino-3-hydroxy-5-methyl-4 isoxazolepropionic acid
AMPK ..... Adenosine 5'-monophosphate-activated protein kinase
ApoE ..... Apolipoprotein E
ApoER2 ..... Apolipoprotein E receptor 2
APP ..... Amyloid precursor protein
Arg ..... Arginine
ATP ..... Adenine triphosphate
Aβ ..... Amyloid β peptide
bisacrylamide ..... N,N'-methylenebisacrylamide
BSA ..... Bovine serum albumin
CAA ..... Cerebral amyloid angiopathy
cAMP ..... Cyclic-adenine monophosphate
CCF.STTG1 ..... Human astrocytoma cell line
cdk5 ..... Cyclin-dependent kinase 5
cDNA ..... Complimentary DNA
CE ..... Cholesteryl ester
cGMP ..... Cyclic-guanosine monophosphate
CHO ..... Chinese hamster ovary
CSF ..... Cerebrospinal fluid
$C_t$ ..... Threshold cycle
CTF ..... Carboxy-terminal fragment
Cys ..... Cysteine
DAF 2 ..... 4,5-diaminofluroscein
DAF 2-DA ..... 4,5-diaminofluroscein diacetate
DAF 2T ..... 4,5-diaminofluroscein triazole
DEPC ..... Diethylpyrocarbonate
DETA/NO ..... DETA-NONOate
dhfr ..... Dihydrofolate reductase
DMSO ..... Dimethyl sulphoxide
DNA ..... Deoxyribonucleic acid
dNTPs ..... Deoxynucleotide-triphosphates
dpm ..... Disintegrations per minute
DTT ..... Dithiothreitol
EA.hy926 ..... Human endothelial cell line
ECL ..... enhanced chemiluminescence
EDTA ..... ethylendiaminetetraacetic acid
EGF ..... Epidermal growth factor
EIA ..... Enzymatic immunoassay
ELISA ..... Enzyme-linked immunosorbent assay
eNOS ..... Endothelial nitric oxide synthase (NOS3)
Ethyl-ITU ..... S-ethylisothiourea
FBS ..... Foetal bovine serum
FH ..... Familial hypercholesterolaemia
FRET ..... Fluorescence resonance energy transfer
GAPDH ..... Glyceraldehyde phosphate dehydrogenase

GSK-3 ..... Glycogen synthase kinase-3
GSNO ..... S-nitroso-L-glutathione
GTP ..... Guanosine triphosphate
H4 ..... Human neuroglioma cell line
$HbO_2$ ..... Oxygenated haemoglobin
HDL ..... High-density lipoprotein
HRP ..... Horseradish peroxidase
IBMX ..... 3-isobutyl-1-methylxanthine
IDL ..... Intermediate-density lipoprotein
IFN-γ ..... Interferon γ
iNOS ..... Inducible nitric oxide synthase (NOS2)
KPI ..... Kunitz-type protease inhibitor
LDL ..... Low-density lipoprotein
LDL-r ..... Low-density lipoprotein receptor
LDS ..... Lithium dodecyl sulphate
LRP ..... LDL-receptor-related protein
LY294002 ..... 2-(4-morpholinyl)-8-phenyl-4H-1-benzopyran-4-one hydrochloride
MetHb ..... Methaemoglobin
MOPS ..... 3-(N-Morpholino)-propanesulfonic acid
mRNA ..... Messenger RNA
NADP ..... nicotinamide adenine dinucleotide phosphate
NADPH ..... nicotinamide adenine dinucleotide phosphate, reduced form
NFTs ..... Neurofibrillary tangles
NMDA ..... N-methyl-D-aspartate
nNOS ..... Neuronal nitric oxide synthase (NOS1)
NO ..... Nitric oxide
NO· ..... Nitric oxide radical
NOS ..... Nitric oxide synthase
NOS1 ..... Neuronal nitric oxide synthase (nNOS)
NOS2 ..... Inducible nitric oxide synthase (iNOS)
NOS3 ..... Endothelial nitric oxide synthase (eNOS)
PAGE ..... Polyacrylamide gel electrophoresis
PAPA/NO ..... PAPA-NONOate
PAS ..... Protein A Sepharose slurry
PBS ..... Phosphate buffered saline
PBS-T ..... Phosphate buffered saline and 0.05 % (v/v) Tween 20
PCR ..... Polymerase chain reaction
PDE ..... Phosphodiesterase
PDK ..... Phosphoinositide-dependent kinases
PDZ ..... Postsynaptic density protein (PSD-95)/
Drosophila discs-large (dlg)/ tight-junction protein (ZO1)
pGC ..... Particulate guanylate cyclase
PHF ..... Paired helical filaments
PI3K ..... phosphotidylinositol-3-OH-kinase
$PIP_2$ ..... PtdIns 2,4-bisphosphate
$PIP_3$ ..... PtdIns 3,4,5-triphosphate
PKA ..... Protein kinase A
PKB/Akt ..... Protein kinase B/Akt
PKC ..... Protein kinase C
PKG ..... Protein kinase G
PMSF ..... Phenylmethylsulphonyl fluoride

PS-1 ..... Presenilin 1
PS-2 ..... Presenilin 2
PTB ..... Phosphotyrosine binding domain
pY ..... Phosphotyrosine
Q-PCR ..... Quantitative polymerase chain reaction
RAP ..... Receptor associated protein
RIA ..... Radioimmunoassay
RIPA ..... Radioimmunoprecipitation lysis buffer
RNA ..... Ribonucleic acid
ROS ..... Reactive oxygen species
RT ..... Reverse transcription
RT-PCR ..... Reverse transcriptase PCR
SDS ..... Sodium dodecyl sulphate
Ser ..... Serine
sGC ..... Soluble guanylate cyclase
SH2 ..... Src homology 2
SH3 ..... Src homology 3
S-HRP ..... Streptavidin conjugated horseradish peroxidase
SH-SY5Y ..... Human neuroblastoma cell line
SR-BI ..... Scavenger receptor class B, Type I
SR-BII ..... Scavenger receptor class B, Type II
SR-BIII ..... Scavenger receptor class B, Type III
TBS ..... Tris buffered saline
TBS-T ..... Tris buffered saline and 0.05 % (v/v) Tween 20
TEMED ..... N, N, N, N'-tetramethylethylenediamine
Thr ..... Threonine
TMB ..... Tetra-methlybenzidine
TNF ..... Tumour necrosis factor
UV ..... Ultra violet
v/v ..... Volume per unit volume
VEGF ..... Vascular endothelial growth factor
VLDL ..... Very-low-density lipoprotein
VLDL-r ..... Very-low-density lipoprotein receptor
w/v ..... Weight (mass) per unit volume
α ..... Anti
τ ..... Microtubular protein tau

# Chapter 1

# GENERAL INTRODUCTION

# 1.0 GENERAL INTRODUCTION

## 1.1 ALZHEIMER'S DISEASE

Alzheimer's disease (AD) is the most common neurodegenerative disease and accounts for approximately two-thirds of all cases of dementia [1]. It is an increasingly acute healthcare issue, particularly in Western societies. Currently, the most comprehensive epidemiological data originates from the US, where according to the census completed in 2000, there were an estimated 4.5 million individuals diagnosed with AD over the age of 65, the majority being in the 75-84 years-old age group [2]. The annual cost of treating AD in the US is currently $80 to $100 billion, a figure which will only increase in years to come [3]. With continual medical advances and an enhanced understanding of aging processes and geriatric care, the size of this elderly population is likely to increase dramatically over the next century. If the number of individuals with AD can be directly correlated as a proportion of the whole population, by 2050 there could be between 11 and 16 million Americans diagnosed with AD-type dementia [2,4].

In the UK, the Alzheimer's Research Trust[1] estimates the current prevalence of AD to be approximately 800,000 individuals; part of a wider population of 6 million patients affected by the disease in Europe. There is indication that the increase in cases in the US over the next few decades is likely to be mirrored in the UK and Europe. As such, this disease represents an increasing demand on healthcare services, especially with the ever-increasing costs of both palliative care and the current limitations of therapeutic modalities. Moreover, there is the effect that this insidious disease has on the quality of life of the patient themselves, as well as the resonance that is experienced in those that care for them.

Alzheimer's disease is a progressive neurological disease resulting in the irreversible loss of neurons, particularly in the cortex and hippocampus. It is a genetically heterogeneous disease that manifests with the primary clinical feature of progressive impairment to memory. In addition there are numerous cognitive function deficiencies such as judgement, decision making, orientation to physical surroundings, and language. These personality changes are all accompanied with specific structural abnormalities in the brain that give a prognosis of AD. Neurological examination and exclusion of other

[1] http://www.alzheimers-research.org.uk/

dementias allows a probable diagnosis of AD to be made. A definitive diagnosis can only be achieved by autopsy [5]. The earliest affected regions of the brain are the entorhinal cortex, hippocampus and basal forebrain, which are all specialised structures in the brain that have a critical role in memory functions. In the early and middle phases of the slow, inexorable progression of AD, the patient's alertness remains along with motor and sensory functions. As the disease takes hold, cognitive function diminishes, accompanied often by a concomitant decrease in motor functions such as gait and coordination. This can often give AD patients an appearance that resembles extrapyramidal motor disorders such as Parkinsonism. Life-expectancy of AD patients can range from 2 to 20 years, although as it is currently an incurable disease it does eventually end in death, most commonly by pneumonia or (unrelated) cardiovascular problems [6].

Pathologically, the disease is characterised by the deposition of extracellular plaques containing β-amyloid (often referred to as senile plaques), as well as intracellular neurofibrillary tangles (NFTs) composed of a hyperphosphorylated form of the microtubular protein tau (τ), and cerebral amyloid angiopathy (CAA) [7]. The β-amyloid found in senile plaques is produced by cleavage of the larger β-amyloid precursor protein (APP) by a series of proteases [8]: the α-, β- and γ-secretases [9,10]. In particular, γ-secretase appears to be responsible for producing a β-amyloid peptide ($A\beta_{42}$) that has pathogenic importance due to its ability to form insoluble toxic fibrils that accumulate in senile plaques [11].

The prevalence and age of onset of AD can vary depending on the diagnostic criteria applied. While acknowledging that population age, geography and ethnicity can affect these studies, AD has a prevalence of approximately 1% among those aged 65 to 69 years of age. The prevalence of the disease increases almost exponentially from about the age of 65 years (in both men and women), such that by 95 years-old there is an incidence of AD in 40 – 50% of patients [1]. The mean age of onset is approximately 80 years [12]. Early-onset AD is defined arbitrarily when the diagnostic features of the disease manifest before the age of 60 to 65 years of age. Approximately 7% of these early-onset cases are familial AD (FAD), showing an autosomal dominant pattern of inheritance and high penetrance [13].

### 1.1.1 Alzheimer's disease – an historical perspective

First identified by Alois Alzheimer, a Bavarian psychiatrist, the disease that now bears his name was presented at a meeting in Tübingen, Germany, in November 1904 [14]. The patient, a 51 year-old woman from Frankfurt, referred to as Auguste D, came under his care originally in 1901 whilst he was as an attending physician at the Frankfurt Asylum. This patient presented with many of the clinical features that are still identified in AD patients today: progressive memory impairment; disordered cognitive function; altered behaviour including paranoia, delusions and loss of social appropriateness; and decline in language functions. Following her death in 1906, a post-mortem revealed brain shrinkage as well as the presence of plaques, neurofibrillary tangles and arteriosclerotic changes. In fact, more recent investigation of the original case file for this patient has revealed her dementia may have resulted from arteriosclerosis of the brain rather than the typical neurodegeneration that characterises AD as we understand it today [15]. The first reference to this disease having acquired the title of *Alzheimer's disease* was in 1910 and attributed to Emil Kraepelin, a key collaborator of Alzheimer's and can be considered a co-discoverer of the disease [16].

Alzheimer pursued a number of interests in the field of neurology, which included psychoses, forensic psychiatry and epilepsy. However, it was his investigation of dementia of degenerative and vascular origin that has remained his legacy. His understanding of the neuropathology of these disorders was both shared and developed with Franz Nissl, who provided Alzheimer with many of the histopathological techniques that were necessary for this investigation. Alzheimer eventually published his findings in 1907, where he presented both the clinical and histopathological findings [17]. He described the neurofibrillary tangles as fibrils of characteristic thickness and impregnability that appear in the centre of otherwise normal cells. Neuritic plaques are referred to as "small miliary foci" that he describes as "storing a peculiar material in the cortex". The clinical changes (memory loss, confusion, paranoia) and pathological features (plaques and tangles) first observed by Alzheimer are now established diagnostic criteria for what we know today as AD.

### 1.1.2 Classification of AD-related cognitive changes

At the time, Alzheimer was not aware of the widespread significance of his discovery; AD was viewed as a distinct and separate form of senile dementia with a highly unique neuropathology. It remained, until the work of Blessed, Tomlinson and Roth in the

1960s, for AD to be considered for the first time as a common basis for senile dementia [18]. In 1976, the notion of AD's uniqueness was further challenged by Robert Katzman in an influential paper which opined, contrary to popular belief, that AD was in fact the most common form of dementia and was the single most likely neuropathological correlate of what was known as senility [19].

Unlike the slow progress to understand and appreciate the neuropathology of AD, our understanding of the cognitive and behavioural changes associated with the disease had virtually been detailed with the first case, with numerous refinements over the decades. This culminated in the mid-1970s with the '*Mini-Mental State Examination*', which attempted to aid clinicians diagnose AD by assessing cognitive changes [20]. A criticism of this method has been the difficulty of standardising its use between patients with varying intelligence levels and backgrounds. This has since been superseded by other assessment procedures. Firstly, in 1994, by the criteria of the American Psychiatric Association's '*Diagnostic and Statistical Manual of Mental Disorders, fourth edition*', and most recently by the criteria set out by the '*National Institute of Neurologic and Communicative Disorders and Stroke–Alzheimer's Disease and Related Disorders Association*' [21]. According to this most recent criteria, AD diagnosis can be sub-classified in order of increasing severity as: 'possible', where patients manifest atypical clinical features, but an alternate diagnosis is not readily apparent; 'probable', where patients show typical clinical syndromes, but without any histologic confirmation; and 'definite', whereby clinical diagnosis has been confirmed with histological evidence.

### 1.1.3 Neurotransmitter-related dysfunctions in AD

Cognitive decline, in whatever guise it may take, is purely the outward manifestation of the AD, indeed its phenotype. However, the disease could not be fully appreciated without a detailed understanding of its biochemical basis, a goal that Alzheimer set himself, but unfortunately did not achieve in his lifetime. Largely due to the limitations of the analysis techniques available in the first half of the 20$^{th}$ century, understanding the mechanisms underlying the disease and the potential for therapies showed little or no progress. However, in the 1960s, Michael Kidd and colleagues started to investigate more fully the ultrastructural changes that underlie AD using electron microscopy [22,23]. Their successful visualisation of the two classical lesions of AD – senile (neuritic) plaques, and neurofibrillary tangles (NFTs) – became the foundation for much research over the following decades.

At around the same time, three separate groups in the UK reported the loss of cholinergic markers in brains of patients diagnosed with AD [24,25,26]. These discoveries were attempts at rationalising the neurotransmitter dysfunctions associated with AD, and hence the neurochemistry of the disease. At the time it was not completely understood how changes in the neurotransmitter, acetylcholine (ACh), had any relevance to the clinical memory defects observed in AD patients. By 1978, Elaine Perry and colleagues had conclusively demonstrated that ACh was variable and usually severely deficient in AD. Furthermore, there were cognitive impairments in AD patients that could be correlated with the severity of ACh decline [27]. This eventually led to the first of what would eventually become an ever expanding list of hypotheses and theories as to the genesis and progression of AD. The cholinergic hypothesis suggested that dysfunctions in ACh containing neurons in the brain (particularly those in the limbic system and associated cortices) were significant contributors to the cognitive impairments observed in AD patients [28]. This eventually led to the development of the first set of suitably effective drugs for the treatment of AD. Tacrine, donepezil, rivastigmine and galantamine all act by inhibiting the ACh degrading enzyme, acetylcholine esterase (AChE) [29].

From a neurochemcial perspective, the cholinergic hypothesis still remains the foundation for the only truly effective pharmacological approach to treating AD. The only other therapeutic method of note is the *N*-methyl-D-aspartate (NMDA) receptor antagonist, memantine, which was first approved for use in 2002 [30]. The NMDA receptor is one of a number of postsynaptic receptors that can be stimulated by glutamate, which is the principal excitatory neurotransmitter found in the brain. Neuronal damage can occur if glutamatergic over-stimulation occurs, in a phenomenon termed excitotoxicity. In neurodegenerative disorders, it is this excitotoxicity that can lead to a dramatic intracellular calcium overload, which initiates a cascade of events that can ultimately result in neuronal death [31]. Memantine is a non-competitive NMDA antagonist that both protects against glutamate-mediated excitotoxicity without any associated activation of the receptor. Although it has been used in isolation, memantine has been demonstrated to be markedly more effective when used in conjunction with an AChE inhibitor, such as donepezil [32].

## 1.2 ALZHEIMER'S DISEASE PATHOLOGY

When discussing AD pathology, the hallmark features that are synonymous with the disease are the amyloid plaques and neurofibrillary tangles. However, it should be noted that these are thought by many to be the 'tombstones' of the disease; they occur late in disease progression and are in themselves unlikely to provide much insight into the disease aetiology and early progression. However, there has been much debate as to the exact temporal deposition of the two lesions types, with respect to which appears first in the brain [33]. Despite this, there is a general consensus that prior to lesion formation there is one or many detrimental biochemical events [34]. If these are appropriately identified, they could be exploited and therapies developed to ameliorate them.

### 1.2.1 Neuritic Plaques

The neuritic plaques of AD are microscopic foci of extracellular amyloid deposition with associated axonal and dendritic injury. In post-mortem tissue, these are generally found in large numbers in the limbic and associated cortices. The plaques are composed of amyloid β-protein deposits, which principally occur in a filamentous form: star-shaped masses of amyloid fibrils. Dystrophic neurites can be found both within these plaques and surrounding them, and are observed to be dilated with ultrastructural abnormalities that include enlarged lysosomes, numerous mitochondria and paired helical filaments (which are generally indistinguishable from those that comprise NFTs). Plaques are intimately associated with microglia expressing cell-surface antigens that indicate an activated state, such as CD45 and HLA-DR [35]. Additionally, plaques are surrounded by reactive astrocytes that display abundant glial filaments. Microglia are usually found within and adjacent to the central amyloid core of the neuritic plaque, whereas astrocytes form a ring around the plaque, with some processes extended towards the central core. The time period over which neuritic plaques develop is not fully understood, but probably evolve over many months or years.

The fibrillary Aβ found in neuritic plaques is predominantly the 42 amino-acid form ($A\beta_{42}$). This is the slightly longer, more hydrophobic form of Aβ and is more prone to aggregation. The bulk of Aβ in the brain is 40 amino-acids long ($A\beta_{40}$), but this too can be found co-localised in plaques [36,37]. Spatially, neuritic plaques have a spherical structure with a cross-sectional diameter of anywhere between 50-200 μm. In addition, the density and degree of compaction of the amyloid that comprises the plaque's core can vary considerably between plaques. Having identified Aβ as the subunit of plaque

amyloid, it was possible to develop sensitive antibodies against Aβ. These were utilised to generate a more complete view of the penetration of neuritic plaques in AD patients' brains [38]. This immunohistochemical staining revealed far more extensive Aβ deposits than had been shown previously using classical silver staining methodologies such as that of Bielschowsky and Bodian [39]. Not all of these deposits were of the compacted, fibrillar appearance associated with classical neuritic plaques. Many plaques within the limbic and association cortices, and virtually all of those in brain regions not implicated in the typical sympatomology of AD (such as the thalamus, caudate, putamen and cerebellum) were observed to have a light, amorphous Aβ immunoreactivity that occurred in a finely granular manner. Using both silver staining (which detected dystrophic neurites) and immunohistochemistry against neuronal/neuritic cytoskeletal proteins, it was revealed that there was little or no detectable neuritic dystrophy in most of these non-fibrillar granular-type plaques. Further investigation revealed that these plaques could also be found in regions that contained many neuritic plaques [40].

This implied the presence of two distinct subclasses of plaques: the more commonly observed neuritic plaques that contain compacted, fibrillar Aβ; and those containing granular, non-fibrillar Aβ deposits. This latter type became known as 'diffuse' plaques or 'pre-amyloid deposits'. Further study revealed that diffuse plaques were comprised primarily of $A\beta_{42}$ with little or no $A\beta_{40}$ immunoreactivity [41]. In contrast, the fibril-rich neuritic plaques generally contained a mix of the two Aβ species. Aetiologically, it was believed that the non-fibrillar Aβ plaques were representative of a lesion precursor to the classical neuritic plaques [42,43]. Moreover, studies with transgenic mice that express the carboxyterminal fragment of mutant human APP showed that they developed diffuse Aβ deposits, followed by fibrillar neuritic/glial plaques that were both thioflavin S-positive and Congo red-positive, which stain senile plaques and amyloid deposits respectively [44]. Further support for this theory came from immunohistochemical investigation of Down's syndrome patients [33,45,46]. These individuals would often display diffuse amyloid deposits as early as their teens; neuritic/glial plaques would not appear for another two decades, by which time the individuals would also begin to display profuse neurofibrillary tangles within regions of the limbic system.

### 1.2.2 Amyloid precursor protein & Aβ processing

Amyloid precursor protein (APP), as its name suggests, is the precursor to Aβ, and is actually a heterogeneous group of ubiquitously expressed polypeptides that can be electrophoretically resolved as mature proteins of between 110 to 140 kDa [47]. The heterogeneity of APP arises from both alternate splicing (to give three major isoforms of 695, 751 and 770 residues) and a variety of post-translational modifications, such as the addition of *N*- and *O*-linked sugars, sulphation and phosphorylation [38,48,49]. The 751 and 770 amino-acid APP splice forms are widely expressed in non-neuronal cells throughout the body, as well as occurring in neurons [50]. However, the 695 amino-acid form is expressed highly in neurons and at very low abundance in non-neuronal cells [51]. The most significant difference between the 751/770 amino-acid form of APP and the 695 amino-acid form is the presence in the former of an exon coding for a 56 amino-acid motif homologous to the Kunitz-type serine protease inhibitors (KPI) [52]. The KPI-containing forms of APP have been observed in human platelets to serve as inhibitors of factor XIa, a serine protease in the coagulation cascade [53]. The expression of APP is very highly conserved and has been detected in all mammals in which it has been sought.

Mature APP is a Type I transmembrane polypeptide, which becomes co-translationally translocated into the endoplasmic reticulum via its signal peptide. From there, it is post-translationally matured through the secretory pathway. Rapidly after biosynthesis, it can acquire *N*- and *O*-linked sugars, whilst its half-life is relatively brief at approximately 45-60 minutes [54]. During and after trafficking through the secretory pathway, APP can undergo a variety of proteolytic cleavages that release secreted derivatives into the vesicle lumen and the extracellular space (see *Figure 1.1*). The first proteolytic cleavage identified occurs at 12 residues $NH_2$-terminal to the single transmembrane domain of the polypeptide [55]. This is performed by the activity designated α-secretase, the result of which is the release of a large soluble ectodomain fragment (α-$APP_s$) into the lumen/extracellular space, whilst an 83-residue carboxy-terminal fragment (CTF) is retained in the membrane [56]. An alternate to APP processing by α-secretase is the cleavage at 16 amino-acids $NH_2$-terminal to the α-cleavage site, by activity designated β-secretase, which generates a slightly shorter ectodomain fragment (β-$APP_s$) and the retention of a 99-residue CTF in the membrane, the C99 fragment [54,57,58]. It is this fragment of APP which is the direct precursor of Aβ: the first residue of the C99 fragment is designated amino-acid 1 of Aβ .

It was long assumed that generation of Aβ was a pathological event. The subsequent cleavage of the C99 fragment by the so-called γ-secretase activity seemed to occur in the middle of the transmembrane domain [58]. As such, it was assumed that this process would require the release of the C99 fragment from the membrane, perhaps through some sort of pre-existing membrane injury, which would then allow access for a soluble protease. This was disregarded, as sensitive Aβ antibodies revealed that APP expressing cells would constitutively release Aβ under normal cellular conditions. In addition, a peptide fragment called p3 was discovered that was produced through sequential cleavage by α- and then γ-secretase [59]. These findings seemed to indicate the Aβ production was metabolically normal, and the peptide was even detectable in cerebrospinal fluid and plasma in healthy individuals throughout life.

The identity of one of the key proteases that process APP has remained elusive for some time until late in 1999 several groups published almost simultaneously the identification of a novel transmembrane aspartic proteinase which exhibited the known properties if β-secretase [60,61,62,63]. The accepted name for the enzyme is now beta-site APP-cleaving enzyme (BACE1). They found that overexpression of this protease would give an increase in β-secretase cleavage products. Moreover, cleavage only occurred at known β-secretase cleavage sites. This was further supported by antisense mRNA inhibition and investigation of subcellular localisation and expression pattern, all of which were consistent with β-secretase. Following the identification of BACE1, a homolog was discovered on chromosome 21, in a region that encodes APP and undergoes triplication in Down's syndrome [64], and termed BACE2. The two proteins shared significant amino acid sequence similarity and is was proposed that BACE2 was also a putative β-secretase [65]. However, expression analysis revealed very low expression of BACE2 in various tissue, but almost undetectable in the brain. In contrast BACE mRNA was found to have high expression in neurons but not glia [61]. Subsequent investigation indicated that BACE2 activity was consistent with cleavage close to the α-secretase site [66].

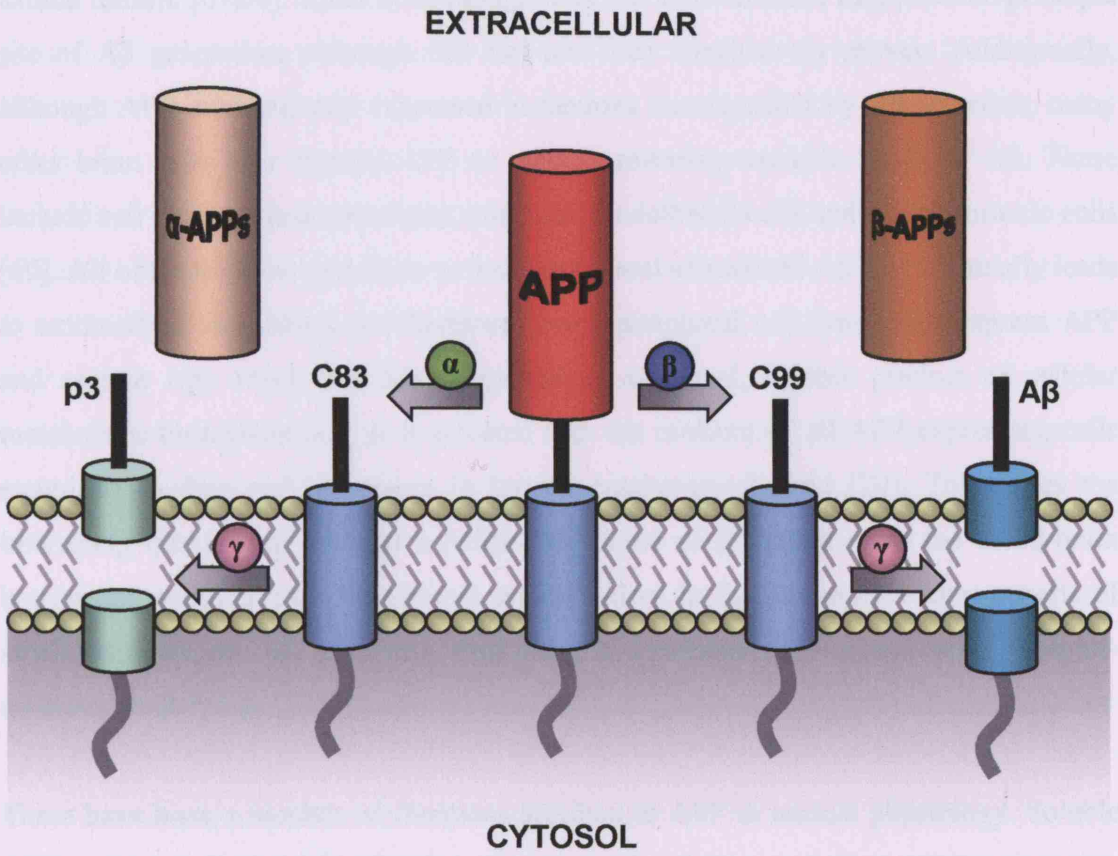


**Figure 1.1 Amyloid precursor protein (APP) processing**

*APP can be processed by either α-secretase or β-secretase. Processing by α-secretase results in the formation of the α-APP$_s$ fragment, and leaves an 83-residue C-terminal fragment (C83) in the plasma membrane. Processing by β-secretase produces the β-APP$_s$ fragment and the C99 fragment. This, when cleaved by γ-secretase produces the amyloid β peptide, which is implicated in AD pathogenesis. Conversely, processing of C83 by γ-secretase produces the p3 fragment, which is a truncated variant of Aβ.*

In neurons, APP can be anterogradely transported by the fast component of axonal transport, and has been detected in axonal vesicles (although not synaptic vesicles) in axonal termini [67,68]. It has been thought that the axon terminal might be the principal site of Aβ generation, although this has not been conclusively proven. Additionally, although APP is abundantly expressed in neurons accompanied by Aβ secretion, many other brain cells also express APP as well as releasing variable levels of Aβ. These include cell types such as astrocytes, microglia, endothelial cells and smooth muscle cells [69]. All of these could contribute to the overall pool of secreted Aβ that eventually leads to extracellular deposition. Furthermore, many peripheral cell types also express APP and secrete Aβ, which has been regarded as a normal, soluble product of cellular metabolism throughout life: it is secreted into the medium of all APP expressing cells examined to date and is present in human cerebrospinal fluid [70]. This raises the interesting question of whether a peripheral source of Aβ could cross the blood-brain barrier and contribute to cerebral Aβ accumulation. In fact, there have been reports of small amounts of Aβ achieving this using a mechanism consistent with receptor-mediated endocytosis [71,72].

There have been a number of functions ascribed to APP in normal physiology. Soluble APPs appear to be capable of acting as an autocrine factor, as well as a neuroprotective and perhaps as a neuritotrophic factor [73,74,75]. The larger 751 and 770-residue APPs both contain a 56 amino-acid KPI motif that allows these isoforms to inhibit serine proteases such as trypsin and chymotrypsin [76]. This has already been shown in platelets, where these APPs can function as an inhibitor of factor XIa, a serine protease, involved in the clotting cascade [77]. Deletion of the APP gene in mice does not seem to confer any increased risk of early mortality or appreciable morbidity [78,79]. The only deleterious effects are cerebral gliosis and locomotor changes in late adult life, although some neurons cultured at birth do appear to have a dimished viability and retarded neurite outgrowth. The inability of APP deletions to manifest a more dramatic phenotype may reflect the close homology of APP to a family of amyloid precursor-like proteins (APLPs). As yet, there does not appear to be any fundamental cellular function that is overtly affected in AD patients with APP mutations. Instead, these mutations generally lead to increased production of the potentially neurotoxic Aβ fragment [80,81].

### 1.2.3 Neurofibrillary Tangles

Many of the neurons in the regions of the brain that are affected by AD (entorhinal cortex, hippocampus, parahippocampal gyrus, amygdala, and the frontal, temporal, parietal and occipital association cortices, as well as certain subcortical nuclei that project into these regions) contain large, non membrane-bound bundles of abnormal fibres that occupy much of the perinuclear cytoplasm. Electron microscopy revealed that most of these fibres consisted of pairs of ~10 nm filaments that were wound into helices (paired helical filaments, or PHFs) with a helical periodicity of ~160 nm [82,83,84]. Interest in these neurofibrillary tangles started in earnest in the mid-1980s with the extensive immunocytochemical and biochemical analyses that suggested they were composed of the microtubule-associated protein tau [85,86]. These PHFs are generally highly insoluble and are partially resistant to detergents such as sodium dodecyl sulphate (SDS) and chaotropic solvents such as guanidine hydrochloride [87]. Isolation of a PHF fraction that could be partially solubilised in detergent or by digestion with proteases, released tau proteins that migrated electrophoretically at a higher molecular weight than normal tau (prepared from NFT-free human or animal brain). The slower migration of this abnormal tau protein was revealed to be due to its hyperphosphorylation; *in vitro* dephosphorylation of PHF derived tau using alkaline phosphatase returned its migration to that of the normal tau protein [88].

It is now known that there is a range of kinases that are capable of phosphorylating tau *in vitro* at various sites. However, it is still not clear if there is a particular kinase, or possibly group of kinases, that are responsible for the principal initiation of the hyperphosphorylation process *in vivo*, which eventually leads to its dissociation from microtubules and subsequent aggregation into the insoluble PHFs [89,90,91]. One study has provided evidence of a dysregulation of cyclin-dependent kinase 5 (cdk5), resulting from the proteolytic cleavage of its regulator subunit p35 to give a fragment (p25) that enables a constitutive activity of cdk5 [92]. This could play a major role in tau hyperphosphorylation, which underlies tangle formation in AD.

### 1.2.4 Genetics of Alzheimer's disease

Despite intensive efforts, the mechanism(s) which lead to synaptic loss and neurodegeneration in AD remain elusive. This incomplete understanding of the disease has impaired the development of suitable animal and cellular models of the disease, which consequently impact the development of therapeutic modalities for patients. Attempts to mimic the disease by perturbation of numerous physiological and genetic factors related to AD have not resulted in models that suitably reflect the spectrum of pathological aberrations. Most often, the factor that is overlooked is simply that AD is a disease of ageing. Therefore, whatever genetic or environmental factors impinge upon the susceptibility to the disease's genesis or progression, the events are inextricably linked with natural ageing processes. Therefore, by inference, age is a clear contributor to one hundred percent of AD cases, regardless of genetic background or predisposition.

In a global sense, these familial forms of AD are relatively rare. However, their importance is significant in elucidating putative pathogenetic pathways of the disease. Linkage analysis and DNA sequencing identified highly penetrant missense mutations in three genes in families with FAD: the gene encoding APP itself on chromosome 21, as well as two similar genes, presenilin-1 (PS-1) on chromosome 14 and presenilin-2 (PS-2) on chromosome 1 [93]. Mutations in PS-1 are generally more common than those in PS-2. The mutations in these genes in patients with early-onset AD appeared to favour the production of the neurotoxic peptide species Aβ42 over the less toxic Aβ40 form [94]. There is some evidence that PS-1 may in fact be the gene for γ-secretase or a co-factor of it [95]. Cultured cells transfected with wild-type APP have been shown to process approximately 10% of the protein into Aβ42: expression of APP or PS-1 mutations can result in an increase in Aβ42 production by a factor of ten [96,97]. This evidence suggests a common mechanism by which mutations in these genes have a deleterious effect and are directly involved in AD pathogenesis. Contrasting with these findings is the lack of any hereditary effect of mutations in the tau gene [1].

However, 90-95% of cases of AD are of late-onset (LOAD) and occur sporadically with no observable mutation in the APP or presenilin genes. Several other factors have been implicated in this form of AD, but the most significant has been apolipoprotein E (see *Section 1.3*), specifically its ε4 allele [93,98,99,100]. Carrying at least one ε4 allele can almost double the lifetime risk of AD, from 15% to 29%, whilst lack of ε4 alleles can reduce the risk of developing AD by 40% [101]. The overall magnitude of the ε4 allele

effect on AD varies between studies, but there does appear to be a dosage effect: disease free survival is lower in homozygous patients than in heterozygotes. It seems that the effect of the ε4 allele on patients with an underlying susceptibility to AD is to shift the average age of onset earlier by approximately 5-10 years in ε4 heterozygous patients, and 10-20 years in ε4 homozygous patients [102,103]. There is also evidence to suggest that apoE2 exhibits a neuroprotective effect [104], putatively through its lower affinity to the lipid peroxidation product 4-hydroxynonenal (HNE) [105] At present, the molecular basis for the effect of apoE on AD pathogenesis remains ill-defined, but the genetic association of this gene to the disease cannot be refuted [106].

## 1.3 APOLIPOPROTEIN E

Apolipoprotein E (apoE) is an apolipoprotein that circulates in plasma and cerebrospinal fluid (CSF), and is involved in regulating lipoprotein metabolism by a number of mechanisms: stabilising lipoprotein particles, activation of co-factors/enzymes or lipid transfer proteins involved in metabolism/remodelling of lipoproteins, and serving as a ligand for lipoprotein receptors [107]. It is a constituent of liver synthesised very-low-density lipoproteins (VLDL), which are primarily involved in the transport of triglyceride from liver to peripheral tissue. ApoE is also found in a subclass of high-density lipoproteins (HDL), participating in cholesterol redistribution. Its major physiological role in lipoprotein metabolism is mediating high-affinity binding of these particles with lipoprotein receptors. Binding initiates uptake of the lipoprotein for degradation and release of lipoprotein cholesterol. There is also evidence of its involvement in intracellular signalling cascades via its receptors and cytoplasmic kinases [108,109].

### 1.3.1 Apolipoprotein E structure and function

The first detailed description of apoE was made in 1973 by Shore and Shore [110]. It is a 34.2 kDa protein with a single 299 amino acid polypeptide. The 3.7 kB gene encoding the protein is located at 19q13.2, with 4 exons and 3 introns, and a mRNA of 1163 bp, which includes an 18 amino-acid signal peptide that becomes cotranslationally removed during processing [111]. A single glycosylation site present at Thr194 results in apoE in humans being secreted as an O-glycosylated protein [112]. First described by Utermann and colleagues in 1977 [113], three major isoforms of apoE exist – APOE ε2, ε 3, and ε4 – giving rise to six recognised genotypes: 2/2, 2/3, 3/3, 4/3/ 4/4, and 4/2. Of these isoforms, APOE ε3 is the most commonly occurring allele in the general population, with a frequency of 0.78, which compares with 0.08 and 0.14 for APOE ε2 and APOE ε4, respectively [107]. The molecular basis for the polymorphism is a single nucleotide substitution resulting in amino acid changes at position 112 and 158 [114]. In apoE3 these are Cys112 and Arg158; apoE2 has Cys158 and apoE4 has Arg112 (see *Figure 1.2*). The broad physiological difference between the three isoforms is in their affinity to the low-density lipoprotein (LDL)-receptor and their interaction with heparin [115].

Limited thrombocytic digestion of apoE has revealed two domains with distinct physical and functional properties. The 22 kDa N-terminal domain mediates receptor binding, and is organised as an anti-parallel bundle of four α-helices [116]. Residues 136-158 of helix 4 are solvent exposed, creating a large positive charge over this area, which is thought to

mediate interaction of the protein with receptors [117]. The 10 kDa C-terminal domain is composed of 3 helices and is less stable than the N-terminal domain. This domain mediates lipoprotein binding, encompassed within residues 244-272. Structural changes in one of the two domains can have an influence on the biological properties of the other [118]. For example, the change in residue 112 of cysteine to arginine present in apoE4 shifts the preference of lipid binding from HDL to VLDL for this isoform, despite this change occurring outside the recognised lipid binding region of the protein [119].

The highest mRNA expression levels of apoE are found in the liver, which is the major source of the protein [120,114]. Here, it is primarily produced by hepatic parenchymal cells and secreted as a component of VLDL. The brain has the second largest concentration of apoE mRNA, at approximately one-third of that found in the liver [121]. The major source of apoE in the brain is from astrocytes, as well as being a major constituent of CSF [122]. Under certain conditions glia and neurons can also produce it [123]. In the brain, apoE has a number of roles:

- Redistribution of lipids, maintaining global cholesterol homeostasis;
- A targeting protein for local redistribution of cholesterol within neural tissue undergoing repair/re-modelling;
- An emerging involvement in developmental processes and synapse formation.

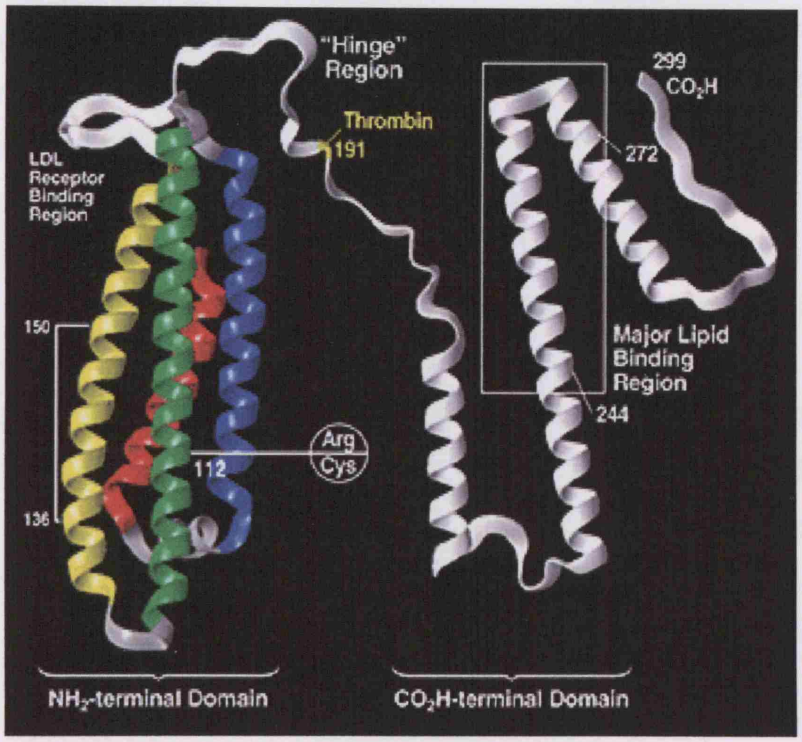


**Figure 1.2 Domain structure of apolipoprotein E as revealed by x-ray crystallography[2]**

*The two polymorphic sites (Cys112 and Arg158) are highlighted as well as the lipid and receptor binding domains. The thrombocytic cleavage site is also indicated, linking the two distinct domains of the protein together.*

[2] Image credit, KH Weisgraber – http://www.gladstone.ucsf.edu/gladstone/php/?sitename=weisgraber

### 1.3.2 Apolipoprotein E in the brain

Interest in apoE has been greatly focussed by the recognition in 1993 that the ε4 allele of apoE was a key susceptibility gene for the development of late-onset AD [101]. This was rapidly followed by a series of studies that endorsed this finding [124,125,126,100,127]. Furthermore, apoE4 had a dose dependent effect on the apparent age of onset of the disease: the ε4/4 genotype decreased the age of onset to 66 years-old; the ε3/4 genotype had an age of onset of 73 years-old; whilst the ε3/3 genotype of 86 years-old. If the ε4 allele is absent and the ε2 allele present (homozygous, ε2/2, or heterozygous, ε2/3) then patients can expect an even later age of onset [101]. Clearly these observations indicate a potentially highly deleterious effect if one is an ε4 hetero- or homozygous individual. It should be noted that the presence of the ε4 allele is neither necessary nor sufficient to instigate disease progression. However, Raber *et al.* have estimated that as much as 95% of individuals in the US that have been diagnosed with AD could potentially be carrying the ε4 allele (single dose or double dose) [128]. This is based on numerous epidemiological studies, and analysis of the percentage of each genotype found in the over-60 year-old population (which they estimate at 46 million) and assuming that approximately 4 million of these have AD.

Prior to the genetic linkage analysis of apoE isoforms with AD, immunohistochemical analysis had already revealed positive staining for the presence of apoE4 in amyloid deposits [100]: apoE4 can form stable complexes with Aβ *in vitro*, whereas apoE3 does not. ApoE is also secreted by macrophages and has been shown to accumulate in regions of damaged/regenerating nerves. This led to the theory that apoE was being utilised as a scavenger of the cholesterol released by damaged neurones and returns these lipids for axonal regeneration [129].

An isoform dependent interaction between the different forms of apoE and tau has been observed [130]. It is thought that apoE3 stabilises microtubules and the cytoskeleton thus maintaining structure/function of neuronal cells [131]. This binding may also inhibit phosphorylation of tau, retarding the formation of paired helical filaments. From this follows the hypothesis that the association of apoE4 with AD is a result of its inability to provide the protective effect that apoE3 mediates [132]. Some controversy exists with regard to the cytosolic presence of apoE; its presence has been shown by immunohistochemistry, but internalisation usually results in degradation by the endosomal pathway, which would have to be avoided to allow a cytoskeletal interaction.

Further to this, apoE is postulated to modify the cytoskeleton and thereby alter neurite extension and branching. Studies have shown that neurite branching is enhanced by the presence of lipid with little or no modification to neurite length. Conversely, the presence of apoE3 can significantly extend the length of neurites [133]. A possible explanation is the enhancement of membrane biosynthesis in the presence of a cholesterol source; apoE and lipid has a similar effect but with the additional response of 'trimming-back' branches to allow long neurite extensions. An isoform response has been observed, where apoE4 displays markedly decreased neurite extension without any inherent toxicity to the cells [134]. ApoE2 has a similar effect to that seen with apoE3. For all three apoE isoforms this effect only appears to occur while in a lipidated form. An explanation for this is likely to be due to the inability of delipidated apoE to bind to cell surface lipoprotein receptors.

### 1.3.3 Apolipoprotein E receptors

Receptor-mediated cellular metabolism of LDL was first described in 1974 by Goldstein and Brown [135]. The liver synthesises a precursor lipoprotein, VLDL, which is converted during circulation to intermediate-density lipoprotein (IDL) and finally to LDL [136]. This is a ligand for receptors on tissues and organs. The majority of LDL receptors expressed in the body are found on liver cells, but virtually all peripheral tissues also express these receptors in varying levels. They are located on specialised indentations of the plasma membrane called caveolae; essentially coated pits that contain within them the ability to form tight complexes with LDL particles. After binding, these particles are internalised via coated pits and vesicles, and the entire LDL particle is delivered to lysosomes where enzymatic hydrolysis disassembles the particle and releases cholesterol for cellular metabolism, in a process known as 'receptor-mediated endocytosis'. Cholesterol itself mediates a feedback loop to maintain cellular cholesterol homeostasis whereby the levels of LDL receptors and cellular cholesterol biosynthesis are regulated.

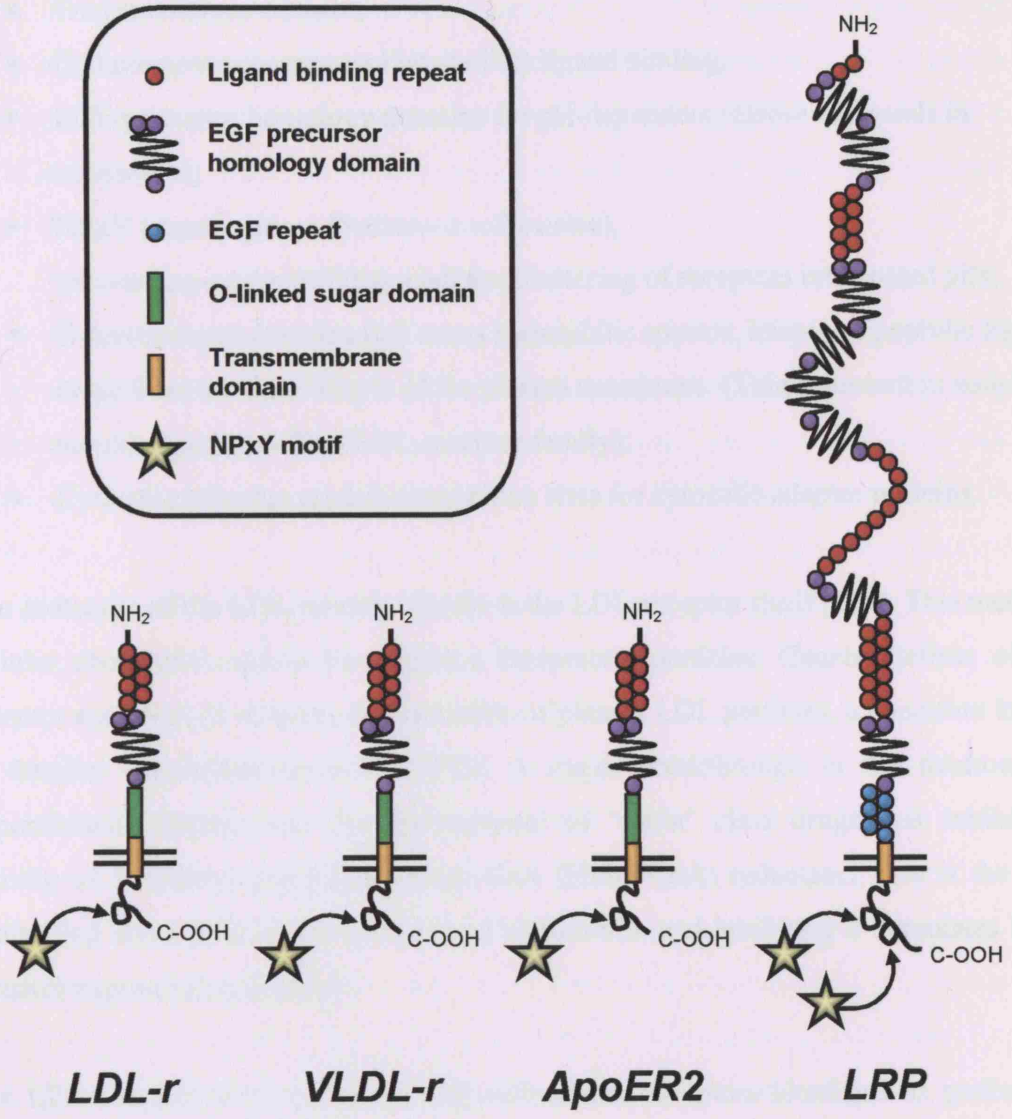


**Figure 1.3 The LDL-receptor gene family**

*Common structural features are highlighted. The ligand binding repeats give rise to the binding specificity. In the LDL-r, the NPxY motif mediates rapid endocytosis and internalisation of the receptor-ligand complex. However, in LRP, apoER2 and VLDL-r, this motif can be involved in signalling pathways via interaction with phosphotyrosine binding (PTB) domain containing proteins.*

Members of the low-density lipoprotein (LDL) receptor family [137] share a number of key structural features (see *Figure 1.3*):

- Transmembrane domain;
- Complement-type repeats that mediate ligand binding;
- EGF-precursor homology domains for pH-dependent release of ligands in endosomes;
- NPxY (*Asparagine – Proline – x – Tyrosine*), tetra-amino-acid motif that mediates clustering of receptors into coated pits;
- O-linked sugar domains that act as hydrophilic spacers, keeping lipophilic ligands away from the lipid bilayer of the plasma membrane. (This is present in some, but not all, members of the LDL-receptor family);
- Cytosolic tails that contain recognition sites for cytosolic adaptor proteins.

The prototype of the LDL-receptor family is the LDL-receptor itself [138]. This mediates cellular cholesterol uptake via lipidated lipoprotein particles. Genetic defects of this receptor can result in massive accumulation of plasma LDL particles, a condition known as familial hypercholesterolaemia (FH). A major breakthrough in the treatment of hypercholesterolaemia was the development of 'statin' class drugs that inhibit the activity of 3-hydroxy-3-methylglutamyl-CoA (HMG-CoA) reductase. This is the rate-controlling enzyme in the biosynthesis of cholesterol, and inhibiting it stimulates LDL-receptor expression in the liver.

The LDL-receptor was one of the first cell-surface receptors identified as performing receptor-mediated endocytosis. It is highly specific to its ligands, apoE and apoB-100. This specificity is a result of the seven ligand-binding repeats present in the receptor: apoE requires repeat 5, and apoB-100 requires repeats 3 to 7, for binding. The LDL-receptors expressed in virtually all tissues at variable levels. Although it is known to be expressed in the brain as well, no critical function of this receptor has been defined, in spite of extensive clinical and experimental study. However, in 2000, Wolozin and colleagues analysed the hospital records of 57,000 patients with respect to the incidence of AD [139]. Those patients being treated with statin-class drugs were found to have a lower AD incidence of 60-73%. This gives a strong correlation between cholesterol metabolism and development of AD, although the precise mechanism that underpins this is unclear at this stage.

The LDL-receptor-related protein (LRP), a key member of the LDL-receptor family, is found most abundantly expressed in hepatocytes and neurones, but also to some degree in virtually all tissue types [140]. At 600 kDa, it is one of the largest members of the LDL-receptor family. It was originally proposed to bind exclusively with chylomicron remnants, as confirmed by biochemical evidence. However, a broader biological role has been revealed, which includes: participation in homeostasis of proteinases and proteinase inhibitors; cellular entry of viruses and toxins; activation of lysosomal enzymes; and cellular signal transduction and neurotransmission.

As with other members of the LDL-receptor gene family, LRP consists of common structural units: ligand-binding repeats, EGF precursor homology domains and EGF-receptor-like repeats, a single transmembrane sequence and a cytoplasmic tail. The ligand-binding repeats occur in four clusters in the extracellular region of the receptor. Each cluster has between two and eleven repeats. The cytoplasmic tail contains two NPxY motifs that act as docking sites for the endocytosis machinery, as well as cytoplasmic adaptor and scaffolding proteins involved in cellular signalling.

In keeping with the multitude of functions attributed to LRP, it is known to bind at least 30 different ligands with high affinity [140]. These ligands include lipoproteins, proteinases, proteinase-inhibitors, extracellular matrix proteins, bacterial toxins, viruses, and various intracellular proteins. The ability of this receptor to bind so many structurally distinct ligands has been determined as a function of the numerous ligand-binding repeats. This was achieved by experiments involving the creation of fusions of ligand-binding repeat clusters and expression of recombinant receptor fragments, as well as deletion analysis. It was revealed that most ligands bind to clusters II and IV, with the majority showing an equal affinity to either, which seems to imply a functional duplication within the LRP sequence. Binding can occur between different ligand-binding repeats, and in some cases can occur across more than one cluster. In total, there are 31 ligand-binding repeats in LRP. This creates unique contoured surfaces and charge distributions that allow multiple ligand-receptor interactions.

### 1.3.4 The low-density lipoprotein receptor gene family and cell signalling

Gene knockout studies of these receptors have revealed their complex physiological requirement beyond ligand endocytosis [137]. One hypothesis was that they might be involved in cellular signalling events. This was postulated after comparison of LDL-

receptors to known signalling receptors that have cytoplasmic tails capable of coupling to intracellular effector pathways, such as mitogen activated protein (MAP) kinases, tyrosine kinases and lipid kinases, or ion channels. The LDL-receptor family receptors have an NPxY tetra-amino-acid motif on their cytoplasmic tails: LDL-receptor has one, while the VLDL-receptor, apoER2 and LRP have multiple copies.

In the LDL-receptor, the presence of the NPxY motif mediates rapid endocytosis of the receptor, implicating it as an internalisation signal for the receptor. Only one motif is necessary and sufficient for this to occur. In LRP, where two of these motifs are found, one or both could interact with cytoplasmic proteins in addition to the cellular endocytic machinery. Well-established signalling pathways involving the receptors for epidermal growth factor (EGF) and insulin use this motif as a means of docking with adaptor proteins via phosphotyrosine binding (PTB) domains. A search for PTB-domain containing adaptor proteins that could potentially interact with LRP revealed two candidate proteins [141]: Disabled-1 (Dab-1) and Fe65. Phosphorylation of the tyrosine residue of the NPxY motif was not required for binding of PTB domain-containing proteins.

Dab-1 plays a critical role in the positional signal of migrating neurons during brain development [142]. It binds specifically to the second NPxY motif of LRP, as well as equivalent sequences in other LDL-receptor family members. Fe65, an adaptor protein that aids the function of other proteins, contains two PTB domains, one of which binds specifically to the NPxY domain of LRP [143]. The other domain has been shown to bind with the NPxY motif found in the cytoplasmic tail of APP. Fe65 expression has been observed in the hippocampus and affected regions of the brain in AD, and is involved in signal transduction events. In mammalian species there exist two Fe65-like proteins, Fe65L1 and Fe65L2, each containing two PTB domains. They can both interact cytoplasmically with APP via one of their PTB domains, while the other domain interacts with LRP [144]. This could create a cytoplasmically-facing complex of APP and LRP, tied together by Fe65, which may have important implications for APP processing. Additionally, LRP has been demonstrated to interact with full length APP on the cell surface membrane [145]. This interaction may also directly influence the rate of amyloidogenic processing of APP, or its clearance from the extracellular environment.

Identification of Dab-1 and Fe65 as LRP tail-binding proteins initiated a search for other proteins that could bind to the tails of other members of the LDL-receptor family, including LRP. A number of adapter and scaffold proteins were discovered, some of which contained PTB-domains whilst others contained PDZ[3] domains [146]. Together, these cytoplasmic tail-binding proteins implicated LRP and members of the LDL-receptor family in numerous regulatory functions: mitogen-activated protein (MAP) kinase signalling, ion channel function, microtubular transport, nitric oxide signalling, and axon guidance.

### 1.3.5 The VLDL-receptor, apoER2 and Reelin signalling

The VLDL-receptor, is almost identical to the LDL-receptor but with an additional ligand binding domain. It can bind apoE with a similar affinity as the LDL-receptor does, however, it is not expressed in the liver, and most expression is found in the heart and skeletal muscle as well as endothelial cells of major blood vessels. An important role for this receptor is in the development of the nervous system where it is involved in neuronal migration: in this process, the VLDL-receptor acts in concert with apoE receptor 2 (apoER2). As with the VLDL-receptor, apoER2 is not expressed in the liver and is almost exclusively limited to the brain and testes (under normal circumstances). It has also been found in atherosclerotic lesions in the vascular walls. The VLDL-receptor and apoER2 are structurally very similar, with the main difference arising from alternate splicing of ligand binding repeats [137].

Studies from a number of groups identified two strains of mice, *scrambler* and *yotari* at were severely ataxic. The defect in both strains of mice was mapped to a mutation in Dab-1. The phenotype of these mice was indistinguishable from *reeler* mice, a strain that had first been established 50 years previously. The phenotype of the *reeler* mice resulted from a recessive mutation in the large secreted protein, Reelin, which is primarily expressed in the nervous system [142]. It is known to affect the development of the neocortex, cerebellum and the spinal cord, in addition to other areas. Loss of Reelin disrupts radial migration and the final position of the neurons. It is secreted by a specialised set of pioneer neurons on the surface of the neocortex, known as Cajal-Retzius neurons, located in close proximity to the endings of radial glial foot processes near the pial surface.

[3] Postsynaptic density protein (PSD-95)/Drosophila discs-large (dlg)/ tight-junction protein (ZO1)

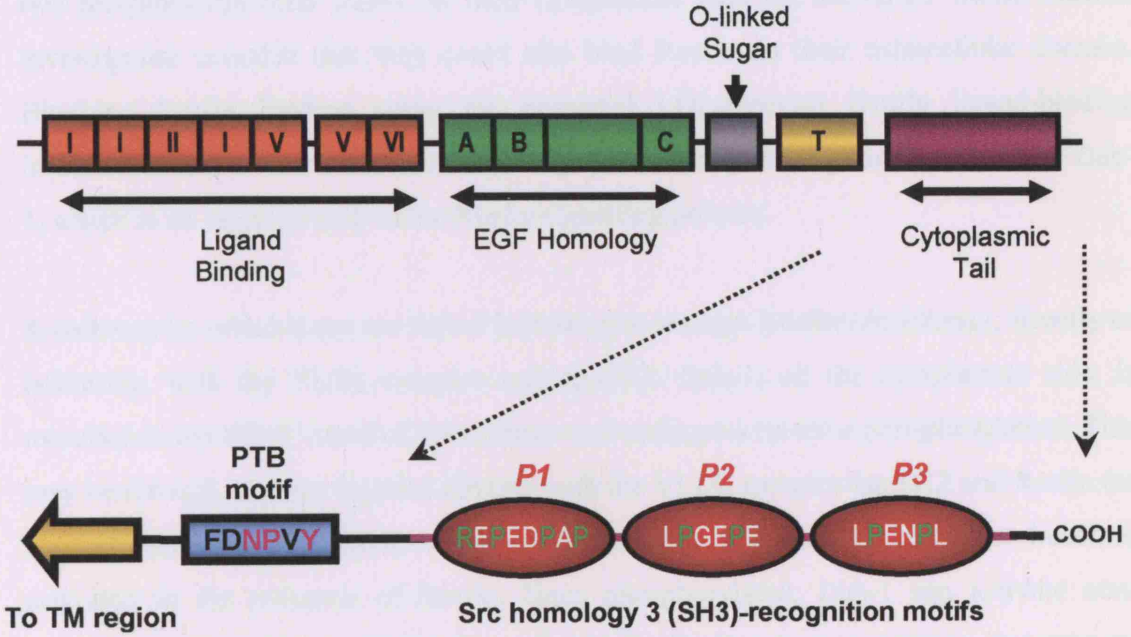


**Figure 1.4 ApoER2 signalling domains**

*The entire structure of apoER2 is illustrated (above), with an expanded view of the cytoplasmic tail (below). The cytoplasmic tail contains numerous proline-rich Src homology recognition motifs (PxxP), which could be putative sites for signal transduction events (P1, P2 and P3 highlighted in red). There is also an NPxY motif (in the blue box), which has an established role in tyrosine phosphorylation mediated signalling events via phosphotyrosine binding domains (PTB). ApoER2 has also been implicated in the regulation of NO release via NOS3 (eNOS).*

The phenotype of these mice was not compounded when double-knockouts of Dab-1 and Reelin were performed, implying that the two proteins worked in a linear pathway [147]. However, Reelin is found in the extracellular space, while Dab-1 is a cytoplasmic adaptor protein, which implied specific receptors for Reelin present on the cell surface. Trommsdorff and colleagues identified that mice lacking the VLDL-receptor apoER2 were also phenotypically similar to *reeler* and *dab1*$^{-/-}$ mice [148]. Similar to LRP, these two receptors can bind Dab-1 on their cytoplasmic tails via the NPxY motif. Further investigation revealed that they could also bind Reelin on their extracellular domain. Blocking Reelin binding using the universal LDL-receptor family ligand-binding inhibitor, receptor-associated protein (RAP), prevented tyrosine phosphorylation of Dab-1, which is an essential step in the Reelin signalling process.

A pathway by which these are linked is starting to emerge. Reelin can interact, directly or indirectly, with the VLDL-receptor and apoER2. Dab-1, on the cytoplasmic side, is recruited to the NPxY motif of the receptor and undergoes tyrosine phosphorylation. This may be through receptor ligation directly with the VLDL receptor/apoER2 and Reelin (or another extracellular protein) or by another membrane tyrosine kinase that becomes activated in the presence of Reelin. Once phosphorylated, Dab-1 can activate non-receptor tyrosine kinases of the Src and Abl family that in turn mediate downstream components. The presence of apoE, which also binds with the extracellular region of these receptors, may significantly modulate the action of Reelin signalling. Additionally, Reelin can activate the protein kinase, PKB/Akt by phosphorylation at Ser473 via the phosphatidylinositol-3-OH-kinase (PI3K) pathway. As PKB/Akt is known to be involved in the up-regulation of NO synthesis via NOS3, this seems to imply Reelin as another contributory factor. A modification to this pathway, possibly by competition of the VLDL receptor/apoER2 by apoE at specific sites in the CNS, could dramatically alter the physiological delivery of NO [149].

Despite its structural similarities to the LDL-receptor, apoER2 is unlikely to function as a receptor for endocytic uptake of lipoproteins [150]. Our laboratory has implicated apoER2 as having the potential to mediate an anti-aggregatory effect of apoE on platelets, with a concomitant increase in intracellular nitric oxide, through a signalling pathway initiated by apoER2 through the interaction of signalling molecules with the cytoplasmic tail of the receptor [151]. Intriguingly, this region is comprised of an additional 59 residues in the cytoplasmic tail (see *Figure 1.4*), encoded by an additional

exon, and is not present in any other member of the LDL-receptor gene family. This cytoplasmic tail contains three potential copies of the minimal Src homology 3 (SH3) binding motif, PxxP. These SH3 domains are found in many intracellular signalling proteins, suggesting that the proline-rich SH3-binding motifs in apoER2 could be involved in signal transduction. These potential functions are in addition to the already well characterised NPxY motif located on the receptor's cytoplasmic tail, implicated in Reelin signalling.

### 1.3.6 High-density lipoprotein (HDL) receptors: SR-BI and SR-BII

As a counterpoint to LDL, the risk of atherosclerosis is inversely proportional to the level of HDL-cholesterol. However, the mechanism of HDL delivery is fundamentally different to the receptor-mediated endocytosis utilised in LDL delivery [136]. HDL acts by a method termed *selective lipid uptake*: after the HDL particle binds to the cell surface, only some of the components of the particle enter the cell (as opposed to the whole lipoprotein/receptor complex, as would be the case with LDL). HDL cholesterol, in the form of cholesteryl ester (CE), is transferred with high efficiency from the particle, after which the lipid-depleted particles dissociate and re-enter the circulation. *In-vivo*, the highest levels of selective uptake are seen in the liver and steroidogenic tissue. The overall HDL-mediated movement of cholesterol from peripheral tissues to the liver is called *reverse cholesterol transport*. In humans, but not in mice, the CE in HDL can also be transferred to other lipoproteins for further transport and metabolism.

Despite this being an established model, the lack of a well defined HDL receptor constrained further development of this field. In 1996, the class B type I scavenger receptor (SR-BI) was unexpectedly shown to be the first molecularly characterised HDL receptor [152]. When expressed on the surface of mammalian cells, this protein bound HDL and mediated selective uptake of HDL lipids. Furthermore, SR-BI was found to be expressed in mice, rats and humans at high levels in precisely those tissues that exhibit the bulk of selective HDL cholesterol uptake *in-vivo* [153]. Temporal and spatial patterns of SR-BI expression during embryogenesis were consistent with the role of SR-BI in delivering cholesterol to the developing foetus [154]. *In-vivo* studies have also established that SR-BI expression was regulated co-ordinately with steroidogenesis in the adrenal gland, testes and ovary, all of which are tissues involved in HDL-CE uptake.

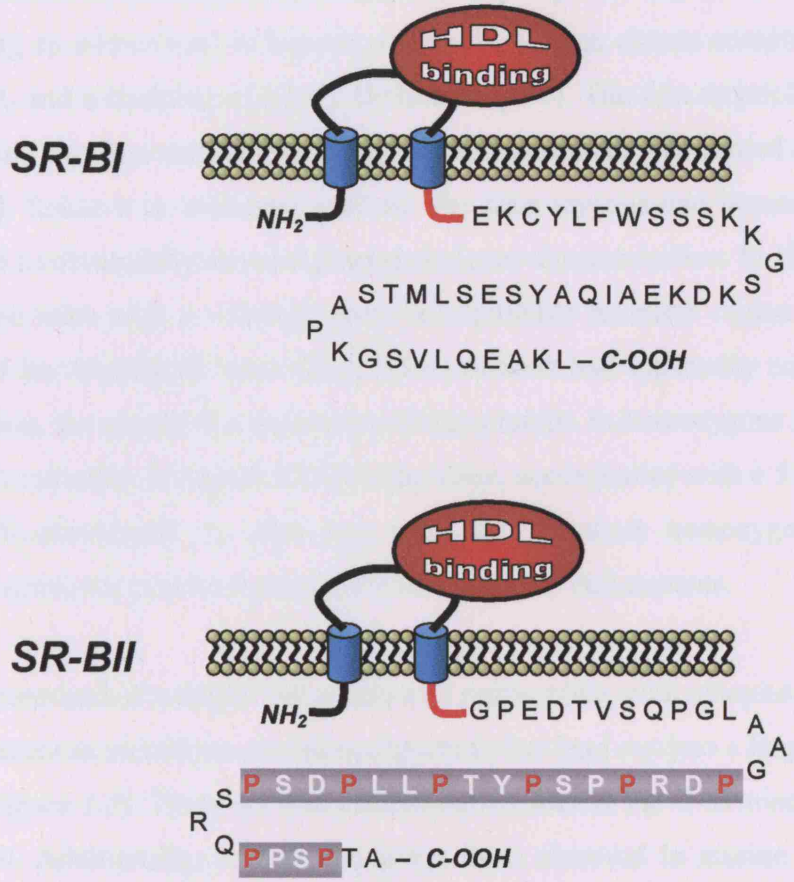


**Figure 1.5 Cytoplasmic tail sequences of SR-BI and SR-BII**

*Illustrated are SR-BI (top) and SR-BII (bottom), with detail of the amino-acid sequences of the cytoplasmic tails of each. Both derive from the same gene: exon skipping of the SR-BI mRNA transcript gives the splice variant, SR-BII. The predominant form is SR-BI, though they both share identical extracellular ligand-binding regions: binding of an HDL particle is shown in the figure. Their cytoplasmic tails are distinct, with SR-BII having several proline-rich PxxP motifs (shaded) that are absent from SR-BI. These could potentially serve as ligands for the protein tyrosine kinase, Src, which is a known stimulator of the PI3K-PKB/Akt pathway.*

The first evidence that SR-BI was directly involved in mediating selective lipid uptake came from the work of Temel *et al.*, where an SR-BI specific blocking antibody inhibited selective uptake of CE from HDL and conversion of HDL-derived cholesterol into steroid hormones in cultured adrenocortical cells [155]. Kozarky *et al.* over-expressed SR-BI (using an adenovirus) in hepatocytes resulting in an almost complete absence of plasma HDL and a doubling of biliary cholesterol [156]. The first targeted disruption of SR-BI (giving rise to a null mutant, i.e. no protein produced) was carried out by Rigotti *et al.* [157]. Relative to wild-type controls, the heterozygous and homozygous SR-BI mutants had a substantially elevated plasma cholesterol concentration. In 1998, Varban *et al.* generated mice with a ~13.5kB insert in a putative promoter region located ~2kb upstream of the first SR-BI exon [158]. This mutation had apparently no effect on the SR-BI protein, but altered the expression of the protein: in homozygous mutants, there was a ~50% reduction in hepatic SR-BI expression, accompanied with a 51% increase in plasma HDL-cholesterol. In other key areas as well these homozygous insertional mutants resemble the previously described heterozygous null mutants.

SR-BI is comprised of a single 509 amino-acid polypeptide, with cytoplasmic N- and C-termini adjacent to membrane spanning sequences that lead out into a large extracellular loop (see *Figure 1.5*). There are two palmitoylation sites at the C-terminal end, Cys462 and Cys470. Additionally, myristoylation has been observed in murine SR-BI. These post-translational modifications may serve an important role in the subcellular localisation of SR-BI in plasma membrane regions, specifically caveolae [159]. This has led to an interest in signal transduction events mediated via SR-BI that eventually activates NOS3 (endothelial NOS or eNOS). Moreover, NOS3 also undergoes subcellular translocation to caveolae (see *Section 1.4.1*). In fact, HDL has been demonstrated to activate NOS3 in a mechanism independent of $Ca^{2+}$ and PKB/Akt, the latter being one of the key regulatory factors of NOS3 mediated nitric oxide biosynthesis [160]. It was discovered that HDL binding to SR-BI gave rise to an intracellular ceramide increase, and that this appeared to be responsible for NOS3 activation. More recently, a pathway has been determined whereby HDL can activate NOS3 via PKB/Akt and MAP kinases [161]. Both these kinases require a phosphorylation signal to become active. This is thought to be catalysed by a Src family tyrosine kinase, which also happens to be an upstream agonist of PI3K.

In 2000, Ikemoto and colleagues identified a protein from rat liver membrane that could interact with the C-terminal of SR-BI via PDZ domains [162]. They named this protein *C-terminal linking and modulating protein* (CLAMP) and it is now known by its generic name, PDZK1. It was shown to have four PDZ domains, although only the first N-terminal domain interacts with SR-BI. It was later shown that co-expression of this protein with the scavenger receptor resulted in an increased level of SR-BI, implying that it may be involved in the stability of the receptor in the plasma membrane. Conversely, this upregulation was accompanied with a 50% reduction in HDL-CE conversion to free cholesterol. This seems to suggest that the interaction of SR-BI with PDZK1 was in someway inhibiting normal delivery of CE to the cells. Members of the LDL-receptor family, such as LRP, are known to interact with PDZ-domain containing proteins through which they can mediate intracellular signal transduction cascades via kinases and other second messengers. It would be interest to investigate whether this could also be the case with SR-BI, and if so whether this occurs by the receptor alone or in concert with LDL-receptor family members.

A newly discovered variant of the scavenger receptor was first described in 1997 by Webb and colleagues [163]. Initially named SR-BI.2, and now known simply as SR-BII, it was discovered by screening a mouse liver cDNA library with degenerate oligonucleotides for human and murine SR-BI. This identified two clones that lacked a 129 nucleotide sequence at its 3' end. This deletion begins at the point on SR-BI where the fifth residue of the cytoplasmic tail would be found and extends through the stop codon of this open reading frame. This exon skipping mechanism alternately splices the SR-BI mRNA to create this variant sequence that encodes SR-BII. To investigate expression of the two splice variants, S1 nuclease protection assays were performed on a number of mouse tissues: liver, testes, adrenal and adipose. This revealed that at least 30% of total expression was attributable to SR-BII, while testes had a 70% preference for this variant of the scavenger receptor.

Further investigation by Webb *et al.* identified the human homologue of SR-BII [164]. Moreover, our group have investigated its sub-cellular location in recombinant Chinese hamster ovary (CHO) cell lines and demonstrated that it was enriched in caveolae, much like SR-BI, indicating that the modifications to the C-terminal end did not affect acylation sites that mediate localisation of the receptor [165]. An analysis of selective HDL-CE uptake and free cholesterol efflux of the two variants revealed SR-BI had a 4-

fold greater efficiency that SR-BII, taking into account the different expression level of the two splice variants. Graf *et al.* studied whether SR-BII was subject to hormonal regulation in a manner similar to SR-BI and its effector, oestrogen [166]. A human liver cell line, HepG2, was exposed to the hormone, 17β-estradiol. This resulted in a dramatic change in expression of the two splice variants. SR-BI expression, which was originally the dominantly expressed receptor, was down-regulated to undetectable levels, whilst SR-BII expression was 3-fold greater than SR-BI. Hormone treatment did not inhibit selective lipid uptake, although even with such an increased SR-BII expression, the level of selective HDL-CE was no more than 75% of the uptake observed by SR-BI. The mRNA levels of the two splice variants were not significantly altered by the hormone, which could indicate that 17β-estradiol does not alter the transcription of the SR-BI/SR-BII, but rather the stability of the protein.

Excluding the first five amino-acids, the cytoplasmic tail of SR-BII is distinct from that found on SR-BI. This would imply differential tail-binding interactions between the two receptors. For example, the PDZK1 interaction, mediated via the terminal 15 amino-acids of SR-BI, is thought to not occur with SR-BII. The tail of SR-BII does, however, contain six PxxP motifs, which can serve as ligands for the protein tyrosine kinase, Src. This is a known stimulator of the PI3K-PKB/Akt pathway. Out of these six Src homology 3 (SH3) domains, two are highly conserved in rat, mouse and hamster sequences. Additionally, a YPTL motif has been identified on SR-BII. This is a consensus Src homology 2 (SH2) domain-binding site, as well being a likely PTB domain site. Both SH2 and SH3 are non-catalytic domains that mediate protein-protein interactions between signalling components downstream of membrane-bound receptors. The presence of these domains on the unique tail sequence of SR-BII implies that this receptor may be capable of a participation in signal transduction mechanisms in a manner quite distinct from SR-BI.

## 1.4 NITRIC OXIDE

Nitric oxide (NO) serves as a ubiquitous intercellular messenger that can modulate cerebral blood flow, thrombosis and neurotransmitter release as well as contributing to morphogenesis and synaptic plasticity [167,168]. It is also important in host response to infection, platelet aggregation and control of smooth muscle tone. However, under conditions of excess formation it can act as a mediator of cyto- and neurotoxicity. Its role as an intercellular messenger is largely due to its ability to diffuse through most cells and tissue with little consumption or direct reaction. As a neurotransmitter, NO is markedly different from others. Most neurotransmitters have an active life of milliseconds after synaptic release. In contrast, NO will persist for seconds, as well as diffusing rapidly, allowing it to encompass several million synapses. It does not require a specific receptor and its action terminates once it reacts with its target substrate.

There is no direct cellular regulation of local NO concentration; control is mediated via its synthesis. Under normal physiological conditions, the amount of NO synthesised is relatively low, but it plays a regulatory role in the function of the nervous system and blood circulation. In the brain, NO acts as a retrograde signalling molecule, where it is transferred from post- to presynaptic nerve terminals. In the postsynaptic terminal it also acts as a second messenger. It has been implicated in functions such as Long-Term Potentiation (LTP) in the hippocampus and Long-Term Depression (LTD) in the cerebellum, as well as a putative involvement in learning and memory [169]. These latter functions may be of greater significance if there is a link between neurodegeneration and elevation/reduction of NO levels.

Nitric oxide has an unpaired electron in its highest orbital, though the highly reactive nature of NO is not simply a result of this [170]. Most other biological molecules are non-reactive to NO as they possess complete orbital pairs. NO is more likely to react with a select range of molecules that also possess an unpaired electron: other free radicals or reactive oxygen species (ROS). One major reaction is with superoxide, a molecule formed by the reduction of molecular oxygen by a single electron, which is a common by-product of the 'leakage' of electrons during the electron transport chain in mitochondria and endoplasmic reticulum [171]. This reacts with NO to form peroxynitrite in a reaction that is largely irreversible. This is normally controlled by the activity of Cu,Zn-superoxide dismutase (SOD). This enzyme converts superoxide to hydrogen peroxide, with an accompanying liberation of molecular oxygen. However, the

rate of formation of peroxynitrite is considerably greater than the rate at which SOD can be active. Peroxynitrite can nitrate aromatic amino acids, react with sulphydryl groups and oxidise lipids, proteins and DNA [172].

### 1.4.1 Nitric oxide synthase (NOS) activity

Synthesis of NO occurs by the conversion of L-arginine to citrulline and NO· by the enzyme nitric oxide synthase (NOS). There are three isoforms of NOS, initially characterised according to the tissue from which they were isolated: neuronal (nNOS or NOS1), endothelial (eNOS or NOS3); or with reference to its transcriptional status, as in the case of inducible NOS (iNOS or NOS2) [173]. As their expression is now known to not be limited to specific tissues, the nomenclature has been updated to reflect this, hence NOS1, NOS2 and NOS3. The use of the older naming convention still persists in most literature, but in this thesis the new nomenclature has been used whenever possible. NOS isoenzymes can be further categorised by their transcriptional regulation: they can be constitutively expressed (NOS1 and NOS3) or inducible (NOS2). All three isoforms share certain common features:

- Bound co-factors (flavin adenine dinucleotide, flavin adenine mononucleotide, heme and tetra hydrobiopterin);
- Enzymatic substrate (L-arginine);
- Co-substrates – ($O_2$ and NADPH).

The activity of the NOS isoenzymes can be summarised below:

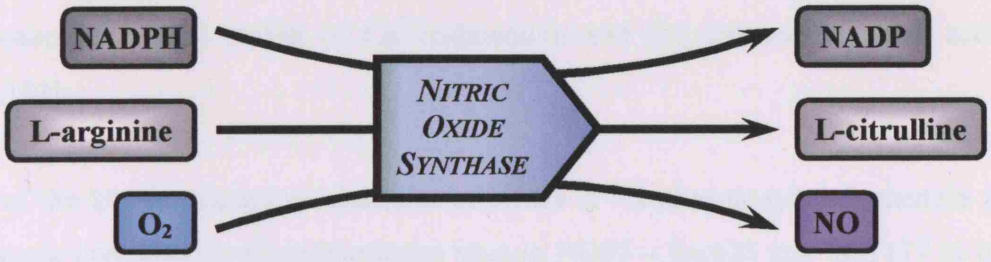


In the brain, NOS3 is found predominantly bound to the plasma membrane of cerebral endothelial cells and regulates cerebral blood flow, although a small population of cells of the hippocampus and dentate gyrus also express it [174]. Both neurons and astrocytes are known to express NOS1, while NOS3 expression has also been observed in

astrocytes. Expression of NOS2 occurs typically after cytokine stimulation in macrophages/ microglia. As stated above, its activity is independent of $Ca^{2+}$ influx, but it may be responsible for excess NO production in diseases such as AD and Parkinson's disease.

### 1.4.2 Regulation of NOS activity

Activation of these enzymes is dependent on several factors and co-factors, in addition to the substrates upon which they act. The action of the constitutive NOS isoenzymes is sensitive to the intracellular $Ca^{2+}$ and calmodulin concentrations [175]. Inducible-NOS also requires the presence of these co-factors for activity as demonstrated by their co-purification with the enzyme, in addition to the main transcriptional regulation by which it is inducible. There is evidence that regulation of NOS1 may extend beyond $Ca^{2+}$/calmodulin influx, mediated via a PDZ domain present on the N-terminal of the NOS1 protein. This domain is known to act as an interaction anchor that allows the enzyme to orient to a subcellular locale [176]. Potentially, it could also be utilised for regulation by phosphorylation, as this has been observed in other PDZ-domain containing proteins [177].

Contrasting with this is the regulation of NOS3 [175]. It can undergo co-translational modification at the N-terminal end by fatty acid acylation: myristoylation at Gly2 occurs, followed by palmitoylation at Cys15 and Cys26 [178,179]. There is evidence that NOS3 must first be membrane bound in order for palmitoylation to occur. Further regulation occurs through the specific localisation of NOS3 to small invaginations of the plasma membrane, caveolae. These are regions where signalling proteins are sequestered. Association of NOS3 with caveolin-1 inhibits the function of the enzyme. This inhibition is weakened by the action of $Ca^{2+}$/calmodulin and the enzyme becomes activated [180,181].

One of the key regulatory mechanisms of NOS3 is via phosphorylation changes [182]. There are two putative phosphorylation sites in NOS3 – Ser633 and Ser1177 in human NOS3 – as well as one in NOS1 – Ser1415 in human NOS1. Phosphorylation of NOS3 enhances NO synthesis independent of intracellular $Ca^{2+}$ concentration. In addition, treatment of endothelial cells with vascular endothelial growth factor (VEGF) or insulin has been shown to produce NO in a PI3K-dependent mechanism. This NO release can be

partially blocked by the action of two structurally dissimilar PI3K inhibitors, wortmanin or LY294002 [183].

The serine/threonine kinase, protein kinase B (PKB), also known as Akt[4], is the cellular homologue of the viral oncogene, v-Akt. It is activated by PI3K, which is further confirmed by its sensitivity to PI3K inhibitors, indicating its downstream effects [184,185]. PKB/Akt had initially been implicated in the endothelial cell response to shear stress whereby an increase in NO synthesis was observed [186]. It has now emerged as a regulator of widely divergent cellular processes, including apoptosis, proliferation and metabolism. It is activated by phosphorylation and there are a number of mechanisms by which this can occur: activation by tyrosine kinase or G-protein-coupled receptors, and stimulation by mechanical processes. Once activated, PKB/Akt can act on a number of protein substrates giving rise to their activation or inactivation. This regulatory function of PKB/Akt on NOS3 activation has been investigated in endothelial cells by the groups of both Dimmeler [187] and Fulton [188].

Fulton's group utilised a wild-type PKB/Akt and a kinase-inactive mutant (K179M) to investigate its action on bovine NOS3 [188]. This study demonstrated that PKB/Akt did phosphorylate NOS3, specifically at Ser1179 (one of the phosphorylation sites present in bovine NOS3), and that this enhanced the enzyme's ability to synthesise NO. In addition, the subcellular localisation of the enzyme was also found to be important for this activation to occur. When a myristoylation/palmitoylation-defective NOS3 mutant was investigated, addition of PKB/Akt did not enhance NO production. Moreover, PKB/Akt had no significant effect on either NOS1 or NOS2, in their native state. To demonstrate this, an N-myristoylation site was added to NOS1, which resulted in a PKB/Akt-mediated enhancement to NO production in a manner similar to wild-type NOS3. This would seem to indicate that the sub-cellular localisation of this enzyme is a key aspect to their activation and function. The action of PKB/Akt on NOS3 was independent of the intracellular $Ca^{2+}$ level. A putative mechanism was proposed whereby the enzyme's sensitivity to calcium-activated calmodulin becomes modified: the addition of a negative charge, via phosphate or aspartate, induces a conformational change in the enzyme that enables activated calmodulin to enter and bind with the enzyme at lower calcium concentrations.

[4] Which is referred to as PKB/Akt whenever possible in this thesis.

Similar work was performed by Dimmeler's group, with emphasis on the shear stress response in endothelial cells [187]. A targeted mutation in the phosphorylation site of human NOS3 at Ser1177 attenuated its activation, which was observed by the lack of any increase in NO production with the addition of PKB/Akt. Furthermore, mutation of the second PKB/Akt site on human NOS3 at Ser 633 showed no effect: phosphorylation and activation of the enzyme occurred and a significant increase in NO production was observed. This suggests that in response to shear stress, it is the Ser1177 site that is responsible for NOS3 activation and a concomitant increase in NO biosynthesis.

### 1.4.3 Brain pathophysiology of NO and oxidative stress

Glutamate-induced activation of NMDA and AMPA/kinase receptors can mediate cell death in focal cerebral ischaemia, as well as in neurodegenerative diseases such as AD and Huntingdon's disease. Moreover, glutamate is the major excitatory neurotransmitter in the corticocortical system [189]. Glutamate neurotoxicity can occur by over-stimulation of these receptors as this leads to an increase in cytosolic calcium levels and activation of $Ca^{2+}$-dependent enzymes, such as NOS. This intracellular increase of $Ca^{2+}$ concentration is transient and returns to a basal level within seconds. One hypothesis is that short-term $Ca^{2+}$ elevation initiates one or more processes that have a delayed neurotoxic effect, consistent with the recorded aetiology of neurodegenerative diseases. It has been observed that cortical cultures treated with NOS inhibitors or removal of arginine can block NMDA neurotoxicity. Addition of haemoglobin, a quencher of NO can induce similar effects. A possible negative feedback loop may exist by the binding of NO to the NMDA receptor, competing with glutamate and inhibiting $Ca^{2+}$ entry [190].

The presence of neurofibrillary tangles, neurite plaques, amyloid angiopathy and granulovacuolar degeneration are established pathological features of AD. These are known to create a great deficit in the cholinergic system, whereby AD brains display a reduction of choline acetyltransferase by 40-90% of the levels found in age-matched clinically-normal patients. Free-radical damage and oxidative stress mediated effects are now considered important factors contributing to AD progression [191], because:

- The concentration of iron is increased in NFT-bearing neurons, and iron is a potent catalyst for the generation of oxyradicals. Additionally, protein modifications catalysed by metal ions and reducing sugars would increase.

- There is an increase in the number of microglial cells and their activation, which can represent a major source of free radicals;

- Degenerating neurons and neurites have an observable increase in lipid peroxidation and resultant membrane disturbances. This could lead to an influx of $Ca^{2+}$ leading to destabilisation of the cytoskeleton and the activation of degrading enzymes.

Amyloid-β has been shown to stimulate NO production in astrocytes. Additionally, clusters of microglia have been observed around Aβ plaques. A possible pathway that has been deduced is the activation of CD4+ T-lymphocytes by Aβ resulting in the production of cytokines such as interferon (IFN)-γ. These cytokines in turn activate microglia that upregulate NOS2 expression as well as produce tumour necrosis factor (TNF)- α, which is also capable of inducing NO production [192].

## 1.5 AIMS OF THESIS

It has been established for well over a decade that individuals carrying one or more copies of the ε4 allele of apoE have an increased susceptibility for developing AD. The mechanisms involved in this process are yet to be fully elucidated. The ability of apoE to modulate the release of NO in endothelial cells, platelets and smooth muscle cells has recently been identified. Moreover, this is an isoform specific effect where apoE4 exposure resulted in an impaired level of NO release than that for apoE3 and apoE2.

I hypothesise that exposure to apoE will give rise to a changed NO response in human brain-derived cells, where this phenomenon will show an apoE isoform differential effect. Broadly, I aim to generate quantified apoE-conditioned medium (*Chapter 2*), characterise human brain-derived cell lines (*Chapter 3*), assay NO release when cells are exposed to apoE (*Chapter 4*), and investigate the signalling pathway within these brain-derived cells (*Chapter 5*). More specifically, the aims of this thesis are:

**AIM 1** *Establish a robust and reliable enzyme linked immunosorbent assay (ELISA) method for measuring the concentration of apoE with conditioned culture media.*

**AIM 2** *Use quantitative polymerase chain reaction (PCR) to survey the expression of apoE receptors, and components of the NO biosynthesis pathway in a panel of human brain-derived cell lines. Suitable cell lines will be identified while gene expression between brain and non-brain tissues will also be compared.*

**AIM 3** *Expose cultured neuronal cell lines to apoE-conditioned medium and assay their response with respect to NO release. For this purpose, an appropriate assay that is accurate and reproducible must be evaluated and established.*

**AIM 4** *Further investigation of the effects of apoE on cultured neuronal cell lines, in particular observing its effect on signalling events within the cells. Immunoblotting techniques will be utilised to monitor phosphorylation changes in key signalling molecules related to NO synthesis.*

# Chapter 2

# MATERIALS & METHODS

# 2.0 GENERAL MATERIALS & METHODS

## 2.1 MATERIALS

All oligonucleotides were made to order by Sigma Genosys (Cambridge, UK). The DNA polymerase, *Taq*, was purchased from Biogene (Kimbolton, UK). The Quantitect SYBR Green I real-time PCR reagents and DNeasy DNA extraction kits were purchased from Qiagen (Crawley, UK). Methanol, ethanol, diethyl ether and chloroform were supplied by VWR International (Poole, UK). All tissue culture plastic-ware unless indicated otherwise in the text were from VWR International. Tetra-methylbenzidine (TMB) substrate kit was supplied by Pierce (Chester, UK). Enhanced chemiluminescence protein biotinylation kit (ECL™), ECL solution for developing Western blots, Hyperfilm nitrocellulose membrane and X-ray developing film were purchased from Amersham Biosciences (Buckinghamshire, UK). All other reagents, unless otherwise stated in the text, were purchased from Sigma-Aldrich Company Ltd. (Poole, UK).

## 2.2 CELL CULTURE METHODS

### 2.2.1 General cell culture

At different stages of this thesis a variety of cell lines were cultured, with a total five distinct cell lines were used throughout the complete project. These included human brain derived cells (all sourced from GlaxoSmithKline, Harlow), endothelial cells and recombinant CHO cells. Details of these cell lines are listed below, including their culture medium formulation:

***SH-SY5Y, human neuroblastoma***

Maintained in Dulbecco's modified Eagle's medium (Sigma) supplemented with 2mM glutamine (1%), non-essential amino-acids (1%) and 10% foetal bovine serum (FBS) (Gibco). Cells were passaged every 4-5 days by brief trypsinisation (see *Section 2.2.2*). *[American Type Culture Collection: CRL-2266]*

***CCF.STTG1, human astrocytoma***

Maintained in RPMI 1640 medium (Sigma) supplemented with 2mM glutamine (1%) and 10% FBS. Cells were passaged every 7 days by brief trypsinisation (see *Section 2.2.2*). *[American Type Culture Collection: CRL-1718]*

***H4, human neuroglioma***

Maintained in Dulbecco's modified Eagle's medium (Sigma) supplemented with 2mM glutamine (1%) and 10% FBS. Cells were passaged every 3-4 days by brief trypsinisation (see *Section 2.2.2*). *[American Type Culture Collection: HTB-148]*

***EA.hy926, human endothelial cell line***

Maintained in Dulbecco's modified Eagle's medium (Sigma) supplemented with 2mM glutamine (1%), penicillin and streptomycin solution (1%) and 10% FBS. Cells were passaged every 6-7 days by brief trypsinisation (see *Section 2.2.2*). These cells were generously provided by Dr CJ Edgell, (University of North Carolina) [193].

***Chinese Hamster Ovary (CHO) cells***

These were based on the mutant CHO cell line, CHOdhfr-, which is deficient in the gene encoding dihydrofolate reductase (dhfr). This enzyme catalyses the reduction of dihydrofolate to tetrahydrofolate, which is an important intermediate in the biosynthesis of proteins and nucleic acids [194]. This cell line was transfected with plasmids that encoded the different human apoE isoforms (in addition to the dhfr gene) to give three new, stably transfected recombinant CHO cell lines [195]: CHO-E2, -E3 and -E4. All three recombinant CHO cell lines, as well as CHOdhfr-, were cultured during this thesis. CHOdhfr- cells were maintained in Iscove's modified Eagle's medium (Sigma) supplemented with 2mM glutamine (1%), 0.05 mM hypoxanthine and 8 $\mu$M thymidine supplement solution (1%), 100 U/ml penicillin and 100 $\mu$g/ml streptomycin supplement solution (1%), non-essential amino-acids (1%) and 10% FBS. CHO recombinant cell lines were maintained in a similar medium to that of CHOdhfr- cells, with the exception that 10% heat-inactivated dialysed FBS (Gibco) substituted the standard FBS, and hypoxanthine/thymidine supplement was not added. CHOdhfr- cells and the three recombinant CHO cell lines were passaged every 4-5 days by brief trypsinisation (see *Section 2.2.2*).

### 2.2.2 Cell maintenance

All cell types were cultured in 25, 75 or 175 $cm^2$ tissue culture flasks, as required. Incubation temperature was maintained at 37 °C, in a humidified atmosphere of 5 % $CO_2$ and 95 % air (Sanyo $CO_2$ incubator MCO-17AI, Sanyo, Japan). Unless indicated

otherwise, all tissue culture work outside of the incubator was performed in a class II microbiological safety cabinet (Envair Ltd., Lancashire, UK), using sterile, disposable plasticware. All cell lines cultured were adherent to the tissue culture flask surface. When cultures reached confluency they would be passaged by trypsinisation.

Briefly, culture medium was aspirated off using a vacuum aspirator with disposable tip (Vacusafe, Integra Biosciences, Switzerland) and cells washed 2 x with warm phosphate buffered saline (PBS) (138 mM NaCl, 10 mM $Na_2HPO_4$, 1.75 mM $KH_2PO_4$ and 2.7 mM KCl.). Cell detachment from the flask was achieved by addition of 0.25 % trypsin-EDTA solution (Sigma, #T4049) such that the cell monolayer was completely covered (equivalent to 0.5, 1 and 2 ml for 25, 75 and 175 $cm^2$ flasks, respectively). Cells were incubated for 3 min at 37 °C with trypsin-ethylene diamine tetra-acetic acid (EDTA). Upon retrieval, flasks were tapped lightly to achieve complete detachment of cells from the culture surface. Culture medium was added to give a total volume of 10 ml, which would also had the effect of diluting the trypsin content of the culture. Cells were split from this stock accordingly at ratios from 1:3 up to 1:20 as required for culture, into fresh tissue culture flasks. To these, fresh medium was added to bring the volume up to 5, 12 and 25 ml for 25, 75 and 175 $cm^2$ flasks, respectively.

### 2.2.3 Viable cell counting

Trypan Blue (Sigma, #93595) stain was used to stain dead cells and determine cell viability during counting. A 100 $\mu$l aliquot of cell suspension was diluted with an equal volume of Trypan Blue stain, and pipetted under the coverslip of a haemocytometer. The number of viable cells present in eight 1 $mm^2$ squares (equivalent to a total volume of $10^{-4}$ $cm^3$) was counted using an inverted phase-contrast microscope (Nikon TMS, Jencons-PLS, UK). After calculating the average number of viable cells per square, the concentration of the cell suspension was calculated using the following equation:

$$\textit{Viable cell count per ml} = \textit{Average count per square} \times \textit{Dilution factor} \times 10^4$$

### 2.2.4 Cryopreservation and retrieval

To create long term storage of reserve cell stocks, cryopreservation was performed. This involved storing cells under liquid nitrogen, whereby a cell suspension is frozen at very low temperature. To prepare cells for storage, between 1 and 5 x $10^6$ cells were

resuspended in 1 ml freezing solution [normal culture medium supplemented with 10 % (v/v) dimethyl sulphoxide (DMSO) and an additional 10% (v/v) foetal bovine serum]. Immediately, cells were transferred to a 1.8 ml cryovial (Life Technologies) and placed in a freezing chamber (Nalgene Cryo 1 °C Freezing Container, Fisher Scientific, Leicestershire, UK). When the isopropanol-containing freeze-container was placed in the -80 °C freezer, its temperature would reduced by 1 °C every minute ensuring a steady decrease in temperature whilst maintaining cell viability. After the cells had reached -80 °C, cryovials were transferred from the freezing chamber to a liquid nitrogen containing tank for long-term storage.

When required, cells were rapidly thawed by brief immersion of the bottom of the cryovial in a 37 °C water bath, before transferring the contents of the vial into an excess of medium in a 12 ml tube. The cells were pelleted at 300 *g* for 5 min in a bench-top centrifuge (Heraeus Megafuge 1.0R), then resuspended in fresh medium and transferred to a 75 $cm^2$ flask and incubated in a 37 °C humidified incubator, as described in *Section 2.2.2*. Following overnight incubation, culture medium was aspirated off and cells washed 2 x with warm PBS. Fresh culture medium was added and cells subsequently subcultured as described previously (*Section 2.2.2*).

## 2.3 MOLECULAR BIOLOGY METHODS

### 2.3.1 Extraction of total genomic DNA from cells

Cellular, or genomic, DNA was extracted using the DNeasy Tissue Kit (Qiagen) following the manufacturer's protocol. Trypsinisation was used to collect adherent cell cultures from a 75 $cm^2$ flask. As per the supplier's instructions, no more than 5 x $10^6$ cells were used in a single extraction so as not to compromise the performance of the DNeasy silica-gel spin columns. Cells were collected by brief trypsinisation (see *Section 2.2.2*) and the culture medium/trypsin solution was transferred to a 12 ml tube. This was centrifuged at 300 *g* for 10 min, after which supernatant was aspirated off.

The cell pellet was resuspended in 200 µl PBS followed by the addition of 20 µl proteinase K and 200 µl buffer AL. Samples were mixed thoroughly by vortexing, then incubated at 70 °C for 10 min before adding 200 µl ethanol and vortexing again. This solution was transferred to a DNeasy spin column placed over 2 ml collection microfuge tube. Following centrifugation for 1 min at 12,000 *g*, the eluted solution in the collection

tube was discarded. After application of 500 μl buffer AW1 to the column, the centrifugation step was repeated as above into a fresh collection tube. Once again, the eluted solution was discarded, and 500 μl of buffer AW2 then added to the column. This was centrifuged at 12,000 *g* for 3 min. The DNA trapped in the column was finally eluted into a clean 1.5 ml Eppendorf tube by adding 100 μl buffer AE to the column and centrifuging for 1 min. Extracted DNA was stored at 4 °C until ready for use.

#### *2.3.1.1 Measurement of DNA concentration*

The concentration of purified DNA was assessed by spectrophotometric measurement of the optical density of the DNA containing solution at a wavelength of 260 nm, as well as 280 nm to measure impurities. The purity of the extracted DNA was determined by the ratio of $A_{260}$ / $A_{280}$, wherein a ratio of 1.7 – 1.9 indicates a high purity of DNA. An $A_{260}$ of 1 OD unit is equivalent to 50 μg/ml DNA in solution. Based on this, the concentration of the eluted DNA could be calculated:

| *Concentration of sample* | = | $A_{260nm}$ | x | *Spectrophotometric conversion rate (= 50)* | x | *Dilution factor* |
|---|---|---|---|---|---|---|

### 2.3.2 Messenger RNA (mRNA) extraction from cultured cells

A large body of work within this project involved real-time PCR analysis of gene expression (see *Section 2.3.6*). This is a technique that can measure the level of gene expression within a particular tissue source, e.g. cultured cells. As such, assaying would require the use of a cDNA template, as opposed to genomic DNA. This, in turn, requires mRNA transcripts to be isolated from which cDNA synthesis can occur by reverse transcription (see *Section 2.3.4*). Extraction of RNA was performed using an organic phenol-chloroform reaction, utilising the commercially available solution TriZOL (Gibco), which contains a mono-phasic solution of phenol and guanidine isothiocyanate.

The RNA extraction procedure is extremely sensitive to RNases that degrade RNA, and are ubiquitously found in all aspects of the general laboratory environment: containers, tips, surfaces, solutions, human skin contact, etc. Therefore, prior to commencement, a dedicated set of Eppendorf tubes and filtered tips had to be autoclaved. All surfaces, including Gilson pipettes had to be washed using RNaseZAP (Ambion, USA) to protect against RNA degradation. To perform dilutions, diethylpyrocarbonate (DEPC) water was prepared by the addition of 0.01% DEPC (v/v) to RNase-free water and then autoclaved before use. Disposable gloves were used throughout the procedure to minimise the risk

RNase contamination. As a further precaution, the entire procedure was performed in a laminar flow vacuum hood.

Cells for RNA extraction were cultured in 60 mm dishes (Nunc). Once cells were sub-confluent, homogenisation was performed with 1 ml TriZOL reagent per dish and the homogenate transferred into an Eppendorf tube. This incubated for 5 min at room temperature to allow complete dissociation of nucleoproteins, after which 200 $\mu$l chloroform was added and the tube shaken by hand for ~15 sec. Samples were then incubated at room temperature for 3 min, followed by centrifugation at 12,000 *g* for 15 min at 8 °C. Separation of solution would occur such that the RNA would be present as a clear aqueous phase at the top of the solution, whilst DNA and proteins would be present in a red/pink lower organic phase layer. Between these two was a distinct, opaque, white interphase layer. The upper RNA-containing aqueous phase was carefully transferred to a fresh tube. RNA precipitation from this solution was achieved by the addition of 0.5 ml isopropanol (Sigma) and incubated for 10 min at room temperature, after which they were centrifuged at 12,000 *g* for 10 min at 8 °C. The RNA would be visible as a small, discreet gel pellet at the bottom of the tube. Supernatant was carefully removed from the tube and the pellet resuspended in 75 % ethanol to wash the pellet. The tube was thoroughly vortexed, then centrifuged for 7500 *g* for 5 min at 8 °C. The extracted RNA was stored in 75 % ethanol at -80 °C until ready to use.

#### *2.3.2.1 Measurement of RNA concentration*

Before proceeding to reverse transcription, it was essential to determine the concentration of the RNA. This was performed spectrophotometrically in the same manner as that for measuring the DNA concentration described in *Section 2.3.1.1.* In this instance, the spectrophotometric conversion is such that 1 OD unit = 40 $\mu$g/ml for RNA (as opposed to 50 $\mu$g/ml for DNA).

#### *2.3.2.2 Assessing RNA quality on a formaldehyde gel*

The quality of the extracted RNA was further assessed by electrophoretic separation on a formaldehyde gel. To prepare samples, RNA pellets were resuspended in DEPC and stored in dry ice to prevent degradation. A gel was prepared with 0.45 g agarose, 1.53 ml 37 % formaldehyde, 3 ml 10 x 3-(N-Morpholino)-propanesulfonic acid (MOPS) buffer, and 25.5 ml DEPC water. This mixture was placed in a microwave oven for ~2 min on medium power, and then poured into a minigel apparatus (Horizon minigel apparatus

from Life Technologies) and allowed to set. A 4 x loading buffer was prepared containing 625 μl formamide, 170 μl 37 % formaldehyde, 125 μl 10 x MOPS buffer, 75 μl bromophenol blue and 5 μl ethidium bromide. The RNA sample loaded on the gel consisted of 5 μl RNA sample with 2.5 μl loading buffer and 2.5 μl DEPC water. A constant voltage of 150 V was applied to the gel and stopped before the bromophenol 'dye-front' reached the end of the gel. The RNA would separate on the gel and was resolved into two distinct bands representing 16S and 28S RNA, which were visualised under UV light.

### 2.3.3 Reverse transcription of RNA to cDNA

Isolated mRNA (described in *Section 2.3.2*) from cells was reverse transcribed into single-stranded cDNA, which could act as a suitable template for PCR. This required the activity of a reverse transcriptase enzyme that can synthesise a DNA sequence based on a RNA template. The reverse transcription process requires the presence of a number of cofactors: deoxynucleotide triphosphates (dNTPs), reverse transcriptase enzyme and an oligo (dT) primer to initiate the reaction. Following this, the cDNA synthesised would provide the necessary DNA template upon which thermostable DNA polymerases can amplify a sequence by PCR (see *Section 2.3.4*).

SuperScript II (Invitrogen) was used for reverse transcription. A reaction mix containing 1 μl oligo(dT), 1 μl dNTPs (Invitrogen), and between 5 ng to 1 μg RNA, all made to final volume of 12 μl with DEPC water was prepared in a fresh RNase-free Eppendorf tube. This was incubated at 65 °C for 5 min, following which it was quickly chilled on ice. The tube was briefly centrifuged, and then 4 μl of 5 x first strand buffer (Invitrogen), 2 μl 0.1 M dithiothreitol (DTT) (Invitrogen) and 2 μl DEPC water were all added to the solution. After mixing the tube gently, it was incubated at 42 °C for 2 min. This was to allow the oligo(dT) primers to anneal to the polyadenylated RNA, following which 1 μl (200 U) of SuperScript II reverse transcriptase was added. The sample were all mixed thoroughly and incubated at 42 °C for a further 50 min to allow first strand cDNA synthesis. The reaction was finally inactivated by transferring tubes into a 70 °C water bath. After the samples had been chilled on ice, 1 μl (2 U) of *E. coli* RNase H was added to each tube to remove any RNA. This digestion was complete after 20 min at 37 °C. The concentration of the newly synthesised cDNA was assessed by the same method used for DNA (see *2.3.1.1*) and stored at -20 °C until ready for use.

### 2.3.4 Polymerase Chain Reaction (PCR) for amplification of DNA

The polymerase chain reaction rapidly amplifies a specific, short target sequence of nucleic acids from a much longer DNA molecule. Either genomic DNA or cDNA can function as template for this reaction. A successful PCR amplification of a target will generate sufficient copies of the PCR product such that it will be in much greater excess that the original template DNA. Once amplified, PCR products can be visualised on agarose gels (see *Section 2.3.5*).

The eventual aim of the majority of analyses in this thesis was to perform quantitative-PCR (Q-PCR), a method whereby the amplification of PCR product at each reaction cycle can be monitored to eventually determine the initial template concentration (see *Section 2.3.6*). This type of PCR requires that the product should not exceed 500 bp, and ideally should be between 100 and 200 bp to ensure the stability of the product when the detectable fluorescent probe is introduced in the reaction. Therefore, PCR products for most targets were designed to be within this size range. Primers were designed using the web-based tool, *GeneFisher*[5], after having retrieved the complete mRNA coding sequences for the various genes from GenBank (via the National Centre for Biotechnology (NCBI) website, *Entrez Nucleotide*).

A reaction mixture prepared for a PCR assay typically comprises a generic set of components: a DNA or cDNA template, a pair of specific oligonucleotide primers that define the two ends of the PCR product, dNTPs, a thermostable polymerase and a reaction buffer containing a specific concentration of $MgCl_2$. After thoroughly mixing the reaction components, samples are placed in a thermal cycler. This is an automated instrument that cycles a series of set temperatures, for varying amounts of time.

The polymerase chain reaction can be delineated into three distinct stages: denaturation, annealing and extension (DNA amplification). The completion of all three stages defines a single PCR cycle:

> ***Denaturation:*** the production of a single-stranded DNA template by heating the sample to at least 95 °C for at ~1 min. This separates the two strands of DNA and generates the template upon which the thermostable DNA polymerase can function.

[5] http://bibiserv.techfak.uni-bielefeld.de/genefisher/

***Annealing:*** the two oligonucleotide primers that define the ends of the PCR product anneal to the separated DNA strands. This stable association of the primer pair with the template DNA occurs within 30–60 s, but is critically dependent upon an annealing temperature, which can be between 50–70 °C dependent on the primers. Therefore, for every primer pair and template combination, the optimal annealing temperature must first be established. This optimisation was achieved using the RoboCycler 40 Gradient Cycler (Stratagene), which allows a simultaneous gradient of annealing temperatures across the heating block to be performed in the same experiment.

***Extension:*** DNA polymerase synthesises a new complimentary oligonucleotide sequence, extending 5' to 3' from the primers, using the existing DNA sequence as a template. This extension phase occurs at the optimal temperature for the thermostable polymerase, which is usually 72 °C. The amount of time needed for this stage depends upon the length of the target sequence. At the end of this extension phase, two double-stranded DNA molecules comprising the region defined by the primers will have been synthesised from the original double-stranded DNA template, and one cycle of the PCR will have been completed. The temperature then returns to 95 °C and the next cycle will commence.

Theoretically, at every PCR cycle the amount of target sequence in the reaction mix will double, resulting in an exponential rise in product. Assuming the presence of a single copy of the target template in the original reaction mixture, after 20 cycles this would result in over a million copies, and after 30 cycles there would be over 100 billion copies. In reality, there are usually numerous copies of a target gene, as the cDNA templates will have been generated from numerous cell sources, and the reaction itself will encounter limiting factors such as availability of free dNTPs and primer as well as progressive heat denaturation of the polymerase enzyme. Upon completion of all PCR cycles, the amplified nucleic acid can then be analysed for size by agarose gel electrophoresis (see *Section 2.3.5*) to ensure the correct sized product has been amplified and no contamination of the reaction has occurred. If real-time PCR (as described in *Section 2.3.7*) were performed utilising an intercalating DNA binding dye, a melt curve analysis could be performed immediately following the PCR to determine product purity. For more information, see *Figure 2.3.3*.

### *2.3.4.1 Basic PCR protocol*

For each PCR, a master mix was prepared by adding the reagents in the order and amounts shown below into 0.5 ml thin-walled PCR tubes (Starlab, Milton Keynes, UK):

| Reaction Component | Volume | Final Concentration |
|---|---|---|
| RNA/DNA-free water | 17.25 µl | – |
| 10 x PCR buffer | 2.5 µl | 1 x |
| 50 mM $MgCl_2$ | 1 µl | 2 mM |
| 10 mM dNTP mix | 0.125 µl | 50 µM |
| 10 mM forward primer | 1 µl | 0.4 mM |
| 10 mM reverse primer | 1 µl | 0.4 mM |
| *Taq* polymerase (5 U/µl) | 0.125 µl | 0.625 U |
| cDNA template (200 ng/µl) | 2 µl | 400 ng |
| **Total reaction volume** | **25 µl** | |

All components of the mix other than the template were prepared in a designated PCR room which was kept free of contaminants. Template was added to the mix outside of this room. Additionally, with each set of experiments, it was necessary to set up a negative PCR control. This was a tube containing all the above listed components, but with cDNA template replaced by RNA/DNA-free water. As described previously, the optimum annealing temperature for reactions was determined by running an annealing temperature gradient on the Robocycler thermal cycling machine. This has a 'hot-top' which eliminates loss of sample through evaporation upon heating. Investigation revealed that all primer sets could be used with similar efficiency at an annealing temperature of 60 °C. Reactions were also performed using the Biometra TRIO-thermoblock (Goettingen, Germany) thermal cycling machine which did not feature a 'hot-top'. In these instances, the reaction mix in each tube had to be covered with mineral oil to prevent sample loss by evaporation. The PCR programme used for all reactions was as follows, and closely matches the conditions used in the real-time PCR machine (see *Section 2.3.7*):

| ***Reaction step*** | ***Temperature*** | ***Time*** | |
|---|---|---|---|
| *Initialisation* | 94 °C | 5 min | |
| *Denaturation* | 94 °C | 20 s | ***45 cycles*** |
| *Annealing* | 60 °C | 30 s | |
| *Extension* | 72 °C | 30 s | |
| *Completion* | 72 °C | 10 min | |

### 2.3.5 Agarose gel electrophoresis of PCR products

Following PCR amplification, the reaction products were analysed using agarose gel electrophoresis. During electrophoresis, the strands of DNA become separated according to their size as they migrate through the agarose matrix from the cathode area towards the anode. The agarose gel was prepared with ethidium bromide, which intercalates between adjacent base pairs of the DNA molecules and allows visualisation of distinct DNA bands on the gel when viewed under UV light. Different agarose concentrations can be used depending on the expected DNA fragment sizes to be resolved. Virtually all PCR products in this thesis were within the region of 100 – 200 bp, which is considered a low molecular weight. For these sizes of products, a 2 % (w/v) agarose gel is recommended. Of note are the PCRs performed in *Chapter 4*, where the expression of soluble guanylate cyclase required amplification of products in excess of 700 bp; in this case the resolving ability of a 2 % agarose gel was still sufficient, so no modification of the protocol was required.

The following protocol describes a typical minigel analysis. The minigel apparatus (Horizon minigel apparatus from Life Technologies) was set up as recommended by the manufacturer. The appropriate weight of agarose (Biogene) was dissolved in Tris-borate EDTA (TBE) buffer [100 mM Tris, pH 8.4, 90 mM boric acid and 1 mM EDTA; diluted from a 10 X stock (Life Technologies)] by heating the mixture in a microwave oven for about 2 min on medium power. As the solution cooled, ethidium bromide (0.5 $\mu$g/ml) was added and the gel then poured into its cast. The gel was left to set for ~30 min at room temperature and then installed within the minigel electrophoresis chamber. A sufficient volume of TBE buffer was added until the surface of the gel was covered. The PCR products were mixed 9:1 with 10 X loading buffer [10 mM Tris-HCl, pH 7.5, containing 50 mM EDTA, 10 % Ficoll 400 (w/v), 0.25 % (w/v) bromophenol blue and 0.25 % (w/v) xylene cyanol FF] and 10–20 $\mu$l of each sample were loaded into each well. Ten $\mu$l of a 1 kb or 100 bp DNA ladder (Life Technologies) were run in an adjacent lane for product size determination. A constant voltage of 150 V was then applied to the gel. The movement of the sample could be observed as the bromophenol blue 'dye-front' migrated down the gel from cathode to anode. When this dye-front was ~1 cm from the bottom of the gel the electrophoresis was stopped. The gel was visualised and photographed on a UV transilluminator connected to a computer operated camera (UVP Epi Chem II Darkroom) and image analysis software (Labworks UVP, Media Cybernetics, USA).

### 2.3.6 Real-time (RT-) PCR

The polymerase chain reaction has proved a powerful tool for many researchers. Quantitative-PCR (Q-PCR) is an extension of this technique, allowing the reaction to be monitored as it progresses. To fully appreciate Q-PCR an understanding of standard PCR should be established. The technique was first developed in the mid-1980s by Kary Mullis and colleagues [196,197]. During PCR a region of a DNA template is amplified at an exponential rate using oligonucleotide-priming sequences that flank the region and a thermostable DNA polymerase, originally isolated from the thermophilic bacterium, *Thermophillus aquaticus*. Beyond the exponential increase in PCR product, a saturation point is eventually reached at which inhibition of the reaction can occur by a number of factors such as reagent limitations, accumulation of pyrophosphate molecules or inhibitors within the template itself. This is termed the 'plateau phase' of the reaction. Additionally, mis-priming of the template or the formation of primer-dimers can give rise to more than one product. Therefore, simply observing the end-point of a reaction is not always the most reliable measure of reaction efficiency and quantification. In Q-PCR, the reaction is monitored during the exponential phase where PCR product continues to accumulate. From this it is possible to perform an extrapolation to determine the initial copy number or relative quantity of a particular gene as expressed within that system [198,199].

Virtually all Q-PCR chemistries utilise fluorescence to measure the accumulation of PCR product, where an increase in fluorescence is detected as more PCR product is formed. Following completion of the reaction a threshold fluorescence is defined beyond which all samples are in the exponential phase of the reaction. This threshold is determined as a function of the background fluorescence, which usually lasts for the first 10-15 cycles of the experiment. When the fluorescence recorded crosses this threshold, it is assumed that their fluorescence is now significantly greater than the background. For each reaction it is possible to establish a cycle number at which the threshold is crossed [200]. This is defined as the Cycle Threshold ($C_t$) and these values are directly proportional to the amount of starting template in the reaction (see *Figure 2.3.1*).

In standard PCR, the mixture is heated and cooled in repeating cycles: template is denatured, allowing annealing of primers that undergo extension by DNA polymerase. These stages are termed the denaturation, annealing and extension steps of PCR. At the end of each cycle, there should theoretically be a doubling of template available for the

next stage, and it is this 'doubling-up' that gives rise to the exponential phase of the PCR. The initial background phase is when the reaction is equilibrating and the concentration of the PCR product is below the detection limits of the machine, whilst the plateau phase at the end is when the reaction reaches rate limiting criteria. These heating and cooling cycles are normally performed using a thermal cycling block.

For Q-PCR it is necessary to both heat and cool the reaction efficiently in addition to reliably measuring and recording the fluorescence as it proceeds over each cycle of the experiment. Before the advent of sophisticated real-time instrumentation, Q-PCR was performed by time course assay whereby a reaction was halted at regular intervals and the PCR product removed. A series of such collections could then be run on an agarose gel and the PCR product visualised by ethidium bromide intercalation (or another intercalating dye) in double-stranded DNA and illuminated by UV irradiation. Using a technique such as densitometric analysis, the PCR product could be quantified relative to a known standard. Overall, this was an unreliable, laborious and largely inconvenient method for quantifying PCR products. Modern real-time PCR was first reported in 1993 by Higuchi and colleagues [201]. Their method was also based on the principle of ethidium bromide intercalation, but this time measurements were performed during the reaction itself and followed by irradiating the reaction mix with UV light. The resulting fluorescence was detected using a charged-coupled device camera. At each cycle number, following the annealing step, a fluorescence reading was recorded and at the end of the reaction this fluorescence was plotted against the cycle number.

There are now three commonly used chemistries for Q-PCR (see *Figure 2.3.1*): 5' nuclease assay probes, molecular beacons and SYBR Green I intercalating dye. These all utilise the generation of fluorescence during the PCR process that is detected by a real-time PCR machine. Both 5' nuclease assay probes and molecular beacons make use of hybridisation probes that enhance the overall specificity of the real-time assay.

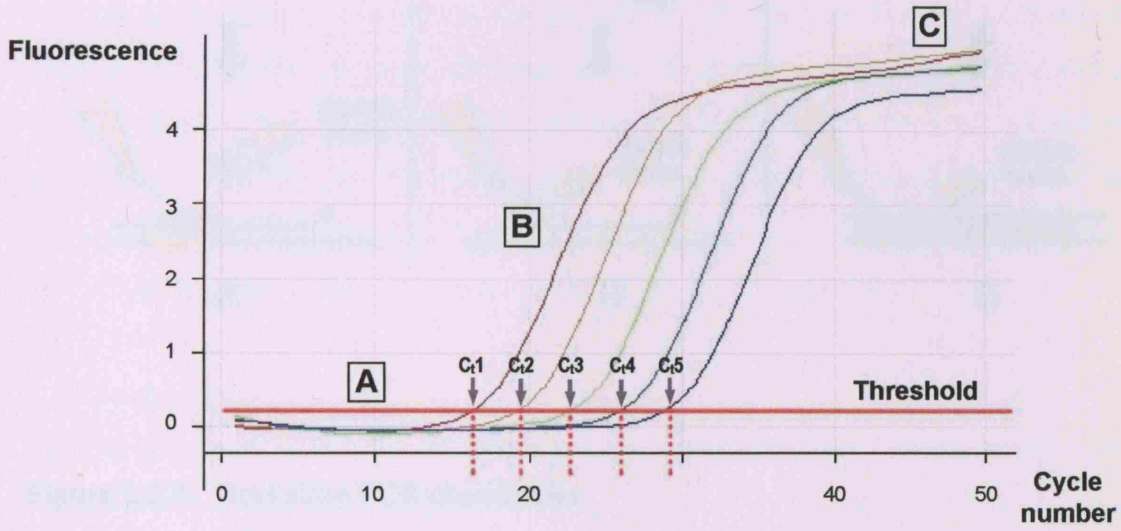


**Figure 2.3.1 Typical quantitative PCR profile.**

*A threshold fluorescence (red line) has been defined, from which different individual cycle ($C_t$) values can be derived. The $C_t$ value is directly proportional to the template copy number of the target gene, whereby a low $C_t$ is equivalent to a high copy number. Each coloured line represents a ten-fold dilution of cDNA template and the same target gene (β-actin) was assayed.*

*A = Initial equilibration period (background fluorescence);*

*B = Exponential phase (detection period);*

*C = Plateau phase (reaction completion).*

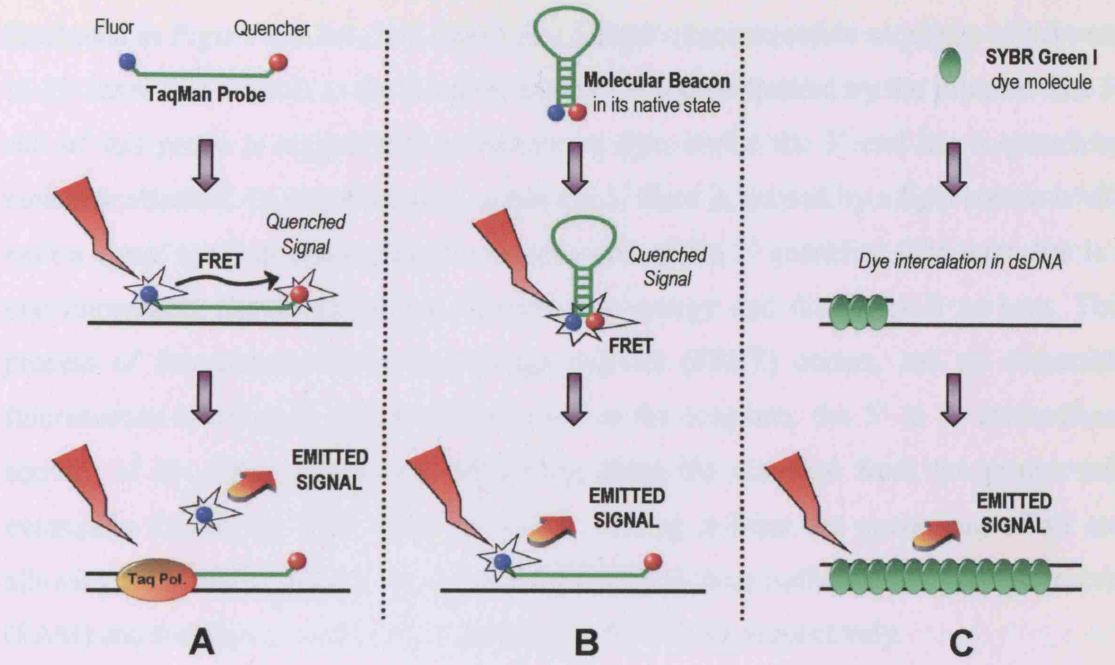


**Figure 2.3.2 Real-time PCR chemistries**

*(A) TaqMan probes: this is a short oligonucleotide sequence that is highly specific to a particular product. It has a 5' fluorescent probe whose signal, whilst in the native state, is quenched by the 3' quenching molecule by fluorescence resonance energy transfer (FRET). Once the probe has annealed to its target, it will be subject to detachment from its oligonucleotide tether by the exonuclease action of* Taq *polymerase, which releases the fluor with a resultant increase in emitted signal;*

*(B) Molecular Beacons: similar to a TaqMan probe, but exists in a hair-pin loop in its native state. This brings the fluor and quencher into close proximity and fluorescence is prevented by FRET. Upon annealing, they become spatially separated, with a concomitant increase in fluorescence;*

*(C) SYBR Green I dye: has a very low level of fluorescence when unbound and free in the reaction mix. During synthesis of double-stranded-DNA, it becomes intercalated between strands, and its fluorescent signal will increase with each successive cycle.*

### *2.3.6.1 TaqMan probes*

Of the 5'nuclease assays, the most commonly utilised is the TaqMan probe [198], illustrated in *Figure 2.3.2 A*. It is essentially a short oligonucleotide sequence of between 15-20 bases that anneals to the template within the region flanked by the primers. The 5' end of this probe is tagged with a fluorescent dye, whilst the 3' end has a quenching molecule attached. In its native state, when the 5' fluor is excited by a light source it will emit a signal that has a wavelength characteristic of the 3' quencher. The quencher is a non-fluorescent chromophore that absorbs this energy and dissipates it as heat. This process of fluorescence resonance energy transfer (FRET) occurs, and no detectable fluorescence is released. Upon hybridisation to the template, the 5' to 3' exonuclease activity of the DNA polymerase advancing along the template from the primer will eventually detach the fluor from the probe, freeing it from the quenching effect and allowing it fluoresce. Commonly used fluors and quenchers include 6-carboxyfluorescein (FAM) and 6-carboxy tetra-methyl rhodamine (TAMRA), respectively.

### *2.3.6.2 Molecular Beacons*

Molecular beacons, like the TaqMan probes, are single stranded oligonucleotides with a fluorescent dye at the 5' end and a quencher at the 3' end [202], illustrated in *Figure 2.3.2 B*. However, the native state of these probes is in a hairpin loop, created by a complimentary sequence of five to seven bases at the 5' and 3' ends. Thus, the fluorophore and the quencher are kept in close proximity to each other, allowing FRET to occur and transfer fluorescence to the quencher. The loop sequence of the probe is designed to be complimentary to a sequence within the target amplicon sequence, as is the case in TaqMan probes. When the molecular beacon approaches the DNA molecule a conformational change occurs in the probe such that the stem region opens up and hybridisation to the target sequence occurs. The incidence of this event distances the fluorophore from the quencher and detectable fluorescence increases. One of the key advantages of the use of molecular beacons is their high specificity. The thermodynamic properties of the probe are such that they greatly favour the formation of the native hairpin loop structure, and therefore remain with the fluorescence quenched. If non-specific binding does occur, the probe will eventually dissociate from the template and re-establish the hairpin loop structure rather than remain hybridised.

The high specificity of molecular beacons can allow them to potentially differentiate between single nucleotide polymorphisms. Therefore, this chemistry lends itself to the

study of allelic discrimination. The disadvantages of molecule beacons result from the stem-loop structure they adopt. These have to be designed very carefully with the thermodynamics of the reaction in mind. If this is not considered they can potentially form other conformations that do not fully quench fluorescence before hybridisation, or do not hybridise at all by having too great a preference for remaining in a hairpin. Moreover, the necessity to include the two regions of complimentary bases at the ends of this oligonucleotide may greatly limit the potential targets for this method as a suitable region on the DNA template must be located to allow this unique structure to form.

### *2.3.6.3 DNA-binding dyes*

This is the natural successor to the original use of ethidium bromide intercalation in the early development of Q-PCR. It is now one of the most commonly used chemistries as it can generally be applied to any existing PCR experiment. Both the TaqMan and Molecular Beacon approaches to Q-PCR require, by their very nature, the synthesis of a specialised oligonucleotide sequence, namely, the probe. DNA binding dyes do not require such a molecule to be synthesised, allowing this chemistry to be utilised in virtually any existing methodology with minimal modification.

The most widely used dye is SYBR Green I, developed by Molecular Probes Inc. (Oregon, USA). When unbound and free in the reaction mix, the dye shows very little fluorescence. When double-stranded sequences of DNA (ds-DNA) are formed as the primer sequences anneal with the template, molecules of the dye begin to intercalate with the strands (see *Figure 2.3.2c*). This intercalation continues along the entire amplicon sequence as polymerisation progresses. This intercalation in ds-DNA gives rise to a rapid increase in fluorescence of the dye molecules, by up to 800- to 1,000-fold. However, at the next denaturation step, all the intercalated dye is released back into the reaction mix. Therefore, all measurements of fluorescence are made after the elongation step. As more PCR product forms at each cycle, the overall fluorescence of the reaction will increase.

The key disadvantage of SYBR Green I dye is its complete lack of specificity. Intercalation occurs with any ds-DNA sequence, including primer dimers and mis-primed reactions. In contrast, TaqMan and Molecular Beacon probes can be highly specific to the amplicon being investigated, and can potentially differentiate single nucleotide differences; this in fact makes these chemistries ideally suited to the analysis of single nucleotide polymorphisms in genes. Although this is not a luxury afforded by

SYBR Green I dye, performing a melt curve analysis immediately following the PCR can elucidate the specificity of this reaction (see *Figure 2.3.3*). This is achieved by increasing the temperature within the thermocycler at 1 °C intervals from the annealing temperature (~55-60 °C) through to a complete denaturing temperature (~99 °C), sampling the fluorescence at each temperature increment. As amplicons denature, fluorescent dye is released into the reaction mix. This will occur at a specific temperature for each reaction product formed. If non-specific binding occurs then more than one peak will be observed in the melt-curve, whereas a specific reaction will show only one peak.

### 2.3.7 Real-time PCR protocol

The real-time PCR was performed using primers listed in *Table 3.1* (*Chapter 3*), after having optimised their activity through a standard PCR protocol, using cDNA template generated from SH-SY5Y and CCF.STTG1 cells. Reaction mixtures were prepared using the Quantitect kit (Qiagen), which contains a ready-prepared 2 x mix of PCR buffer, dNTPs, $MgCl_2$, *Taq* polymerase and SYBR Green I dye. For each reaction, the master mix was prepared by adding the reagents in the order and amounts shown below into 0.2 ml thin-walled PCR tubes (Starlab, Milton Keynes, UK):

| Reaction Component | Volume | Final Concentration |
|---|---|---|
| RNA/DNA-free water | 8.5 µl | – |
| 2 x Quantitect mix (PCR buffer, dNTPs, $MgCl_2$, *Taq* polymerase, SYBR Green I dye) | 12.5 µl | 1 x |
| 10 mM forward primer | 1 µl | 0.4 mM |
| 10 mM reverse primer | 1 µl | 0.4 mM |
| cDNA template (200 ng/µl) | 2 µl | 400 ng |
| **Total reaction volume** | **25 µl** | |

Reactions were performed using the RotorGene RG3000 (Corbett Research, Cambridge, UK). This machine has two unique operational features: (1) the reaction temperature is regulated by the action of forcing heated or cooled air into the central reaction chamber, and (2) the reactions were are placed in a rotor which continually centrifuges during the experiment, a process which maintains complete uniformity of temperature between reactions (sample to sample variance is ± 0.01 °C according to the manufacturer).

The following programme was used for all Q-PCR experiments:

| *Reaction step* | *Temperature* | *Time* | |
|---|---|---|---|
| *Initialisation* | 50 °C | 2 min | |
| *Enzyme activation* | 95 °C | 10 min | |
| *Denaturation* | 95 °C | 15 s | ***45 cycles*** |
| *Annealing / Extension* | 60 °C | 1 min | |

The *Taq* polymerase included in the Quantitect mix is a 'hot-start' *Taq*. This enzyme is supplied in an inactive state and has no enzymatic activity at ambient temperatures. As a result, the formation of misprimed products and primer-dimers during reaction setup is eliminated. Once the reaction temperature is increased to 95 °C, the enzyme enters into its activated state allowing PCR to commence and DNA polymerase activity to proceed. Immediately following the 45 cycles of PCR, a melt curve analysis was performed by heating the plate from 60°C to 99°C and measuring SYBR Green I dissociation from the amplicons (see *Figure 2.3.3*). This gives a measure of reaction specificity, whereby a single peak in a first derivative plot was indicative of a single amplification product, whereas multiple peaks implied co-amplification of several cDNA species.

The copy number of mRNA-derived cDNA in each sample was calculated from a standard curve generated with the use of known amounts of genomic DNA, which was then serially diluted from $10^0$ (undiluted, stock DNA template) through to $10^{-6}$; the data presented in *Figure 2.3.1* is in fact taken from a serially diluted template. The housekeeping gene, β-actin, was targeted in this reaction, allowing a standard curve to be plotted based on the $C_t$ values generated. Each set of PCR conditions was performed in triplicate, and an average reading taken for data analysis.

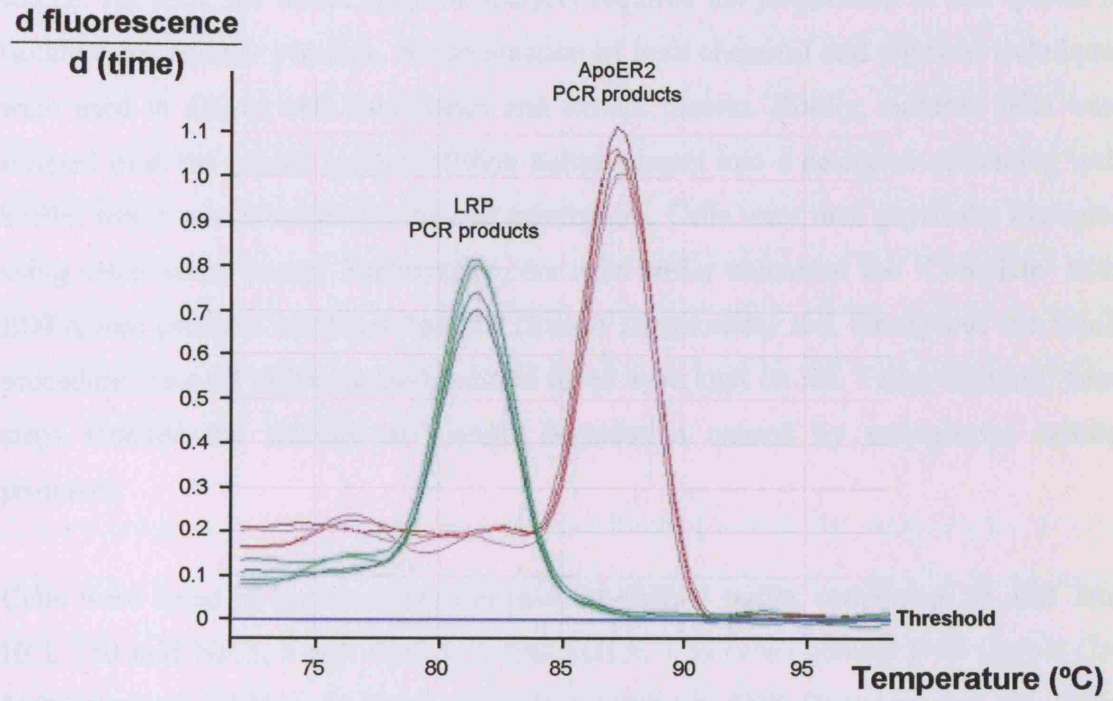


**Figure 2.3.3 Melt curve analysis of PCR products**

*Melt curve performed immediately following a real-time PCR programme. Samples are heated from 55 °C to 99 °C. Two sets of experiments are presented, each with 4 individual reactions performed (each with its own trace): the green traces represent reactions for apoER2 receptor; the red traces represent reactions for the receptor, LRP. As the temperature increases, the PCR products start to denature. If a single PCR product is present without any contaminant or artefactual product, a single, well-defined peak should be observed. This peak represents the release of intercalated DNA binding dye (in this instance SYBR Green) at a temperature specific to that particular PCR product.*

## 2.4 PROTEIN EXTRACTION AND ANALYSIS

### 2.4.1 Cell Lysate Preparation

All protein analyses in this thesis were performed with cellular material as the protein source. As such, the initial stage of analysis required the preparation of cell lysates to isolate these cellular proteins. A combination of both chemical and physical techniques were used to disrupt cell membranes and extract protein. Briefly, cultured cells were scraped from the plastic surface of their culture vessel into a detergent-containing lysis buffer, which would solubilise the cell membranes. Cells were then physically disrupted using shear stress forces. Furthermore, the lysis buffer contained the 'Complete' Mini EDTA-free protease inhibitor cocktail (Roche Diagnostics) and throughout the whole procedure ice-cold buffers were used and tubes were kept on ice. Taken together, these steps reduced the amount of protein degradation caused by endogenous cellular proteases.

Cells were lysed in radioimmunoprecipitation (RIPA) buffer containing 50 mM Tris-HCl, 150 mM NaCl, 1 mM EDTA, 1 mM EGTA, 1 % (v/v/) nonidet P-40 (Igepal CA-360) detergent, 0.1 % (w/v) Na-deoxycholate, and 0.1 % SDS. Once prepared, this buffer could be stored at 4 °C until required. Immediately prior to use, 2 mM Na-orthovanadate, 20 mM Na-pyrophosphate, and 1 mM PMSF were added. To this, one tablet of 'Complete' Mini EDTA-free protease inhibitor cocktail was added for every 10 ml of lysis buffer prepared. This complete lysis buffer was kept on ice during the preparation of the cell lysates and was not stored long-term.

Monolayer cultures were grown to confluency in 60 mm dishes and washed in warm PBS, followed by ice-cold PBS. When required, 500 µl lysis buffer was pipetted into each dish. Cells were quickly scraped and collected in a 1.5 ml tube. A 19 G needle and syringe was used to create shearing forces as the cells were drawn up and down five times through the needle. Lysates were then left on ice for 30 min with constant agitation before the detergent-insoluble cellular fraction was pelleted by centrifugation for 10 min at 13,000 rpm and 4 °C. The supernatant was subsequently transferred to a fresh tube and assayed for protein concentration using the Bradford assay (see *Section 2.4.2*). Lysates were batched out and frozen at 4 °C for use within a week, or at 20 °C for longer-term storage.

### 2.4.2 Bradford assay

All protein quantifications in this thesis were performed using the 'Bio-Rad Protein Assay Kit' (Bio-Rad, Hemel Hempstead, UK). This assay is based on Marion M Bradford's observation that there is a shift from 465 nm to 595 nm of the acidic solution of Coomassie Brilliant Blue G-250 as a result of its binding to proteins [203]. It was established by Spector that a dye-albumin solution had a constant extinction coefficient over a 10-fold concentration range [204]. Consequently, Beer's Law (wherein absorbance is proportional to the product of molar absorptivity, light path length and concentration of the compound in solution) has been applied for accurate quantification of protein concentration having selected an appropriate ratio of dye volume to sample concentration. This assay was used for quantification of both cell lysate protein extracts and antibodies used in other assays.

A standard curve ranged from 0-20 $\mu$g protein/50 $\mu$l was used for every assay. This was performed by triplicate dilutions of an appropriate protein standard, usually bovine serum albumin (BSA), or immunoglobulin G (IgG) for antibody quantification. These were prepared in 0.1 mM NaOH to a final volume of 50 $\mu$l. Triplicates of the unknown samples were also diluted in 50 $\mu$l of distilled water. The standards and the unknown samples were added to appropriate wells of a 96-well plate. To each well, 250 $\mu$l of freshly diluted Bio-Rad dye reagent (final concentration 20%, v/v) was added. After 10 min incubation at room temperature, the $OD_{595}$ was measured using a Dynex plate-reader (Dynex Technologies, West Sussex, UK). The concentration of the standards versus their $OD_{595nm}$ were plotted, and the test sample concentrations were determined from this standard curve.

### 2.4.3 Polyacrylamide gel electrophoresis (PAGE)

To analyse the protein content of a complex mix of proteins, lysates had to be fractionated according to size. Most commonly, this is achieved through the use of sodium dodecyl sulphate-polyacrylamide gel electrophoresis (SDS-PAGE). However, in this thesis, an alternative method was utilised, based on the NuPage gel system developed by Invitrogen (Paisley, UK). Essentially, this method is based on identical principals to SDS-PAGE, but lithium dodecyl sulphate (LDS) is used instead of SDS as a denaturing agent. Additionally, fractionation can occur at a faster rate and the gels have a greater storage time. PAGE requires only microgram amounts of protein and the method can be performed quickly and simply.

The eventual goal of PAGE is the separation of polypeptides within a complex mixture according to molecular size. The buffer system used contains the ionic detergent LDS, which dissociates all the proteins within the mixture into their individual polypeptide subunits. When proteins are heated to 70 °C in the presence of excess LDS and a reducing agent [β-mercaptoethanol or dithiothreitol (DTT)], the proteins become denatured and bind LDS in a constant LDS:weight ratio (1.4:1). This results in every polypeptide having a constant negative charge per mass unit since intrinsic charges of the polypeptide become insignificant. During electrophoresis, the LDS-polypeptide complexes migrate towards the anode. Owing to the molecular-sieving properties of the gel, their mobilities are inversely proportional to the $\log_{10}$ of their molecular weights. Sample protein molecular weights can therefore be estimated if standard proteins of known molecular weight are applied to the same gel.

Polyacrylamide gels are formed as a result of acrylamide monomer polymerisation into long chains, which then become cross-linked by compounds such as N,N'-methylenebisacrylamide (bisacrylamide). The polymerisation reaction is initiated by ammonium persulphate and accelerated by N,N,N',N'-tetramethylethylenediamine (TEMED). TEMED acts by catalysing the formation of free radicals from persulphate, which then initiate polymerisation. The effective linear range of polypeptide separation of polyacrylamide gels is greatly influenced by the percentage acrylamide in the polymerisation mixture and the amount of crosslinking, such that smaller proteins can be separated as the acrylamide concentrations is increased. The cross-links created by bisacrylamide not only provide the gel with rigidity, but form pores through which the LDS-polypeptide complexes pass. As the bisacrylamide:acrylamide ratio increases, the size of these pores decrease. A ratio of 1:29 is most commonly used, which generates a gel capable of resolving polypeptides that differ in molecular weight by as little as 3 %.

To obtain a higher resolution of polypeptide separation from a large, dilute sample applied to the gel, a discontinuous gel system is used. This system utilises both stacking and resolving gel layers that differ in salt concentration, pH, acrylamide concentration or a combination of these. The sample is applied to a stacking gel with high porosity [usually 4 % (w/v) acrylamide], which serves to concentrate the LDS-polypeptide complexes into an extremely narrow zone (or stack) before they enter resolving layer of the gel. This resolving gel has a larger percentage of acrylamide, and therefore has

greater molecular-sieving properties, allowing separation of complexes into sharp polypeptide bands according to their molecular weight.

Gradient polyacrylamide gels, with increasing acrylamide concentration through the resolving gel, are now extensively used. There are a number of advantages to using gradient gels, over single percentage gels; gradient gels resolve proteins covering a wide range of molecular weights on a single gel and also promote sharpening of protein bands during migration. The LDS-polypeptide complexes migrate through the pores until the decreasing pore sizes impede their progress.

In this thesis, the NuPage gel electrophoresis technique was used throughout to fractionate a complex protein mixture before Western blotting (see *Section 2.4.4*). All gels and buffers were purchased from Invitrogen. Throughout, pre-cast 4-12 % gradient Bis-Tris gels were used. This gel provided a resolving capability comparable to a 4-20 % Tris-glycine gels, as would be used in SDS-PAGE. Gels were supplied in plastic cassettes for use in the 'Mini cell Xcell II' (Invitrogen) electrophoresis tank, and contained sodium azide preservative. Before use, the accompanying gel comb was removed from the cassette and wells washed thoroughly with 1 x running buffer to remove this preservative. Both 12-well (Invitrogen, #NP0322) and 17-well (Invitrogen, #NP0329) gels were used, dependent on the number of samples that required analysis.

#### *2.4.3.1 Electrophoresis*

Before running samples, their concentration was determined by Bradford assay (see *Section 2.4.2*) and all sample concentrations normalised by dilution with distilled water. Electrophoresis procedure followed was as per the manufacturer's instruction. Briefly, samples were mixed 3:1 with 4 x LDS sample loading buffer (Invitrogen, #NP0007) and 9:1 with 10 x sample reducing agent (Invitrogen, #NP0004) in 1.5 ml Eppendorf tubes. The lids of the samples tubes were pierced with a single perforation (to prevent pressure build-up) and placed in a heating block set to 70 °C for 5 min. Following this, tubes were gently centrifuged in a desktop centrifuge to collect any material that may have condensed on the inner surfaces of the tube. MagicMark XP Western protein standard (Invitrogen, #LC5602) was used, which provided a broad range molecular weight marker (20-200 kDa), and was ready to use without the need for denaturation or heating. Sample and marker were loaded on the gel: 20 µl of sample and 2 µl of marker on a 12-well gel; 10 µl sample and 1 µl marker on a 17-well gel. After loading the electrophoresis chamber

was filled with 1 x MES running buffer (Invitrogen, #NP0002) containing 0.25% antioxidant solution (Invitrogen, #NP0005). Gels were run in the 'Mini-cell Xcell II' gel tank at 200 V for 35 min. Following this, the gel was removed from its cassette and then subjected to either Coomassie staining *(Section 2.4.3.5)*, or Western blotting *(Section 2.4.4)*.

### *2.4.3.2 Coomassie staining of polyacrylamide gels*

Protein bands on gels can be detected using an easily visualised reagent that reacts with any protein irrespective of biological activity. The most simple and most commonly used technique is Coomassie blue staining, which has a sensitivity of 0.1-0.5 μg protein per band. This method was used to detect the purity of proteins that had been isolated using affinity chromatography. Following polypeptide separation by PAGE, the gel was transferred to a container holding about 50 ml of Coomassie stain: 0.25 % (w/v) Coomassie brilliant blue R-250, 50 % (v/v) methanol and 10 % (v/v) glacial acetic acid. Staining took place at room temperature over 30 min with shaking. Following gel staining, excess stain was removed by destaining in successive volumes of destain: 30 % (v/v) methanol and 10 % (v/v) glacial acetic acid. The destained gel was then washed and stored in distilled water for visualisation.

### 2.4.4 Western blotting

Antibodies have a crucial role to play in the specific detection of small quantities of antigen within a complex mixture of proteins. Two immunodetection methods were used in this thesis: Western blotting and immunoprecipitation (see *Section 2.4.6*). Western blotting is a method that involves the fractionation of antigens from a complex mixture of proteins by electrophoresis, which are then probed and labelled using specific antibodies. The distinction between this and immunoprecipitation (IP) is that in IP the lysate is enriched for a particular target antigen before application on a gel.

In both instances, proteins are separated by size on a gel and then transferred to a nitrocellulose membrane. On this membrane, protein binding sites are blocked before exposure to primary antibody against the target antigen. This reduces the amount of non-specific binding of the primary antibody to the membrane. Unbound primary antibody is washed off. A secondary antibody, which has been conjugated with horseradish peroxidase (HRP), is applied and directed against the primary antibody (i.e. an anti-IgG antibody). After removing unbound secondary antibody, chemiluminescence is used to visualise the antigens. Luminescence describes the emission of light resulting from the release of energy from a substance in an excited state. In chemiluminescence, the excitation results from a chemical reaction. The ECL detection system (Amersham Biosciences) involves the oxidation of luminol by HRP in the presence of chemical enhancers, such as phenols. The light emitted is at a wavelength of 428 nm and can be detected by a short exposure to blue-light sensitive autoradiography film. The Western blotting procedure is schematically summarised in *Figure 2.4.1*.

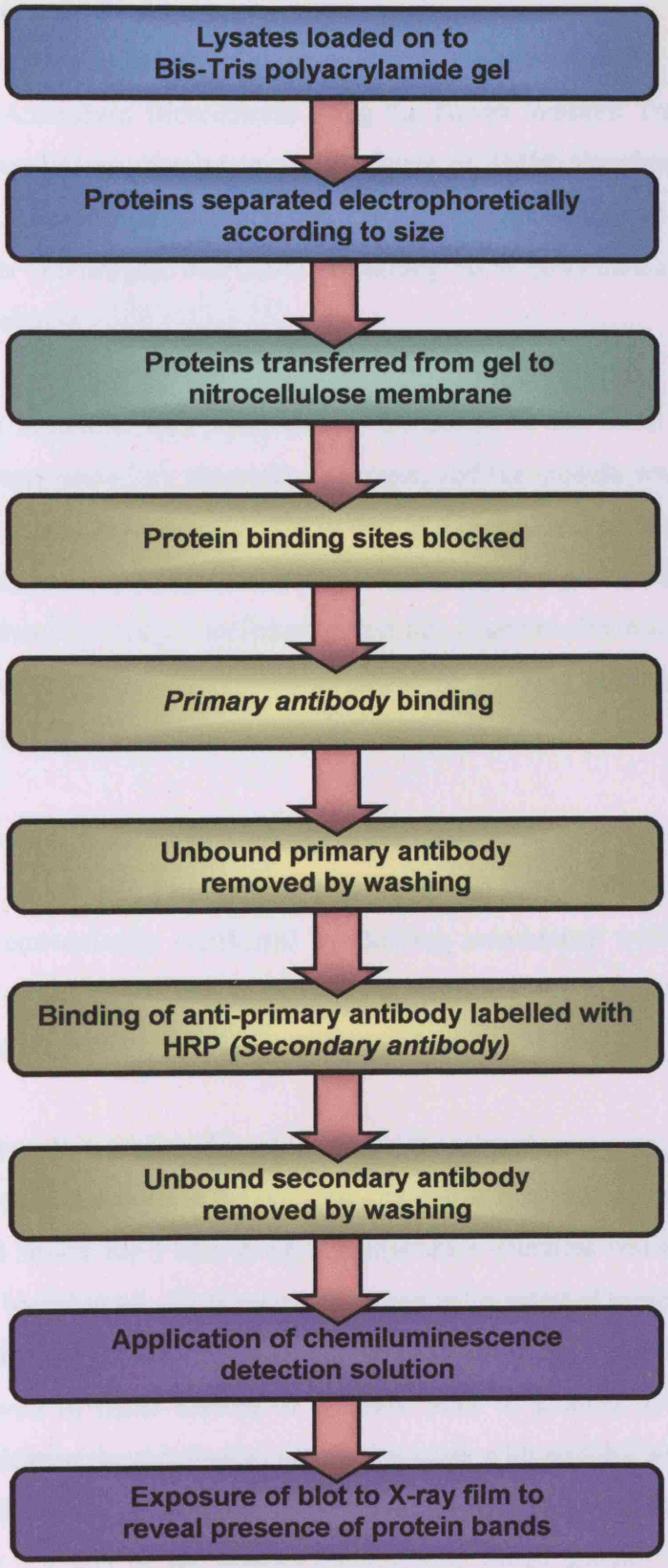


**Figure 2.4.1 Schematic representation of the Western blot procedure**

*A chart depicting the stages of a complete Western blot, from sample being loaded on the gel, sample transfer, probing with primary and secondary antibodies, and finally development of by exposure to autoradiography film.*

### *2.4.4.1 Sample transfer*

Proteins were transferred from polyacrylamide gels to Hybond ECL nitrocellulose membranes (Amersham Biosciences) using the Novex Western Transfer Apparatus. A piece of nitrocellulose membrane and 2 sheets of 3MM absorbent paper (Whatman, Maidstone, UK) were cut to the correct gel size and pre-soaked in transfer buffer: 1 x transfer buffer (Invitrogen, #NP0006) containing 10 % (v/v) methanol and 0.1 % (v/v) antioxidant solution.

This transfer sandwich was positioned in the centre of the Xcell II Blotting Module (Invitrogen) surrounded by pre-soaked sponges, and the module was filled with transfer buffer (formulation listed above). Illustrated in *Figure 2.4.2* is the composition of the blotting chamber as it would have been setup for a single gel transfer, although up to 2 gels can be simultaneously transferred within this chamber. Deionised water was poured around the transfer block to prevent overheating. Blotting occurred over 90 min at a constant current of 125 mA.

### *2.4.4.2 Ponceau S staining to confirm sample transfer*

The transfer of samples from polyacrylamide gel to nitrocellulose membrane could be rapidly and conveniently confirmed by staining membranes with Ponceau S (Sigma, #P7170) red dye solution. This is a reversible staining solution that will stain any protein bands present on the membrane.

Following sample transfer, The membrane was placed in a tray and a few drops of Ponceau S solution added. After ensuring the whole blot was covered, it was incubated on an orbital shaker for 1 min at room temperature. Distilled water was used to destain and remove background, allowing visualisation of transferred protein on the membrane. This was performed routinely during the Western blotting procedure to confirm protein transfer as well as equal loading of samples, prior to probing by immunoblotting. To completely destain the membrane, repeated washes with distilled water were performed. Further confirmation of sample transfer could be achieved by Coomassie blue staining (see *Section 2.4.3.5*) of the polyacrylamide gel, which should reveal a much lower protein content (if any) compared to that before transfer.

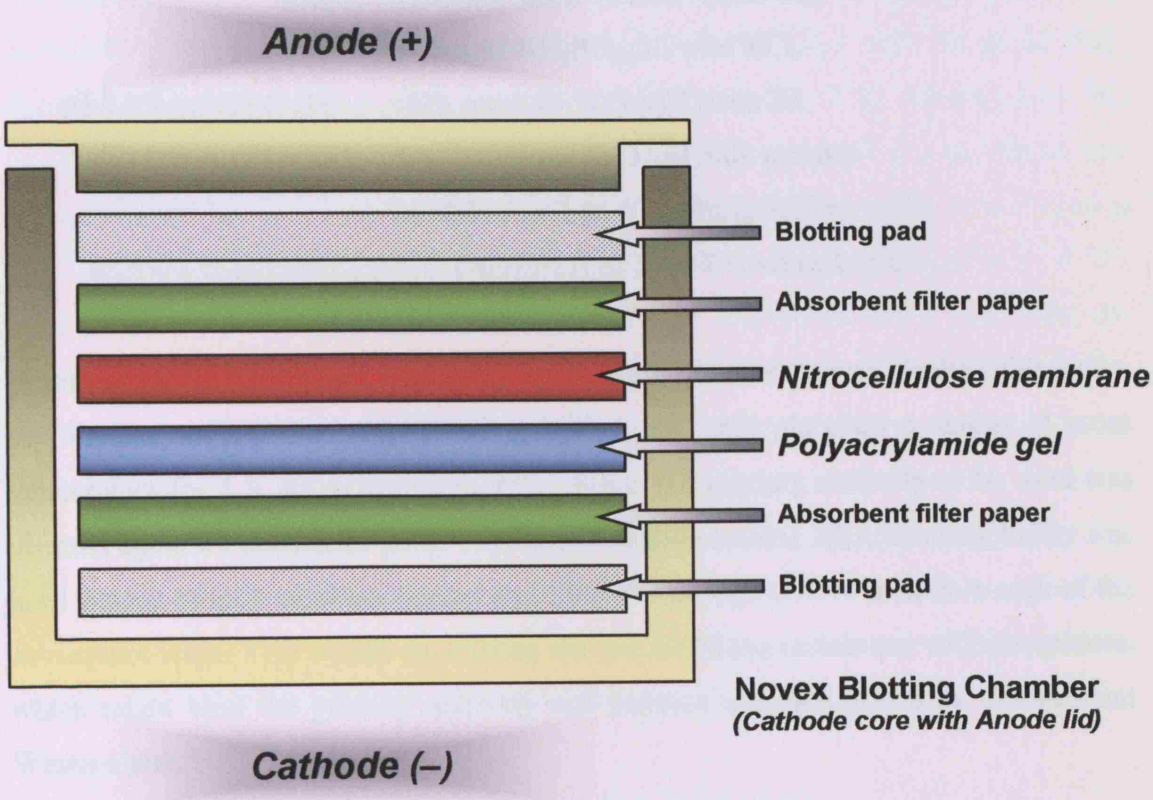


**Figure 2.4.2 Schematic representation of Western blot transfer chamber**

*The blotting chamber is composed of a cathode core with an anode lid, which when assembled creates an impermeable case around the central contents of the chamber. Within, a sandwich is formed by filter papers, the polyacrylamide gel and the nitrocellulose membrane, on to which the electrophoresed proteins are transferred. Surrounding this sandwich are layers of foam blotting pads. All components of the blotting sandwich were pre-soaked in transfer buffer containing 10 % methanol.*

### 2.4.5 Immunoblotting

To immunoblot the nitrocellulose membrane, the following solutions were required:

*Tris buffered saline (TBS)* ..... 10 mM Tris-HCl, pH 7.5 and 150 mM NaCl.
*TBS-T washing buffer* ..... TBS and 0.05 % (v/v) Tween 20.
*PBS* ..... 138 mM NaCl, 10 mM $Na_2HPO_4$,
1.75 mM $KH_2PO_4$, 2.7 mM KCl.
*PBS-T washing buffer* ..... PBS and 0.05 % (v/v) Tween 20.
*Milk blocking buffer* ..... 5 % (w/v) non-fat dried milk powder
in PBS-T or TBS-T washing buffer.
*BSA blocking buffer* ..... 5 % (w/v) BSA in TBS-T washing buffer.

Before exposing membranes to primary antibody, the membrane was blocked. Generally, this method utilised the milk blocking buffer, and took place on a shaker at room temperature for 1 h, or overnight at 4 °C. When the primary antibody to be used was directed against a phosphate group (e.g. anti-phosphotyrosine), BSA blocking buffer was used instead of milk blocking buffer, and TBS-T washing buffer was used in each of the subsequent steps. This avoids incubating the nitrocellulose membrane with phosphates, which might bind the primary antibody and increase the background of the resultant Western blot.

Primary antibodies were optimally diluted in BSA/milk blocking buffer or PBS-T washing buffer and incubated with the membrane on a shaker, either overnight at 4 °C or 1 h at room temperature. The membrane was then thoroughly washed 3 x 10 min with wash buffer. Secondary antibodies were diluted in either PBS-T or TBS-T washing buffers and incubated with the membrane for 1 h at room temperature. After repeating the washing steps, the membrane was visualised using an enhanced chemiluminescence (ECL) substrate, according to the manufacturer's instructions (Amersham Biosciences). The blot was secured in a film cassette and briefly exposed to X-ray film (Hyperfilm ECL, Amersham Biosciences).

### 2.4.6 Immunoprecipitation

Immunoprecipitation involves the specific removal of an antigen from a complex mixture of proteins by an antibody. Following antibody/antigen complex formation, the antibody binds to a matrix and becomes immobilised, thereby separating the immune complex

from the protein mixture. Immunoprecipitation was achieved using Protein A sepharose beads (Sigma). A 50 % slurry was used throughout, which was prepared by diluting a given volume of Protein A in an equivalent volume of PBS, which is henceforth termed PAS.

For basic immunoprecipitation reactions, 1 mg/ml cell lysates (see *Section 2.4.1*) were subjected to pre-clearing. This involved incubating cell lysates with 50 µl of PAS. Samples were incubated on a rotating wheel for at least 1 h at 4 °C. Subsequently, the beads were isolated from the lysate and discarded, which removed any molecules that had a high non-specific binding activity. The primary antibody was added to the lysate at a 1:100 dilution and samples incubated overnight on a rotating wheel h at 4 °C. Following immune complex formation, 25 µl of PAS was added to the lysate and the antibody/antigen complexes allowed to bind to this matrix during a 3 h incubation on a rotating wheel at 4 °C. Bound immune complexes were separated from the rest of the cell lysate proteins by centrifugation and then subjected to two washing steps with 500 µl of lysis buffer (see *Section 2.4.1*). The immunoprecipitates were resuspended in 50 µl 1 x LDS sample loading buffer and 5 µl reducing agent. After heating to 70 °C for 5 min, the immunoprecipitates were loaded on to a 4-12 % Bis-Tris gradient gel and the standard Western blotting protocol followed (see *Section 2.4.4*)

### 2.4.7 Stripping and re-probing the nitrocellulose membrane

Membranes were sometimes re-probed in order to visualise different antigens on the same blot. This required the blots to be stripped of all antibody content and targeted again with new antibody. A stripping buffer was prepared which contained 7.6 g Tris-base, 20 % (w/v) SDS and 7.0 ml β-mercaptoethanol, made up in 100 ml distilled water and pH adjusted to 6.8. Following the first immunodetection, blots were washed 3 x 10 min with TBS-T washing buffer to remove any ECL solution. Membranes were then incubated in stripping buffer for 30 min at 50 °C. Following this, blots were washed a further 3 x 10 min in TBS-T wash buffer, blocked and subjected to a second round of immunodetection according to the standard protocol detailed in *Section 2.4.4*.

## 2.5 ENZYME-LINKED IMMUNOSORBENT ASSAY (ELISA) FOR MEASUREMENT OF apoE CONCENTRATION

One of the eventual objectives of this project is to investigate the physiological effects of exposing human brain derived cells to apoE. To this end, recombinant CHO cells (described in *Section 2.2.1*) were cultured that secreted all three apoE isoforms. Media collections were performed with these cells, with the culture medium enriched with secreted apoE. Following this, it was necessary to develop a method for measuring the concentration of apoE in this conditioned medium. This was because it was essential to know the concentration of apoE used to incubate target cells with, and to ensure that variations between the different isoforms were normalised and concentrations remained consistent between experiments. There are potentially a number of methodologies available to achieve this, including radioimmunoassay [205], immunonephelometry [206,207] and radial immunodiffusion.

Antibodies raised against apoE are now commonly available and can be supplied from a range of companies. Using these antibodies, it is possible to develop an enzyme-linked immunosorbent assay (ELISA) that can be used to accurately and reliably measure the concentration of apoE in serum [208,209,210]. This is a largely cost-efficient method that is relatively simple to setup and can be used to measure a large number of samples during a single experiment. An ELISA had previously been developed in the laboratory and had been successfully applied in a number of studies [211,195,212,213]. However, the capture antibody and apoE standards utilised for this assay were no longer available. Therefore, investigation was required to determine suitable replacements for these reagents.

Within the area of ELISA, there are a number of distinct approaches that can be followed. These include direct and in-direct assays, sandwich and competitive reactions. Furthermore, the enzymatic detection method can be attuned to specific experimental methods. The method developed in this instance was a direct sandwich ELISA (see *Figure 2.5.1*). This utilises two separate antibodies, both against the target antigen, in this case apoE. The principle of this technique is to affix a capture antibody to a solid phase, which in this instance is the plastic surface of a 96-well plate. The sample is applied to this pre-coated membrane and an antigen-antibody interaction occurs. Following removal of unbound sample, a detection antibody is applied, which also interacts with antigen.

Thus, a sandwich is formed comprised of antibody–antigen–antibody. A further wash is performed to remove any unbound detection antibody. For measurement, the detection antibody is conjugated to an enzyme that is active when exposed to its substrate. In this instance, horseradish peroxidase (HRP) was used, which reacts with it substrate: 3, 3', 5, 5'-tetramethylbenzidine (TMB) substrate. The reaction of HRP with TMB results in a visible colour change in each well such that the solution shifts from clear to blue. The reaction is halted using sulphuric acid ($H_2SO_4$), which results in another colour change from blue to yellow. The intensity of this colour is directly proportional to the concentration of the target molecule.

### 2.5.1 General ELISA protocol

As this was a revision of an existing protocol, the essential framework of the assay was already in place, with only two of the reagents requiring re-assessment. The assay required the use of three buffer solutions:

*Blocking Buffer*..... 50 mM Tris.HCl (pH 7.4), 150 mM NaCl, 1 mM $MgCl_2$.
*Assay Buffer*..... 50 mM Tris.HCl (pH 7.4), 150 mM NaCl,
0.01 % (v/v) Tween-40, 0.05 % (w/v) gamma-globulin.
*Washing Buffer*..... 10 mM Tris.HCl (pH 7.4), 150 mM NaCl,
0.05 % (w/v) Tween-20.

All buffers were stored at 4 °C for up to a month. Prior to use in the ELISA, blocking buffer and assay buffer were supplemented with 1 % (w/v) and 0.5 % (w/v) bovine serum albumin (BSA) (Sigma) respectively. These buffers would then be filtered through 0.22 μm vacuum filters (Corning). Following addition of BSA, the buffers remain fresh for one week when kept at 4 °C.

With a multi-channel pipette (Anachem), a 96-well Nunc Maxisorp immunoassay microtitre plate (VWR International) was coated with 100 μl per well polyclonal goat anti-human apoE (Diasorin, US) *capture* antibody (at 2.5 μg/ml in PBS, pH 7.4) and left covered overnight at 4 °C. At each step of the assay, plates were covered securely with sealing tapes. Moreover, incubation steps were performed at room temperature (unless otherwise stated) on an orbital shaker. Washing steps were repeated using a programmed Dynex plate washer (Dynex Technologies, West Sussex, UK) set to wash each well five times sequentially with 300 μl wash buffer per well at each step. Following an overnight

incubation, excess capture antibody was decanted from the wells and 350 μl/well of blocking buffer was added to block non-specific binding sites on the plastic solid phase. After 1 h incubation at 37 °C, the plates were washed.

The plates were then incubated for 1 h at room temperature with 50 μl/well of samples and standards, which were added in triplicate and diluted as required in assay buffer. The standard used was a calibrated serum standard (Technoclone, Surrey, UK) that had a stock apoE concentration of 43 μg/ml. This was diluted using assay buffer into standards ranging from 10 ng/50 μl (≡ 0.2 μg/ml) to 1 ng/50 μl (≡ 0.02 μg/ml) apoE concentration. In addition to standards and samples, a buffer-only control was applied that would define the background signal when no known apoE was present in the reaction. After washing the plates, 50 μl biotinylated goat anti-human apoE (Biogenesis) *detection* antibody (at 1 μg/ml in assay buffer plus 1% goat serum) was added to each well. The plates were incubated for 1 h at room temperature

Following another wash step, 100 μl of streptavidin–horseradish peroxidase (S-HRP) conjugate (diluted 1:2,000 in assay buffer) was added to each well. After 30 min incubation at room temperature the plates were washed as before. ApoE quantification was determined by adding 100 μl/well of freshly prepared TMB substrate: equal volumes of 0.004 % (v/v) $H_2O_2$ (substrate) and TMB (dye). The colour reaction (from colourless to blue) was allowed to proceed for exactly 10 min with the plates gently shaken. The reaction was stopped by the addition of 100 μl/well of 2 M $H_2SO_4$. The absorbance at 450 nm ($OD_{450nm}$) was immediately measured using a Dynex microplate reader (Dynex Technologies, West Sussex, UK).

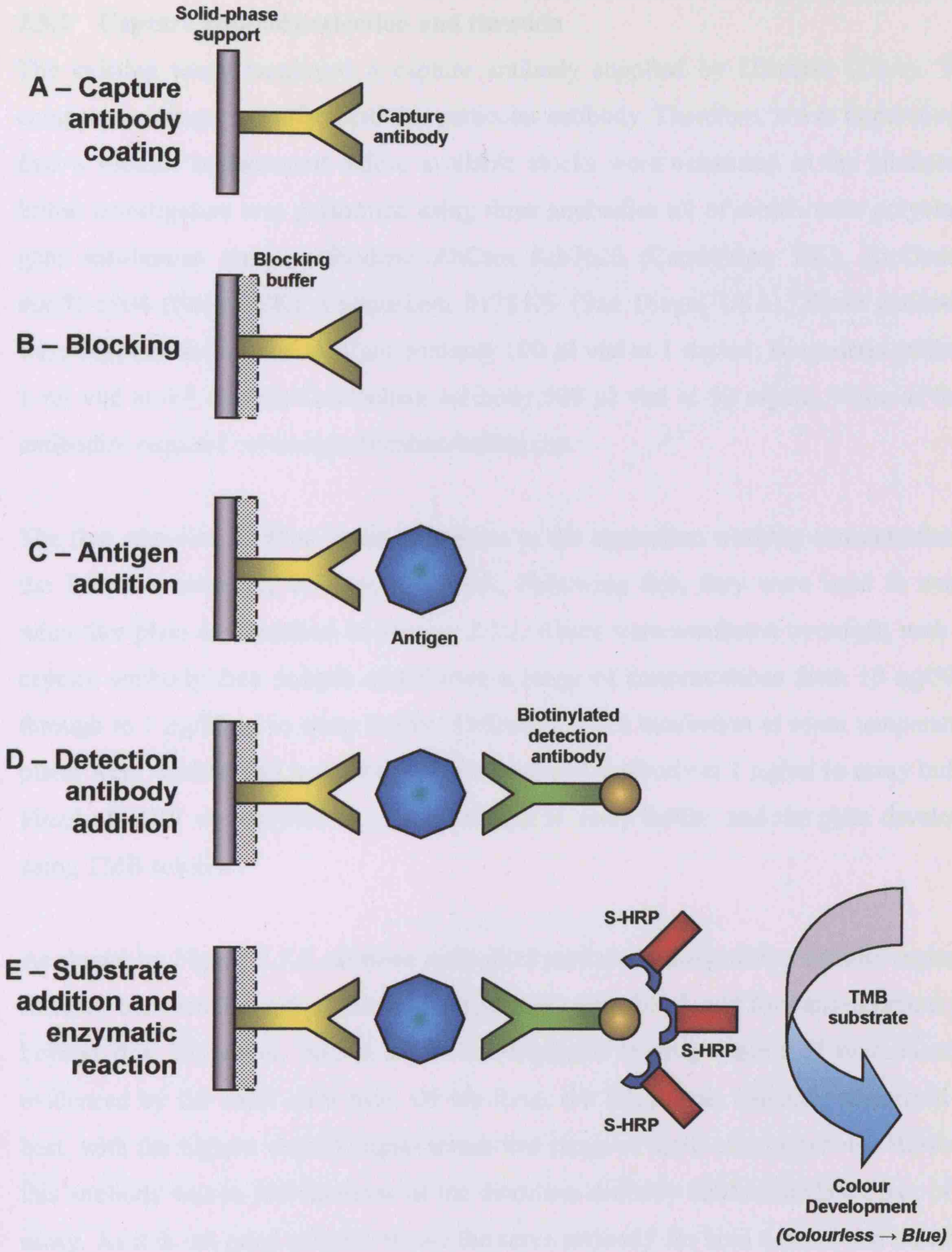


**Figure 2.5.1 Schematic representation of the stages of the direct sandwich ELISA.**

*(A) Capture antibody attached to solid phase (96-well plate surface).*

*(B) Excess antibody washed off and blocking buffer applied.*

*(C) Excess blocking buffer washed off and antigen (samples and standards) applied.*

*(D) Excess antigen washed off and biotinylated detection antibody added.*

*(E) Excess antibody washed off and streptavidin-HRP (S-HRP) added. Enzymatic reaction of HRP achieved by the addition of TMB substrate, resulting in colour development. Enzymatic reaction stopped by addition of 2 M $H_2SO_4$.*

### 2.5.2 Capture antibody selection and titration

The existing assay employed a capture antibody supplied by Diasorin (USA). This company no longer manufactured this particular antibody. Therefore, it was imperative to find a suitable replacement before available stocks were exhausted in the laboratory. Initial investigation was performed using three antibodies all of which were polyclonal goat anti-human apoE antibodies: AbCam #ab7620 (Cambridge, UK), BioGenesis #0650-1904 (Poole, UK), Calbiochem #178479 (San Diego, USA). These antibodies were supplied as follows: AbCam antibody 100 $\mu$l vial at 1 mg/ml; Biogenesis antibody 1 ml vial at 6.8 mg/ml; Calbiochem antibody 500 $\mu$l vial at 92 mg/ml. None of these antibodies required column purification before use.

The first step was to dilute these antibodies to the equivalent working concentration of the Diasorin antibody, 2.5 $\mu$g/ml in PBS. Following this, they were used to coat a microtitre plate as described in *Section 2.5.1*. Plates were incubated overnight with the capture antibody then antigen added over a range of concentrations from 10 ng/50 $\mu$l through to 1 ng/50 $\mu$l in assay buffer. Following a 1 h incubation at room temperature, plates were washed and wells loaded with detection antibody at 1 $\mu$g/ml in assay buffer. Finally S-HRP was applied at 1:1,000 diluted in assay buffer, and the plate developed using TMB solution.

As shown by *Figure 2.5.2*, all three antibodies performed well, with a definite region of linearity between 0 ng/50 $\mu$l (blank reading) and ~6 ng/50 $\mu$l, and for concentrations just beyond this. Moreover, results across the triplicate reading were well reproduced as evidenced by the short error bars. Of the three, the Biogenesis antibody performed the best, with the highest overall signal across this range of apoE concentrations. However, this antibody was in fact the same as the detection antibody used in the latter part of the assay. As it is not good practice to use the same antibody for both capture and detection purposes due to the potential of unforeseeable interactions, it was decided not to use this antibody. Therefore, further efforts were focussed on the next most suitable antibody, namely that from Calbiochem.

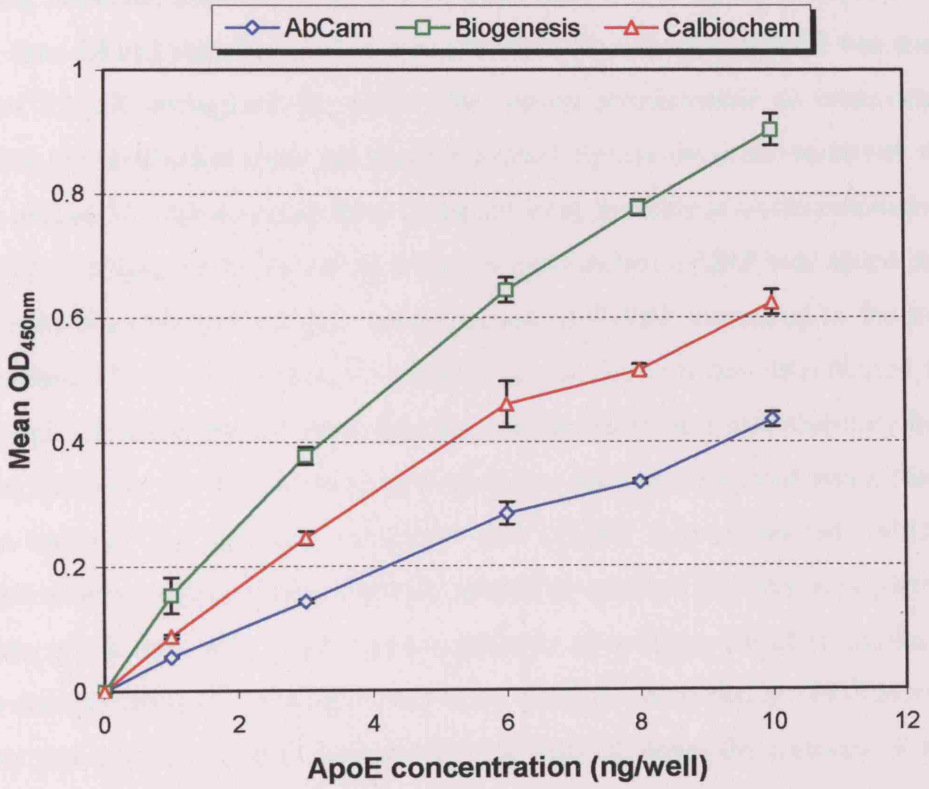


**Figure 2.5.2 Investigation of potential new capture antibodies for apoE ELISA.**
*Analysis of three polyclonal goat anti-human apoE capture antibodies used in the existing apoE ELISA protocol. Antibodies investigated were from AbCam, Biogenesis and Calbiochem. Data shown represents triplicate readings performed simultaneously on the same 96-well microtitre plate (± standard error). An assay buffer-only control set of wells was used to create a background reading, which was subtracted such that an apoE concentration of 0 ng/50 µl gave a mean $OD_{450}$ of 0.*

Before progressing to titration of the capture antibody, it was necessary to determine if there was any potential cross-reactivity between this antibody, the detection antibody and S-HRP. Cross-reactivity between the two antibodies was assayed by performing an ELISA without the addition of any antigen. The experimental conditions for this experiment were: capture antibody used to coat the plate at a concentration of 2.5 μg/ml in all wells; detection antibody used at a concentration of 2.0 μg/ml in triplicate in the first row, then diluted serially 1:2, 1:4, and 1:8 down the columns; S-HRP was used at a dilution of 1:1,000 throughout the plate. The results demonstrated no cross-reactivity between the two antibodies (data not shown). Following this the cross-reactivity with S-HRP was evaluated: capture antibody was used to coat the plate at a concentration of 2.5 μg/ml; neither antigen or the detection antibody were added; S-HRP was added at 1:500 (to investigate the effect of a higher concentration of S-HRP compared to the standard assay condition of 1:1,000 dilution) in triplicate in the first row and then diluted serially 1:2, 1:4, and 1:8 down the columns. Results demonstrated no cross-reactivity between the coating antibody and S-HRP conjugate (data not shown). In a final assay, the cross-reactivity between the detection antibody and S-HRP was evaluated, which also determined whether any detection antibody would be retained in wells after plate wash: plates were not coated with either capture antibody or antigen; detection antibody was used at a concentration of 1.0 μg/ml in all wells; S-HRP was added at 1:500 in triplicate in the first row and then diluted serially 1:2, 1:4, and 1:8 down the columns. Results of this assay confirmed no detectable signal, indicating no detection antibody being retained in the wells, which also implies no biotinylated antibody present for S-HRP to bind with (data not shown).

The titration of the capture antibody was performed by varying the concentration of the antibody used to coat the plates, but retaining all other features of the assay constant. As such, an antigen concentration of apoE was used uniformly across the plate at 6 ng/50 μl, detection antibody was used at 1.0 μg/ml, and S-HRP was maintained across the plate at 1:1,000. The concentration of capture antibody was varied from 0.25 μg/ml through to 6 μg/ml. A greater order of magnitude of varying this concentration was not necessary as it was already determined that the Diasorin capture antibody was optimal at 2.5 μg/ml. The kinetics of antibody/antigen interaction would largely be similar between the two antibodies as they are both targeting the same antigen, although there could be variation in the epitopes recognised by each antibody. In addition to an assay with antigen at 6 ng/50 μl, another set of wells was run as well, but with no antigen present (a buffer-only

control) to determine if changes in the antibody concentration would promote any cross-reactivity with the detection antibody and S-HRP.

The results of this titration experiment are shown in *Figure 2.5.3.* At a very low capture antibody concentration (0.25 – 0.5 μg/ml) the variability in the signal was too great. However, at much higher antibody concentrations (> 1.75 μg/ml) signal strength was compromised. The optimum concentration for use in the ELISA was determined to be 1.5 μg/ml: this represented the highest concentration of this antibody that could be applied before absorbance readings begin to diminish. Another titration assay was performed to confirm this particular concentration as optimal before subsequent use in the ELISA.

### 2.5.3 Detection antibody biotinylation

The detection polyclonal anti-human apoE antibody (Biogenesis, #0650-1904) was biotinylated using ECL Protein Biotinylation Module (#RPN2202) (Amersham Biosciences). This kit also contained the S-HRP (#RPN1231) used in the ELISA. Biotinylation was performed following the manufacturer's instructions. Briefly, the antibody was diluted in 40 mM bicarbonate buffer (from the kit) to give a working concentration of 1 mg/ml and a volume of 2.5 ml. To this, 100 μl biotinylation reagent was added and the solution was left to incubate for 1 h at room temperature. Meanwhile, a Sephadex G25 column was prepared by passing through 5 ml PBS containing 1 % (w/v) BSA (pH 7.5), followed by 20 ml PBS. These column washes were discarded. The biotinylated antibody solution was placed on the column and allowed to absorb into the Sephadex matrix, whilst unbound solute passed through the column. The biotinylated antibody was eluted from the column with 5 ml PBS; fractions of 500 μl were collected in 1.5 ml Eppendorf tubes.

Collected fractions were analysed spectrophotometrically to determine which fraction contained eluted antibody. These fractions were collected and the remainder discarded. A Bradford assay (see *Section 2.4.2*) was performed, using IgG standards to determine the eluted antibody concentration. The eluted biotinylated detection antibody was measured as 800 μg/ml according to this assay.

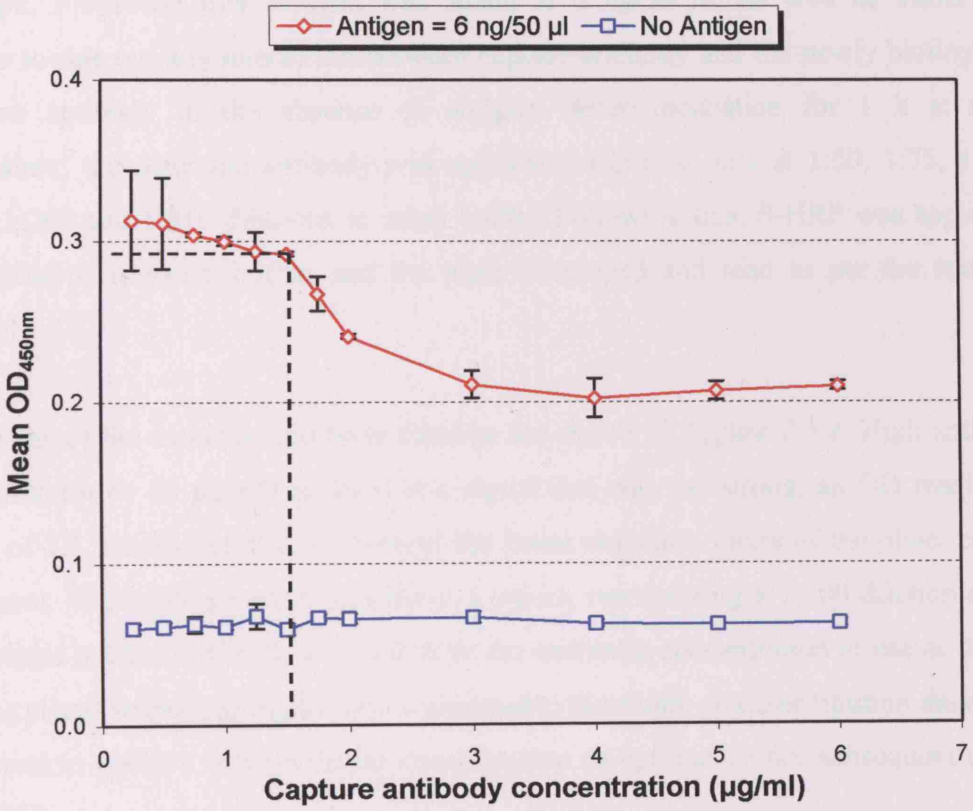


**Figure 2.5.3 Capture antibody titration.**

*The Calbiochem polyclonal goat anti-human apoE capture antibody was titrated to determine the optimum concentration for use in ELISA. Antibody concentration was varied from 0.25 µg/ml to 6 µg/ml in assay buffer. Detection antibody was maintained at 1.0 µg/ml and S-HRP used at 1:1,000 in assay buffer. Antigen was kept constant at 6 ng/50 µl apoE concentration, in addition to a set of assays performed in the absence of antigen. Each point represents triplicate readings on a plate (± standard error). The dashed line represents the optimum capture antibody concentration determined (1.5 µg/ml) and this was the concentration used in subsequent assays.*

### 2.5.4 Detection antibody titration

Having prepared fresh biotinylated detection antibody, this too had to be titrated to determine the optimum concentration for use in the ELISA. This was achieved by preparing a plate coated with capture antibody at 1.5 μg/ml per well and incubating overnight. Following this, antigen was added at 6 ng/50 μl, as well as buffer-only controls to rule out any interaction between capture antibody and the newly biotinylated detection antibody in the absence of antigen. After incubation for 1 h at room temperature, the detection antibody was applied in triplicate sets at 1:50, 1:75, 1:100, 1:150, 1:200 and 1:250 dilutions in assay buffer. Following this, S-HRP was applied at 1:100 dilution in assay buffer, and the plate developed and read as per the standard protocol.

The results of the detection antibody titration are shown in *Figure 2.5.4.* High antibody concentrations (> 10 μg/ml) resulted in a signal that was too strong: an OD reading in excess of 1.5 is considered to be beyond the linear detection limits of the plate reading equipment. The antibody concentration at 8 μg/ml, representing a 1:100 dilution of the biotinylated antibody, was determined to be the optimum concentration to use as it gave a strong signal without going beyond a reasonable threshold. Another titration assay was performed to confirm this particular concentration as optimal before subsequent use in the ELISA.

### 2.5.5 Streptavidin-HRP titration

As this was another key component in the ELISA protocol, this too was titrated. In this instance, the capture antibody was used to coat the plates at 1.5 μg/ml. The plates were loaded with antigen at 6 ng/50 μl in one set of wells and another set with buffer-only to determine if there was any interaction between S-HRP and the capture antibody (any detection antibody applied should not bind to anything and would therefore be washed off the plate). Detection antibody was applied at 8 μg/ml. Following this, S-HRP was applied at a range of dilutions in assay buffer: 1:2,000, 1:1,500, 1:1,000, 1:500, 1:250, 1:100. The rest of the protocol was performed as previously described. Altering the dilution factor of S-HRP had very little effect on the overall signal strength obtained at the end of the ELISA (data not shown). Therefore, the 1:1,000 dilution that was currently being used in the assay was maintained for all subsequent assays using the newly optimised capture antibody and detection antibody concentrations.

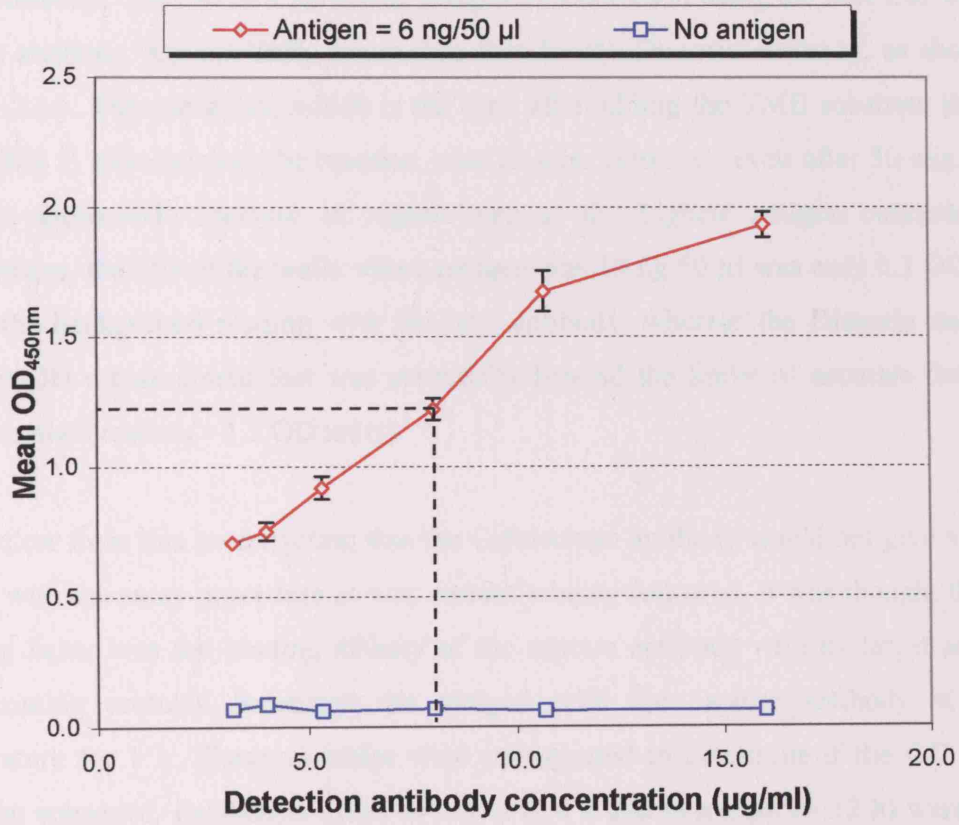


**Figure 2.5.4 Detection antibody titration.**

*The Biogenesis polyclonal goat anti-human apoE detection antibody was titrated to determine the optimum concentration for use in ELISA following biotinylation and quantification by Bradford assay. Calbiochem capture antibody was maintained across the assay at 1.5 µg/ml. Antigen used was at an apoE concentration of 6 ng/50 µl. Detection antibody was varied, from a stock concentration of 800 µg/ml, by dilutions in assay buffer ranging from 1:50 (16 µg/ml) through to 1:250 (3.2 µg/ml). S-HRP was maintained at 1:1,000 in assay buffer. In addition, a set of assays were performed in the absence of antigen. Each point represents triplicate readings on a plate (± standard error). The dashed line represents the optimum detection antibody concentration determined (8.0 µg/ml) and this was the concentration used in subsequent assays.*

### 2.5.6 Optimisation of overall ELISA protocol

Much of the success of an ELISA is reliant on the ability of the capture antibody to both coat the solid-phase suitably and also interact with antigen with high affinity and specificity. All subsequent stages in the assay can be adversely affected if this does not occur correctly. The OD at a particular antigen concentration using the new Calbiochem capture antibody was markedly lower than that for the Diasorin antibody, as shown in *Figure 2.5.5*. The end-point, which is the time after adding the TMB substrate that the 2M $H_2SO_4$ is added to halt the reaction, was 15 min. However, even after 30 min, there was no appreciable increase in signal even at the highest antigen concentration. Furthermore, the OD of the wells where antigen was 10 ng/50 $\mu$l was only 0.3 OD units above the background reading with the new antibody, whereas the Diasorin antibody gave an OD measurement that was essentially beyond the limits of accurate detection with this plate reader (> 1.5 OD units)

It was clear from this investigation that the Calbiochem antibody would not give suitable results with the assay procedure as was currently being followed. It was thought that the limiting factor was the binding affinity of the capture antibody with its target antigen. The existing protocol incubated the antigen with the capture antibody at room temperature for 1 h. These variables were investigated to determine if the OD values could be enhanced. Incubation times of 1 h, 2 h, 4 h and overnight (> 12 h) were used, with incubation temperatures of 4 °C, room temperature and 37 °C. These data are summarised in *Figure 2.5.6*. All experiments performed at 4 °C resulted in low ODs, with little or no change observable as incubation time was increased. Incubating at room temperature enhanced the OD measurements, but still were not suitably distinct from the background OD readings (data not shown). Conversely, incubating the antigen with the capture antibody at 37 °C gave a markedly higher OD measurement, even after a 2 h incubation. Leaving the samples to incubate overnight greatly enhanced this signal, and returned them to a level that was in the same order as that for the Diasorin antibody (see *Figure 2.5.6*). Therefore, the protocol for use with the Calbiochem capture antibody was modified: following incubation overnight at 4 °C, excess antibody was decanted off and, after blocking non-specific binding sites, the antigen was applied, which was incubated overnight at 37 °C. The remainder of the ELISA protocol was followed as per the general method detailed in *Section 2.5.1*.

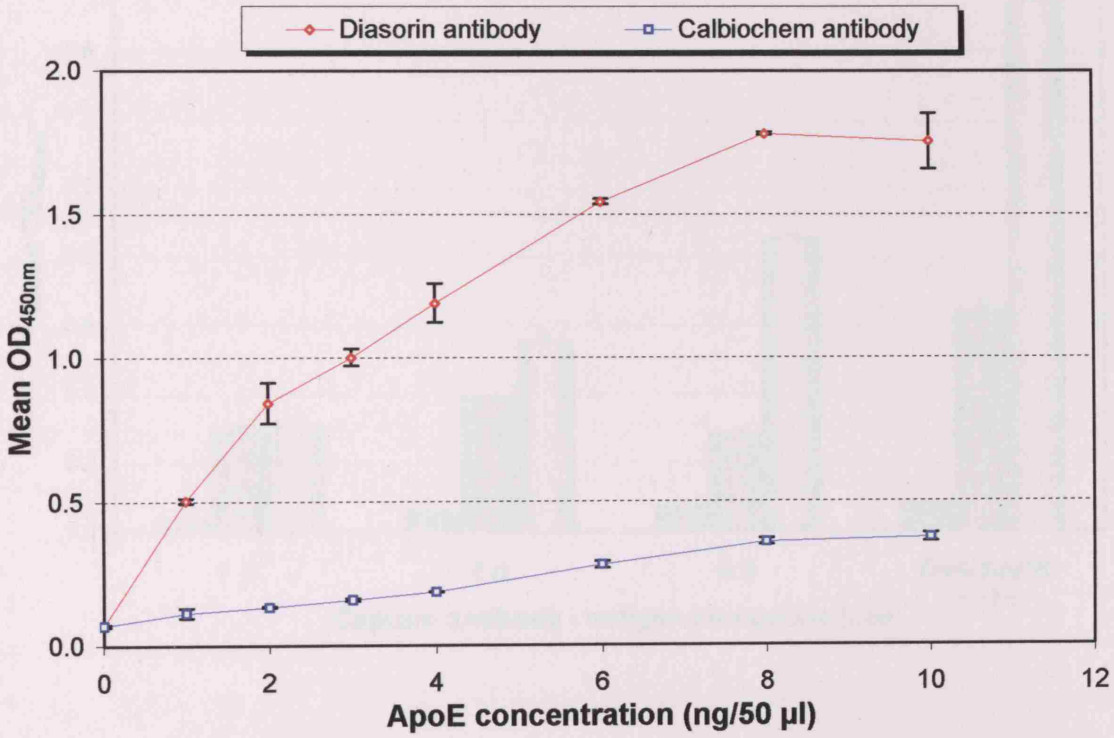


**Figure 2.5.5 Comparison of Diasorin and Calbiochem capture antibodies**

*Both capture antibodies were applied to ELISA microtitre plates at their appropriate optimal concentrations: Diasorin = 2.5 µg/ml; Calbiochem = 1.5 µg/ml. Following overnight incubation, wells were incubated with apoE serum standards for 1 hour at room temperature, then probed with detection antibody (8 µg/ml), and S-HRP 1:1,000 dilution in assay buffer. Assay endpoint was 15 min after addition of TMB substrate. Each point represents triplicate readings (± standard error).*

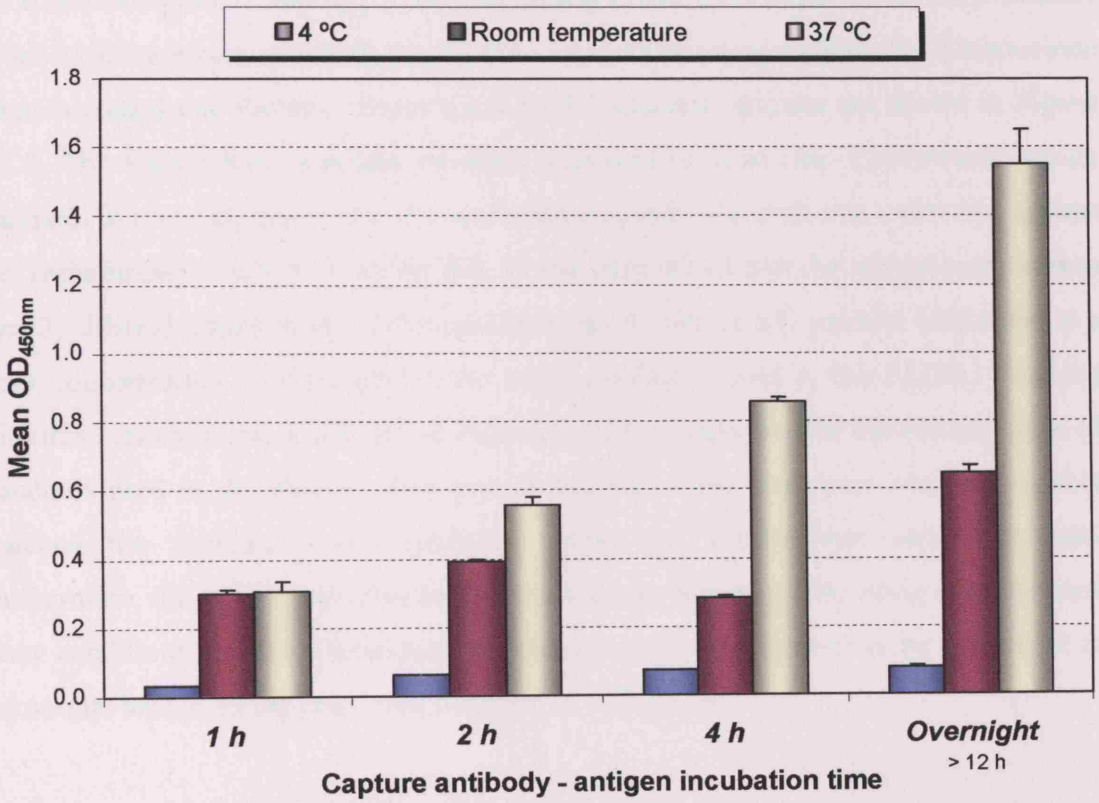


**Figure 2.5.6 Effects of incubation time and ambient temperature during antigen binding, by capture antibody on the microtitre plate**

*A microtitre plate was prepared by overnight incubation with capture antibody at 1.5 µg/ml. Following this, antigen was applied at a concentration of 8 ng/50 µl. Samples were incubated according to the different conditions investigated: incubation times of 1 h, 2 h, 4 h, and overnight (>12 h); incubation temperatures of 4 °C, room temperature, and 37 °C. Following this, detection antibody was applied at 8 µg/ml, and S-HRP 1:1,000 dilution in assay buffer. All assays were stopped 30 min after addition of TMB substrate. Data shown represent triplicate readings, with standard error displayed above each bar.*

### 2.5.7 Assessment of new apoE standard

In addition to the capture antibody, the manufacturer of the serum standard used in the current ELISA method, Technoclone, no longer supplied this reagent. As a replacement, recombinant human apoE3 from Calbiochem (#178475) was used. This was supplied at a stock concentration of 340 ng/µl, and was diluted using assay buffer in the same manner as the existing serum standard. An ELISA was performed using both the Technoclone serum standard and the new recombinant apoE3 standard. Results are shown in *Figure 2.5.7*. The Calbiochem standard deviated significantly from the Technoclone serum standard. In order to rectify this, the recombinant apoE3 standard was calibrated against the Technoclone standard. Through this, it was determined that the recombinant human apoE3, although supplied at a stock concentration of 340 µg/ml, actually functioned at a stock concentration of 170 µg/ml in the assay conditions used in this ELISA. Working with this concentration, a new set of dilutions were prepared within the normal range of standards used in the ELISA. This gave a standard curve that more comprehensively matched the standard curve generated using the Technoclone serum standard. Furthermore, the apoE concentration in human serum was measured using the optimised assay conditions and the Calbiochem standard, and was determined to be equivalent to the normal human serum apoE concentration of ~50 µg/ml.

### 2.5.8 Detection limits of ELISA with new reagents

Having established the optimum concentrations of the various reagents in the apoE ELISA, the detection limits of the assay could be established. This minimum sensitivity limit defines the lowest concentration of apoE that the assay can detect with any accuracy. This value is linked to the background OD reading of the assay. At this lower end of the ELISA scale, minor changes in colour can be amplified as significant changes in concentration. The detection limit was determined by performing an ELISA according to standard protocol: capture antibody 1.5 µg/ml in PBS; detection antibody 8 µg/ml in assay buffer; S-HRP 1:1,000 in assay buffer. However, instead of the normal range of concentrations of the standard, a much lower standard range was used: serial doubling dilution from 6.0 ng/50 µl through to 0.09 ng/50 µl. The sensitivity limit has been determined as a function of the background OD measured, and defined as 2 x the standard deviation (SD) of this measurement. From *Figure 2.5.8*, the background OD reading is 0.061, with an SD of 0.04. This gives a sensitivity limit $OD_{450nm}$ of 0.069, which is equivalent to an apoE concentration of ~0.049 ng/50 µl. Thus, the sensitivity limit of this assay is equivalent to 0.977 ng of apoE per ml of sample, or ~1 ng.

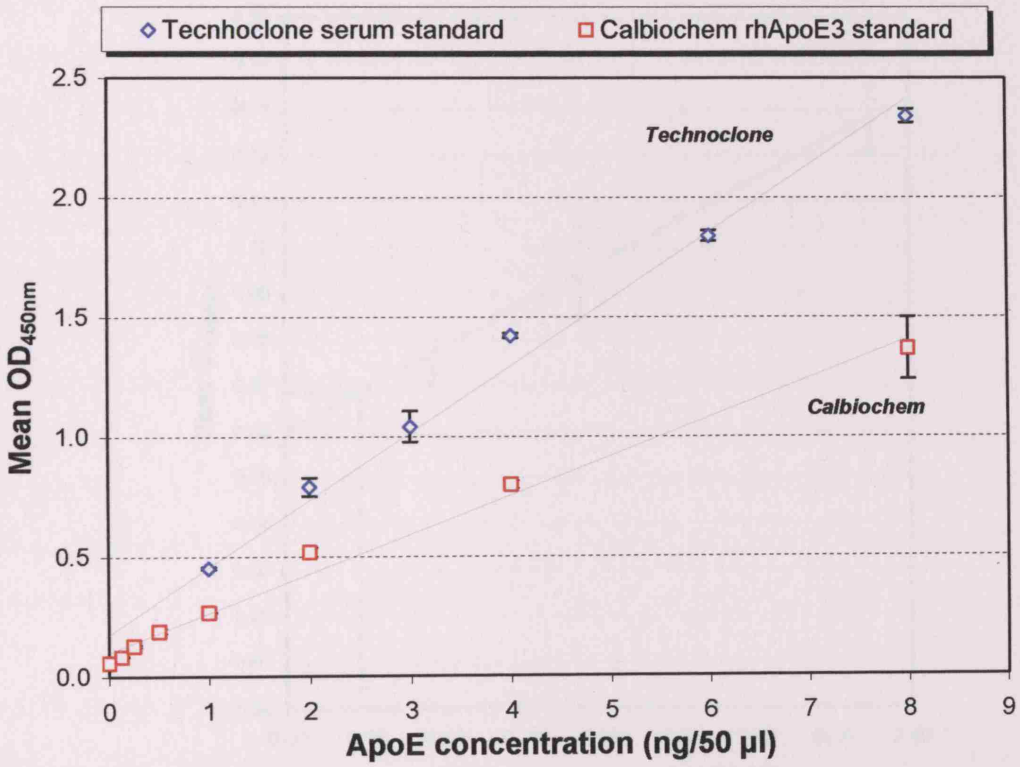


**Figure 2.5.7 Investigation of a potential new apoE standard for use in the ELISA**

*Technoclone's serum standard and Calbiochem's recombinant human apoE3 were diluted in assay buffer to give an equivalent set of standards. These were used in an ELISA in which an optimised set of conditions was used: capture antibody at 1.5 µg/ml, samples incubated overnight at 37 ºC, detection antibody at 8 µg/ml, S-HRP 1:1,000 dilution in assay buffer. Assay endpoint was 30 min after addition of TMB substrate. Each points represents triplicate readings (± standard error).*

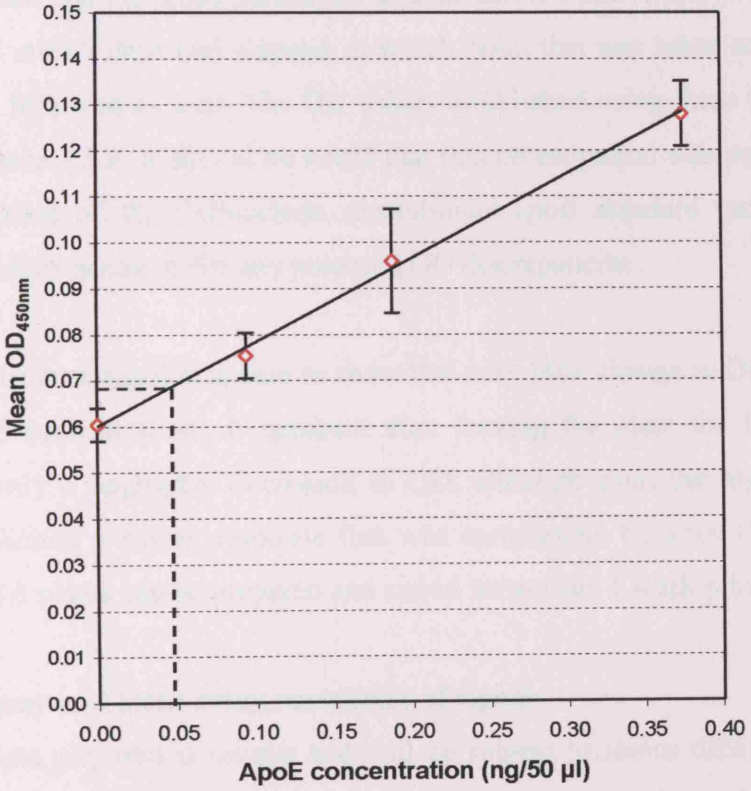


**Figure 2.5.8 Determination of detection limit of optimised apoE ELISA.**

*The assay was performed as described in* Section 2.5.11 *using newly calibrated recombinant apoE3 standards across a range from 0.03-6.0 ng/50 µl, but only up to 0.375 ng/50 µl have been plotted. Each point represents triplicate readings on a plate (± standard error). The full set of standards extending beyond the points shown follow a linear relationship between measured OD and apoE concentration, as assessed by Microsoft Excel. The sensitivity limit has been determined by the OD reading at 1.5 x OD above the background OD reading, which is 0.06 units. The detection limit is shown on the curve as a dashed line. This is equivalent to 3.4 ng apoE per ml in a sample.*

### 2.5.9 Investigating potential for an extended storage of prepared ELISA plate

It is recommended that when performing an ELISA, the microtitre plate should be prepared no more than 24 h prior to the time of initial use. However, to investigate whether this was necessarily the case, 2 plates were prepared as normal by coating wells with 1.5 μg/ml capture antibody and stored at 4°C. Following overnight incubation, one plate was taken out and a normal ELISA protocol was followed with a range of standards applied to the plate and the assay performed to conclusion. Meanwhile, the second plate remained at 4°C until 7 days had elapsed, at which point this was taken and the normal ELISA protocol followed as well. The OD values established using these two plates are displayed in *Figure 2.5.9*. It should be noted that this investigation was performed prior to the re-calibration of the Calbiochem recombinant apoE standard (as described in *Section 2.5.7*), which accounts for any potential OD discrepancies.

The results of this investigation appear to show that very little change in OD measured at equivalent apoE concentrations is apparent after leaving the plate for 1 week. There appears to be only a negligible decreased in OD, although even the highest standard concentration elicited a strong response that was comparable between the two plates. Therefore, ELISA plates can be prepared and stored for at least 1 week prior to their use.

### 2.5.10 Intra-assay and inter-assay variability of signal

Each ELISA plate prepared is unique and will be subject to minor differences in both initial preparation and use throughout the assay. However, the ability to deliver accurate results requires a degree of reproducibility and consistency between plates. To this end, an investigation was performed to determine the intra-assay and inter-assay variability on a single plate and across a range of plates, respectively. This was achieved using pooled plasma samples taken from 7 individual human donors. The plasma was diluted appropriately (usually around 1:1,000 to 1:2,000) in assay buffer and a normal ELISA protocol followed. Normally, as least one triplicate set of wells would be treated with this plasma sample. However, to determine the intra-assay variability, a single plate had 10 of its wells loaded with 50 μl/well of plasma each at different (i.e. non-sequential) positions across the plate. For inter-assay variability, plasma samples from 12 unique ELISAs were compared, each run on different plates and on different days.

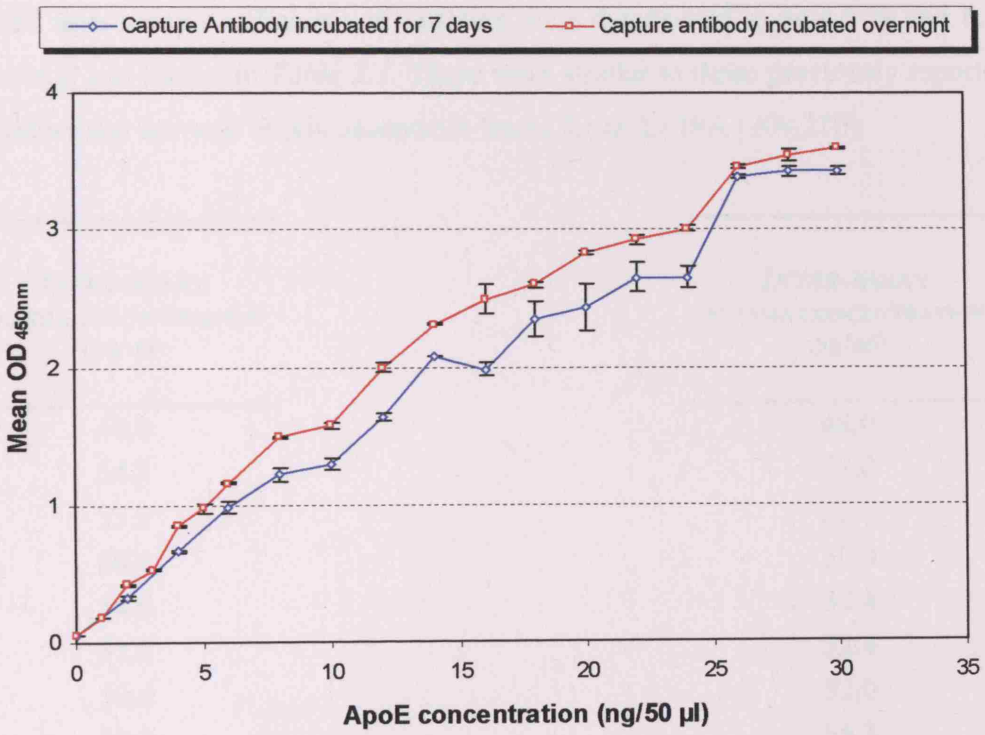


**Figure 2.5.9 Investigation of extended storage of prepared ELISA microtitre plate**

*Two microtitre plates were setup identically with wells coated with capture antibody at 1.5 µg/ml and stored at 4 ºC. Following overnight incubation, one plate was taken and a normal ELISA protocol was performed. The second plate was stored for 7 days before taking it from cold storage and a normal ELIA performed. Each point represents triplicate readings at each apoE concentration (± standard error).*

To determine the variability between these readings, the coefficients of variation (CVs) was calculated using the following equation:

$$CV = \frac{\text{Standard deviation (SD)}}{\text{Mean average}} \times 100$$

The CV values determine the degree of variation both within and between assays. The intra- and inter-assay coefficients of variation were determined to be 4.5 % and 6.1 %, respectively, and shown in *Table 2.1.* These were similar to those previously reported in the literature and are well within acceptable limits for an ELISA [209,210].

| *INTRA*-ASSAY PLASMA CONCENTRATION (μg/ml) | | *INTER*-ASSAY PLASMA CONCENTRATION (μg/ml) |
|---|---|---|
| 49.0 | | 48.0 |
| 54.3 | | 52.0 |
| 53.0 | | 52.0 |
| 60.1 | | 50.0 |
| 54.6 | | 50.4 |
| 51.1 | | 52.4 |
| 50.4 | | 52.0 |
| 57.3 | | 55.3 |
| 55.0 | | 54.2 |
| 53.0 | | 49.6 |
| — | | 48.0 |
| — | | 49.0 |
| **10** | ***n*** | **12** |
| **53.8 μg/ml** | ***AVERAGE*** | **51.1 μg/ml** |
| **3.3** | ***SD*** | **2.3** |
| **6.1 %** | ***CV*** | **4.5 %** |

**Table 2.1 Intra- and inter-assay reproducibility of apoE ELISA.**

*Pooled plasma from 7 human volunteers was diluted in assay buffer and used in a apoE ELISAs. In the first instance, a single plate contained 10 wells with this plasma, in non-sequential positions across it, used to determine the intra-assay variability. The inter-assay variability was determined by measuring samples on 12 unique plates, performed at different time. Normal ELISA protocol was followed. The CV values for intra- and inter-assay variability were calculated from the equation CV = (SD/mean) x 100.*

### 2.5.11 Summary of ELISA development

In conclusion, the apoE ELISA was re-developed using an existing protocol, but with new sources for the capture antibody, apoE standard and a modification of the actual procedure itself. Summarised below is the new ELISA protocol:

- Coat wells of a 96-well microtitre plate with 100 $\mu$l per well capture antibody (1.5 $\mu$g/ml in PBS, pH 7.4) cover securely and incubate overnight at 4 °C.
- Decant off capture antibody the following day.
- Wash 5 times with 300 $\mu$l/well washing buffer.
- Add 350 $\mu$l/well blocking buffer, cover securely and incubate plate at 37 °C for 1 h.
- Wash plate 5 times with washing buffer.
- Add 50 $\mu$l per well antigen (samples and standards) to give a range of standards (Calbiochem recombinant human apoE3; 49 $\mu$g/ml stock concentration) and samples within the limits of this standard curve. All diluted in assay buffer.
- Allow antigen to incubate (securely covered) with the capture antibody: incubate overnight at 37 °C.
- Wash plate 5 times with washing buffer
- Add 50 $\mu$l per well biotinylated detection antibody (8 $\mu$g/ml in assay buffer) supplemented with 1 % goat serum. Incubate securely covered for 1 h at room temperature with constant agitation.
- Wash plate 5 times with washing buffer.
- Add 100 $\mu$l per well S-HRP solution, diluted 1:1,000 in assay buffer. Securely cover and incubate for 30 min at room temperature with constant agitation
- Wash plate 5 times with washing buffer.
- Add 100 $\mu$l per well TMB substrate. Cover with aluminium foil and incubate at room temperature for 30 min with constant agitation
- Enzymatic reaction stopped by application of 100 $\mu$l per well 2M $H_2SO_4$.
- Plates read using a plate reader, and data entered into Microsoft Excel for analysis.

## 2.6 STATISTICAL ANALYSIS

Values in text and figures were expressed as the mean ± standard error of the mean, unless stated otherwise. Statistical differences between means were determined using Student's *t*-test and considered significant if $p<0.05$. All analyses were performed using Microsoft Excel (Microsoft Office Professional Edition, 2003).

# Chapter 3

# CHARACTERISATION OF NEURONAL CELL LINES BY QUANTITATIVE POLYMERASE CHAIN REACTION

# 3.0 CHARACTERISATION OF NEURONAL CELL LINES BY QUANTITATIVE POLYMERASE CHAIN REACTION

## 3.1 INTRODUCTION

As described in *Chapter 1*, the eventual aim of this thesis is to identify whether apoE can mediate an isoform differential effect on neuronal cell lines, including the release of nitric oxide. As a preliminary exercise, it is necessary to identify suitable cell lines that can be utilised for this purpose. This will become the model system from which all further analyses can be performed. Selection of the optimum cell line(s) will have a significant effect on the eventual investigations performed.

The cell line(s) selected must meet a selection of criteria to be considered suitable for further investigation. They must express cell surface receptors that will allow apoE to bind and undergo endocytosis. This provides the 'first-line' interface between the cells and the ligand (apoE). A number of receptor types have been investigated, including members of the LDL-receptor gene family (LDL-r, VLDL-r, LRP and apoER2) and HDL receptors (SR-BI and SR-BII). The capability of these cells to generate nitric oxide will be conferred by the presence of one or more of the NO synthesising isoenzymes, NOS. Moreover, the expression of the NOS3 regulatory kinase, PKB/Akt, was also investigated; PKB/Akt has been demonstrated to perform a vital function in the regulation of NO release, especially in low $Ca^{2+}$ conditions. Together, these various factors – *receptor binding, nitric oxide synthesis,* and *regulation of the nitric oxide response* – can be considered as essential mediating points that allow apoE to propagate a message from the cell surface to eventually modulate NO release.

A number of the receptors studied are of particular interest due to their potential for mediating a signalling function, specifically: LRP, VLDL-r, apoER2, and the SR-BII splice variant. Putatively, apoE binding to these receptors on the extracellular surface of a cell could result in the recruitment of signalling molecules intracellularly resulting in the initiation of a signalling cascade, or the modification of one. As such, investigating the expression of these receptors could be very revealing; the presence of these receptors may be indicative of particular signalling functions within neuronal cells that could be modified by apoE, whether these be related to NO release or not.

There are a number of methods available for assaying gene expression, including competitive reverse transcriptase- (RT-) PCR, conventional RT-PCR and Northern blot analysis [214,215,216]. However, in this instance, the assay method employed has been quantitative real-time PCR utilising SYBR Green I intercalating dye chemistry. This was deemed a suitable technique as it required no special probes to be synthesised, nor the need to modify existing PCR protocols. Initially, gene expression was assessed using only SH-SY5Y and CCF.STTG1 cells, largely to establish that this technique could be utilised effectively. Beyond this, expression of these genes was measured through the use of *TaqCell* plates; microtitre plates that carried cDNA from a panel of 38 different human cell lines, 12 of which were derived from the brain. This allowed a unique assessment of gene expression in multiple cell lines from a diverse range of tissue sources. Furthermore, the presence of cDNA templates of known copy number on these plates allowed the mRNA copy number of the genes under investigation to be determined using this assay method.

## 3.2 SPECIALISED MATERIALS & METHODS

### 3.2.1 Cell culture and sample preparation

In order to verify and optimise PCR procedures in this chapter, SH-SY5Y neuroblastoma and CCF.STTG1 astrocytoma cell lines were cultured according to the protocols detailed in *Section 2.2.1*. These two cell lines were selected as they were suitable representatives of the two main populations of cell types found in the brain; SH-SY5Y representing neuronal cells and CCF.STTG1 representing astrocytic cells. When cells were sub-confluent, genomic DNA and RNA were extracted, as detailed in *Section 2.3.1* (DNA) and *Section 2.3.2* (RNA). Extracted RNA was used as a template for single-stranded cDNA synthesis by reverse transcription, described in *Section 2.3.3*. The cDNA transcripts provided the template for subsequent PCR investigation (see *Section 2.3.4*).

### 3.2.2 PCR optimisation

As described in *Section 2.3.1*, PCR primers were determined using the web-based primer design application, *GeneFisher*[6], and are listed in *Table 3.1*. Primer design was based on the complete mRNA coding sequences of the target genes. Amplicons were designed to be between 100-200 bp to ensure maximum PCR efficiency for detection of products with the intercalating fluorogenic dye, SYBR Green I (see *Section 2.3.6.3*). Reactions were performed on a standard thermal cycler to ascertain the optimal annealing temperature. Once established, reactions were then performed using the real-time PCR thermal cycler (RotorGene RG3000) and reaction mixtures containing the Quantitect SYBR Green I dye (see *Section 2.3.7*), to investigate whether the primers and optimised reaction conditions could suitably measure gene expression. For reference, the expression of a housekeeping gene (β-actin) was used with 10-fold serially diluted DNA templates to give a range of concentrations from $10^0$ through to $10^{-6}$. This allowed generation of a standard curve that could then be used to determine the level of expression of the target genes. As the copy number of β-actin was not known, expression of target genes were measured relative to that of β-actin on an arbitrary scale.

### 3.2.3 Preparation of *TaqCell* plates

For complete analysis of gene expression, a human cell line and primary cell '*TaqCell*' masterplate [217,218] was prepared. The plate contained cDNA samples for 38 human primary cell and cell lines on a 96-well plate; details of these cell lines are displayed in

[6] http://bibiserv.techfak.uni-bielefeld.de/genefisher/

*Table 3.2.* Briefly, total RNA was extracted from the different cell lines for reverse transcription. Also included were two neuroblastoma cell lines, IMR-32 and SH-SY5Y, which had been differentiated into more neuron-like morphologies with extended neurites. This was achieved in IMR-32 cells by treating cell cultures for 7 days with 1 μM retinoic acid. For SH-SY5Y cells, differentiation was achieved by supplementing their growth medium for 7 days with 1 mM dibutryl cAMP, 100 ng/ml 2.5S nerve growth factor, 10 μg/ml gangliosides, and 0.5 μM sodium butyrate. Fifty micrograms of RNA from each cell line was reverse transcribed (as detailed in *Section 2.3.*3) and the cDNA diluted into 96-well plates. Upon completion, each well contained 5 μl of cDNA reverse transcribed from 50 ng total RNA from each of the different cell lines in duplicate across the 96-well plate. The prepared plates were stored at -80 °C until required for use.

### 3.2.4 Quantitative RT-PCR with *TaqCell* plates

To each well of cDNA template (5 μl), a 20 μl reaction mix was added containing 12.5 μl '2x PCR mastermix' (comprising optimal amounts of SYBR Green I, $MgCl_2$, dNTP and Taq polymerase), 1 μl of 10 μM forward primer, 1 μl of 10 μM reverse primer, and 5.5 μl water. Real-time PCR assay was performed on an ABI 7700 Sequence Detection system (Applied Biosystems) running the cycling conditions: 50 °C for 2 min, 95 °C for 10 min, 45 cycles of 95 °C for 15 s, and 60 °C for 1 min. Immediately following this reaction, melt curve analysis was performed by heating the plate from 60 °C to 99 °C and measuring SYBR Green I dissociation from the amplicons. This allowed determination of reaction specificity. The copy number of mRNA-derived cDNA in each sample was calculated from a standard curve generated with the use of known amounts of plasmid or genomic DNA. Housekeeping genes, β-actin and GAPDH, were measured for reference to verify that all samples were integral and of comparable quality. Genomic DNA contamination of the original RNA samples was negligible (<10 copies genomic DNA/50ng RNA), as shown by TaqMan assay of genomic sequence for 10 genes in replicate samples taken through the reverse transcription procedure, but with the reverse transcriptase omitted.

| GENE | *GENBANK* ACCESSION NUMBER | PRIMER | SEQUENCE 5' – 3' | PRODUCT SIZE |
|---|---|---|---|---|
| LDL-r | NM00527 | Forward | GCGAAGATGCGAAGATATCGATG | 172 bp |
| | | Reverse | CCGGTTGGTGAAGAAGAGGTAG | |
| VLDL-r | NM003383 | Forward | CTGCAGCCATTGCTGTTGATTGG | 173 bp |
| | | Reverse | CCAGTAAACAAAGCCAGACAGTG | |
| LRP | NM002332 | Forward | GATCCCAATGACAAGTCAGATGC | 173 bp |
| | | Reverse | ATGCCATTGGTCACCACGTCTTC | |
| ApoER2 | D50678 | Forward | GCGGAACTATTCACGCCTCA | 74 bp |
| | | Reverse | TGCGATTGGTGGCAACTTC | |
| SR-BI | Z22555 | Forward | GGTCCCTGTCATCTGCCAA | 85 bp |
| | | Reverse | CTCCTTATCCTTTGAGCCCTTT | |
| SR-BII | Z22555 | Forward | TCCTGAGGACACCGTGAGC | 123 bp |
| | | Reverse | GAGGCTCAGGCTGTGG | |
| NOS1 | AH005382 | Forward | TGCTGCGATGCAATGCTT | 117 bp |
| | | Reverse | GACGGCCATGTTCCAGT | |
| NOS2 | NM153292 | Forward | ACAAGCCTACCCCTCCAGAT | 104 bp |
| | | Reverse | CCTGGCCAGATGTTCCTCTA | |
| NOS3 | A519768 | Forward | CCTGGAGAATGAGCAGAAGG | 109 bp |
| | | Reverse | GTTGACCATCTCCTGATGGAA | |
| PKB/Akt | M95936 | Forward | TCACTGCGCTGAAGTATGCCTTC | 171 bp |
| | | Reverse | CGCGAGTGCAAGTACTCAAGAG | |
| β-actin | X00351 | Forward | AGGCTACGAGCTGCCTGACG | 215 bp |
| | | Reverse | GTAGTTTCGTGGATGCCACAGGACT | |

**Table 3.1 Primers designed to investigate gene expression by real-time PCR**

*Complete list of primers used in this present study, with GenBank accession numbers and expected product sizes. All primers designed using GeneFisher and synthesised to order by Sigma-Genosys (Cambridge, UK). Primers were designed for amplification from cDNA template.*

*LDL-r* ..... *low-density lipoprotein receptor;*
*VLDL-r* ..... *very-low-density lipoprotein receptor;*
*LRP* ..... *LDL-receptor-related protein*
*ApoER2* ..... *apolipoprotein E receptor 2;*
*SR-BI / BII* ..... *scavenger receptor class B Type I / Type II;*
*NOS1* ..... *neuronal nitric oxide synthase;*
*NOS2* ..... *inducible nitric oxide synthase;*
*NOS3* ..... *endothelial nitric oxide synthase;*
*PKB/Akt* ..... *protein kinase B;*
*β-actin* ..... *ubiquitously expressed housekeeping gene for real-time PCR standardisation/quantisation.*

| CELL LINE NAME AND TISSUE SOURCE | CELL LINE INFORMATION | REFERENCE |
|---|---|---|
| ***Vessel Wall*** | | |
| AO-SMC- (unstimulated) | Aortic smooth muscle cells | CC-2571[A] |
| AO-SMC+ (serum stimulated) | Aortic smooth muscle cells | - |
| HCA-EC | Human coronary artery endothelial cells | CC-2585[A] |
| HCA-SMC | Human coronary artery smooth muscle cells | CC-2583[A] |
| Bladder-SMC | Bladder smooth muscle cells | GSK[B] |
| ***Liver*** | | |
| Chang | Liver cells | CCL-13[C] |
| HepG2 | Hepatocyte carcinoma | HB-8065[C] |
| WRL68 | Liver carcinoma | CL-48[C] |
| ***Blood*** | | |
| Lymphocytes | Primary culture | - |
| Macrophages (monocyte-derived) | Primary culture | - |
| THP-1 (unstimulated) | Monocytic | TIB-202[C] |
| Neutrophils | Primary culture | - |
| CMK-86 | Megakaryocyte | GSK[B] |
| M-07e | Megakaryocyte | ACC104[D] |
| UT7-Epo | Megakaryocyte | [219] |
| ***Bone/Cartilage*** | | |
| C20A4 | Chondrocytes | [220] |
| HOS | Osteosarcoma cells | CRL-1543[C] |
| MG63 | Osteosarcoma cells | CRL-1427[C] |
| SAOS2 | Osteosarcoma cells | HTB-85[C] |
| HAC60 | Articular chondrocytes | GSK[B] |
| ***Astrocytoma/glia*** | | |
| 1321N1 | Brain astrocytoma | 86030402[E] |
| C13 | Immortalized immature microglial cell | GSK[B] |
| Hs-683 | Glioma | HTB-138[C] |
| CCF.STTG1 | Astrocytoma | CRL-1718[C] |
| ***Neuroblastoma*** | | |
| H4 | Brain neuroglioma | HTB-148[C] |
| IMR32- NCA240 | Neuroblastoma | CCL-127[C] |
| IMR32+ NCA240 | Neuroblastoma | - |
| SK-N-MC | Neuroblastoma | HTB-10[C] |
| SK-N-SH | Neuroblastoma | HTB-11[C] |
| SH-SY5Y- (undifferentiated) | Neuroblastoma | CRL-2266[C] |
| SH-SY5Y+ (differentiated) | Neuroblastoma | - |
| NT-2 precursor cells | Ntera/D1 cell line, derived from a human teratocarcinoma, represents a committed neuronal precursor stage of differentiation | CRL-1973[C] |
| ***Others*** | | |
| Prostate SMC | Prostate smooth muscle cells, primary, p3 | GSK[B] |
| HK-2 | Kidney, cortex, proximal tube, HPV-16 transformed | CRL-2190[C] |
| ***Parental Background Cells*** | | |
| HEK 293 | Embryonic kidney | CRL-1573[C] |
| HeLa | Epithelial cervical adenocarcinoma | CCL-2[C] |
| COS-1 | Kidney fibroblast-like, derived from CV-1 cells, transformed with origin-defective mutant of SV-40 coding for T-antigen | CRL-1650[C] |
| MRC-9 | Foetal lung fibroblast (female) | CCL-212[C] |

**Table 3.2 Human primary cells and cell lines present on the *TaqCell* plate.**

*Details of cell lines, with tissue source and reference number/supplier information.*

*A = Cambrex Bioproducts, New Jersey, USA;*

*B = GlaxoSmithKline (GSK) in-house collection, Harlow, UK;*

*C = American Type Culture Collection (ATCC);*

*D = German Collection of Microorganisms and Cell Cultures (DSMZ);*

*E = European Collection of Cell Cultures ECACC)*

## 3.3 RESULTS

### 3.3.1 Standard PCR assay to test primers

Before primers were used in *TaqCell* plate assays, it was important to verify that each chosen pair would selectively amplify their target under identical conditions. This was done using cDNA templates from CCF.STTG1 and SH-SY5Y cells, selected due to their representation of the two main cell types found in the brain: neuronal and astrocytic. Reactions were performed in a standard thermal cycler, followed by visualisation by agarose gel electrophoresis. The aim was to generate a single band corresponding to the correct product size, with no obvious contamination by artefactual bands, mispriming, or primer-dimer complexes.

The final results from this investigation are shown in *Figure 3.1*, which represents a set of PCRs performed using the primer sets listed in *Table 3.1*. For every target gene, multiple primer sets were designed and investigated (data not shown). Those that gave the most intense single product without mispriming were isolated and their annealing temperatures investigated in a further round of PCRs. The goal was to develop a uniform programme that could be used for all primer sets. This was in order to simplify the quantitative PCR process that would follow on, allowing a number of genes to be investigated in simultaneous reactions without having to modify the overall conditions within the machine real-time PCR thermocycler. The programme eventually elucidated was 50 °C for 2 min, 95 °C for 10 min, followed by 45 cycles of 95 °C for 15 s, and 60 °C for 1 min, which was based on the Quantitect SYBR Green I manufacturer's recommended protocols and the average melting temperature of the primer sets (which corresponds to their annealing temperature). All primer sets appeared to function well at these conditions, although a range of temperatures ± 2 °C of the optimal annealing temperature could be utilised for all primer sets (data not shown).

Shown in *Figure 3.3* are reactions performed at these conditions, followed by agarose gel electrophoresis: potential apoE receptors (see *Figure 3.1.A*); NOS isoenzymes, PKB/Akt and the housekeeping gene β-actin (see *Figure 3.1.B*). Each reaction was performed with identical conditions, whereby 400 ng of cDNA temple were used in a reaction mixture containing identical concentrations of PCR components (i.e. primers, dNTPs, $MgCl_2$, *Taq*, water), and finally run to an identical programme on the thermal cycler.

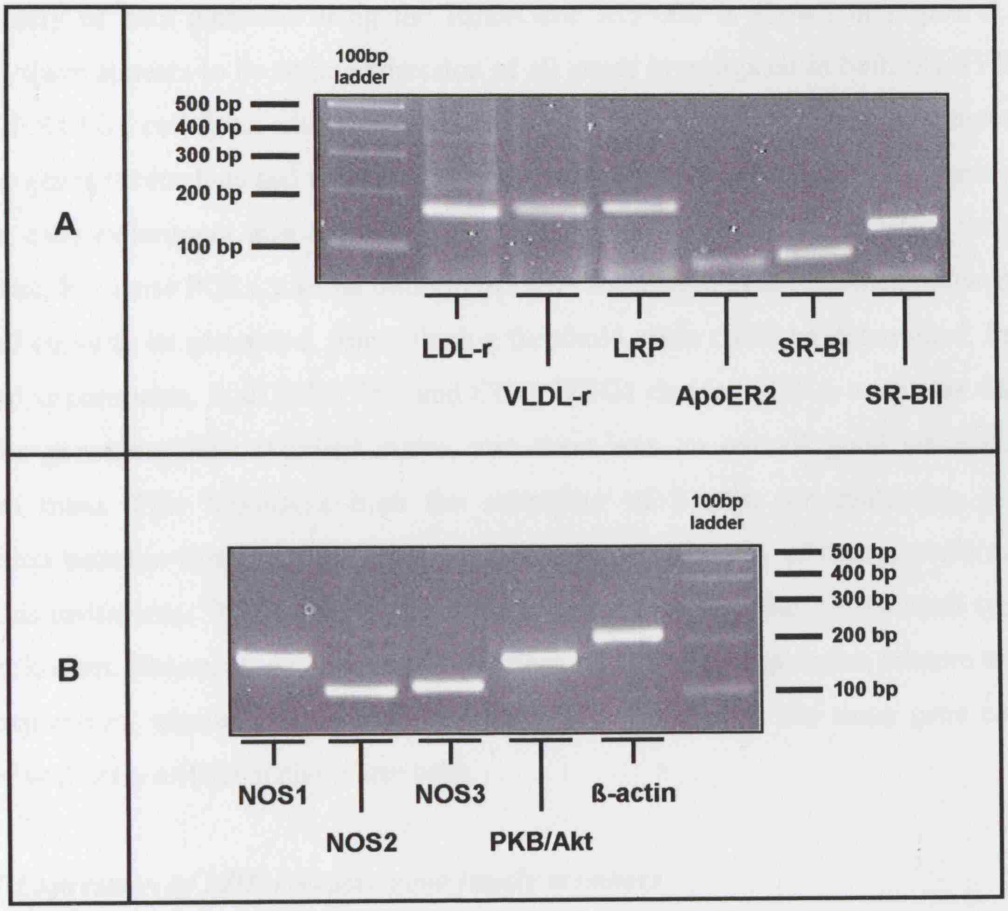


**Figure 3.1 PCR products of genes being investigated**

*Reactions were performed using cDNA template derived from cultured SH-SY5Y cells in a standard thermal cycler and products separated by 2 % agarose gel electrophoresis. Also included is one of the ubiquitously expressed housekeeping genes, β-actin, used to standardise/quantify gene expression of the other target genes. Detailed below are the expected product sizes of each PCR product:*

*(A) Lipoprotein receptors*

*LDL-r..... 172 bp*

*VLDL-r..... 173 bp*

*LRP..... 173 bp*

*apoER2..... 74 bp*

*SR-BI..... 85 bp*

*SR-BII..... 123 bp*

*(B) NO biosynthesis elements*

*NOS1..... 117 bp*

*NOS2..... 104 bp*

*NOS3..... 109 bp*

*PKB/Akt..... 171 bp*

*β-actin ..... 215 bp*

### 3.3.2 Gene expression investigation using RotorGene RG3000 thermal cycler

A summary of data gathered using the RotorGene RG3000 is shown in *Figure 3.2.* Overall, there appears to be some expression of all genes investigated in both SH-SY5Y and CCF.STTG1 cell lines, although the actual level of expression is variable between both the genes themselves and the two cell lines. In addition to reactions for the genes of interest, each experiment also included a set of reactions using primers targeting the β-actin gene. For these PCRs, a serial dilution of DNA template was used, which allowed a standard curve to be generated, from which a threshold cycle could be determined. In a series of experiments, both SH-SY5Y and CCG.STTG1 derived cDNA templates were used for generating this standard curve, and there was an overall good correlation between them. This highlights both the suitability of β-actin for evaluating gene expression between these two cell-lines, and the general reliability of assays performed using this instrument. The actual copy number of β-actin genes within the two cell types was not known. Hence, all data generated has been measured as expression relative to β-actin expression, wherein 1.0 unit of expression is equivalent to the same gene copy number as β-actin mRNA within these cells.

#### *3.3.2.1 Expression of LDL-receptor gene family members*

The expression of apoE related receptors and protein kinase B (PKB/Akt) are displayed in *Figure 3.2 A.* The observed relative expression of LDL-r was good in SH-SY5Y cells (1.050 units), with the CCG.STTG1 cells showing about half this expression level (0.630 units). This was also the case for the VLDL-r, with SH-SY5Y cells expressing 0.433 units compared to 0.209 units in CCG.STTG1. LDL-receptor-related protein (LRP) expression was relatively low in SH-SY5Y cells. However, in CCG.STTG1 cells, there was a marked increase in expression of this receptor (2.648 units in CCG.STTG1 cells, compared with 0.181 units in SH-SY5Y cells). Expression of apoER2 was very low in both cell types: 0.011 units in SH-SY5Y cells and 0.037 units in CCG.STTG1 cells. Although expression in the CCG.STTG1 cells was about 3-fold higher, both are of a similar order of magnitude, which is problematic when attempting to determine in which cell type (neuronal or astrocytic) this receptor is predominantly expressed. Despite this, it is significant that expression of apoER2 has been demonstrated in these two cell lines. This is a positive observation, which will be important for further investigation, largely because the main function of apoER2 (in concert with VLDL-r) is considered to be its involvement in signalling events rather than receptor-mediated endocytosis of apoE

containing lipoproteins, which is the main function of the other LDL-receptor gene family members.

### *3.3.2.2 Expression of SR-BI and SR-BII*

Both of these HDL receptors showed good expression in both SH-SY5Y and CCG.STTG1 cells (see *Figure 3.2 A*). In both instances, CCG.STTG1 cells appeared to have approximately 2-fold higher expression compared to SH-SY5Y cells. However, the expression of SR-BII was the predominant form found in both cell types, with 1.7 x in SH-SY5Y and 1.6 x in CCG.STTG1 cells with respect to SR-BI expression. The expression of SR-BII requires the splicing out of the stop codon of the SR-BI mRNA sequence, with the addition of a new exon sequence. The occurrence of this event is considered relatively infrequent, resulting in SR-BI expression being predominant in human cells such as HepG2 and THP-1 [165].

### *3.3.2.3 Expression of NOS isoforms and PKB/Akt*

Overall, expression of the NOS isoenzymes (see *Figure 3.2 B*) reveals a very low expression, particularly of NOS1 and NOS3. It was only the expression of the inducible form, NOS2, in SH-SY5Y cells that was significantly high. This was still only 0.043 units, which is dramatically lower than any of the receptor expression levels observed. However, as basal NO levels remain relatively low, there may be no real requirement for these cells to have high NOS levels. Certainly, they express them at a very low copy number, but this may be sufficient for the cell's purposes. Also featured on *Figure 3.2 A* are data for PKB/Akt expression within these two cell lines, which appears to be relatively high. Therefore, this regulatory element of NOS3 activity is present at substantial levels. The disparity between PKB/Akt and NOS3 expression is likely due to PKB/Akt being a signalling molecule for a number of pathways other than NOS3, which would entail relatively high expression.

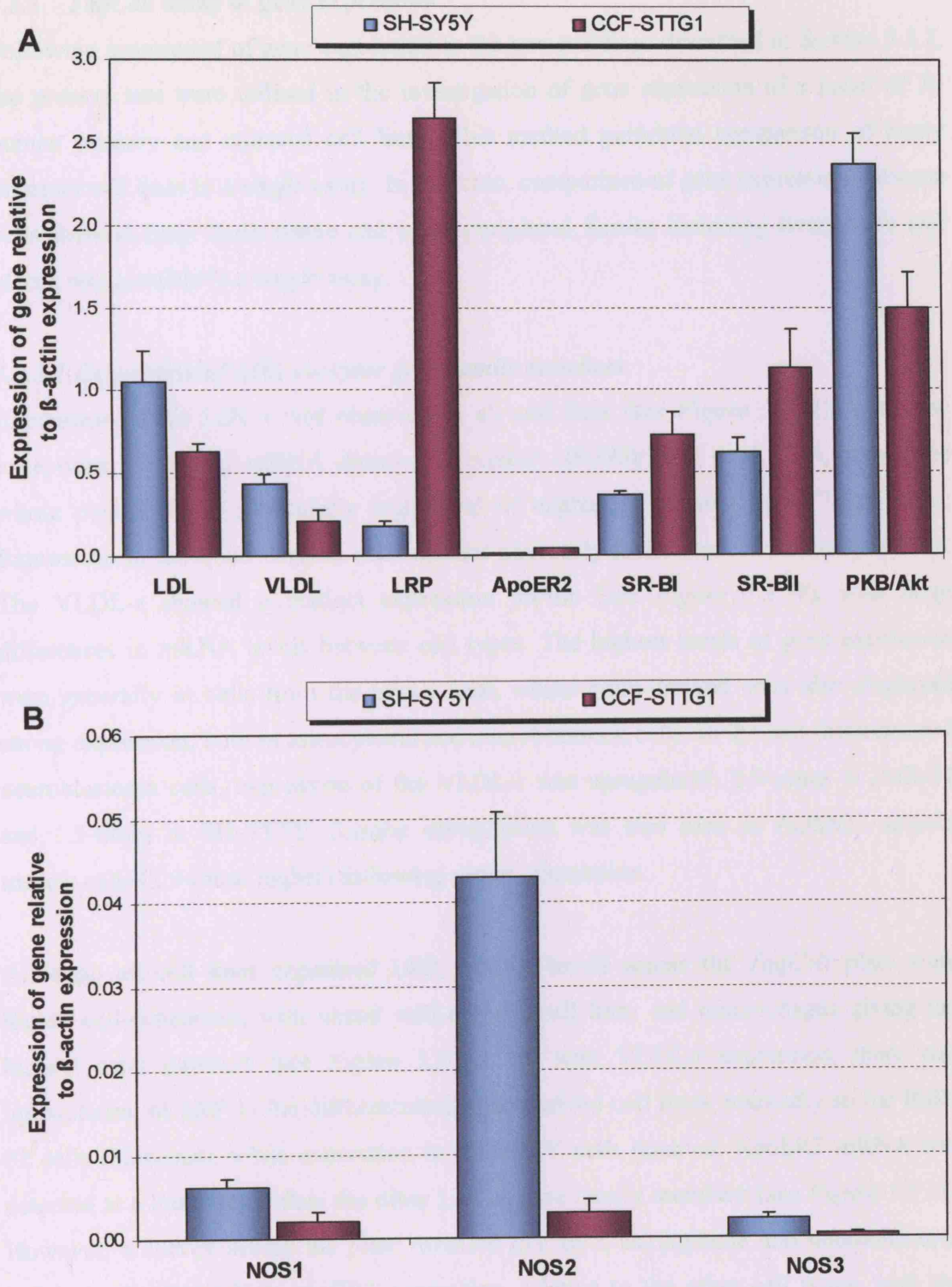


**Figure 3.2 Real-time PCR investigation using *RotorGene* instrument**

*(A) LDL-receptor gene family members (LDL-r, VLDL-r, LRP and apoER2), HDL receptors (SR-BI and SR-BII) and PKB/Akt;(B) NOS isoforms. Reactions performed using cDNA templates from SH-SY5Y and CCF.STTG1 cells. Gene expression levels determined on an arbitrary scale relative to β-actin expression. Plotted data represent the mean of quadruplicate reactions for each primer set (± standard error).*

### 3.3.3 *TaqCell* assay of gene expression

Following assessment of gene expression in the two cell lines described in *Section 3.3.2*, the primers sets were utilised in the investigation of gene expression of a panel of 38 human primary and cultured cell lines. This method permitted comparison of many different cell lines in a single assay. In this case, comparison of gene expression between cells derived from brain tissue and other peripheral tissues including liver, bone and blood, was possible in a single assay.

#### *3.3.3.1 Expression of LDL-receptor gene family members*

Expression of the LDL-r was observed in all cell lines (see *Figure 3.3 A*). With few exceptions, copies of mRNA detected exceeded 100,000/50ng total RNA across the whole plate, with a particularly high level of expression present in UT7-Epo cells. Expression in the brain-derived cells did not obviously differ from the other cell lines. The VLDL-r showed a distinct expression profile (see *Figure 3.3 B*), with large differences in mRNA levels between cell types. The highest levels of gene expression were generally in cells from the vessel wall, whilst brain-derived cells also displayed strong expression, both in astrocytoma and neuroblastoma cells. In the two differentiated neuroblastoma cells, expression of the VLDL-r was upregulated: 2.9-times in IMR-32 and 1.5-times in SH-SY5Y. Similar upregulation was also seen in AOSMC smooth muscle cells (2.9-times higher) following serum stimulation.

Although all cell lines expressed LRP, mRNA levels across the *TaqCell* plate were highly cell-dependent, with vessel wall-derived cell lines and macrophages giving the highest copy numbers (see *Figure 3.3 C*). As with VLDL-r expression, there was upregulation of LRP in the differentiated brain-derived cell lines, markedly so for IMR-32 cells (32-times), while expression in SH-SY5Y cells doubled. ApoER2 mRNA was detected at a lower level than the other LDL-r gene family members (see *Figure 3.3 D*). However, a survey across the plate revealed that both astrocytoma and neuroblastoma cell lines displayed high apoER2 expression, relative to the other cell types, with the greatest level found in H4 neuroglioma cells. Differentiated IMR-32 cells showed a 30% rise in apoER2 mRNA, consistent with increased expression of LDL-r and VLDL-r, whereas this was not seen in SH-SY5Y cells, which expressed 55% less apoER2 mRNA than undifferentiated cells.

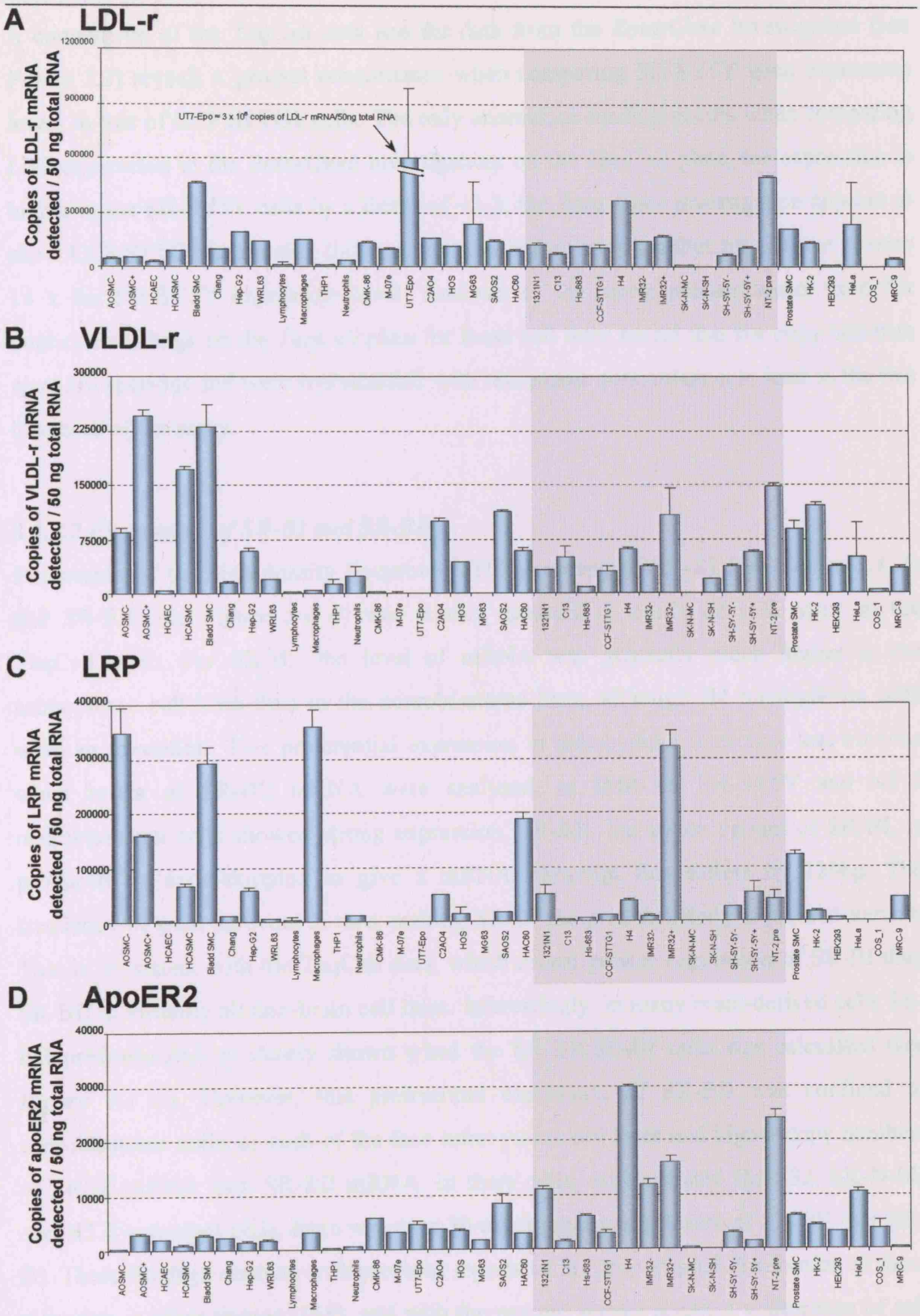


**Figure 3.3** ***TaqCell*** **plate assay of LDL-receptor gene family expression**

*Levels of mRNA were measured in 38 human cell lines and primary cells for (A) LDL-r, (B) VLDL-r, (C) LRP and (D) apoER2. Data shown represents the mean of a duplicate measurement (± standard error) of mRNA copy numbers in 50ng of reverse transcribed total RNA from the same batch of cells. Note: scaling on y-axis of each graph differs. In all figures, brain-derived cell lines are highlighted within the shaded boxes.*

A comparison of the *TaqCell* data and the data from the *RotorGene* investigation (see *Figure 3.2*) reveals a general concordance when comparing SH-SY5Y gene expression levels to that of CCF.STTG1 cells. The only anomalous reading occurs when comparing LRP expression in the *RotorGene* investigation: on the *TaqCell* plate, the expression is higher in the SH-SY5Y cells by a factor of ~2-3; the *RotorGene* investigation appears to show CCF.STTG1 expressing this receptor at a higher copy number by a factor of over 14 x the SH-SY5Y expression level. Analysis of the direct measurements from the duplicate readings on the *TaqCell* plate for these cell lines reveal that the copy numbers were not spurious and were reproducible with reasonable concordance, at least in the two instances of the assay.

#### *3.3.3.2 Expression of SR-BI and SR-BII*

Expression of the high-density lipoprotein (HDL) receptors, SR-BI (see *Figure 3.4 A*) and SR-BII (see *Figure 3.4 B*) was readily apparent in nearly all cell types on the TaqCell plate. For SR-BI, the level of mRNA was generally much higher in the astrocytoma cell lines than in the neuroblastoma lines, although H4 neuroglioma cells were an exception. This preferential expression in astrocytoma lines was less obvious when levels of SR-BII mRNA were analysed, as IMR-32, SH-SY5Y and NT-2 neuroblastoma cells showed strong expression. SR-BII, the splice variant of SR-BI, is produced by exon-skipping to give a mRNA transcript that differs by 129bp. The frequency of such an event is rare, making SR-BI the predominantly expressed variant. This is consistent with the TaqCell data, which reveal greater expression of SR-BI than SR-BII in virtually all non-brain cell lines. Interestingly, in many brain-derived cells SR-BII predominated as clearly shown when the SR-BII:SR-BI ratio was calculated (see *Figure 3.4 C*). However, this preferential expression of SR-BII was confined to neuroblastoma cells, as each of the four astrocytoma cell lines had higher copy numbers of SR-BI mRNA than SR-BII mRNA. In three cells, differentiated IMR-32, SK-N-SH and NT-2 precursor cells, there was over 30-times greater expression of SR-BII than SR-BI. These findings contrast with previous reports of the proportional distribution of these receptors in other tissues [165], and with the present survey across a wide range of cell types. However, this finding is supported by the assay performed using the *RotorGene* instrument, which seems to indicate that this is a notable phenomenon (see *Figure 3.2 A*).

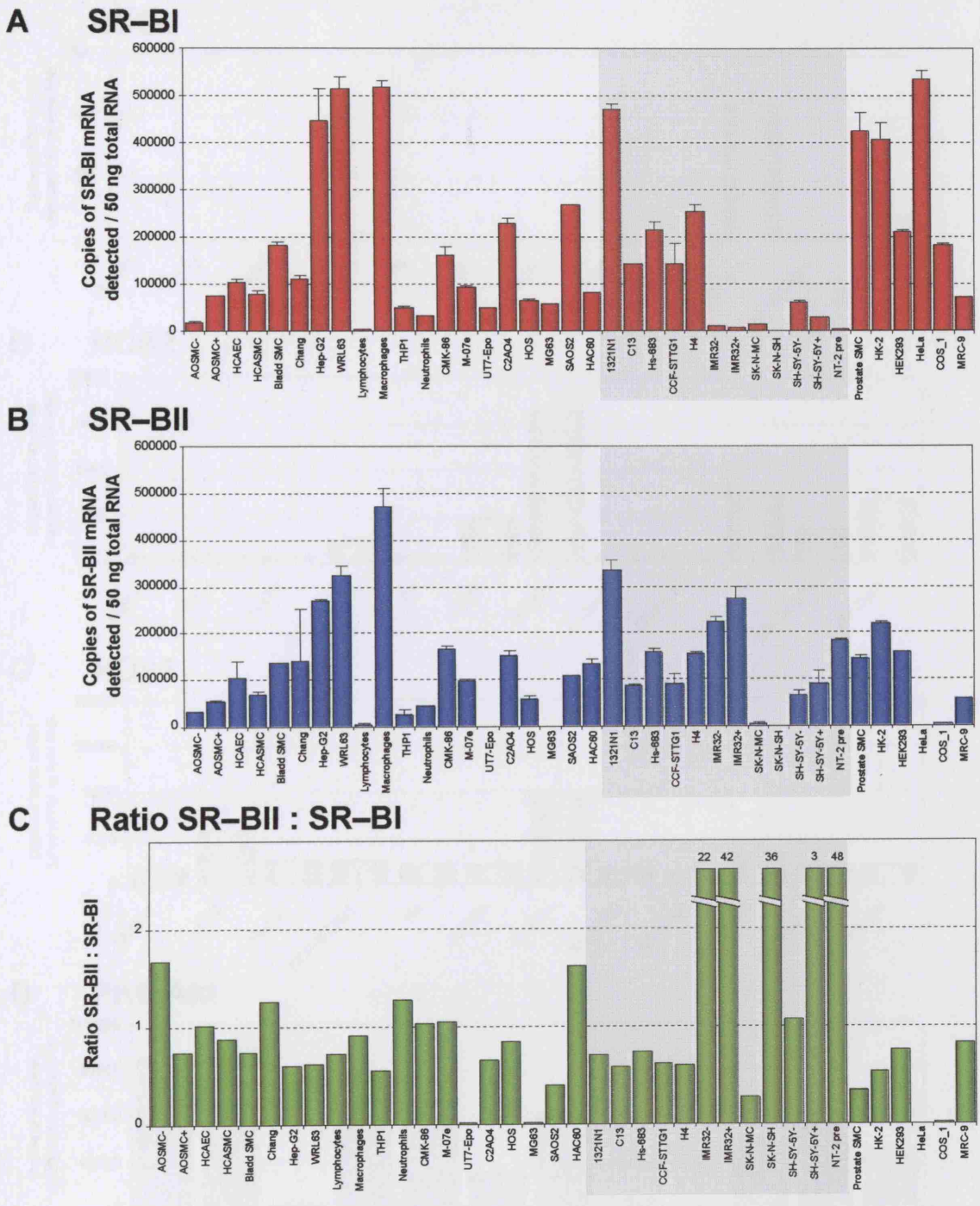


**Figure 3.4 TaqCell plate assay of HDL receptor expression**

*Levels of mRNA were measured in 38 human cell lines and primary cells for (A) SR-BI and (B) SR-BII. Data shown are the mean of a duplicate measurement (± standard error) of mRNA copy numbers in 50ng of reverse transcribed total RNA from the same batch of cells. (C) Calculated ratio of SR-BII : SR-BI mRNA expression. Brain-derived cell lines are highlighted; five cell lines gave ratios greater than 2.0 (IMR-32 +/-, SK-N-SH, SH-SY5Y +/-), in four cases markedly so, and their individual ratio values are shown above the bars. In all figures, brain-derived cell lines are highlighted within the shaded boxes.*

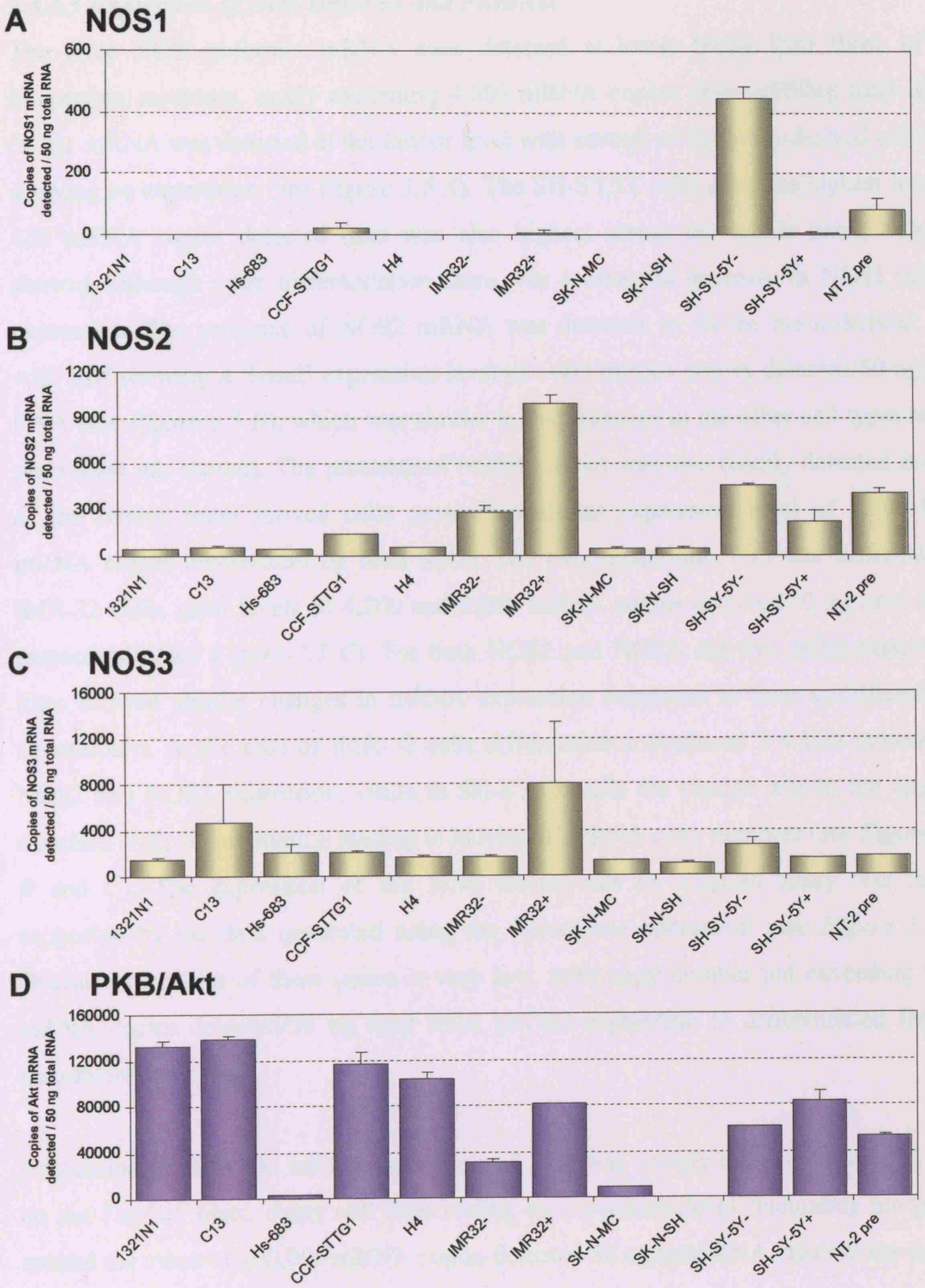


**Figure 3.5** ***TaqCell*** **plate assay of NOS isoform and PKB/Akt expression**

*Levels of mRNA were measured in 38 human cell lines and primary cells for (A) NOS1, (B) NOS2, (C) NOS3 and (D) the NOS3 regulatory kinase, PKB/Akt. Results are shown only for the brain-derived cells and represent the mean of a duplicate measurement (± standard error) of mRNA copy numbers in 50ng of reverse transcribed total RNA from the same batch of cells. Note that the scaling on the y-axis of each graph differs.*

### *3.3.3.3 Expression of NOS isoforms and PKB/Akt*

The three NOS isoform's mRNA were detected at lower levels than those of the lipoprotein receptors, rarely exceeding 4,000 mRNA copies detected/50ng total RNA. NOS1 mRNA was detected at the lowest level with several of the brain-derived cell lines showing no expression (see *Figure 3.5 A*). The SH-SY5Y cells gave the highest level of 430 mRNA copies detected (and was also highest across the whole plate; data not shown), although upon differentiation there was a dramatic decrease in NOS1 mRNA expression. The presence of NOS2 mRNA was detected in all the brain-derived cells with half showing a 'basal' expression level of ~400 mRNA copies detected/50 ng total RNA (see *Figure 3.5 B*), which was similar to that detected in the other cell types on the plate (data not shown). The presence of NOS3 mRNA was also readily detected and ten of the twelve brain-derived cells gave a consistent expression level of 1,500-3,000 mRNA copies detected/50 ng total RNA. The two exceptions, C13 and differentiated IMR-32 cells, gave levels of 4,200 and 8,000 mRNA copies detected/50 ng total RNA, respectively (see *Figure 3.5 C*). For both NOS2 and NOS3, the two differentiated cell lines showed similar changes in mRNA expression compared to their undifferentiated counterparts. In the case of IMR-32 cells differentiation produced 3-4-fold increases in NOS2 and NOS3 expression, while in SH-SY5Y cells the change was in the opposite direction with differentiation leading to halving of mRNA copy numbers (see *Figures 3.5 B* and *C*). The expression of the NOS isoenzymes by *TaqCell* assay was largely supported by the data generated using the *RotorGene* instrument (see *Figure 3.2 C*). Overall expression of these genes is very low, with copy number not exceeding 9,000 mRNA copies detected/50 ng total RNA (NOS2 expression in differentiated IMR-32 neuroblastoma cells).

Expression of PKB/Akt mRNA (see *Figure 3.5 D*) was usually high across all cell types on the *TaqCell* plate, many cell lines having an expression level fluctuating marginally around the mean of 100,000 mRNA copies detected/50 ng total RNA. Most brain-derived cells also showed good expression of PKB/Akt mRNA, with values similar to other cell lines and in some cases exceeding them. The three highest expressing lines were the 1321N1, C13 and CCF.STTG1 astrocytoma cells, which each gave levels of ~120,000 mRNA copies detected/50 ng total RNA. Differentiation of IMR-32 and SH-SY5Y cell lines produced 170% and 40% increases in expression, respectively, to about 80,000 mRNA copies detected/50 ng total RNA compared to the undifferentiated forms.

## 3.4 DISCUSSION

The characterisation of cell lines is an important initial step in this study. By defining which genes are expressed in these cells, it is possible to identify suitable cell lines for further exploration of NOS signalling pathways. It details those genes that may be of greater importance when attempting to establish a mechanism or pathway by which apoE might mediate an effect on neuronal cells, and whether there is an isoform specific difference. Furthermore, this work opens the possibility to assay cells that are lacking in a particular gene's expression. For example, the expression of PKB/Akt in Hs-683 glioma and SK-N-SH neuroblastoma cells was extremely low relative to other brain-derived cell lines (see *Figure 3.5 D*). If this kinase has a direct effect on NO synthesis via the activation of NOS3, as has been observed in non-neuronal cells [188], it could be postulated that a qualitatively reduced degree of NOS3 activation would occur in a neuronal cell line with a very low level of PKB/Akt protein.

Two cell lines were initially investigated (SH-SY5Y and CCF.STTG1) representing the two main populations of functional cells in the CNS (neuronal and glial cells). The cells were grown in the absence of any selective factors. From these cultures, DNA and RNA were extracted, with the RNA acting as a template for reverse transcriptase to generate cDNA. This became the template DNA source for investigating gene expression. Quantitative real-time PCR was used to measure mRNA expression levels of a range of genes involved in apoE metabolism and NO biosynthesis, focusing on genes encoding receptors capable of binding apoE-containing lipoproteins. The generic probe, SYBR Green I, which intercalates into the double-strand DNA amplicons, was used to monitor PCR reactions rather than a synthetic oligonucleotide-based reagent specific for each gene. However, all assays were sensitive and specific, as judged by rigorous electrophoretic and melt curve analyses of primer pairs prior to their use in both the *RotorGene* instrument and the *TaqCell* plates. The use of quantitative PCR can be highly sensitive and present a very compelling view of gene expression within a cellular system. However, individual assays give only information on mRNA levels; in particular, whether a gene is expressed by a cell line, its copy number relative to other cell lines, and to other genes investigated. It does not follow, however, that mRNA levels are a true reflection of protein expression; an important consideration when evaluating the data presented. Moreover, it gives absolutely no indication on the functional activity of a particular protein, such as pSer1177 residue of NOS3 and the pSer473/Thr308 sites of PKB/Akt (further data with regard to this aspect presented in *Chapter 5*).

The LDL-r is the archetypical cell-surface receptor mediating endocytosis of its ligand, in this case apoE or apoB100, to allow delivery of lipid nutrients. It is expressed in virtually all cells and tissues at variable levels, which the findings in *TaqCell* plates confirm. The LDL-r is widely expressed in brain and, as apoB100 and LDL are absent from cerebrospinal fluid [221], it appears that their role in lipid transport and cholesterol homeostasis is fulfilled by apoE [221,129]. Structurally, the VLDL-r and apoER2 are very similar to the LDL-r and to each other; both bind apoE3 and apoE4 with similar affinities [222,223]. The VLDL-r is abundantly expressed in heart and skeletal muscle and adipose tissue, all of which actively metabolise fatty acids acquired from triglyceride-rich lipoproteins [224,225]. In contrast, apoER2 is absent from these tissues. Moreover, its reported predominate expression is to be found in brain, with a widespread distribution [226]. Subsequent immunohistochemical studies also revealed VLDL-r expression in brain, including hippocampal cortical neurons and microglia, particularly those associated with senile plaques [149,227]. Data from the *TaqCell* plates were consistent with this tissue distribution, including the strong expression of VLDL-r and apoER2 across most of the brain-derived cell lines.

Studies in mice that lack both VLDL-r and apoER2 have highlighted key roles for these receptors in neuronal migration and development of the nervous system. The double knockout mice have marked behavioural and neuroanatomical features, which includes cerebellar dysplasia and severe ataxia, and disruption of cortical layering. This phenotype is identical to the mutant mouse strains, *Scrambler* and *Reeler*, which have dysfunctional forms of the intracellular adaptor protein, Disabled-1 (Dab-1) [228], and the large secreted signalling glycoprotein, Reelin [142,228], respectively. Genetic and biochemical studies now group these disparate proteins into a common signalling pathway in which Reelin binds with high-affinity to VLDL-r or apoER2, an interaction which promotes Dab-1 binding to the cytoplasmic NPxY motifs of both receptors [229]. This initial Reelin signal stimulates tyrosine phosphorylation of Dab-1, which can then activate a variety of downstream signalling components [229,230,137].

At 600 kDa, LRP is much larger than the other LDL-r family members studied and contains two NPxY motifs and one tyrosine-based YxxL motif. It has broad binding specificity with over 30 different ligands many of which are internalised, interestingly via the alternative endocytic signalling motif, YxxL, which dominates [231]. In addition, several adaptor and scaffold proteins, including Dab-1, potentially bind the cytoplasmic

NPxY motifs of LRP and, although biochemical and physiological details are incomplete, numerous regulatory functions are suggested, including mitogen-activated protein (MAP) kinase signalling, ion channel function, microtubular transport, and axon guidance [140,137,232]. Genetic association studies suggest a direct link between LRP and AD, as the C766T polymorphism in exon 3 of LRP is under-represented [233]. However, although brains of AD patients with CT or TT genotypes contain higher levels of LRP [234] and circumstantial evidence suggests that LRP promotes Aβ clearance [235], the relationship remains controversial [236]. Similarly, polymorphisms in the VLDL-r [149,227] and apoER2 [237] have been identified and are suggested to be risk factors for AD, but further studies are needed to verify these possibilities.

Scavenger receptor class B, type I mediates the selective uptake of cholesteryl esters from HDL without degrading the particles. It was the first authentic HDL binding protein to be characterised [152], although other ligands including apoE are now recognised [238]. A splice variant, termed SR-BII, was subsequently identified; this results from skipping exon 12 [165,164] to produce a receptor with a different C-terminal cytoplasmic tail, but identical extracellular binding region, to that of SR-BI. This implies differential functions; for example, the interaction between C-terminal SR-BI and PDZK1, a scaffolding protein [239], would not occur with SR-BII. On the other hand, cytoplasmic SR-BII contains six PxxP motifs, two being conserved in rat, mouse and hamster, which are potential ligands for tyrosine kinases or adaptor proteins with Src homology 3 (SH3) domains (see *Figure 1.5*) [165]. The presence of these motifs, which are also found in cytoplasmic apoER2 [151], suggests that SR-BII may initiate signalling pathways that cannot be mediated by SR-BI; although speculative, this is an exciting possibility given the preferential expression of SR-BII in many brain-derived cell lines (see *Figure 3 C*). The higher expression of SR-BII in these brain-derived cells would seem to indicate a specific necessity for its presence, which may be related to the unique tail sequence of SR-BII, thought to be involved in cell signalling events that SR-BI is incapable of participating in.

Copy numbers of NOS mRNA transcripts were generally low in all cells, although presumably adequate to maintain basal NO levels that are biologically functional without being cyto- or neurotoxic. Under normal physiological conditions, relatively little NO is synthesised and it appears that cells only transcribe NOS genes at low levels. Indeed, production of NO commonly reflects the catalytic activity of the enzyme, which depends

on intracellular $Ca^{2+}$ concentrations, the availability of substrates or co-factors, and an array of heterologous protein partners [240]. Both NOS1 and NOS3 are constitutively transcribed, whereas NOS2 expression is induced by cytokines, such as IFN-γ. Recently, phosphorylation at Ser1177 has emerged as a key regulatory mechanism of NOS3 activity, most likely because the enzyme can then bind calcium-activated calmodulin at low calcium concentration. The phosphorylation of NOS3 can be mediated by protein kinase A (PKA) or adenosine 5'-monophosphate-activated protein kinase (AMPK), but is accomplished more frequently by protein kinase B (PKB; also termed Akt), which also helps regulate apoptosis and cellular proliferation and is itself phosphorylated and activated by phosphatidylinositol (PI) 3-kinase [241]. Here, we have measured NOS and PKB/Akt mRNA transcripts in each cell line, which as discussed above may not accurately reflect protein levels. Thus, although the data identifies cells that express the three isoenzymes and the key activator of NOS3, the measurement of NOS proteins and a functional assessment of NO synthesis must await additional investigations. Moreover, there are other NOS regulatory pathways that could have been investigated, including mitogen activated protein kinase (MAP kinase) and glycogen synthase kinase (GSK). In this particular investigation, the emphasis was placed on PKB/Akt as this is a well-documented pathway, whose interaction with NOS has been well-characterised.

During this study it was not considered necessary to investigate the expression of apoE itself by quantitative PCR analysis. Production of apoE in the brain is largely controlled by astrocytes, oligodendrocytes and ependymal layer cells, and hence, under normal conditions, CCF-STTG1 astrocytoma cells would produce very low levels of apoE [242,243], whilst SH-SY5Y and other neuroblastoma cell lines would produce only insignificant or undetectable amounts [244]. Moreover, estimating apoE expression would not have aided any subsequent work, as experiments were designed such that the contribution of any endogenous apoE would be minimal.

In summary, this study has demonstrated that receptors recognising apoE are widely expressed in brain-derived cell lines. Of note, was the strong expression of apoER2 in these cells, which we have previously implicated in apoE-mediated stimulation of NO release in platelets and endothelium, and the preferential expression of the splice variant SR-BII, which is rich in cytoplasmic SH3 motifs, over wild-type SR-BI. The finding that differentiation of the neuroblastoma cell lines, IMR-32 and SH-SY5Y, results in clear changes in expression of apoER2 and the VLDL-r should also be noted. As indicated

earlier, these receptors have co-operative functions in Reelin-dependent neuronal migration and it will be of interest to determine whether differentiation of these cells influences Reelin signalling, including downstream effectors. Finally, these data helps identify suitable human brain cells for investigating apoE-mediated biosynthesis of NO and whether apoE4 and apoE3 have differential effects. Thus, the common models of neurons and astrocytes, SH-SY5Y and CCF.STTG1 cells, both appear suitable as they express adequate levels of apoER2, as well as NOS3 and PKB/Akt. Furthermore, the 4-10-fold increases in apoER2 expression in H4 neuroglioma, NT-2 precursor and IMR-32 neuroblastoma cells would also be interesting to investigate and determine whether they are associated with enhanced NO release when stimulated with apoE.

# Chapter 4

# ASSAYING RELEASE OF NITRIC OXIDE FROM NEURONAL SH-SY5Y CELLS FOLLOWING EXPOSURE TO APOLIPOPROTEIN E

# 4.0 ASSAYING RELEASE OF NITRIC OXIDE FROM NEURONAL SH-SY5Y CELLS FOLLOWING EXPOSURE TO APOLIPOPROTEIN E

## 4.1 INTRODUCTION

The characterisation of cell lines presented in *Chapter 3* identified a number of cell lines that would be suitable for investigating the response of neuronal cells to apoE exposure, specifically SH-SY5Y neuroblastoma and H4 neuroglioma cell lines. As described in *Chapter 2,* a robust sandwich ELISA protocol to measure apoE concentration was developed, which could be used to quantify the apoE content of conditioned medium from cultured stably-transfected recombinant CHO cell lines secreting apoE. Having established these foundational tools, they could now be utilised to determine whether apoE exposure results in a physiological response in brain-derived cells, and whether this displayed an isoform differential effect with respect to apoE4 relative to apoE3/E2. To this end, it was necessary to apply an assay that would reliably and repeatedly measure the level of NO (or a derivative compound) within this biological system. This could then be used to demonstrate whether exposure to the different apoE isoforms results in a change from the basal level of cellular NO biosynthesis, and if so whether these are increases or decreases in NO concentration.

### 4.1.1 Methods for assaying NO

There are a number of methods available to measure NO within a biological system. Generally, they all measure the change in a downstream effect of NO release; the formation/accumulation of products such as citrulline (the product of NOS enzyme activity), nitrate/nitrite (degradation products of NO), or cyclic-GMP (NO secondary messenger). If a change can be monitored in any of these, then a change in NO can be inferred. Additionally, some assays can be monitored in real-time, whilst others require that lysates be prepared at specific times in a discontinuous manner. Ultimately, each assay has its own distinctive degree of sensitivity, and each can vary considerably in the ease and cost of initial set up, all of which are factors that must be considered before large-scale throughput of samples.

As described in *Chapter 1,* nitric oxide is produced by the action of NOS isoenzymes that catalyse the oxidation of the guanidino nitrogen of L-arginine, converting it into L-

citrulline with the liberation of NO as a by-product. Constitutively expressed NOS1 and NOS3 synthesise low levels of NO, in the picomolar to nanomolar range, whereas the inducible NO-synthase (NOS2) can produce NO in the nanomolar to micromolar range [245]. The measurement of NO in any biological system can be highly problematic due to sensitivity issues: NO has a very short half-life (< 5 s) and a low basal concentration, further compounded by its free-radical nature that results in a particularly unstable molecule [170]. Therefore, directly measuring NO is not an approach that is technically feasible. However, assaying derivatives of NO is widely utilised in numerous methods. Within a biological system, NO can undergo a number of degradation reactions:

$$2 \cdot NO + O_2 \rightarrow 2 \cdot NO_2$$

$$\cdot NO + \cdot NO_2 \rightarrow N_2O_3 + H_2O \rightarrow \mathbf{2\ NO_2^-}$$

$$2 \cdot NO_2 \rightarrow N_2O_4 + H_2O \rightarrow \underset{\text{Nitrite}}{\mathbf{NO_2^-}} + \underset{\text{Nitrate}}{\mathbf{NO_3^-}}$$

$$\cdot NO + O_2 \rightarrow \mathbf{NO_3^-}$$

Eventually, the products formed are nitrite ($NO_2^-$) and nitrate ($NO_3^-$), highlighted above. One of the first approaches to NO measurement was based on monitoring the level of nitrite and nitrate within a system, which is a logical approach as these are relatively stable end products [246]. However, the relative levels of nitrate and nitrite produced can vary from one system to another. So, to achieve a good estimation of NO production, the sum of nitrite and nitrate concentrations is taken. In practice, rather than measure two different products, samples are subject to treatment by nitrate reductase, which catalyses the reduction of $NO_3^-$ into $NO_2^-$, which therefore means only nitrite need be assayed. A number of methods are available for nitrite measurement, including the Griess colorimetric assay, the haemoglobin assay, and a chemiluminescence analysis.

The Griess assay utilises a two-step diazotization reaction [247]. In the first stage, $NO_2^-$ is reacted with sulphanilamide (Griess reagent 1) to produce the diazonium ion. This ion is then coupled to *N*-(-1-naphthyl)ethylenediamine (Griess reagent 2) to form a chromophormic azo derivative. The formation of this azo complex can be monitored by measuring the absorbance at 540 nm. The Griess reaction is a relatively simple and fast method for detecting nitrite levels, and can be performed in a 96-well plate format for high-throughput of samples. However, it has a detection limit range in the micromolar range [248], which in a picomolar to nanomolar producing system is not sensitive

enough. For enhanced sensitivity, a fluorimetric method is also possible, which is based on the reaction of nitrite with 2,3-diaminonapththalene, under acidic conditions, to produce the fluorescent product 1-(*H*)-napthotriazole [248]. This method is supposedly 50–100 times more sensitive than the spectrophotometric method, but is still not within the sensitivity limits of a non-concentrated NOS system as is being used here.

The haemoglobin assay is based on the direct oxidation reaction of oxygenated, ferrous haemoglobin ($HbO_2$) by NO to produce the ferric form, methaemoglobin (MetHb), and $NO_3^-$ [247]. There is an associated absorbance spectrum shift for haemoglobin during this reaction, which can be monitored spectrophotometrically. This method does not require any specialised apparatus and gives a relatively sensitive measurement of NO release. However, it does require a constant amount of $HbO_2$, which can be difficult to achieve as many commercially available stocks are contaminated with MetHb. Additionally, $NO_2^-$ is also known to react with $HbO_2$ to form MetHb. Thus, it is virtually impossible to differentiate between NO and its decomposed product.

By far the most sensitive method available at present for assaying NO release is the chemiluminescence method. It also has the advantage of monitoring a reaction in real-time, which is in fact a necessity of this method. It has a generally recognised sensitivity in the femtomolar ($10^{-15}$) range, but in some setups can even assay attomolar ($10^{-18}$) concentrations of (extrapolated) NO [247]. The method based on the reaction between NO and ozone, resulting in the liberation of energy in the form of light:

$$\cdot NO + O_3 \rightarrow \cdot NO_2 + O_3$$

$$\cdot NO_2 \rightarrow NO_2 + h\nu_{\text{Light}}$$

The method was originally designed for measuring NO in gaseous samples, as there was much interest in the levels of NO as a pollutant in air [248]. It has since been adapted for aqueous samples, which requires an additional step to drive samples into an aqueous phase. Unfortunately, this technique requires very expensive and specialised equipment that are not readily available in the laboratory.

Alongside the Griess reaction, another commonly used method of NO detection is the NO electrode, based on the principle that applying a potential to an aqueous solution

containing NO will result in the electrochemical activation of NO [248]. The electrode acts as a probe, which is coated in a membrane that allows NO to diffuse through but remains impermeable to other ions of larger molecules that are electrochemically active in the solution. The NO released is measured as a change in current and can be used to monitor NO release in real-time when connected to a data plotter or computer. Additionally, sensitivity within the nanomolar range has been observed, and can routinely be used for measuring sub-micromolar NO levels in an aqueous solution [249]. The main criticism of this technique is the possibility for interference of measurements, either through electrical disturbances or the physical disturbances of adding substrates to initiate the activity of NOS.

In general, the methods of NO measurement described here have one or more failings: they can be expensive to initially setup, requiring specialised reagents; the equipment required is often specialised and can be susceptible to interference; they can be relatively insensitive or just not sufficiently quantitative. An alternative method is to assay the activity of NOS through the use of radiolabelled substrates, [$^{3}$H]-arginine or [$^{14}$C]-arginine, to follow enzymatic progress. As described in *Section 1.4.1*, NOS catalyses the reaction of arginine, nicotinamide adenine dinucleotide phosphate (NADPH) and oxygen to produce citrulline, NADP and NO [250]. Therefore, this assay monitors the conversion of radiolabelled arginine into radiolabelled citrulline, and the concentration of liberated NO can be inferred from this. However, to prepare samples, endogenous arginine must first be removed from the system, achieved by passing samples through a Dowex ion-exchange column; this technique is also used at the end of the assay to remove radiolabelled-arginine and allow measurement of the newly-synthesised radiolabelled-citrulline in the eluate [251]. It is essential, therefore, that this ion-exchange column should effectively remove all arginine within a solution, which can then be recovered as an eluate by standard ion-exchange chromatographic methods. As this is a radioactive assay, monitoring the release of NO in real-time is not possible, although this is not an overly critical aspect of the method.

Of greater concern, however, is that this assay assumes that arginine is metabolised solely by NOS. In fact, arginine serves a number of other functions, including: whilst as a free amino-acid, it serves as an intermediate in the urea cycle, and thus can be converted firstly into ornithine, and then into proline, glutamate and glutamine, which are three common amino acids in many proteins; it can also generate many non-protein nitrogen-

containing compounds, such as creatine, polyamines, agmatine and NO [252]. All of these (with the exception of NO synthesis) are under the operation of numerous enzymatic pathways, and all will consume some of the arginine load within a cell. Clearly, therefore, these reactions will also consume a certain quantity of radiolabelled arginine that will not be available for conversion to citrulline. Furthermore, there are pathways to convert citrulline back into arginine as part of the urea cycle through the production of argininosuccinate (AS) via AS synthetase (ASS) [253]. If this occurs, a radioassay will underestimate the inferred level of NO in the system, although it can be circumvented by addition of excess non-radioactive citrulline into the sample before assay.

As well as the methods described above, there are further assays available, such as electron paramagnetic resonance assay, gas chromatography, and mass spectrometry [246]. Again any of these could have been utilised, if it were not for one or more potential problems: setup cost; requirement for specialised equipment; insufficient sensitivity in some instances; potentially the need for specialist knowledge regarding routine operation to ensure that consistent and high quality results are achieved.

### 4.1.2 Diaminofluroscein (DAF) fluorescence assay

As alluded to in the previous discussion, the numerous methods for measuring NO release are far from ideal and a 'perfect' assay has yet to be developed. However, a promising method for assaying NO was first detailed in 1998 by Kojima and colleagues [254,255]. They described the use of the fluorescent probe 4,5-diaminofluroscein diacetate (DAF-2 DA), which was utilised for the bio-imaging of intracellular NO in tissue sections [254,255,256]. This cell-permeable fluorescein derivative compound becomes hydrolysed by intracellular esterases to liberate the cell-impermeable 4,5-diaminofluroscein (DAF-2). When DAF-2 becomes nitrosylated by NO within the cell, a highly fluorescent derivative is formed, DAF-2 triazole (DAF 2T) (see *Figure 4.1.1*), which can then be detected by a fluorimeter. This method is relatively quick and easy to setup. Moreover, as this assay is performed by a fluorimeter, measurements can be taken in real-time over a specified time frame, especially if connected to appropriate computer-based sampling software.

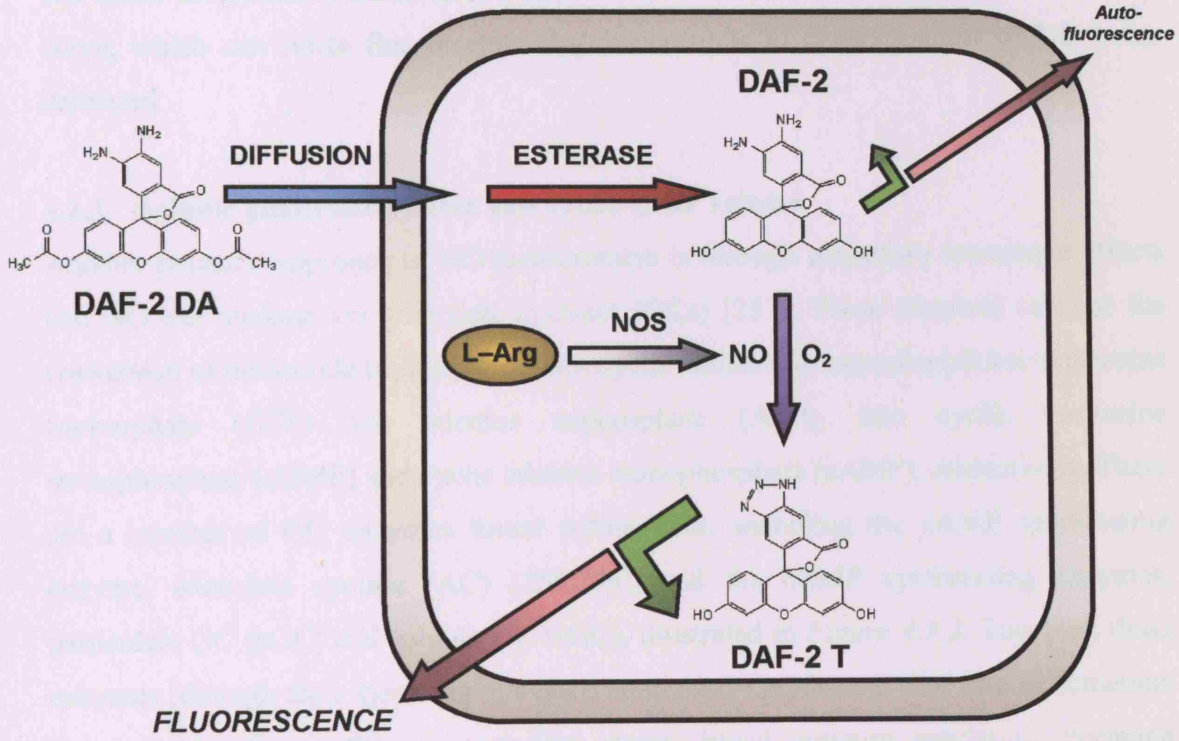


**Figure 4.1.1 Reaction of DAF-2 with NO to produce DAF-2 T**

*The non-fluorescent probe, DAF-2 DA, permeates the cell membrane, wherein cytosolic esterases hydrolyse the diacetate group to release the relatively non-fluorescent DAF-2 dye. Intracellular L-arginine (L-Arg) acts as the substrate for nitric oxide synthase (NOS) to produce NO, which in turn reacts with DAF-2 in the presence of $O_2$ to produce DAF-2T, its triazole fluorescent derivative. DAF-2 has a low level of auto-fluorescence that will be detected when measuring the fluorescence of a sample. Therefore, all recordings made during an assay will include a basal level of fluorescence arising from DAF-2, in addition to the NO-derived DAF-2 T that would ideally be measured in isolation.*

For the purposes of assaying NO release in the neuronal cells being utilised in this chapter, this method appeared ideally suited. It can measure NO release in the micromolar range, and the assay is performed in real-time. This allows a number of different treatment conditions to be assessed in a single experiment. Additionally, if an NO donor compound is included as a positive control, it is feasible to generate a standard curve, which can relate fluorescence absorbance units to concentrations of NO bolus delivered.

### 4.1.3 Soluble guanylate cyclase and cyclic-GMP release

Another potential approach to NO measurement is through secondary messenger effects that NO can mediate via guanylate cyclases (GCs) [257]. These enzymes catalyse the conversion of nucleotide triphosphates into cyclic nucleotide monophosphates: guanosine triphosphate (GTP) and adenine triphosphate (ATP), into cyclic guanosine monophosphate (cGMP) and cyclic adenine monophosphate (cAMP), respectively. There are a number of GC enzymes found within cells, including the cAMP synthesising enzyme, adenylate cyclase (AC) [258,259], and the cGMP synthesising enzymes, particulate GC (pGC) and soluble GC (sGC), illustrated in *Figure 4.1.2*. Together, these enzymes (through their synthesis of cGMP and cAMP) perform a vital role in numerous signal transduction pathways, including vision, blood pressure regulation, hormone response, and virtually any effect that NO has within cells [260,261,262].

Particulate-GCs have a single membrane spanning region with an amino-terminal extracellular ligand binding domain, whilst the carboxy-terminal intracellular region has three distinct domains: a kinase-like domain, a catalytic domain, and a dimerisation domain [263]. Activation of this enzyme occurs through the ligand binding domain, which recognises peptide hormones, specifically natriuretic peptides such as atrial natriuretic peptide (ANP), brain natriuretic peptide (BNP), and C-type natriuretic peptide (CNP) [264]. Particulate-GCs function as either homodimers or heterodimers, the association of which is facilitated by the dimerisation domain [265].

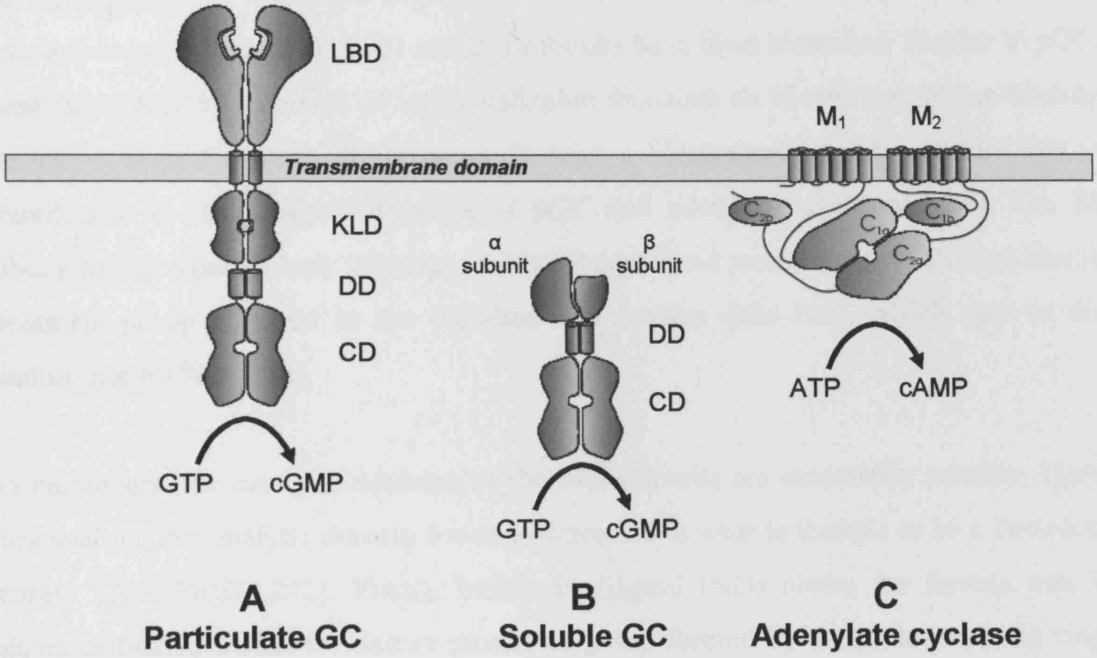


**Figure 4.1.2 Structural organisation of the cyclases**

*Illustrated are the three cyclases, particulate guanylate cyclase (pGC), soluble guanylate cyclase (sGC), which catalyse the conversion of GTP to cGMP, and adenylate cyclase (AC), which catalyses the conversion of ATP to cAMP.*

*(A) The single polypeptide chain of pGC contains an extracellular ligand binding domain (LBD), a single transmembrane domain, and an intracellular region comprised of a kinase-like domain (KLD) and a single catalytic domain (CD). These cyclases function as homodimers which require the dimerisation domain (DD) for their formation.*

*(B) Soluble GCs function as heterodimers of α and β polypeptide chains, each containing a single catalytic domain.*

*(C) The single polypeptide chain of adenylate cyclase contains two transmembrane domains ($M_1$ and $M_2$) and a cluster of cytoplasmic regions that form the catalytic centre of this enzyme [258].*

*Illustration adapted from Kobia and Gorczyca1, 2000 [263].*

Soluble-GCs are largely cytosolic and are the best known target of NO, whereby cGMP acts as nitric oxide's physiological mediator in vasodilatation and neuromodulatory functions [266]. As illustrated in *Figure 4.1.2*, sGC is composed of α and β subunits. Two α (α1 and α2) and two β (β1 and β2) subunits have been identified. Similar to pGC, these subunits are composed of easily definable domains: an N-terminal haeme-binding domain; a central subunit dimerisation domain; a C-terminal catalytic domain that is homologous to the catalytic domains of pGC and adenylate cyclases [267]. The β1 subunit serves a particularly important role as it contains a protoporphyrin IX type haeme prosthetic group attached to the histidine 105 residue (His-105), which acts as the binding site for NO [268].

As monomers, the catalytic domains of the two subunits are essentially inactive. Upon dimerisation, the catalytic domain becomes activated in what is thought to be a three step process [269,270,271,272]. Firstly, before the ligand (NO) binds, the ferrous iron is pentacoordinated within the haeme prosthetic group formed by the protoporphyrin ring. Once NO binds to the ferrous iron, a nitrosyl complex is formed, and the ferrous iron becomes hexacoordinated, with a resultant 4-fold increase in enzyme activity above the basal level. Finally, there is a breakage of the His-105 link with the porphyrin ring, which releases the ring and allows the iron to be pulled out (which remains hexacoordinated with a nitrosyl group). The result is a conformational change in the catalytic domain, and the enzyme is now said to be in its activated state with a 100-fold increase in catalytic activity [271], and a cumulative increase in activity of 400-fold over the basal level. These steps are illustrated in *Figure 4.1.3*.

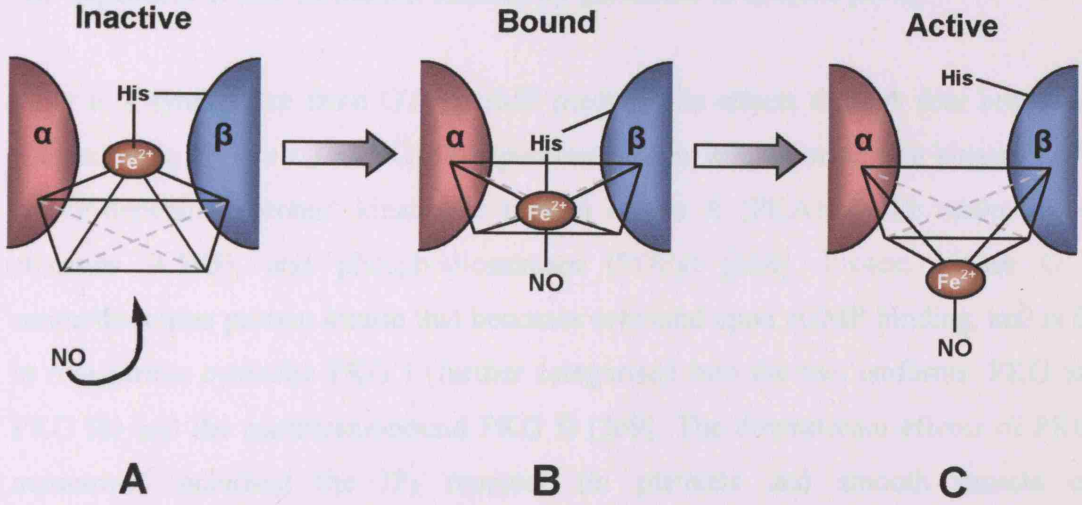


**Figure 4.1.3 Activation steps of sGC**

*(A) In its inactive form, the protoporphyrin ring containing the haeme prosthetic group exists as a 5-coordinated haeme, attached to the β subunit via the His-105 residue;*

*(B) Once NO enters, a nitrosyl bond is formed with the ferrous ion, and a 6-coordinated haeme group is created;*

*(C) Finally, the link with His-105 is broken, resulting in complete activation of the enzyme's two catalytic domains, one on each of the α- and β-subunits.*

Co-expression studies have revealed that subunit dimerisation occurs in a strictly heterodimeric fashion of one α and one β subunit, which is essential for creating a catalytically active enzyme [273]. Moreover, despite there being two forms of each subunit type, the only sGC isoforms that have been show to exist physiologically are $\alpha_1\beta_1$ and $\alpha_2\beta_1$, with respect to enzymes that can actually convert GTP to cGMP [274]. Although all sGC subunits are known to be expressed in the brain, at least at the level of mRNA [275,276], the most abundantly expressed is the $\alpha_2\beta_1$ heterodimer [277]. This has been shown to be associated with synaptic membranes, where the $\alpha_2$ subunit C-terminal amino acids associate with the PDZ[7] domain [278]. This may position the enzyme close to the NMDA (N-methyl-D-aspartic acid) receptor and also NOS1 which itself binds to the PDZ domain [176]. This could potentially be the basis for the efficient stimulation of NO-dependent cGMP formation induced by glutamate in neurons [279].

After it is synthesised from GTP, cGMP mediates its effects through four broad targets (illustrated in *Figure 4.1.4*): cGMP-dependent protein kinase, or protein kinase G (PKG); cAMP-dependent protein kinase, or protein kinase A (PKA); cyclic nucleotide-gated channels (CNG); and phosphodiesterases (PDEs) [268]. Protein kinase G is a serine/threonine protein kinase that becomes activated upon cGMP binding, and is found in two forms: cytosolic PKG I (further categorised into the two isoforms, PKG Iα and PKG Iβ) and the membrane-bound PKG II [269]. The downstream effects of PKG are numerous, including the $IP_3$ receptor (in platelets and smooth muscle cells), phospholamban (in smooth muscle cells), vimentin (in granulocytes and lymphocytes), the phosphatase inhibitor G substrate (in cerebellar Purkinje cells), and subunits of myosin light chain phosphatase [280,281,282,283]. All are mediated via protein phosphorylation. Cyclic-AMP can also interact with PKG, but does so with 50-fold less sensitivity than cGMP. Likewise, cGMP can activate PKA, but with 50-fold less sensitivity compared to cAMP [282].

Of particular significance when considering the use of a cGMP-based assay for the measurement of NO release is the activity of phosphodiesterases [284]. These enzymes catalyse the hydrolysis of the 3'-phophodiester bond of cGMP to yield 5'-GMP (as well as degradation of cAMP into 5'-AMP). Phosphodiesterases were first identified in the mid-1980s as three isoenzymes; at present 21 human PDE genes are recognised within

[7] Postsynaptic density protein (PSD-95)/*Drosophila* discs-large (dlg)/tight-junction protein (ZO1)

11 families and over 60 confirmed isoforms [285]. Any assay that measures NO release through the monitoring of cGMP changes must consider the activity of PDEs. Degradation of cGMP will obviously reduce the level of cGMP measured, with possibility of readings reaching zero if PDEs have sufficient time to act on the cGMP content of a particular lysate. Hence, a PDE inhibitor must be included within any cellular system studied. Inhibitors to specific PDE families or classes are available. However, a commonly utilised compound is 3-isobutyl-1-methylxanthine (IBMX), which is a non-specific, but wide-ranging, PDE inhibitor. Application of IBMX during the preparation of cell lysates will prevent cGMP degradation and hence allow its accumulation over time. A summary of the cGMP synthesis pathway and potential downstream effects is illustrated in *Figure 4.1.4.*

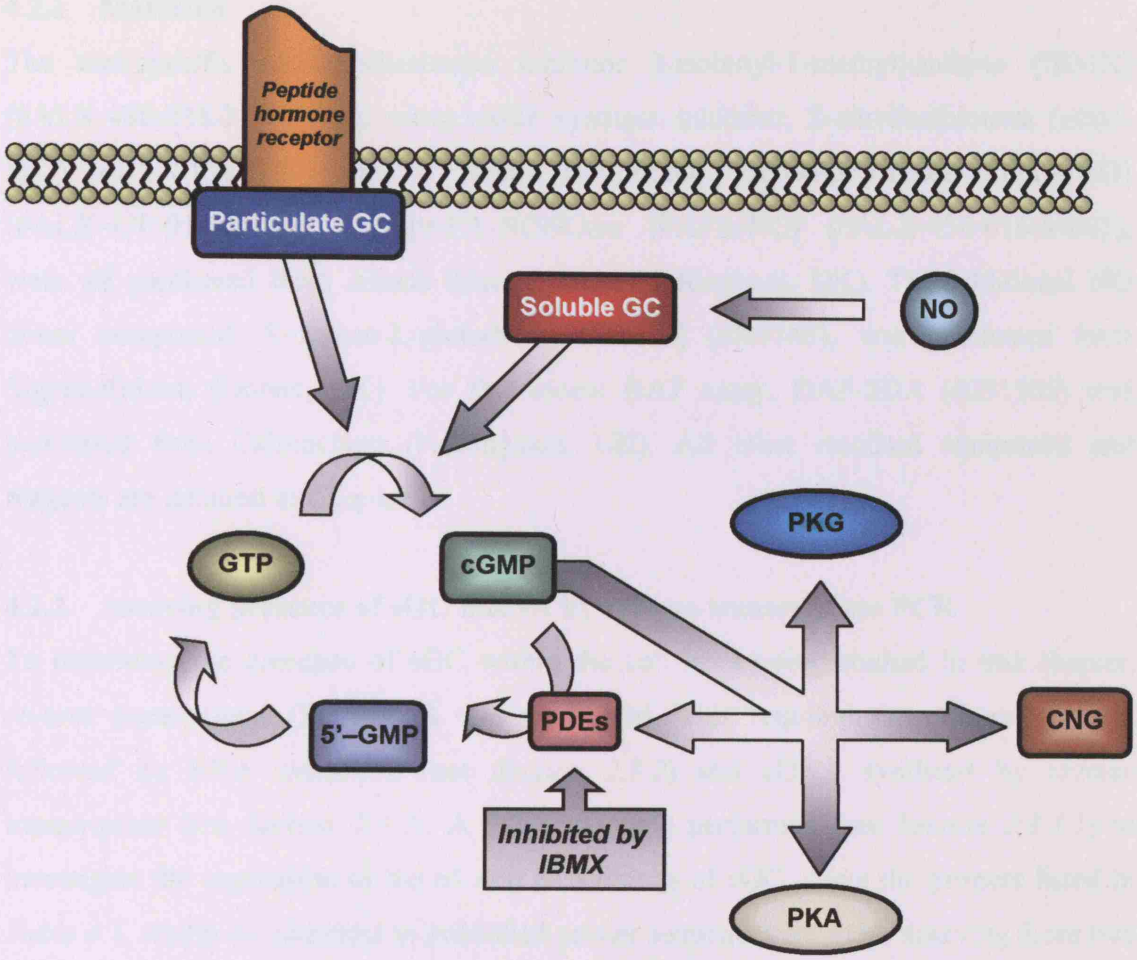


**Figure 4.1.4 The cyclic-GMP synthesis pathway and downstream effects**

*Cyclic-GMP can be synthesised by the action of either particulate guanylate cyclase (pGC) or soluble guanylate cycalse (sGC). The transmembrane pGC enzyme becomes activated by peptide hormone, which act as a ligand for its extracellular region. The cytosolically located sGC becomes activated through the conformational change induced by binding of NO to the haeme moiety of sGC. In both instances, the enzymes catalyse the conversion of GTP to cGMP. Downstream, the intracellular effects of cGMP are mediated by the activation of cGMP dependent protein kinases (PKG) and cAMP-dependent protein kinsaes (PKA) as well as cyclic nucleotide gated channels (CNG). Furthermore, cGMP regulates the activity of phosphodiesterares (PDEs), which degrade cGMP to 5'-GMP (which is then the substrate for the formation of GTP). This ensures that cGMP is kept at a basal concentration. Activity of PDEs can be inhibited using compunds such as IBMX, if it is desired to retain the synthesised cGMP.*

## 4.2 SPECIALISED MATERIALS AND METHODS

### 4.2.1 Materials

The non-specific phosphodiesterase inhibitor 3-isobutyl-1-methylxanthine (IBMX) (#ALX-480-038-M500), the nitric oxide synthase inhibitor, S-ethylisothiourea (ethyl-ITU) (#ALX-270-025), and NO donor compounds, DETA-NONOate (DETA/NO) (#ALX-430-014-M005) and PAPA-NONOate (PAPA/NO) (#ALX-430-016-M005), were all purchased from Alexis Biochemicals (Nottingham, UK). The additional NO donor compound, S-nitroso-L-glutathione (GSNO) (#N4148), was purchased from Sigma-Aldrich (Dorset, UK). For fluorescent DAF assay, DAF-2DA (#251505) was purchased from Calbiochem (Nottingham, UK). All other standard equipment and reagents are detailed in *Chapter 2*.

### 4.2.2 Assaying presence of sGC mRNA by reverse transcriptase PCR

To determine the presence of sGC within the cell lines being studied in this chapter, reverse transcriptase (RT-) PCR was performed. This required the culture of cells, followed by RNA extraction (see *Section 2.3.2*) and cDNA synthesis by reverse transcription (see *Section 2.3.3*). A PCR was then performed (see *Section 2.3.4.1*) to investigate the expression of the α1 and β1 subunits of sGC, using the primers listed in *Table 4.1*, which are identical to published primer sequences for these assaying these two genes [275].

| GENE | PRIMER | SEQUENCE (5' – 3') | PRODUCT SIZE |
|---|---|---|---|
| sGC $\alpha_1$ | Forward | CTGATTTTCCCAGAGTTTGAA | 764 bp |
| | Reverse | CTTAGGGAAGAAGTAGTAA | |
| sGC $\beta_1$ | Forward | GCTGCAAGCAAAGTCCTC | 447 bp |
| | Reverse | GATGCGTGATTCCTGGGT | |

**Table 4.1 Primers for PCR amplification of sGC subunits α1 and β1**

*Primer sequences were identical to those used by Budworth and colleagues for assaying the expression of human sGC subunits [275]. For this present study, primers were synthesised to order by Sigma-Genosys (Cambridge, UK). The expected product sizes for the reactions are also detailed.*

The PCR cycling conditions for this reaction are detailed below:

| *Reaction step* | *Temperature* | *Time* | |
|---|---|---|---|
| *Initialisation* | 95 °C | 15 min | |
| *Denaturation* | 95 °C | 1 min | |
| *Annealing* | 53 °C | 1 min | ***35 cycles*** |
| *Extension* | 72 °C | 1 min | |
| *Completion* | 72 °C | 10 min | |

### 4.2.3 Assaying presence of sGC subunit protein by Western blot

Having established the expression of sGC within cell lines, the presence of this enzyme was also investigated at the protein level. For this, polyclonal rabbit anti-human antibodies targeting the α1 sGC subunit (Sigma, #G4280) and β1 sGC subunit (Sigma, #G4405) were used. Cells were cultured in 60 mm dishes, then lysed (see *Section 2.4.1*), quantified by Bradford assay (see *Section 2.4.2*), subject to electrophoresis on a polyacrylamide gel (see *Section 2.4.3*), then Western blotted (see *Section 2.4.4*). The primary antibodies were diluted as follows in 1 % (w/v) non-fat dried milk powder in TBS-T: anti-α1 antibody diluted 1:20,000, anti-β1 antibody diluted 1:10,000. In both instances, the secondary antibody was goat anti-rabbit IgG conjugated to HRP (Sigma, #A4916) diluted 1:5,000 in 1 % (w/v) non-fat dried milk power in TBS-T.

### 4.2.4 Cell culture

#### *4.2.4.1 General cell culture*

All assays described in this chapter were performed using SH-SY5Y, CCF.STTG1, H4 or EA.hy926 cell lines. All were cultured according to the conditions and protocols described in *Section 2.2*.

#### *4.2.4.2 Preparation of apoE-conditioned medium*

ApoE conditioned medium was prepared by culturing CHO-apoE recombinant cells, as well as CHOdhfr- cells (see *Section 2.2.1*) that provided a negative control medium for treating cells. At different stages, all three CHO-apoE cell lines were cultured. For media collection, cells were grown to confluency in 75 $cm^2$ flasks. Normal culture medium was aspirated off and the cells washed 2 x with warm PBS. Cells were then grown in CD-CHO medium (Gibco, #10743-011) supplemented with 100 U/ml penicillin and 100 μg/ml streptomycin, and 2mM glutamine. Following 24 h incubation, medium was

collected from the cells and trasnferred to a fresh tube. If required, cell monlayers could be washed again with PBS and fresh CD-CHO collection medium added. Otherwise, cells were discarded.

Collected conditioned medium was filtered through a 0.20 μm syringe filter (Sartorius Minisart, Epsom, UK). Following this, the apoE concentration was determined by sandwich ELISA, detailed in *Section 2.5.* All apoE conditioned media (E3, E4 and E2) were adjusted such that their concentrations were equivalent. In addition, CHOdhfr- medium was also assayed, which indicated no detectable levels of apoE within the collected medium. For assays where a higher concentration of apoE was required, medium was passed through a Vivaspin 20 spin concentrator (Vivascience, Epsom, UK). This device allowed up to 20 ml of a given solution to be concentrated by passing it through a polyethylsulphone (PES) filter with a pore size designed to retain anything in solution above a certain molecular weight, whilst any proteins of a smaller size pass through the filtration membrane are eluted. In this instance a 30,000 Da pore size was used, which allowed concentration of the 34 kDa apoE protein present in the medium. The concentrator also features a 'dead-stop' of 50 μl, which is the volume of concentrated solution that is always retained and prevents 'drying-out' of the filtrating membrane. The concentrator adopts the same form as a 50 ml universal container. It was placed placed in a desktop centrifuge (Heraeus Megafuge 1.0R) for up to 1 h at 300 *g*, with the ambient temperature set to 4 °C.

### 4.2.5 DAF fluorescent assay

The DAF assay was performed to assess the increase in NO within a cellular system over a given time period. The assay was carried out on SH-SY5Y cells, cultured in a 48-well tissue culture plate. Cells were treated with conditioned CD-CHO medium from CHO-E3, CHO-E4 or CHOdhfr- cells. Additionally, control-conditioned medium (from CHOdhfr- cells) containing the NO donor compound, PAPA/NO, was also prepared.

#### *4.2.5.1 Pre-treatment of cells with DAF-2 DA*

The protocol requires cells to be pre-treated with DAF-2 DA before exposure to treatment medium. Due to its high photosensitivity, whenever possible DAF was handled in the dark. A range of DAF concentrations were prepared by the dilution of the stock DAF solution (5 mM concentration in DMSO) in 0.25 % (w/v) BSA solution to give an

initial diluted DAF concentration of 0.2 mM. This was further diluted in 1 M HEPES buffer to give a final concentration between 5 μM to 0.05 μM, as required.

Culture medium was aspirated off the cells on the 48-well plate. After washing 3 x with 0.5 ml/well warm PBS, cells were loaded with 200 ml/well DAF solution at the required dilution. The plate was wrapped in foil and incubated for 1 h at 37 °C.

#### *4.2.5.2 Fluorescent assay protocol*

Following pre-treatment of the cells with DAF, cells were exposed to the required treatment medium, prepared as described in *Section 4.2.5.2*. In addition, the NO donor compound PAPA/NO was used, prepared in 10 mM NaOH to give a final working concentration of 50 μM in control-conditioned medium. Furthermore, some wells were treated with conditioned medium (apoE and control medium) containing 20 μM ethyl-ITU. This is a nitric oxide synthase inhibitor, which should abolish any NO generating effects that a particular medium may have. Each well of cells was treated with 500 μl/well with the appropriate treatment medium. Whilst keeping the plate covered, it was quickly placed inside the CytoFluor 4,000 (Applied Biosystems, Warrington, UK) fluorescent plate reading machine, which had been set to emit an excitation signal at 485 nm and measure emission at 530 nm. The fluorescence was sampled every 2 min and recorded by the attached computer software to give a complete experiment duration of 4 h. Collated data were transferred to Microsoft Excel for further analysis.

### 4.2.6 Cyclic-GMP enzymatic immunoassay (EIA)

Concentrations of cGMP were measured with the Assay Designs Inc. Correlate-EIA™ Direct Cyclic-GMP Enzyme Immunoassay Kit (#900-014), from Metachem Diagnostics (Nottingham, UK). The assay consisted of a 96-well plate, pre-coated with a goat anti-rabbit IgG capture antibody and a detection antibody that was directed against cGMP. The plate had 12 break-away strips of wells such that a column of 8 wells could be used at a time. The whole kit and its contents were stored at 4 °C until required for use; specifically, the plate was stored in a sealed foil desiccator to prevent entry of any moisture.

The kit utilises a competitive immunoassay in order to determine the concentration of cGMP within samples loaded in the wells. All samples were treated with HCl, which functions both as a lysis reagent and, according to the accompanying documentation, as

an inhibitor of endogenous PDEs to stabilise cGMP. As such, no other PDE-inhibitor was used to supplement the treatment medium. Within each well of the plate, a polyclonal anti-cGMP antibody binds in a competitive manner with cGMP from either the standards/samples or an alkaline phosphatase (AP) conjugated cGMP molecule. Once excess reagents were washed from the wells, a substrate was added that reacts with AP and a colour change is observed. The OD of each well was measured using a plate-reader that will show an inversely proportional relationship between the OD value and cGMP concentration. The ODs of the standards can then be plotted, allowing cGMP concentrations of the samples to be determined. To further enhance the sensitivity when samples with low concentrations are being assayed, all samples and standards can be acetylated: a process that enhances the binding affinity of cGMP to its antibody.

#### *4.2.6.1 Preparation of cell lysates for assay*

The EIA kit was used to measure cGMP concentration in cultured SH-SY5Y cells grown in 6-well tissue culture plates. Cells were treated with conditioned medium from CHO-E3, CHO-E4 or CHOdhfr- cells, prepared in the manner described in *Section 4.2.4.2*. In addition, cells were treated with control-conditioned medium containing either 300 μM DETA/NO or 300 μM GSNO nitric oxide donors, both prepared initially in 0.1 M NaOH as they are activated in a physiological pH solution, such as cell culture medium.

Once ready, cells in individual wells were washed 2 x with warm PBS, and 1 ml/well warm treatment medium added as appropriate: E3- or E4-conditioned medium, control-conditioned medium, and NO donor containing control-conditioned medium. Plates were incubated for 6 h at 37 °C before harvesting. For this, treatment medium was aspirated off and 0.5 ml/well trypsin/EDTA solution added. Once all cells had detached from the surface of the well (as observed by phase-contrast microscopy), cell suspensions were transferred to 1.5 ml Eppendorf tubes. Following centrifugation at 13,000 rpm for 10 min, supernatant was aspirated off and the cell pellet resuspended in 100 μl 0.1 M HCl added and samples incubated for 10 min at room temperature. To ensure complete cell lysis, tubes were subject to rapid freeze-thawing using a Dewer-flask containing liquid nitrogen and a 37 °C water bath: samples were transferred alternately between each container, four times. Following this, samples were vortexed briefly and centrifuged. Finally, lysates were transferred to fresh tubes and stored at -20 °C for long-term storage, or at 4 °C for up to a week.

#### *4.2.6.2 Cyclic-GMP EIA procedure*

The assay was performed according to the manufacturer's instructions, with all samples and standards acetylated. Briefly, standards were prepared by serial dilutions of the cGMP standard (5,000 pmol/ml stock concentration) in 0.1 M HCl to give a highest concentration cGMP standard of 10 pmol/ml, down to 0.08 pmol/ml. The acetylation reagent was prepared by mixing acetic anhydride with triethylamine (both provided with the kit) at a ratio of 1:2, respectively. This reagent was added to each sample and standard such that every 200 µl of solution was supplemented with 10 µl acetylation reagent. Once prepared, all tubes were vortexed for at least 2 sec each, and then left to incubate overnight at 4 °C.

The required strips of the pre-coated assay plate were retrieved from 4 °C storage. To each well, 25 µl/well *pink neutralising reagent*, followed by 50 µl of samples or standards as appropriate. Immediately after this, 25 µl/well *blue conjugate* was added, followed by 25 µl/well *yellow antibody* solution. The plate was covered with film and incubated for 2 h at room temperature with constant agitation using an orbital shaker. Following this, the plate was washed 3 x with 200 µl/well manufacturer's wash solution (Tris-buffered saline containing detergents). Then, 100 µl/well p-nitrophenyl phosphate (p-Npp) substrate was added and the plate incubated for 1 h at room temperature without any shaking *or* covering. To stop the reaction, 25 µl of stop solution was added to each well and the plate immediately transferred to a plate reader to measure the OD at 405 nm.

### 4.2.7 Cyclic-GMP radioimmunoassay (RIA)

Similar to the EIA protocol described above, this radioimmunoassay (RIA) utilises the competitive interaction between cGMP of a standard/sample and a known content of labelled cGMP within the reaction. While in EIA, the cGMP was conjugated to alkaline phosphatase, in RIA the cGMP is radiolabelled with $^{3}H$, which can then be assayed by liquid scintillation counting. Garthwaite's group has developed a RIA that is sensitive and robust [286], having been used successfully to measure cGMP release in a number of studies [287,288,289]. The identical RIA was used in this present study.

#### *4.2.7.1 Preparation of cell lysates for assay*

The cGMP response was assayed using SH-SY5Y cells treated with conditioned medium containing apoE3, apoE4, apoE2 or control-conditioned medium from CHOdhfr- cells. Additionally, the NO donor, PAPA/NO (50 µM prepared in 10 mM NaOH), was used as

a positive control to establish whether a response could be achieved in this system. The SH-SY5Y cells were cultured in 12-well plates until they reached sub-confluency. The different conditioned media were prepared such that equivalent concentrations of apoE were present, as described in *Section 4.2.4.2*. Furthermore, all treatment media contained 1 mM IBMX (prepared in DMSO, to give a final DMSO working concentration of 0.1 %), which would inhibit the breakdown of cGMP by the activity of endogenous phosphodiesterases. All dilutions, as well as the NO donor containing treatment medium, were prepared using control-conditioned medium (CHOdhfr-).

Culture medium was aspirated off and the cells were washed 2 x with warm PBS. Each well was then loaded with 0.5 ml of the appropriate treatment medium and the plates returned to the 37 °C incubator. Each well of cells on the 12-well plate represented a particular time-point over which the assay was monitored, with a time-points ranging from 1 min to 120 min post-exposure to the medium. At the completion of a time-point, the plates were removed from the incubator and the treatment medium aspirated off. Cells were washed briefly 1 x with ice-cold PBS, following which they were treated with 200 µl inactivation buffer (50 mM Tris.HCl, 4 mM EDTA, pH 7.4) supplemented with 10 % (v/v) trypsin/EDTA. After incubation for 10 min at room temperature with this solution, the lysates were collected from the wells and the samples boiled using a heat-block set at 100 °C. Lysates were stored at -20 °C for long-term storage, or at 4 °C for up to a week.

#### *4.2.7.2 Cyclic-GMP RIA procedure*

All solutions were prepared using the Tris.HCl/EDTA inactivation buffer described above. All standards were prepared, in 1.5 ml Eppendorf tubes, as duplicates using a stock cGMP standard of 8 pmol, which was serially diluted to give a range of concentrations, from 8 pmol/tube through to 0.25 pmol/tube. Additionally, a 'blank' standard of 10 µM was included, which was a saturating concentration of cGMP that would give the zero value for the analysis. Finally, a tube containing inactivation buffer only was added as a negative control.

All samples (prepared as described in *Section 4.2.7.1*) were initially centrifuged at 12,000 rpm for 4 min at 4 °C. A fresh set of 1.5 ml tubes were prepared, each containing 50 µl radiolabelled [$^3$H]-cGMP, and to each tube was added 100 µl of sample. Additional tubes contained standards (100 µl) and [$^3$H]-cGMP (50 µl/tube). Finally, to all tubes, 50 µl of

anti-cGMP antibody was added, the tubes vortexed and incubated on ice and placed in a in a 4 °C refrigerator for 2 h. Following this, the antibody content of the tubes was precipitated out using ammonium sulphate, $(NH_4)_2SO_4$. To each tube, 1 ml ice-cold saturated $(NH_4)_2SO_4$ solution was added, vortexed thoroughly and then incubated on ice for 5 min. The tubes were then centrifuged at 12,000 rpm for 4 min at 4 °C to precipitate the antibody, which would be visible at the bottom of the tube as a distinctive white deposit. Supernatant was aspirated from all tubes, and the precipitate was resuspended in 1 ml distilled $H_20$.

Meanwhile, scintillation vials for radioactive counting were prepared by the addition of 5 ml scintillant. When ready, samples in distilled water were vortexed in order to homogenise the antibody/antigen pellet. From each tube, 950 µl was transferred into a appropriately labelled and prepared scintillation vial. After addition, the tubes were capped tightly and vortexed vigorously to prevent emulsification, before being placed in processing racks for scintillation counting using the LS 6500 multi-purpose scintillation counting system (Beckman Coulter, Buckinghamshire, UK). Scintillation counts were recorded by this machine as disintegrations per minute (dpm) for each vial. Upon completion, the complete data was transferred to Microsoft Excel for further analysis.

## 4.3 RESULTS

### 4.3.1 DAF fluorescent assay to monitor NO release

The DAF fluorescent assay was investigated as a strong potential candidate assay for monitoring NO release. There are a number of benefits that this approach offers: real-time measurement of NO, negating the need to produce cell lysates; a variety of cell conditions and treatments which can be monitored within a single experiment; and all data are directly logged electronically using a computer connected to the fluorimeter, providing more direct means of analysing measurements.

Presented in *Figure 4.3.1* is a typical set of data generated by this assay. SH-SY5Y cells were cultured in a 48-well plate. When ready to use, they were washed with warm PBS then pre-treated with varying concentration of DAF 2-DA, in this instance 2 μM, 1 μM and 0.5 $\mu$M concentrations. During the pre-treatment stage, the fluorescent compound permeates the cell membrane to be cytosolically internalised. Following this, cells were exposed to control-conditioned medium that contained 100 μM of the nitric oxide donor compound, PAPA/NO. Cells were assayed at 2 min intervals over a time-course of 4 h. As these were preliminary experiments, no attempt was made to calibrate measured fluorescence against known NO concentrations. As such, the fluorescence absorbance in arbitrary units was used as the measurement in this assay. This figure illustrates how variations in the concentration of DAF 2-DA pre-treatment can markedly affect the overall fluorescence measured during the assay. Furthermore, after ~40 minutes, the system appears to reach a saturation point beyond which no more DAF nitrosation occurs, which likely represents the point at which PAPA/NO has liberated all NO that it is capable of delivering to the cells.

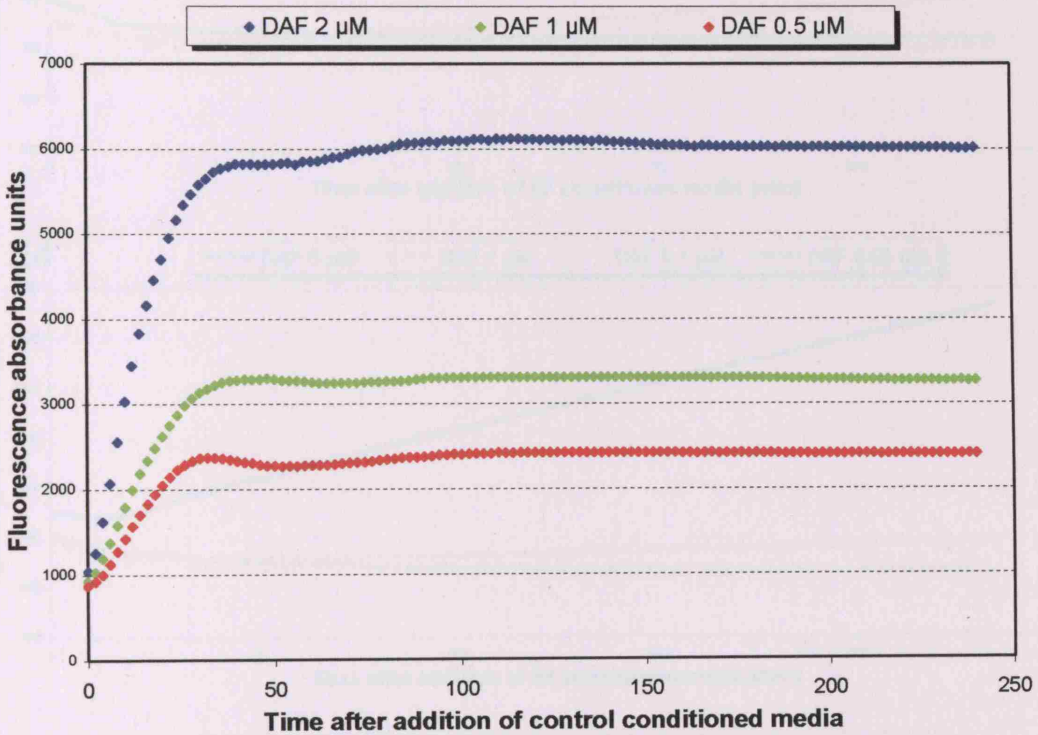


**Figure 4.3.1 Response of SH-SY5Y cells to treatment with PAPA/NO following varying concentrations of DAF 2-DA pre-treatment and monitored by DAF fluorescent assay**

*Following pre-treatment with varying concentrations of DAF 2-DA (0.5 µM, 1 µM and 2 µM), SH-SY5Y cells were exposed to control-conditioned medium (CHOdhfr-) containing 100 µM PAPA/NO, an NO donor compound that liberates NO with a half-life pf 15 min at pH 7.4 and 37 ºC. Fluorescence was sampled every 2 min over a complete 4 h time-course. At each time-point, individual wells were measured in triplicate by the fluorimeter. The mean averages of these were calculated and represent each datum point on the above graph.*

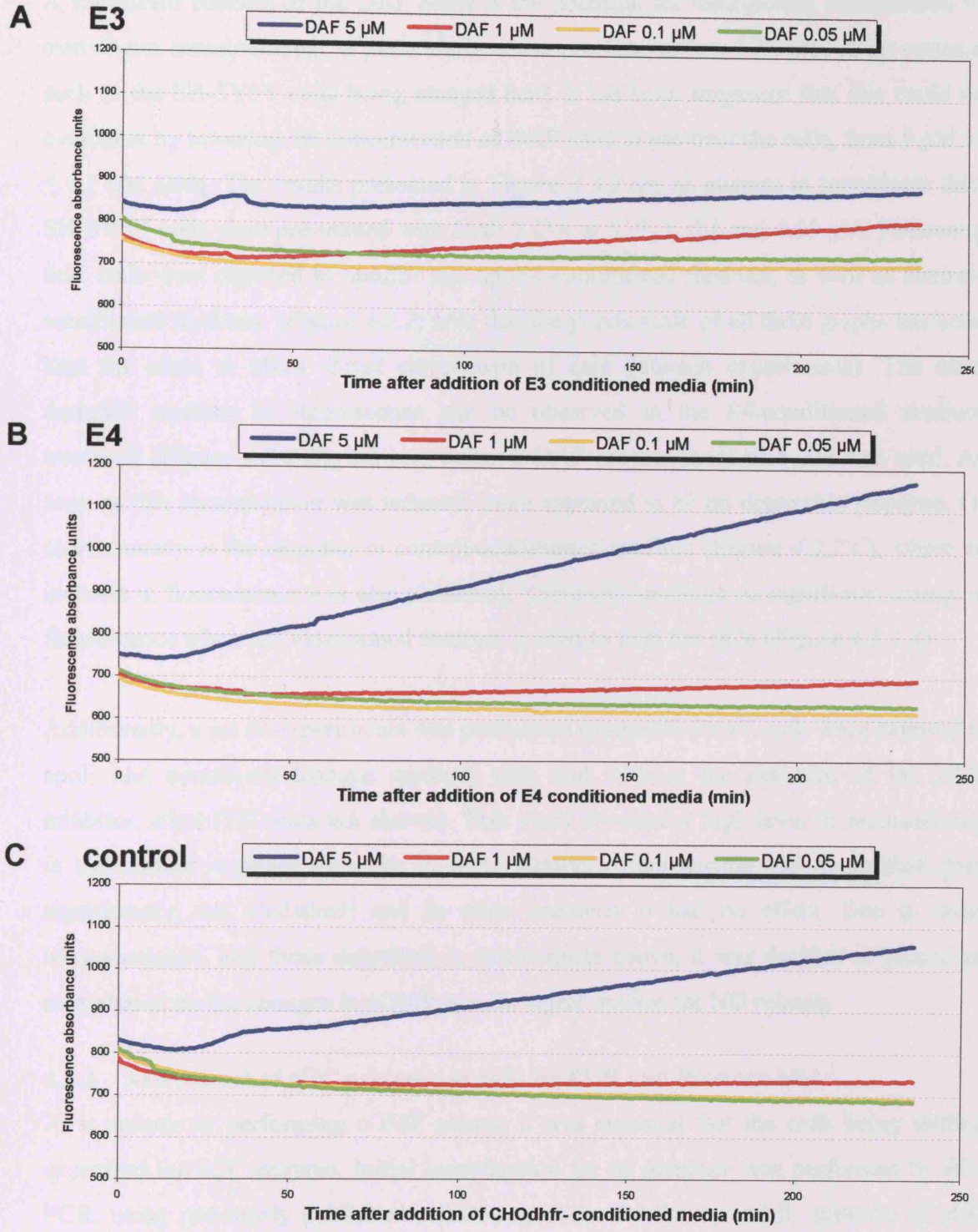


**Figure 4.3.2 DAF assay of SH-SY5Y cells' exposure to conditioned medium**

*Cells were exposed to equivalent concentrations of (A) E3, (B) E4, and (C) control-conditioned medium, following pre-treatment with DAF 2-DA at 0.05 µM, 0.1 µM , 1 µM and 5 µM. Fluorescence was sampled every 2 min over the 4 h time-course. At each time-point, individual wells were measured in triplicate by the fluorimeter software. The mean averages of these were calculated. The graphs presented are computer-determined lines of best-fit of these data to represent the fluorescence response.*

A significant concern of the DAF assay is the potential for background fluorescence to overwhelm measurements, a particularly acute problem in low NO producing systems such as the SH-SY5Y cells being assayed here. It has been suggested that this could be overcome by lowering the concentration of DAF used to pre-treat the cells, from 5 μM to ≤ 0.1 μM [290]. The results presented in *Figure 4.3.2* are an attempt to investigate this. SH-SY5Y cells were pre-treated with DAF 2-DA at 5, 2, 1, 0.1 and 0.05 μM. Following this, cells were exposed to apoE3- and apoE4-conditioned medium, as well as control-conditioned medium. (*Figure 4.3.2*; note that the y-axis scale of all three graphs has been kept the same to allow direct comparison of data between experiments). The most dramatic increase in fluorescence can be observed in the E4-conditioned medium treatment (*Figure 4.3.2 B*), but only when a DAF pre-treatment of 5 μM was used. As soon as this concentration was reduced, there appeared to be no detectable response. Of more concern is the response to control-conditioned medium (*Figure 4.3.2 C*), where an increase in fluorescence was also measured. There appears to be no significant change in fluorescence when E3-conditioned medium is used to treat the cells (*Figure 4.3.2 A*).

Additionally, a set of experiments was performed where SH-SY5Y cells were exposed to apoE and control-conditioned medium with and without the presence of the NOS inhibitor, ethyl-ITU (data not shown). This study revealed a high level of inconsistency in the cellular response detected: in some instances fluorescence was diminished (but, significantly, not abolished) and in other instances it had no effect. Due to these inconsistencies, and those described in experiments above, it was decided to pursue an assay based on the changes in cGMP as a surrogate marker for NO release.

### 4.3.2 Assessment of sGC presence in cells by PCR and Western blot

As a prelude to performing cGMP assays, it was essential that the cells being studied expressed the sGC enzyme. Initial investigation for its presence was performed by RT-PCR, using previously published primer sequences for the $\alpha_1$ and $\beta_1$ subunits of sGC [275]. To check that reverse transcription of extracted RNA to cDNA had been processed correctly, an additional PCR was performed using primers to target the ubiquitously expressed housekeeping gene β-actin (see *Chapter 3, Table 3.1*) (data not shown). The results of this investigation revealed that the cell lines used in this chapter (SH-SY5Y, CCF.STTG1, H4 and EA.hy926) all expressed the two subunits of sGC, at least at the mRNA level (see *Figure 4.3.3*).

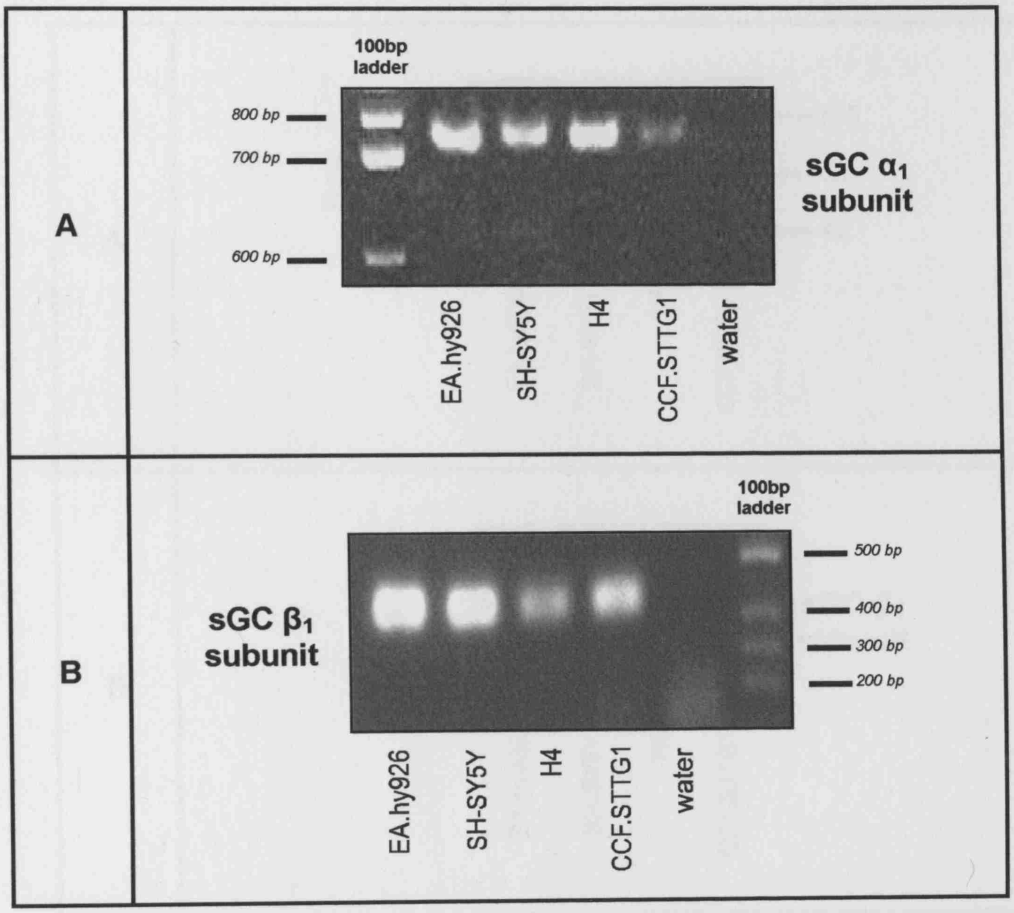


**Figure 4.3.3 Reverse-transcriptase PCR investigation of sGC expression in a range of human cell lines**

*The expression of (A) $\alpha_1$ and (B) $\beta_1$ subunits of sGC were investigated by PCR. For each reaction, 300 ng of cDNA from each cell line (EA.hy926, SH-SY5Y, H4 and CCF.STTG1) was used. Negative control was a PCR with template replaced by water. Expected product sizes: sGC $\alpha_1$ subunit 764 bp; sGC $\beta_1$ subunit 447 bp. For reference, 100 bp ladders are included showing relative sizes of the different PCR products. All products were run on a 2% agarose gel and visualised by ethidium bromide staining.*

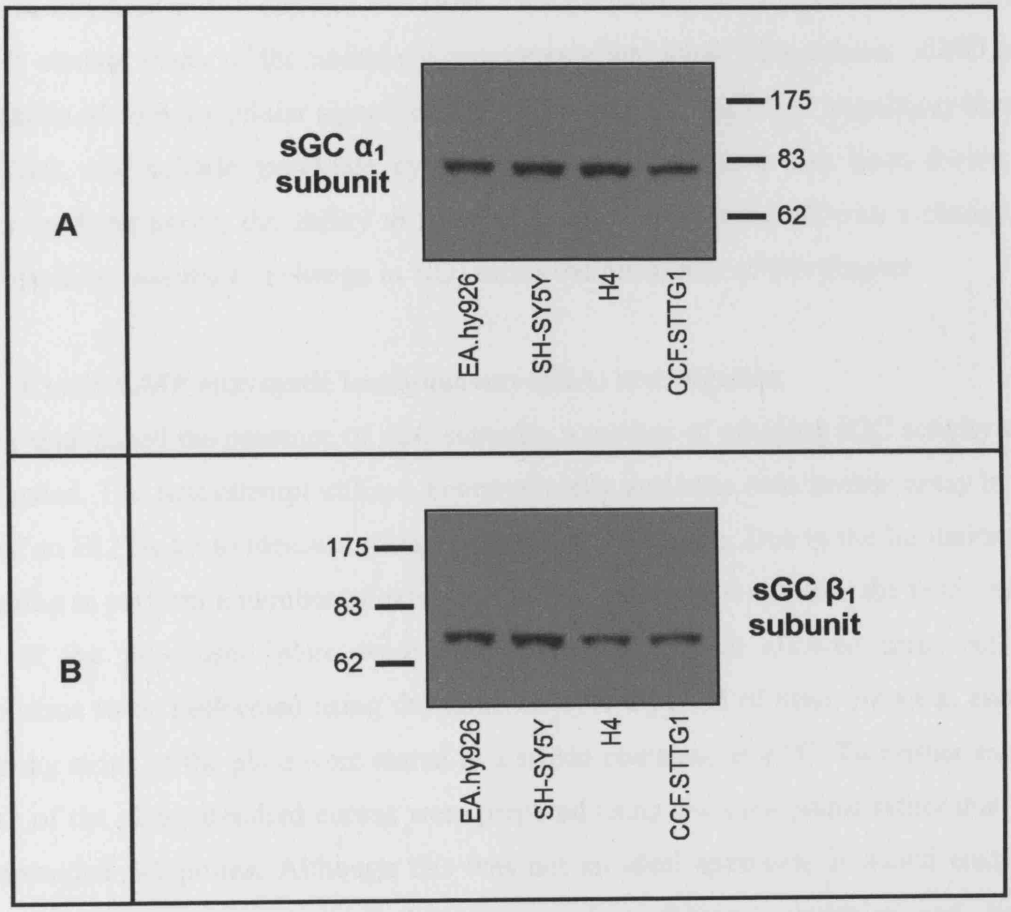


**Figure 4.3.4 Immunoblot investigation of sGC subunit expression in a range of human cell lines**

*The presence of (A) $\alpha_1$ and (B) $\beta_1$ subunits of sGC were investigated by Western blotting. Antibodies used detected $\alpha_1$ subunit at ~80 kDa and $\beta_1$ subunit at ~70 kDa. Lysates from a range of cell lines were tested: EA.hy926, SH-SY5Y, H4 and CCF.STTG1. Protein bands were visualised by HRP chemiluminescence. Pre-stained protein markers were also included to enable estimation of molecular weights (not shown).*

For further validation, an immunoblot was performed using antibodies to target the $\alpha_1$ and $\beta_1$ subunits of sGC, shown in *Figure 4.3.4*. This demonstrated that all four cell lines contained the two sGC subunit proteins. Combined with the quantitative PCR data discussed in *Chapter 3*, it appears that these cells (in particular SH-SY5Y, CCF.STTG1 and H4) contain many of the necessary components that allow biosynthesis of NO and propagation of an intracellular signal: nitric oxide synthases, the NOS3 regulatory kinase (PKB/Akt), and soluble guanylate cyclase. Although they have also been shown to express apoE receptors, the ability to respond to stimulation by apoE with a change of cGMP (and, by inference, a change in NO) forms the remainder of this chapter.

### 4.3.3 Cyclic-GMP enzymatic immunoassay (EIA) investigation

Having established the presence of sGC subunits, a method of assaying sGC activity was investigated. The first attempt utilised a commercially available colorimetric assay in the form of an ELISA kit to measure changes in cGMP production. Due to the limitations of attempting to perform a number of experiments on a single 96-well plate, the break-away strips of the pre-coated plate were used separately, which allowed three sets of experiments to be performed using the same kit over a period of time. Between assays, remaining strips of the plate were stored in a sealed container at 4 °C. To further extend the use of the plate, standard curves were prepared using 3-4 data points rather than the recommended 5-6 points. Although this was not an ideal approach, it would enable a broad preliminary evaluation of the assay against different variables and lysate preparations.

Displayed in *Figure 4.3.5* are two typical standard curves achieved using this assay. Due to this being a competitive assay, the higher the cGMP concentration of the sample/standard being assayed, the lower the OD measured. As discussed, it would have been preferable to have a wider range of cGMP concentrations for the generation of this standard curve. The manufacturer's recommendations for standards range from 50 pmol/ml through to 0.08 pmol/ml, with the standard curve following an almost sigmoidal pattern. For the purposes of these early experiments, only those that remained within a relatively linear region of the standard curve were included: from 0.08 pmol/ml to 10 pmol/ml. It should be also noted that at 10 pmol/ml, the OD measured was virtually 0 after subtraction of background fluorescence. The documentation accompanying the kit stated the assay should detect cGMP concentrations up to and exceeding 100 pmol/ml, a feature that could not be accurately substantiated with the available data.

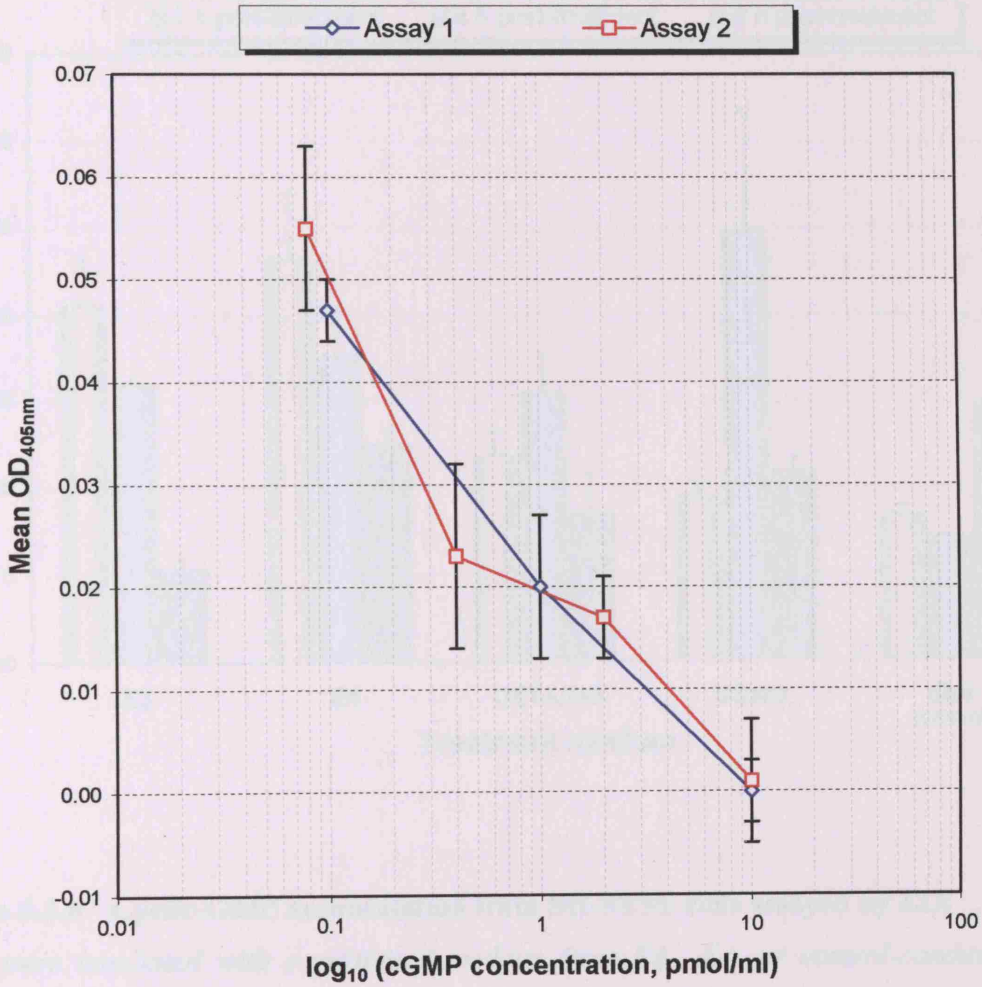


**Figure 4.3.5 Standard curves generated by cGMP EIA protocol**

*Data were collected from two separate assays, and optical densities have been corrected for background fluorescence. All samples were acetylated prior to their addition and duplicate measurements were performed at each concentration. Sample treatment was identical in both experiments. Each datum-point represents a mean average of duplicate measurements (± standard error).*

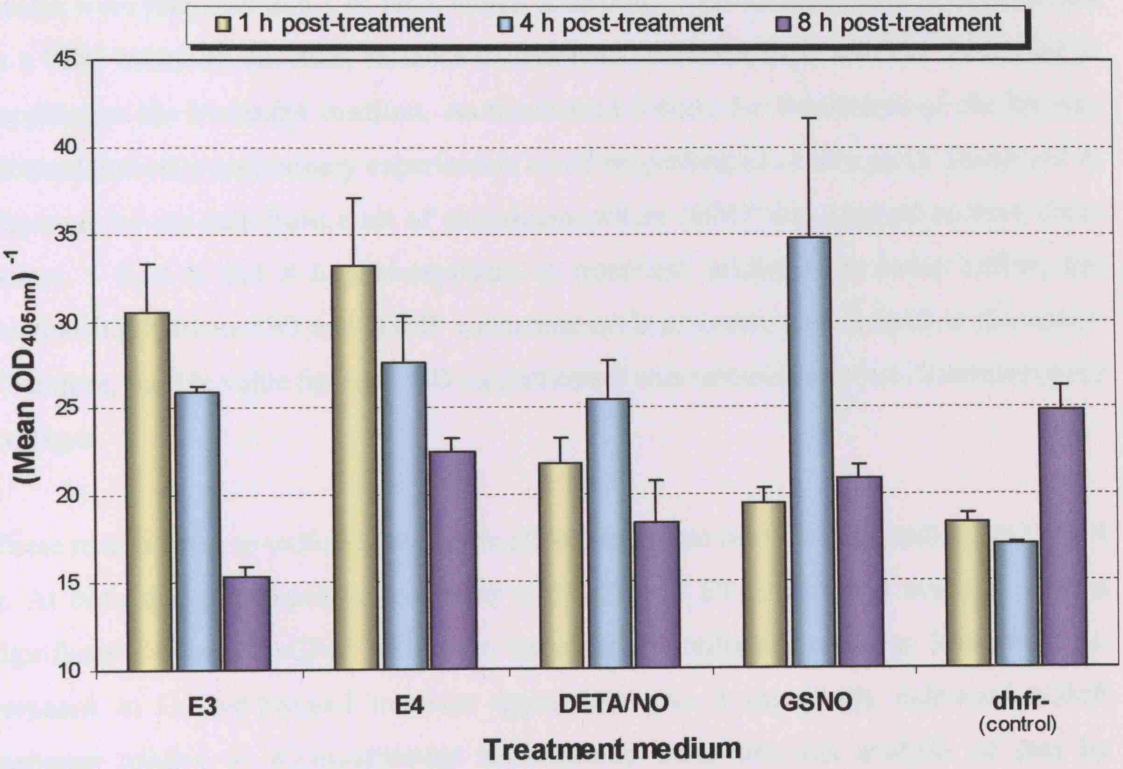


**Figure 4.3.6 Cyclic-GMP accumulation from SH-SY5Y cells assayed by EIA**

*Cells were incubated with conditioned medium from E3-, E4- or control-conditioned medium, or with NO donor compound (DETA/NO and GSNO), and assayed at 1 h, 4 h and 8 h post-exposure. Lysates were prepared at these time-points and cGMP assay performed using the EIA kit. For each lysate, duplicate measurement were performed on the 96-well plate; as this is a competitive assay, OD measurements are inversely proportional to the actual cGMP concentration within each reaction, therefore all ODs were inverted by calculating the 1/x (where x = OD) value for each measurement. As such, each bar represents the (mean average OD)$^{-1}$ of a duplicate of measurements (± standard error of inverted measurements).*

For assays, 6-well plates were seeded with SH-SY5Y cells at 0.1 x $10^6$ cells per well 24 h previous to treatment. Cells were treated with E3-, E4- or control-conditioned medium. As positive controls, two NO donor compounds, DETA/NO and GSNO, were used, both added at 300 μM (in 10 mM NaOH). All treatments were performed in duplicate. Cell lysates were prepared in 0.1 M HCl, which according to the manufacturer's protocol acts as a PDE inhibitor. As such, in these experiments, no other PDE inhibitor was used to supplement the treatment medium. As mentioned before, the limitations of the kit size dictated that only preliminary experiments could be performed on this plate. Displayed in *Figure 4.3.6* are data from a set of experiment where cGMP was assayed at three time-points: 1 h, 4 h and 8 h post-exposure to treatment medium. As noted before, the relationship between OD and cGMP concentration is inversely proportional in this assay. Therefore, the 1/x value for each OD measurement was calculated before determining the averages.

These results seem to indicate detectable cGMP increases over control medium at 1 and 4 h. At both these time-points, treatment with E3- and E4-conditioned medium gives a significantly elevated cGMP level over the control-conditioned medium. Moreover, the response to E4-conditioned medium appears to give a marginally enhanced cGMP response relative to E3-conditioned medium exposure, although analysis of data by Student's T-test reveals that this is not significant: at the 1 h time-point, P = 0.76, whilst at 4 h this is 0.66. However, when analysing the relationship between apoE3 and apoE4 exposure relative to control-conditioned medium, the results are apparent: T-testing give P values of 0.12 and 0.18 for E3- and E4-medium exposure, respectively. A similar observation can be made at the 4 h time-point. Rather intriguingly, both E3 and E4-conditioned medium gave a dramatic decrease in cGMP release between 4 h and 8h. In particular, exposure to E3-conditioned medium displayed a 41 % decrease in cGMP during this 4 h period until 8 h post-exposure to medium. However, during the equivalent time-period when exposed to control-conditioned medium, a 35 % increase in cGMP can be observed.

The response to NO donor compounds follow a similar trend to each other: an elevation in cGMP release between 1 h and 4 h exposure, which then returns to a basal level by 8 h. This is particularly noticeable in the cells treated with GSNO, where a 75 % increase in cGMP occurs during this time period, which returns to back to the level 1 h level to a relatively basal level by 8 h.

Beyond this point the cells' resources are either being exhausted or the cells are responding to shock in some way such that regardless of treatment medium, the cGMP concentrations all tend towards a similar value of 0.1 – 0.2 pmol/ml. This was also the case in the control-conditioned medium treatment, where the cGMP concentration was initially at a relative baseline, but then started to increase after the first 4 h. These cells are clearly capable of producing cGMP in response to an NO increase as evidenced by the responses to both DETA/NO and GSNO. However, the response to apoE was less pronounced. Although initially cGMP levels were high, there was a rapid decrease during the first 4 h, which continued until the end of the assay. Furthermore, there was no distinct difference between cells treated with either E3- or E4-conditioned medium. Cells treated with E4 medium appeared to have a slightly higher cGMP concentration over those treated with E3 medium. Having only performed the experiments with duplicate readings, it is very difficult to conclusively state whether or not this is a physiologically and statistically significant difference. Furthermore, as detailed previously, HCl was used to prepare the lysates and was reported to act as a PDE inhibitor. There is a possibility that if a compound such as IBMX were utilised, a more pronounced cGMP response may have been observed.

### 4.3.4 Radioimmunoassay of cGMP concentration

Due to the limitations of the enzymatic assay that became apparent during investigation, another assay method was considered. A radioimmunoassay technique for monitoring the concentration of cGMP had been developed by Garthwaite's group and had proven a successful and sensitive assay method [286]. The reagents for this assay were readily available, which allowed a number of investigations to be performed.

Shown in *Figure 4.3.7* is a typical standard curve generated by this assay. It follows an expected sigmoidal pattern, with a region of relative linearity between 0.5 pmol/tube and 4 pmol/tube. Despite minor differences in OD measured between individual assays, the overall inter-assay variability was very consistent (data not shown). It should be noted that unless otherwise stated all subsequent experiments performed using this protocol were done so in the presence of the non-specific PDE inhibitor 3-Isobutyl-1-methylxanthine (IBMX), which would stabilise any synthesised cGMP before it could be degraded by endogenous PDEs.

### 4.3.5 Cyclic-GMP RIA optimisation: time-course and cell culture conditions

An initial investigation of the response of SH-SY5Y cells was performed using time-course assays, from 1 min up to 8 h post-treatment. However, it was discovered that after 15-20 min, cell adherence was greatly diminished with a significant number of cells becoming detached and floating in suspension. When the treatment medium was aspirated off the wells, these cells would be lost and therefore incapable of contributing towards the cell lysate. In a system such as this where NO release is likely to be very low, loss of any cellular material before the preparation of the lysate would greatly attenuate the overall signal. Furthermore, such a phenomenon introduces an unnecessary degree of inconsistency to experiments to such an extent that comparison of different assay variables becomes unreliable over extended time-courses. A similar event is likely to have occurred during the preparation of lysates for the EIA investigation (described in *Section 4.3.3*), but had, in that instance, been overlooked.

Due to the potential for this form of cellular detachment to occur, assays were performed at 10 min post-treatment. This would give a reasonable view of how the cells were responding before any wholesale loss of cells occurred. However, one consequence of this modification to the protocol was that DETA/NO was no longer suitable for the assay. With a half-life of 20 h, this compound would not be capable of generating enough NO during a 10 min exposure. In comparison, PAPA/NO has a half life of 15 min, which is far more suitable for a short exposure time [291].

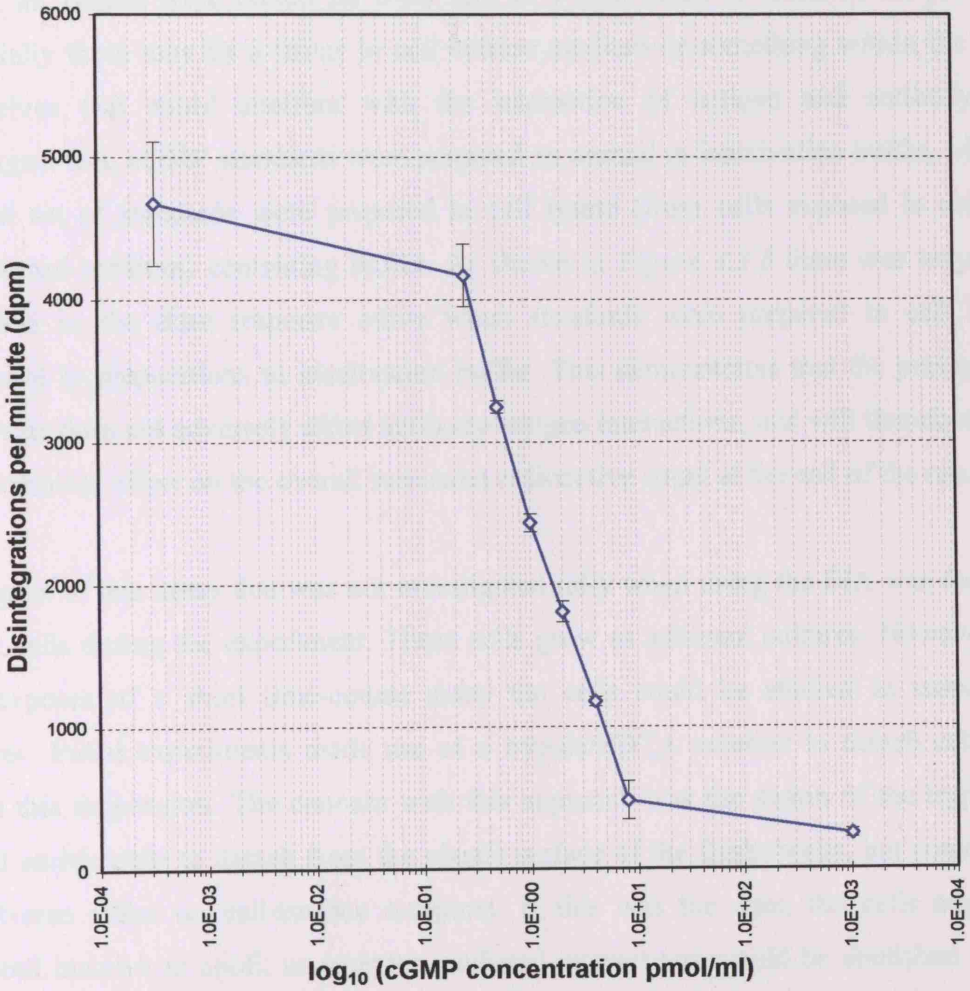


**Figure 4.3.7 Standard curve generated by cGMP RIA protocol**

*Dose-response of measured disintegrations per min (dpm), by liquid scintillation counting, to increasing concentrations of cGMP standards. Samples and standards were treated with the same reagents and handled identically. The lowest concentration, at $1x10^{-8}$ pmol/tube, represents essentially a buffer only sample. The highest concentration, at 1,000 pmol/tube, represents a saturating concentration of cGMP such that virtually all free antibodies in solution is sequestered by radiolabelled cGMP. Each point represents the average dpm count measured from duplicate scintillation vials (± standard error).*

Lysates for the RIA were prepared using a Tris/EDTA inactivation buffer. This buffer would both inactivate endogenous enzymes and lyse cells. Following collection in this buffer, all lysates were boiled for 5-10 min in a heat block to denature all proteins. Potentially there may be a factor in cell culture medium or something within the cells themselves that could interfere with the interaction of antigen and antibody. To investigate this, cGMP standards were prepared as normal in inactivation buffer, while a parallel set of standards were prepared in cell lysate (from cells exposed to control-conditioned medium) containing buffer. As shown in *Figure 4.3.8* there was very little deviation in the dose response curve when standards were prepared in cell lysate compared to preparations in inactivation buffer. This demonstrates that the presence of cell lysate does not adversely affect antibody/antigen interactions, and will therefore have no discernible effect on the overall measured radioactive count at the end of the reaction.

An aspect of this assay that was not investigated fully when using the EIA was the state of the cells during the experiment. These cells grow as adherent cultures. However, for the purposes of a short time-course assay the cells could be studied as suspension cultures. Initial experiments made use of a trypsin/EDTA solution to detach cells and create this suspension. The concern with this approach was the action of the trypsin: it would enable cells to detach from the plastic surface of the flasks/wells, but could have an adverse effect on cell-surface receptors. If this was the case, the cells might be rendered inactive to apoE, as receptor mediated interactions would be abolished by the action of trypsin/EDTA on cell surface receptors. The results presented in *Figure 4.3.9* seem to support this scenario. Cell suspensions were generated by incubating with trypsin/EDTA, followed by exposure to either E3-conditioned medium or medium prepared with the NO donor, GSNO. Little or no cGMP release was detectable in the cells treated with E3 medium, even 2 h post-treatment. A similarly poor response was observed if the conditioned medium were concentrated or diluted 10-fold (data not shown). Additionally, control-conditioned medium produced a similar output as E3-conditioned medium in this experiment (data not shown so as not to avoid confusion with datum-points of the E3 response curve, as they deviate very little from these points). In contrast, there was a pronounced release of cGMP when cells were treated with GSNO, with the peak saturation of response occurring ~60 min post-treatment.

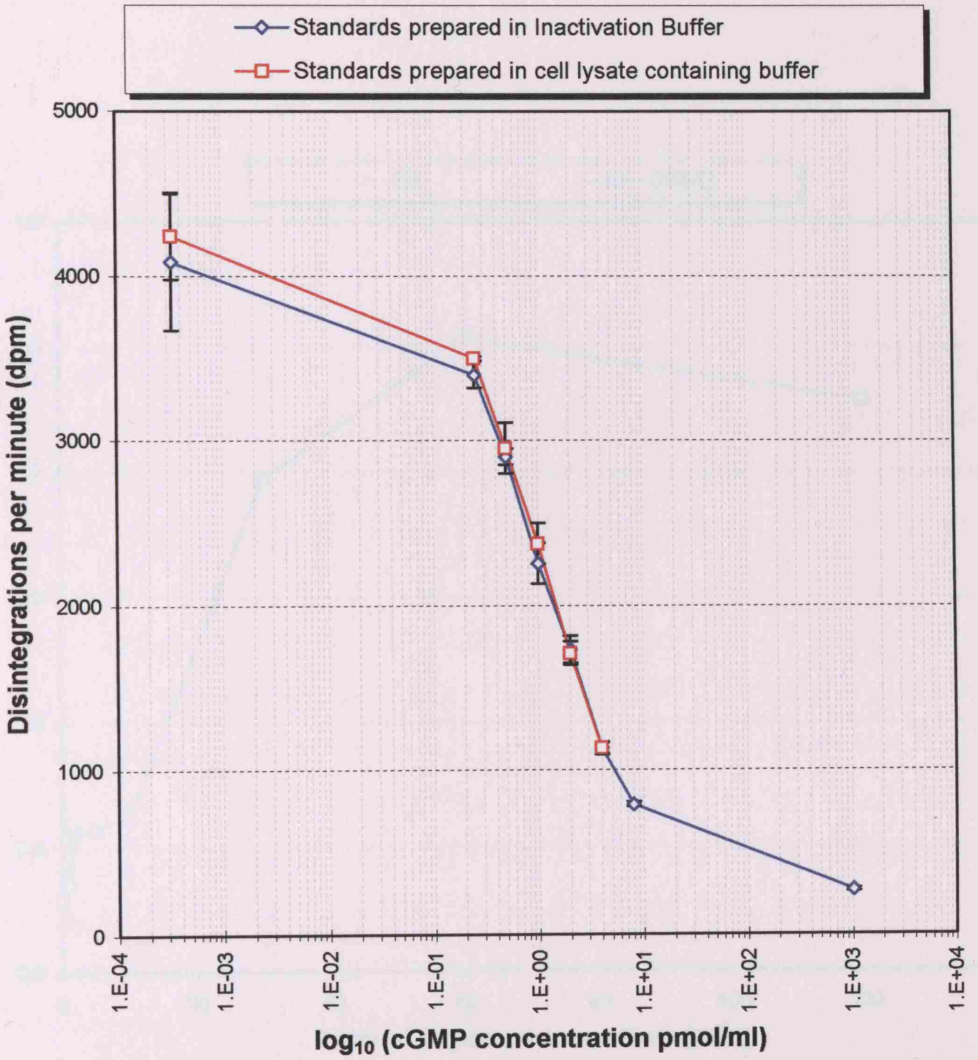


**Figure 4.3.8 Comparison of cGMP RIA standards prepared in either cell lysate-containing buffer or Tris.HCl/EDTA inactivation buffer**

*Cyclic-GMP standards were prepared as normal for RIA, in the Tris.HCl/EDTA containing inactivation buffer. In parallel, stock cGMP was diluted serially with SH-SY5Y lysate containing buffer. A no-cGMP control was also included (zero value on graph). Both sets of standards were prepared by identical serial dilutions and were measured in duplicate. Standards at 8 pmol/tube and 1,000 pmol/tube were not included with the cell lysate standards as these were the stock cGMP and blank cGMP control, respectively. Each point represents the average dpm counts of duplicate measurements (± Standard error).*

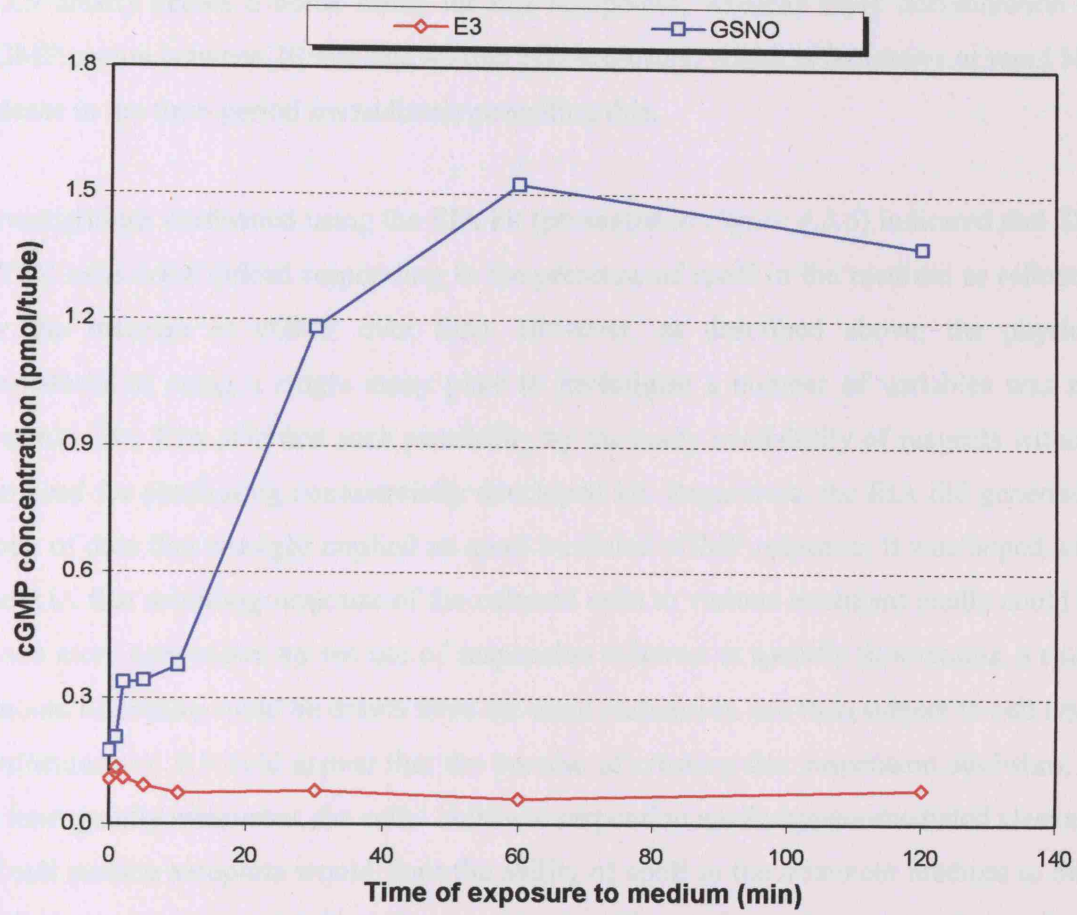


**Figure 4.3.9** **Response of *trypsinised* SH-SY5Y cells to E3-conditioned medium and the NO donor compound, GSNO**

*This RIA was performed on cell suspensions generated by treatment with trypsin/EDTA. Cells were treated with either E3-conditioned medium or control-conditioned medium containing 300 μM GSNO. At each time-point, a sample of cell suspension was removed and treated with inactivation buffer, then boiled. Each point represents a single assay point. Both E3 and GSNO treatments were performed in the presence of the non-specific PDE-inhibitor, IBMX.*

In the above investigation, GSNO was used as a positive control as a mean of generating cGMP in a suspension culture of SH-SY5Y cells. As this assay was performed over the course of 2 h, it was felt that this NO donor would have been more suitable than a NONOate compound such as PAPA/NO. Indeed, the response curve presented in *Figure 4.3.9* clearly shows a bolus effect for this compound, whereby rapid accumulation of cGMP occurs between 20 min and 40 min post-exposure, which is indicative of rapid NO release in the time-period immediately preceding this.

Investigations performed using the EIA kit (presented in *Figure 4.3.6*) indicated that SH-SY5Y cells were indeed responding to the presence of apoE in the medium as reflected by the increase in cGMP over time. However, as described above, the physical limitations of using a single assay plate to investigate a number of variables was not feasible. The RIA afforded such possibility by the ready availability of reagents without the need for purchasing commercially developed kit. Regardless, the EIA did generate a body of data that strongly implied an apoE mediated cGMP response. It was hoped with the RIA that sampling response of the cultured cells to various treatment media could be made more convenient by the use of suspension cultures: at specific time-points, a small amount of culture could be drawn from the main suspension and then subject to cell lysis. Unfortunately, it would appear that the process of creating this suspension abolishes, or at least greatly attenuates, the cells' ability to respond to apoE: trypsin-mediated cleavage of cell surface receptors would limit the ability of apoE in the treatment medium to bind with such receptors and initiate the putative signalling pathway that eventually results in detectable cGMP biosynthesis. Based on this evidence, further investigations using the RIA were performed using adherent cultures, as indeed were used throughout the EIA-based investigations.

### 4.3.6 Cellular NO release in response to apoE

Having established that assaying adherent cells was most suitable for subsequent investigation, cells were treated with apoE-conditioned medium from all three isoforms as well as experiments using control-conditioned medium (negative control) and PAPA/NO (positive control). Time-course assays were eschewed in favour of assaying at 10 min post-treatment to avoid the potential complication of cell detachment from the surface of the wells. *Figure 4.3.10* shows the response of these cells to the different media using three different concentrations (1/10 x dilute, 1 x neat, and 10 x concentrate). Following a 24 h incubation of recombinant CHO cells in serum-free CD-CHO medium,

the collected medium were assayed by apoE ELISA (see *Section 2.5*) to determine their apoE content. These were then adjusted to an equivalent concentration of 30 μg/ml by dilution with control-conditioned medium. Following this, the appropriate treatment concentrations were prepared: dilution in control-conditioned medium to give a 1:10 dilute sample, or passed through a spin concentrator to give a 10 x concentrate sample (see *Section 4.2.4.2*). Therefore, cells would be exposed to 3, 30 and 300 μg/ml sample concentrations. Individual wells of cells were treated with 500 μl medium supplemented with 1 mM IBMX. Additionally, cells were treated with control-conditioned medium and the NO donor PAPA/NO (50 μM). Lysates were prepared following 10 min exposure to the treatment medium, and the results are presented in *Figure 4.3.10*. For reference, exposure of SH-SY5Y cells to control-conditioned medium for 10 minutes gave a mean dpm reading of 4,623 (± 71, standard error).

The data seem to indicate that an isoform differential effect on SH-SY5Y cells with respect to cGMP production is occurring. As there is an inversely proportional relationship between scintillation counts and the derived cGMP concentration in this assay, a low dpm count indicates a high cGMP concentration and vice versa. By this rationale, it appears that E3 medium stimulated the highest production of cGMP and that the response from the three media types seems to indicate a trend of E3 > E2 > E4 with respect to the production of cGMP. This is further supported by comparing the change in dpm against cells treated with control-conditioned medium (values given as figures in *Figure 4.3.10*). However, these data actually represents only a very minor change in dpm count from the basal response: the biggest change in dpm count is given by the exposure of SH-SY5Y cells to undiluted E3-conditioned medium, with a 12.57 % decrease in radioactivity count. This equates to a change from 4,623 (± 71) to 4,042 (± 57) disintegrations per minute. Applying these figures to the RIA standard curve (see *Figure 4.3.7*) this is still within the plateau region that represents the lowest concentrations of cGMP. According to the standard curve, a dpm measurement at 4,623 and 4,042 represents cGMP concentrations of ~0.0001 and ~0.01 pmol/mol, respectively. If this is broadly the range by which the measured dpm changes during this experiment, there is an equivalent 1 % change in cGMP. For the other treatment medium conditions, this value is considerably less. Of note, however, is that this change in dpm was measured after only a 10 min exposure to the different treatment media.

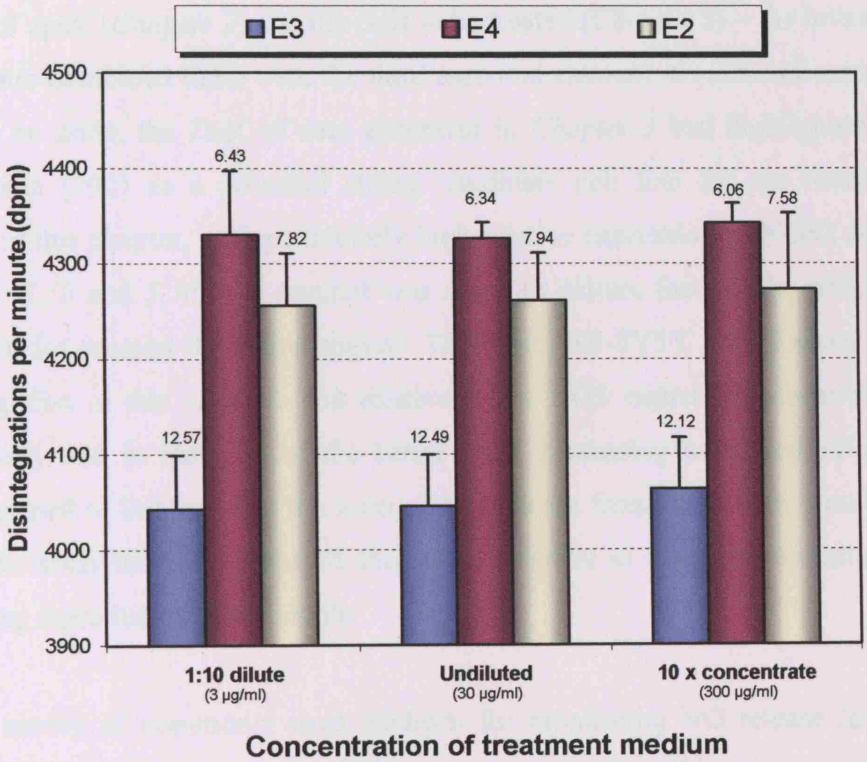


**Figure 4.3.10 Production of cGMP in SH-SY5Y cells in response to apoE isoforms at varying concentrations**

*SH-SY5Y cells lysates, prepared after 10 min exposure to treatment medium, and assayed for cGMP production by RIA. Data presented is an investigation of two variables: (1) the three apoE isoforms, E2, E3 and E4; (2) varying the concentration of the medium to give 1:10 dilute (≡3 µg/ml), 1 x neat (≡30 µg/ml), and 10 x concentrate (≡300 µg/ml). Results represent the mean of 6 individual cell samples, each assayed once in the same experiment (± standard error). The number listed over each bar indicates the percentage decrease in dpm of each treatment medium measured against the control-conditioned medium basal response (≡ 4,623 dpm ± 71 standard error). A decrease in radioactivity count is equivalent to an increase in cGMP production, although due to the sigmoidal relationship between cGMP concentration and dpm count, this percentage value is merely an arbitrary indicator of cGMP production and is not a true reflection on actual cGMP biosynthesis. Please note the shortened y-axis scale to accommodate the data presented.*

## 4.4 DISCUSSION

The aim of this chapter was to treat neuronal cells with apoE and monitor the effect it had on NO release. Having established the foundational tools required for this – namely the source of apoE (*Chapter 2*) and the cells to be treated (*Chapter 3*) – the investigations in this chapter combined these with the third essential element: a means of assaying NO release. As an aside, the *TaqCell* data generated in *Chapter 3* had highlighted IMR-32 neuroblastoma [292] as a potential strong candidate cell line for the investigations performed in this chapter, with particularly high relative expression of NOS2 and NOS3 (see *Figure 3.5b* and *3.5c*). An attempt was made to culture these cells, which proved unsuccessful for reasons that were unclear. Therefore, SH-SY5Y cells formed the basis for investigation in this chapter. The relatively low NOS expression observed in SH-SY5Y (which was in fact one of the better NOS expressing brain-derived cell lines studied), seemed to indicate that the level of NO release from these cells would be low. As such, the assay method employed should be sensitive to low NO concentrations, as well as being reproducible and reliable.

An initial survey of commonly used methods for monitoring NO release (e.g. Griess colorimetric assay, NO electrode, [$^3$H]-arginine assay, chemiluminescence) failed to identify a suitably sensitive method that did not require specialised and expensive equipment. Eventually, two assay types were investigated, either of which could potentially have proven a successful technique for monitoring this postulated physiological response: the DAF fluorescent assay, and the monitoring of cGMP release in response to changes in intracellular NO.

The DAF assay initially seemed very promising. The SH-SY5Y cells responded very well to the NO donor compound, PAPA/NO (*Figure 4.3.1*). However, the response to apoE treatment was more variable. As shown in *Figure 4.3.2*, the cells did respond to apoE treatment, particularly E4-conditioned medium (*Figure 4.3.2 B*), but unexpectedly a similar response was observed when control-conditioned medium was added (*Figure 4.3.2 C*). This indicates that the response observed with E4-conditioned medium treatment may not be a 'real' response, and perhaps could be a product of DAF-2 auto-fluorescence. This is the most significant concern with the DAF assay: the near identical absorbance and fluorescence maxima of both DAF-2 and DAF-2T.

During the process of NO release, both DAF-2 and DAF-2T will exist simultaneously within cells, although the intensity of their fluorescent output upon excitation is appreciably distinct, with DAF-2T being considerably higher than DAF-2. Nevertheless, any measurement of DAF-2T is accompanied by a simultaneous sampling of DAF-2, in a process known as auto-fluorescence. In a system with very high NO yield, the contribution of this DAF-2 auto-fluorescence is negligible; DAF-2T fluorescence can be more than 180-fold greater than DAF-2 [293]. However, in a low NO producing system, such as endothelial or neuronal cell cultures, the level of auto-fluorescence may be too indistinct to allow an effective separation. This has been demonstrated by Dirsch's group, where treatment of endothelial cells with 5μM DAF-2 gave the same level of fluorescence regardless of whether the cells were activated to release NO or not [294]. A similar problem of auto-fluorescence was observed by Chatton and colleagues, testing the ability to measure NO release in HEK293 human embryonic kidney cells [295]. Furthermore, this group also observed that the fluorescence detected using this system was highly sensitive to divalent cations such as $Ca^{2+}$ and $Mg^{2+}$.

A potential solution, at least to the problem of auto-fluorescence, was suggested by Dirsch's group. Their approach was to reduce the concentration of DAF-2 used in the pre-treatment stage from 5 μM to 0.1 μM [290]. When the concentration of DAF-2 was reduced to $\leq$ 0.1 μM, a difference in fluorescence was detectable, although this was accompanied by a concomitant reduction in overall fluorescence. In this investigation, a similar approach was followed, reducing the concentration of the DAF-2 used to pre-treat cells. However, as soon as it was reduced to 1 μM, there was virtually no change in intracellular DAF-2T fluorescence, which seems to imply that no associated change in NO released was observable (see *Figure 4.3.2*). Although minor fluctuations occurred, the overall trend shows no response. Reducing the DAF-2 concentration further to 0.1 μM and 0.05 μM gave essentially the same response. Looking closely, the 1 μM DAF pre-treatment does show a minor increase in fluorescence over the 4 hour time period, but it is not significantly over the baseline fluorescence to allow an NO response that could be detected using this assay. The aim of reducing the DAF-2 concentration was an attempt to reduce the level of auto-fluorescence produced within the system and measure only the real NO release response. However, in one study where neuronal cells were used, a DAF-2 concentration of 10 μM was used [296], although this work was primarily focussed on the DAF assay as a means of visualising NO release under the microscope rather than monitoring its response over a time-course.

In general, the DAF assay results were disappointing. Further experiments were performed, in addition to the figures presented, and in each instance anomalous measurements were observed. For example, one set of experiments involved treating cells with medium that contained the non-specific NOS inhibitor, ethyl-ITU. Little or no reduction in fluorescence was observed between cells treated with ethyl-ITU and those without, and in some instances the fluorescence was actually higher. A further concern was the consistency and reproducibility of results: when a particular set of treatment conditions was explored for a second or third time, results could show significant variance despite efforts to retain uniformity between experiments. Although there are likely to be unavoidable discrepancies between experiments (e.g. non-identical cell numbers being treated, variations in the concentrations of apoE-conditioned medium used to treat the cells, minor changes in medium composition between experiments, and of course operator errors) efforts were made to keep conditions as consistent as possible between experiments. Despite this, the fluorescence measured could change dramatically between experiments. This was further compounded by the optics utilised by the fluorimeter since they did not read an entire well, but rather certain points across it. Potentially, this could include reading blank parts of the well, which would skew the overall measurement for that well at that time-point. This was a distinct possibility as SH-SY5Y cells cannot be cultured as confluent monolayers due to their morphological feature of possessing extensions, which precludes the ability to form such a monolayer. Moreover, over-confluency tends to result in morphological changes that could affect their normal physiological responses. However, in practice this does not seem a significant feature as the graphs plotted do not obviously indicate any unexpected shifts across the time-course.

Following on from this, the potential of assaying cGMP changes was evaluated as a means of defining the changes in NO release within this cell system. Two cGMP assays were studied in this chapter, both based on the competitive interaction of an anti-cGMP antibody against labelled cGMP of known concentration and the unlabelled cGMP of unknown concentration derived from a cell lysate.

The first to be investigated was an enzymatic assay, which was in the form of an ELISA. The assay was purchased as a kit, which contained all buffers and solutions, including cGMP standards. According to the manufacturer's guidelines, this assay should have been capable of detecting NO release in the sub-picomolar range, quoting a sensitivity of

0.16 – 100 pmol/ml. Therefore, it could potentially have been a highly successful assay method. In reality it proved problematic, even before samples were assayed. To test the responsiveness of the kit, initial assessment was achieved through addition of cGMP standards to the plate and recording the OD values measured. The measurements differed significantly from those quoted in the kit's manual. Of particular concern was that the 0.1 pmol/ml standard gave an OD measurement of ~ 0.05 (see *Figure 4.3.5*). As this was a competitive assay, a low cGMP concentration should generate a high OD. For reference, the manufacturer's guidelines state that the OD at this concentration should be ~ 0.3. Although this is a value 6-fold greater than that which has been achieved in this present study, this still represents a relatively low OD, and ideally a complete set of standards should generate ODs ranging from a near zero value through to 1.0, but crucially not exceeding this due to limitations in plate reading optics.

Although the OD measurements for standards did show a degree of reproducibility between experiments, at least in the two assays presented in *Figure 4.3.5*, the low ODs make this a very imprecise measurement. Once the concentration of the standard was increased to 10 pmol/ml, the OD value was close to 0, which precluded the ability of this kit to measure any cGMP concentration beyond this point. Furthermore, the range between this and the lowest concentration standard is no more than ~0.06 OD units, which is a very limited range of ODs to monitor changes within. Additionally, a third experiment was performed, with standards ranging from 50 pmol/ml to 2 pmol/ml (produced by serial dilutions). The OD measurements from this experiment were not similar to the measurements from the initial assays at all, neither did they approach the manufacturer's examples. Although the assays presented in *Figure 4.3.5* show a reasonably reproducible set of data, the potential for spurious data to be generated is an obvious concern.

This particular kit is well-established and has been used in a number of other applications and studies where cGMP concentration has been measured [297,298,299]. In these studies, cGMP was assayed in a range from picomolar to nanomolar concentrations. Thus, it should have been a suitable assay for the cellular system in this study. The inability to establish this assay in our lab is disappointing, and an explanation for this is difficult to reach. The most obvious reason would be that this was a defective kit: the 96-well plate may not have been sufficiently coated with the capture antibody (anti-IgG); the IgG used could have been defective; one of the other reagents may not have performed as

well as it should have done; or one of the components of the kit (plate or reagents) may have been compromised during transit or storage. As the same kit was used for all the preliminary experiments, it was not possible to verify this. There are also potentially operator errors, for example when diluting standards or preparing reagents and samples. Certainly, the cGMP measurements for the test samples that were assayed would likely have been considerably higher had a dedicated PDE inhibitor such as IBMX been included in the cell lysis buffer, rather than relying on HCl to achieve this. This would have helped prevent cGMP degradation and enhanced the measurement made. However, this does not explain the results generated with the standards, as these should have matched much more closely the OD values quoted by the manufacturer.

Following assessment of the cGMP EIA, a radioimmunoassay was investigated. This method utilised the same principle as that for the enzymatic assay, with the notable exception of the use of radiolabelled cGMP as the means of monitoring the cGMP content of standards and samples. Having optimised the experimental conditions, this assay was used to analyse SH-SY5Y cells treated with conditioned medium containing the three apoE isoforms at concentrations varying from undiluted, through to a 1:10 dilution and a 10 x concentrate using a spin column concentrator. The results of this seemed to indicate that an isoform differential effect was occurring with respect to cGMP concentration changes, as displayed in *Figure 4.3.10*. As with the cGMP EIA results, the level of radioactivity counted within each scintillation vial is inversely proportional to the cGMP content within the samples.

Treating the cells with apoE4-conditioned medium appeared to affect the cGMP concentration the least, especially when compared with cells treated with apoE3-conditioned medium. Relative to cells treated with control-conditioned medium (that gave an average radioactivity count of 4,623 dpm), exposure to apoE4 gave an approximately 6% decrease in radioactivity, compared to a 12% decrease with apoE3-conditioned medium. However, the results presented in *Figure 4.3.10* are in some respects misleading; they are a representation of the cellular response of these cells based on the radioactive disintegrations per minute, and not an extrapolation to calculate the actual cGMP concentration as determined via the assay's standard curve. When this is performed, all the dpm counts presented are somewhat unreliable due to the flattening of the cGMP concentration/radioactivity count relationship at the extremities of the standard curve (see *Figure 4.3.8*). As such, scintillation counts greater than ~ 4,000 dpm are very

difficult to quantify with any degree of accuracy. Although a cGMP concentration can be ascribed to radioactivity counts at this range, they are at the limits of accuracy, and ideally the dpm counts should be within the region of linearity in the middle of the standard curve (see *Figure 4.3.8*). This is also true for very radioactivity counts that are indicative of a very high cGMP concentration; in this instance, the samples could easily be diluted to bring these counts to within the region of linearity, which is obviously a far more straightforward resolution than in the case (as it is in this present study) where the dpm is too high

This assay does seem to have proven an aspect one of this thesis' hypotheses – whether human brain derived cell lines can respond to apoE exposure by changing the level of NO release, in this case inferred through its secondary messenger cGMP. However, as discussed above, these results are tempered by the overall low level of response observed within this cellular system. Moreover, the conclusion is supported by the data obtained through the cGMP EIA experiments. As presented in *Figure 4.3.6*, exposure to apoE4 appeared to upregulate cGMP levels relative to apoE3 exposure at 1 h and 4 h post-exposure, and this difference was maintained even after 8 h. Neither the cGMP EIA or the RIA sets of data are completely comprehensive, and can even be considered incomparable due to the distinct exposure times used for both assays: during the EIA experiments, cells were treated over an 8 h time-course, with the first lysate prepared 1 h post-treatment, whereas for RIA all experiments were performed using a 10 min exposure to apoE-conditioned medium. This could help explain the disparity between the results, but is far from conclusive. In addition, the results generated using the DAF assay (see *Figure 4.3.2*) also indicated that apoE4 generated the highest level of NO release relative to apoE3, which supports the EIA data and argues against the trend observed with RIA. However, the DAF assay also demonstrated an NO biosynthesis in response to cells treated with control-conditioned medium, which certainly diminishes the overall veracity of these results.

The findings of the different assays investigated in this chapter do seem to indicate that SH-SY5Y calls are sensitive to the presence of exogenously applied NO, as evidenced by the effect of the numerous NO donors utilised. Moreover, cells seemed to show a low-level response to apoE exposure. However, these data has not been completely unassailable and the ability of apoE exposure to affect the NO biosynthesis pathway in these cells has not been completely characterised. As became clear through the progress

of this study, a key issue that requires significant attention is identifying a suitable assay method for monitoring NO release.

At the outset, an assay was required such that it could: be easily reproducible; generate results that would be accurate; be a true reflection of NO release, whether this was monitored directly or indirectly; and allow a relatively high throughput of samples. The methods investigated all have certain distinct advantages and disadvantages, but the cGMP RIA was by far the most consistent method used. This was likely due to the unique opportunity for performing numerous optimisation and assessment investigations prior to making use of this assay in earnest. Despite these shortfalls, the results are indicative of an apoE effect, although this represent only a 1% change in cGMP concentration, but it would have benefited from a more sensitive assay method if the gross physiological response of these cells were to be properly established in the context of nitric oxide release response.

During this study, SH-SY5Y cells did show a response when exposed to NO donors, whereas the evidence for an apoE-mediated response was inconclusive. However, this does not exclude the possibility that there is an apoE-mediated link to NO release in the brain. Before rejecting such a link, it is essential to carry out further investigations in other human neuronal cell lines, as well as primary neuronal cell cultures derived from rats. Moreover, it is conceivable that a more subtle or different sequence of signalling events could be occurring at the submolecular level; this possibiliyty was investigated in *Chapter 5*.

# Chapter 5

# APOLIPOPROTEIN E AND SIGNALLING PATHWAYS IN SH-SY5Y NEURONAL CELLS

# 5.0 APOLIPOPROTEIN E AND SIGNALLING PATHWAYS IN SH-SY5Y NEURONAL CELLS

## 5.1 INTRODUCTION

Having established a suitable source of quantifiable apoE-conditioned media (*Chapter 2*) and suitable human brain-derived cells for treatment with this apoE (*Chapter 3*), the investigations in *Chapter 4* attempted to combine these foundational factors with a method for measuring NO biosynthesis. Although some response to apoE was detectable in these cells, these measurements were far from conclusive, largely due to concerns regarding assay sensitivity and reproducibility. Response to nitric oxide donor compounds was far more successful with a change in NO detectable either directly by fluorescence increases in the DAF assay, or indirectly by assaying the presence of the secondary messenger cGMP by enzymatic assay or radioimmunoassay. Moreover, the effect of NO donors in these cells demonstrates their capacity to respond to the presence of NO in a typical manner. However, in the context of apoE mediated effects, a view must be taken that encompasses not only this 'end' effect but also upstream regulatory processes that initiate at the cell-surface and are propagated through various intermediaries.

The cell line characterisation performed in *Chapter 3* indicated that these cell lines possessed the numerous features necessary to allow apoE to modify the synthesis of NO: relevant cell-surface receptors that would allow cells to interact with circulating apoE; one or more of the NOS isoenzymes that actually synthesis NO; and the NOS3 regulatory kinase, protein kinase B (PKB), which is also referred to as Akt[8]. The function of this kinase is to activate NOS3 and reduce its sensitivity to $Ca^{2+}$ influx for activation. Furthermore, reverse transcriptase PCR and Western blotting performed in *Chapter 4*, revealed that these cells also expressed soluble guanylate cyclase, which catalyses the formation of cGMP. All of these are important milestones in the propagation of putative events that initiate with apoE and eventually stimulate (or impede) nitric oxide release. A hypothesis can be postulated that states that exposure to apoE will initiate a signalling event in these cells, which will start on a cell-surface receptor and result in modifying NO synthesis. If a signalling pathway can be shown to be affected by the presence of

[8] To avoid confusion, this kinase will be referred to as PKB/Akt in this chapter. However, in some instances (e.g. describing an antibody) only Akt will be used, but this still refers to the same kinase.

apoE, this would be a significant validation of the general hypothesis proposed in *Chapter 1*: exposure to apoE has an effect on the release of NO in the brain.

The proposed pathway under investigation in this chapter can be described generally:

- ApoE containing lipoprotein particle binds alone, or in concert with another molecule, to the extracellular ligand binding domain of a cell-surface receptor (apoER2, VLDL-r), whose function is primarily signal transduction rather than receptor-mediated endocytosis of bound ligands;

- Intracellularly, there is a recruitment of signalling molecules or adaptor proteins that propagate the signal within the cell; further downstream regulatory events occur through sequential phosphorylation and dephosporylation events involving an indeterminate number of kinases and phosphatases;

- The signalling endpoint (with respect to a physiological response) occurs either with the activation of NOS3 such that it becomes $Ca^{2+}$ insensitive, or activation of transcription factors that upregulate the expression of inducible NOS2.

Within this chapter, three elements of this pathway have been explored, namely: the apoE receptor, apoER2; NOS3 regulating kinase, PKB/Akt; and the NOS3 enzyme itself. All of these can undergo phosphorylation events in the regulation of their activity and represent distinct phases of the signalling pathway, described earlier: initiation (apoER2), propagation (PKB/Akt) and activation (NOS3). As with any other signalling pathway, there are numerous other components involved, particularly with respect to the propagation of signal. Additionally, the initiation stage could involve a number of other receptors, e.g. very-low-density lipoprotein (VLDL) receptor, LDL-receptor-related protein (LRP), or the high density lipoprotein scavenger receptors (SR-BI and SR-BII). Moreover, they may achieve this in concert with apoER2 [230], or may function in parallel with it. There is also potential for apoE to activate expression of the inducible NOS2 [300,301,302,303] and neuronal NOS1 [304], although in this study the focus is on NOS3.

The NOS3 regulatory kinase, Akt, is a component of the larger phophoinositide-3-kinase (PI3K) pathway [305]. The activity of Akt is dependent upon the activation by

phosphorylation of PI3K, which in turn propagates this signal to Akt. The instigating reaction of this pathway is the phosphorylation of the 3'-hydroxyl group of the inositol rings of phosphatidylinositol (PtdIns), all by the action of PI3K:

| | | |
|---|---|---|
| Phosphatidylinositol<br>*PtdIns* | ⟶<br>***PI3K*** | PtdIns 3-phosphate<br>*PtdIns(3)P* |
| PtdIns 4-phosphate<br>*PtdIns(4)P* | ⟶<br>***PI3K*** | PtdIns (2,4)-bisphosphate<br>*PtdIns(2,4)$P_2$* |
| PtdIns (4,5)-bisphosphate<br>*PtdIns(4,5)$P_2$* | ⟶<br>***PI3K*** | PtdIns (3,4,5)-triphosphate<br>*PtdIns(3,4,5)-$P_3$* |

There exist three classes of mammalian PI3 kinases, with the first category subdivided into two – giving classes IA, IB, II and III – based on structural distinctions of the monomers that comprise the final enzymatic heterodimer [306]. Despite this, they all share a similar range of substrates (i.e. the PtdIns) and are affected by common inhibitory factors such as Wortmannin and 2-(4-morpholinyl)-8-phenyl-4H-1-benzopyran-4-one hydrochloride (LY294002). Their expression is not uniform and ubiquitous in all tissues, but is thought to be selectively expressed in fully differentiated non-proliferating cells with different PI3K classes present in different spatial locations [307].

The first characterisation of PI3K was provided by analysis of bovine brain, identifying the two subunits that comprise the enzyme: the 724 amino acid p85α subunit, and the 1068 amino acid p110α subunit. The catalytic activity of the enzyme resides in the p110α subunit, whilst the p85α subunit contains regulatory domains that control its activity. In fact, the p85α subunit contains a number of independently folded domains, including two SH2 domains and one SH3 domain. Of note in this thesis is the presence of SH3 motifs, which are found in the cytoplasmic tails sequences of both apoER2 and scavenger receptor, SR-BII. The intracellular tails of these receptors could act as putative activation points for the PI3K pathway, possibly via phosphorylation changes propagated from one domain to another. The two subunits associate via a helical region located towards the carboxy terminal end of p85α, which in turn associates with the amino-terminal p85 recognition site of p110α. Located at the carboxy-terminus of this subunit is the catalytic domain of what will eventually become the PI3K heterodimer [305].

Numerous cellular processes have been implicated as part of the PI3K pathway. These include DNA synthesis, cell survival, membrane ruffling, oxidative burst, cytoskeletal rearrangements, glucose transport, vesicle trafficking, receptor internalisation, and oocyte maturation. This diversity of function reflects the multitude of downstream effector molecules upon which PI3K mediates a regulatory function. These include the GTPase Rac, Akt protein kinase, Glut4 glucose transporter, p70S6 kinase (which has also been implicated in tau hyperphosphorylation in AD [308]) and protein kinase C [309,184]. Of these, the serine/threonine protein kinase, Akt, has been studied in some depth in this particular study.

The discovery of Akt started with the investigation of the spontaneously lymphomatous AKR/J breed of mice in 1977 [310]. The Akt8 virus, which is a derivative of the transforming T8 virus, was isolated from a spontaneous thymic lymphoma of these mice. This had the capability of producing malignant transformation *in vitro*, but required a helper virus for propagation. A decade later, the molecular cloning of the Akt8 provirus revealed a viral genome containing both viral and non-viral, cell-related sequences. The non-viral component sequence was designated *v-akt*, as it was thought to be the viral oncogene of the Akt8 virus and harboured its ability to transform cells *in vitro* [311]. This same study established two human homologues of the *v-akt* oncogene, *AKT1* and *AKT2*, which were cloned [312]. Following on from this, the cellular homologue, *c-Akt*, was identified, and this is now commonly known simply as Akt, or protein kinase B (PKB) or RAC PK (related to protein kinases A and C) [313].

Akt is a member of the cyclic-AMP-dependent protein kinase A/protein kinase G/protein kinase C (AGC) super family of protein kinases, which have structural homologies in their catalytic domain and activation mechanism [314]. In mammalian tissues, three PKB/Akt genes have been identified: PKBα/Akt1, PKBβ/Akt2 and PKBγ/Akt3, which are found on chromosomes 14q32, 19q13 and 1q44, respectively. The tissue distribution of the PKB/Akt isoforms has been investigated in mice [315], which revealed ubiquitous expression of the α and β isoforms. However, PKBγ was not detected in several tissues where α and β isoforms were highly expressed, although relatively high expression of this isoform was detectable in brain and testis. The predominant isoform was PKBβ, which displayed high expression in insulin target tissues, such as fat cells, liver and skeletal muscle.

The three PKB/Akt isoforms share extensive structural similarities, with a greater than 80% homology at the amino acid level [316]. With regard to their structural features, three distinct functional domains can be defined, illustrated in *Figure 5.1.1*. Firstly, there is the amino-terminal pleckstrin homology (PH) domain, which mediates protein-protein and protein-lipid interactions. It consists of approximately 100 amino acids and resembles the 3-phosphoinositide binding domain in other signalling molecules [317]. This PH domain can interact with membrane lipid products such as PtdIns(3,4,5)$P_3$, which is produced through the action of PI3K. Moreover, biochemical investigation has demonstrated that the PH domain of PKB/Akt has a similar affinity for both PtdIns(2,4)$P_2$ and PtdIns(3,4,5)$P_3$ [314]. Thus, the upstream activator of PKB/Akt is PI3K, although there is also a less direct pathway, e.g. the action of insulin is mediated via initial phosphorylation of PtdIns(4,5)$P_2$, which stimulates the PtdIns(3,4,5)$P_3$-dependent kinases, PDK1 and PDK2, and hence activation of PKB/Akt [185,318] (see *Figure 5.1.1*).

The kinase catalytic region of PKB/Akt is located after the PH domain in the central region of the molecule. This mediates phosphorylation of substrate proteins and has a high degree of similarity to those in PKA and PKC, which led to its initial nomenclature as RAC PK (related to PKA and PKC). The final domain is the approximately 40 amino acid carboxy-terminal regulatory tail domain. Significantly, both these domains have serine and threonine domains that require phosphorylation in order for PKB/Akt to be activated. The actual sites of these residues within each domain vary slightly between the three PKB/Akt isoforms. The threonine residue within the kinase domain is at position 308, 309 and 305 of Akt1, 2, and 3, respectively, whereas the second residue, serine, is located in the regulatory domain at positions 473, 474 and 472, and are detailed in *Figure 5.1.1*.

When the level of $PIP_3$ rises, for example by growth factor activation of receptor tyrosine kinases and PI3K, there is an associated increase in binding of $PIP_3$ to the PH domain of PKB/Akt. This causes a conformational change in PKB/Akt and its translocation to the plasma membrane. At this location, PKB/Akt is phosphorylated and activated by the action of PDK1 on the threonine residue. It is thought that in its native state within the cytosol, the tertiary structure of PKB/Akt is such that PDK1 cannot access the threonine site. Once the PH domain is bound with $PIP_3$ and conformational change occurs, this masking effect is abolished and the enzyme can undergo its first activation. Following

activation, the enzyme translocates again, this time from the membrane to various subcellular compartments to initiate whichever signalling events are necessary. Phosphorylation at Thr308 will only partially activate the enzyme; complete activation only occurs when the Ser473 is also phosphorylated. This process can involve the action of PDK2, as well as PDK1.

Downstream of PKB/Akt activation are its effects on NO synthesis. This is well characterised and has been discussed in *Chapter 1, Section 1.5.1.* In the present investigation, it is hypothesised that exposure of neuronal cells to apoE will instigate a signalling cascade propagated through the apoER2 receptor to resulting in PI3K-mediated activation PKB/Akt and a subsequent change in NO synthesis through the action of NOS3.

## 5.2 SPECIALISED MATERIALS AND METHODS

All assays performed in this chapter utilised cultures of SH-SY5Y neuroblastoma cells as the target cell line. They were cultured according to the standard protocols, described in *Section 2.2.1*. Cells were cultured in 60 mm dishes (Nunc) in preparation for treatment with different media and to prepare cell lysates, each dish representing an individual time-point for an assay course. The cells would be exposed to conditioned medium from recombinant CHO cells; three cell lines were cultured – apoE3, apoE4 and the non-transfected CHOdhfr- line. The latter would be used to generate control-conditioned medium that would be free of any recombinant apoE (confirmed by ELISA), thereby acting as a negative control to be run in parallel with treatment with E3- and E4-conditioned media. Following collection, medium was passed through a 0.20 μm syringe filter and assayed by sandwich ELISA (see *Section 2.5*). This allowed the different conditioned media to be adjusted to an equivalent concentration prior to treating the cells.

Once cultures of SH-SY5Y cells were sub-confluent, they were ready for treatment and preparation of lysates. The normal culture medium was aspirated off and each dish washed with warm PBS, followed by addition of 500 μl desired treatment media. Dishes were returned to incubate at 37 °C. At the appropriate time-point, treatment media was aspirated off the cells and ice-cold PBS applied to try and halt any cellular activity. Lysates were prepared according to the protocol defined in *Section 2.4.1*, after which their protein concentration was assessed by Bradford colorimetric assay (see *Section 2.4.2*). Following this, lysates were kept at -20 °C for long-term storage or at 4 °C for up to a week.

Based on protein concentrations, as determined by the Bradford assay, lysates were diluted in distilled water to give equivalent concentrations. These were then loaded onto 4-12% Bis-Tris polyacrylamide gels for electrophoretic separation (see *Section 2.4.3*). The resulting products were transferred to nitrocellulose membranes (see *Section 2.4.4.1*) prior to performing a Western blot (see *Section 2.4.5*). The presence of three proteins were assayed in this study, including their phospho-modified variants: apoER2, PKB/Akt and NOS3. The details of the antibodies, including their dilutions and relevant secondary antibodies, are listed in *Table 5.1*.

| 1° Antibody *(species)* | 1° Antibody Supplier | 1° Antibody Dilution & Buffer | 2° Antibody | 2° Antibody Dilution in wash buffer | MW |
|---|---|---|---|---|---|
| **α-apoER2** *(goat)* | Santa Cruz # sc-10113 | 1:1,000 in 5% BSA /TBS-T | Mouse α-goat IgG HRP-conj. | 1:5,000 in 5% Marvel /TBS-T | ~ 130 kDa |
| **α-pY20** phosphotyrosine *(mouse)* | Zymed # 03-7700 | 1:1,000 in 5% BSA /TBS-T | Sheep α-mouse HRP-conj. | 1:5,000 in 5% Marvel /TBS-T | *(as apoER2)* |
| **α-Akt** *(rabbit)* | CST # 9272 | 1:1,000 in 5% BSA /TBS-T | Goat α-rabbit IgG HRP-conj. | 1:5,000 in 5% Marvel /TBS-T | 60 kDa |
| **α-Akt pSer473** phospho-Akt *(rabbit)* | CST # 9271 | 1:1,000 in 5% BSA /TBS-T | Goat α-rabbit IgG HRP-conj. | 1:5,000 in 5% Marvel /TBS-T | 60 kDa |
| **α-Akt pThr308** phospho-Akt *(rabbit)* | CST # 9275 | 1:1,000 in 5% BSA /TBS-T | Sheep α-mouse IgG HRP-conj. | 1:5,000 in 5% Marvel /TBS-T | 60 kDa |
| **α-NOS3** *(goat)* | Santa Cruz # sc-653 | 1:1,000 in 5% BSA /TBS-T | Mouse α-goat IgG HRP-conj. | 1:5,000 in 5% Marvel /TBS-T | 140 kDa |
| **α-NOS3 pSer1177** phospho-eNOS *(rabbit)* | CST # 9571 | 1:1,000 in 5% BSA /TBS-T | Goat α-rabbit IgG HRP-conj. | 1:10,000 in 5% Marvel /TBS-T | 140 kDa |

**Table 5.1 Complete list of antibodies utilised in this chapter**

*Antibodies used for both Western blotting and immunoprecipitation procedures. All 2° antibodies were purchased from Sigma-Aldrich (Poole, UK)*

*MW* = *Molecular weight of antigen*

*HRP-conj.* = *HRP-conjugated antibody*

*Santa Cruz* = *Santa Cruz Biotechnology (Middlesex, UK)*

*Zymed* = *Zymed Laboratories – Cambridge Bioscience Ltd (Cambridge, UK)*

*CST* = *Cell Signalling Technologies (New England Biolabs, Herts., UK)*

Gels were loaded dependent on the capacity of the well, which varied with the number of lanes available on the gel. Initially 12-well gels were utilised, which allowed 20 µl sample to be loaded. Once high throughput of lysate analysis was required, 17-well gels were used, each allowing a maximum of 10 µl per sample, although in this study no more than 8 µl was used to prevent any overspill or sample contamination. Prior to running on the gel, samples were assayed for protein content (Bradford method as described above and detailed in *Section 2.4.2*) and diluted in lysis buffer to give a concentration of 1 µg/µl.

Immunoblotting of PKB/Akt, apoER2 and NOS3 was performed by standard Western blot of cell lysates (see *Section 2.4.5*). However, to investigate expression of their phosphorylated forms, immunoprecipitation was performed as detailed in *Section 2.4.6*. In these instances, the antibody for the non-phosphorylated form of the protein functioned as the precipitating agent. Following this, enriched lysates were electrophoresed on a 4-12% Bis-Tris gel (as described in *Section 2.4.3.4*), which was followed by probing with the appropriate phospho-specific antibody. For investigating apoER2 phosphorylation, lysates were precipitated using an α-apoER2 antibody. Following this, lysates were electrophoresed as described above then immunoblotted using an antibody against phosphotyrosine.

In some instances, blots were stripped and reprobed following initial immunoblotting. This was particularly the case when investigating the presence of phospho-modified proteins. The procedure for reprobing blots has been described in *Section 2.4.7*.

## 5.3 RESULTS

Before being used to treat SH-SY5Y cells, the concentration of the apoE in the conditioned medium was measured by ELISA (see *Section 2.5*). Concentrations of the two apoE conditioned media were adjusted to give a final concentration of 2.5 μg/ml. Furthermore, control-conditioned medium was also assessed to confirm that no apoE was present in this treatment medium. Cells were exposed to E3-, E4-, or controlled-conditioned medium. At the appropriate time point, the treatment medium was aspirated off and cells treated with ice-cold lysis buffer. To ensure homogenisation of the protein and cellular content of the lysates, all samples were repeatedly passed through a 19G needle, which allowed shear stress to disrupt all cellular membranes and liberate protein content of the cells. Having prepared the lysates, their protein concentration was determined by Bradford assay, based on which lysates were adjusted to give equivalent protein concentrations. For loading, 1 μg/μl of sample was mixed with loading buffer and boiled for 5-10 min prior to separation by 4-12 % Bis-Tris gel electrophoresis. Standard Western blotting procedure was followed as described in *Section 2.4.3 – 5.*

### 5.3.2 Detection of apoER2 and its phosphorylated form

In a putative signalling pathway, the first step would be binding of ligand to its cell surface receptor, which would then instigate downstream activation. Here, the receptor under investigation is apoER2, the expression of which in SH-SY5Y cells has already been demonstrated in *Chapter 3*. The investigations in that chapter confirmed the presence of apoER2 mRNA. In this chapter, the apoER2 functional protein was being assessed.

Presented in *Figure 5.3.1* are lysates of SH-SY5Y cells produced over 6 h time-course after exposure to either control- (*Figure 5.3.1 A*), E3- (*Figure 5.3.1 B*) or E4-conditioned medium (*Figure 5.3.1 C*). The presence of apoER2 over the time course was judged by immunoblotting with α-apoER2 antibody. This shows a consistent product resolved at the expected band size, equivalent to ~ 130 kDa.

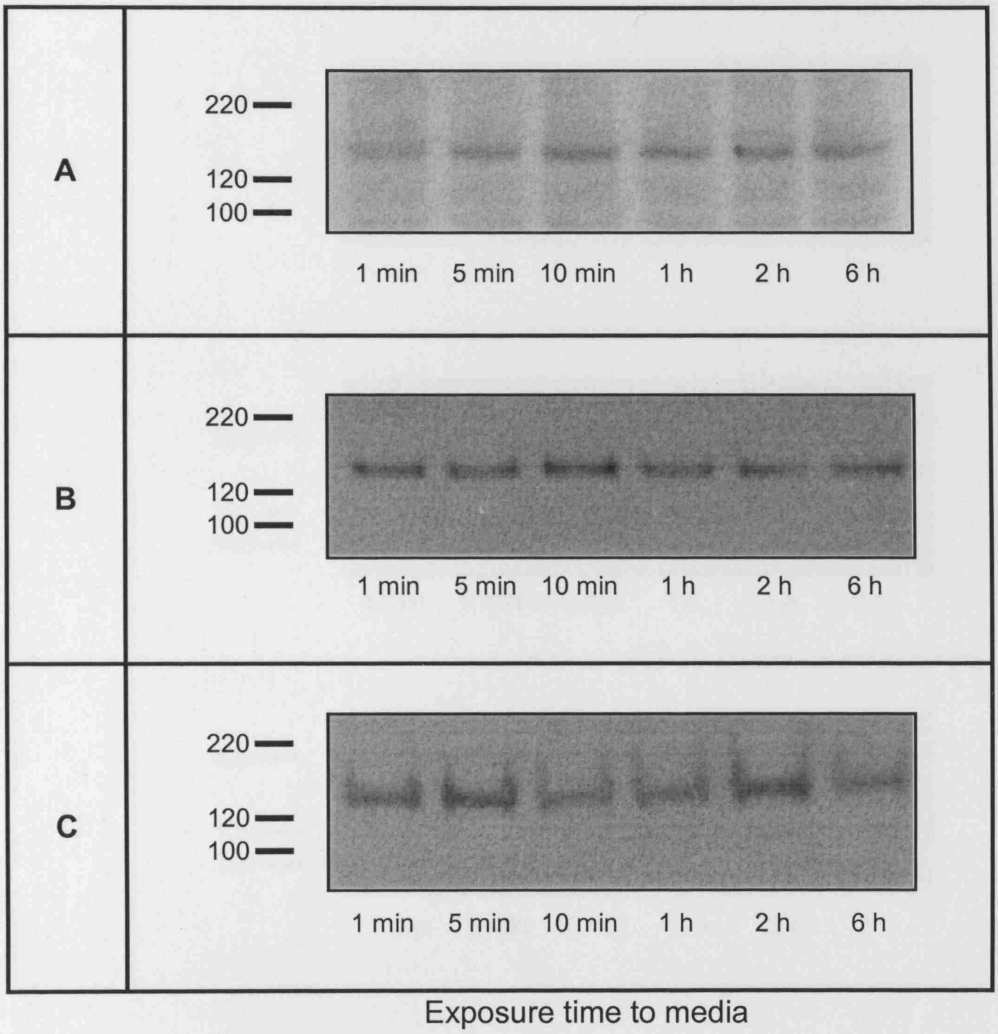


**Figure 5.3.1 Exposure of SH-SY5Y cells to E3- or E4-conditioned media does not affect the expression of apoER2**

*Cultured SH-SY5Y cells were exposed to CHO-conditioned medium for 1, 5 and 10 min, then 1, 2 and 6 h. Expression of apoER2 was assessed by immunoblotting with α-apoER2 antibody. Marker on the left hand edge represents molecular weight size markers (kDa); apoER2 ≡ ~ 130 kDa.*

*(A) CHOdhfr-; (B) CHO-E3; and (C) CHO-E4 treatment medium.*

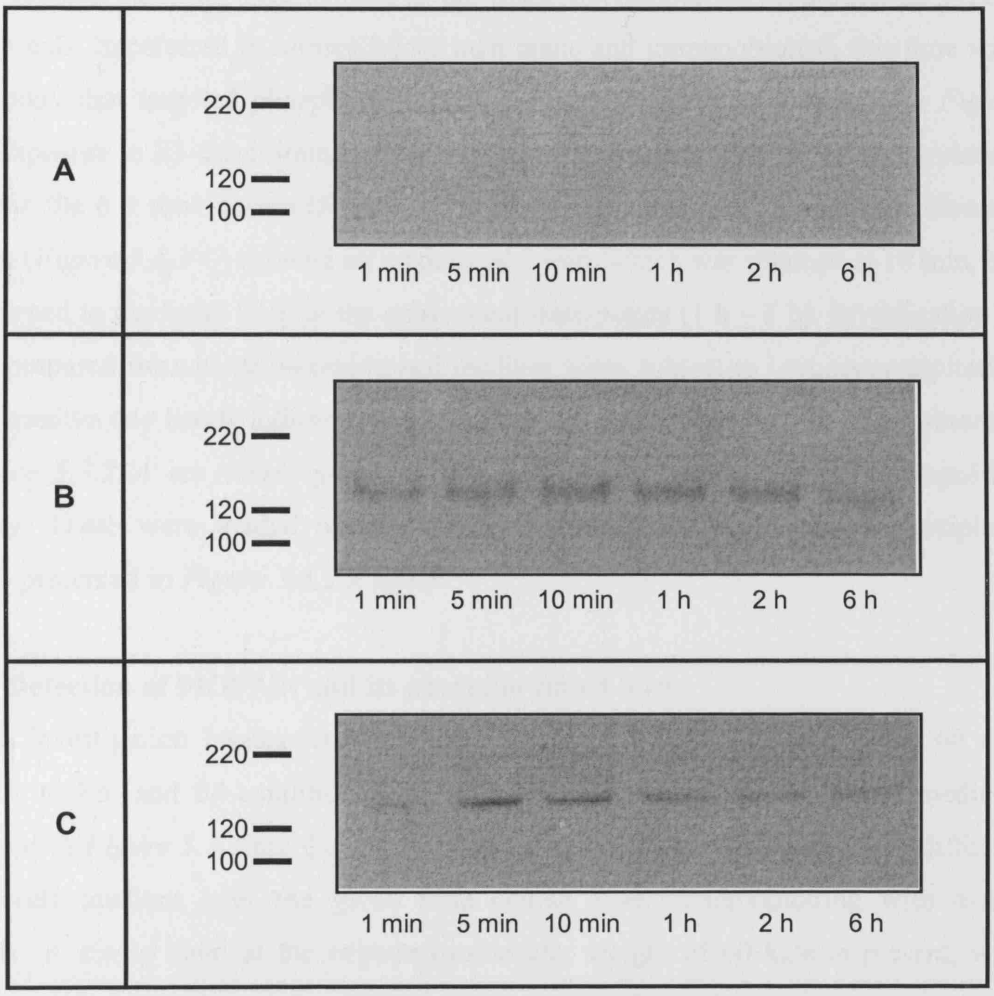


**Figure 5.3.2 SH-SY5Y cells exposed to E4-conditioned medium show tyrosine phosphorylation of apoER2, which does not occur when treated with E3-conditioned medium**

*Cultured SH-SY5Y cells were exposed to CHO-conditioned medium for 1, 5, and 10 min, then 1, 2 and 6 h. Lysates were immunoprecipitated using α-apoER2 antibody, and the enriched lysates immunoblotted with α-pY20 antibody. Marker on the left hand edge represents molecular weight size markers (kDa); apoER2-pY ≡ ~ 130 kDa .*

*(A) CHOdhfr-; (B) CHO-E3; and (C) CHO-E4 treatment medium.*

To investigate phosphorylation changes to this receptor, lysates were immunoprecipitated using α-apoER2 antibody to enrich for this component of the protein mix in the lysate. These enriched samples were subject to the same electrophoretic separation on 4-12% Bis-Tris gels, transferred to nitrocellulose membrane and immunoblotted, this time with an antibody that targeted phosphotyrosine, α-pY20. This result is presented in *Figure 5.3.2.* Exposure to E3-conditioned medium did not appear to modify the phosphorylation state over the 6 h time course (*Figure 5.3.2 B*), whereas treatment with E4-conditioned medium (*Figure 5.3.2 C*) showed an increase at 5 min, which was retained at 10 min, but had returned to the basal level at the subsequent time-points (1 h – 6 h). Investigation of lysates prepared from control-conditioned medium when subject to immunoprecipitation did not resolve any bands following immunoblotting. For relative comparison, presented in *Figure 5.3.2 A* are these lysates investigated by immunoblotting with α-apoER2 antibody. These were loaded onto gels at the same time as the immunoprecipitate samples presented in *Figure 3.3.2 A* and *B*.

### 5.3.2 Detection of PKB/Akt and its phosphorylated forms

For this investigation lysates were prepared following 1, 2, 5, 10, 20, 30 and 60 min exposure to E3- and E4-conditioned medium, as well as control conditioned medium. Displayed in *Figure 5.3.3* are the lysate signals produced when exposed to the different conditioned medium over the given time course after immunoblotting with α-Akt antibody. A single band at the expected molecular weight of 60 kDa is present, with consistent intensity between the different treatment media and across the time-course. This is in agreement with the results presented in *Chapter 3 (*see *Section 3.2.3.3*), where expression of Akt was readily detectable in SH-SY5Y cells. Treatment with control-conditioned medium showed a stable expression of PKB/Akt over the time-course (*Figure 5.3.3 A*). Although there are minor inconsistencies between time-points, these are most likely due to experimental variation. Likewise, treatment with either E3-conditioned medium showed no change in PKB/Akt over during the 60 min exposure (*Figure 5.3.3 B*), as well as during treatment with E4-conditioned medium (*Figure 5.3.3 C*). This implies that apoE does not have an effect on transcription or protein turnover, whether during short exposure (1-5 min) or over a longer period (10-60 min).

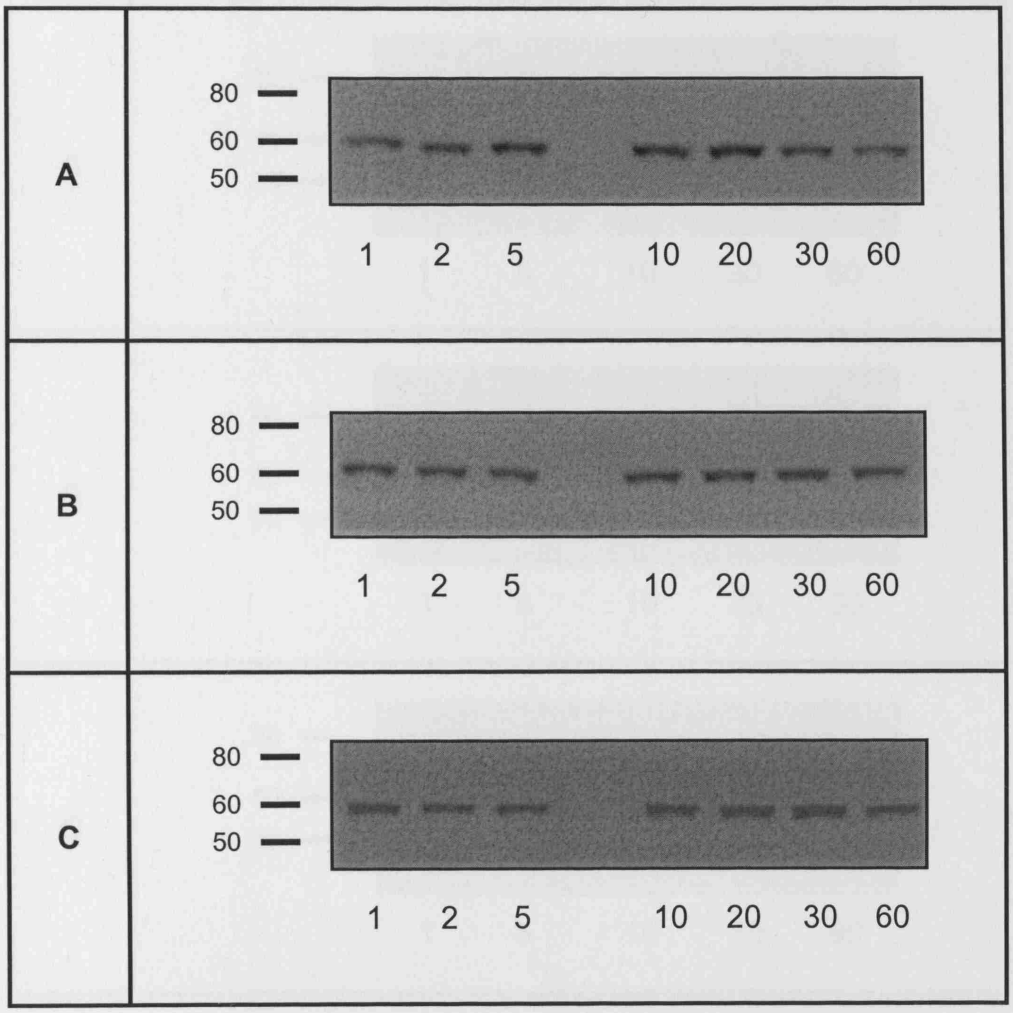


**Figure 5.3.3 Incubation of SH-SY5Y cells with E3-, E4- and control-conditioned medium has no effect on expression of PKB/Akt**

*Cultured SH-SY5Y cells were exposed to CHO-conditioned medium for 1, 2, 5, 10, 20, 30 and 60 min before preparation of cell lysates and subject to Western blot with α-Akt antibody. Marker on the left hand edge represents molecular weight size markers (kDa); PKB/Akt ≡ 60 kDa.*

*(A) CHOdhfr-; (B) CHO-E3; and (C) CHO-E4 treatment medium.*

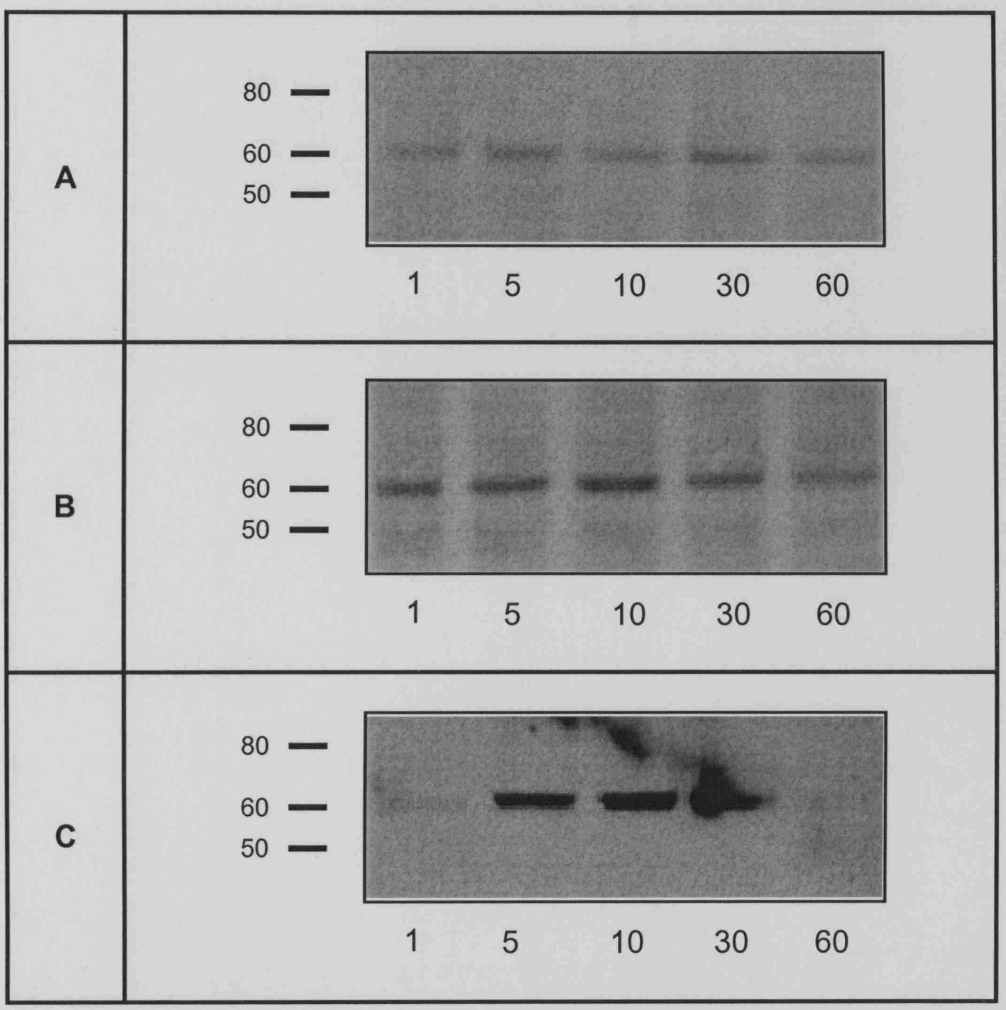


**Figure 5.3.4 Incubation of SH-SY5Y cells with apoE4 increases phosphorylation of PKB/Akt at Ser473**

*Cultured SH-SY5Y cells were exposed to CHO-conditioned medium for 1, 5, 10, 30 and 60 min before preparation of cell lysates. Lysates were immunoprecipitated using α-Akt antibody, and the enriched lysates immunoblotted with α-Akt-pSer473 antibody. The immunoprecipitate representing the 30 min time-point in (C) could be anomalous due to the presence of a slight artefact on the film across this band. Markers on left hand edge represent size markers (kDa); PKB/Akt-pSer473 ≡ 60 kDa.*

*(A) CHOdhfr-; (B) CHO-E3; and (C) CHO-E4 treatment medium.*

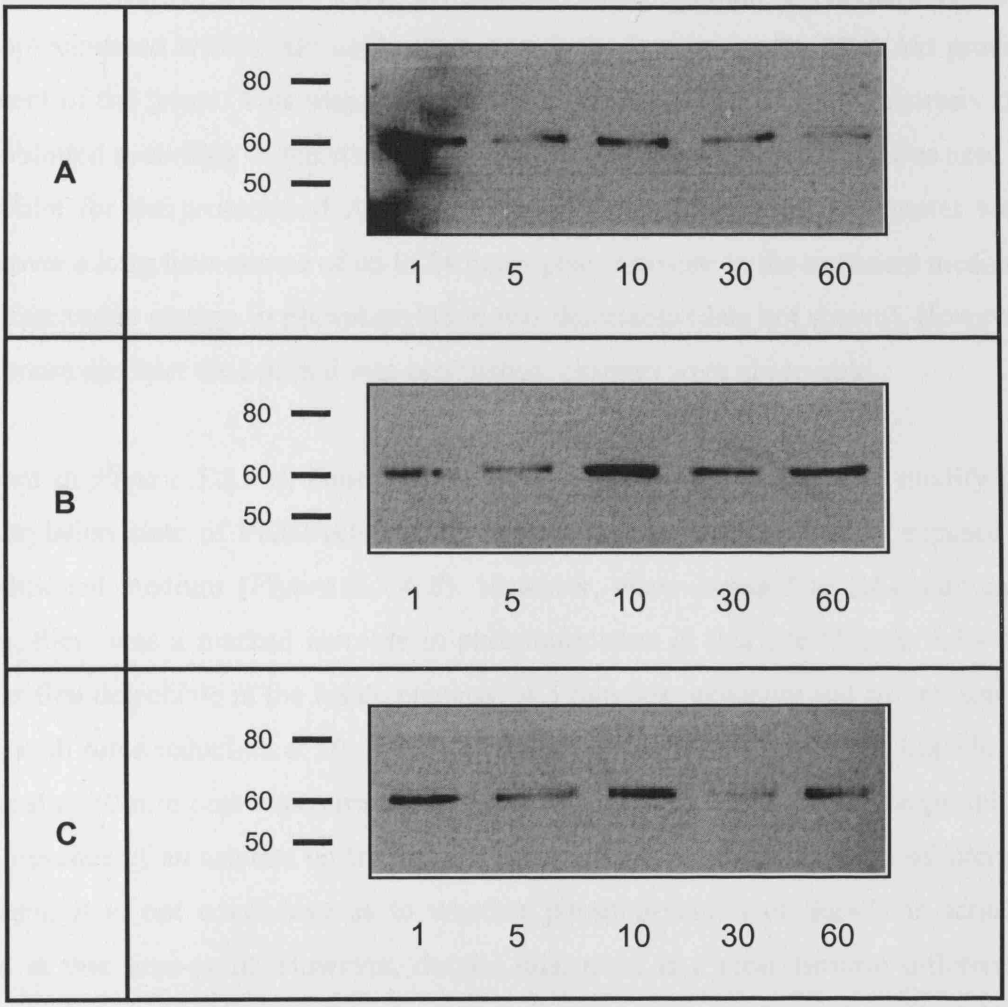


**Figure 5.3.5 Western blot of SH-SY5Y cells treated with E3-, E4- or control-conditioned media and immunoblotted to detect phosphorylation of PKB/Akt at Thr308**

*Cultured SH-SY5Y cells were exposed to CHO-conditioned medium for 1, 5, 10, 30 and 60 min before preparation of cell lysates. Lysates were immunoprecipitated using α-Akt antibody, and the enriched lysates immunoblotted with α-Akt-pThr308 antibody. Marker on the left hand edge represents molecular weight size markers (kDa); PKB/Akt-Thr308 ≡ 60 kDa.*

*(A) CHOdhfr-; (B) CHO-E3; and (C) CHO-E4 treatment medium.*

Phosphorylation changes to PKB/Akt were assayed by immunoprecipitation, and these results are presented in *Figure 5.3.4* and *Figure 5.3.5* for residues Ser473 and Thr308, respectively. Firstly, lysates were pre-cleared using Protein A-Sepharose, then immunoprecipitated with α-Akt antibody to enrich the lysates for the PKB/Akt protein component of the lysate. This was separated by 4-12 % Bis-Tris gel electrophoresis and immunoblotted according to the standard protocol. The appropriate antibody was used to immunoblot for the presence of Akt-pSer473 and Akt-pThr308. Initially, lysates were studied over a long time-course of up to 24 hours post-exposure to the treatment medium, but no discernible change in phosphorylation was detectable (data not shown). However, when a more succinct time period was established, changes were observable.

As shown in *Figure 5.3.4 A*, control-conditioned media did not appear to modify the phosphorylation state of PKB/Akt-Ser473, and this was also noted in cells exposed to E3-conditioned medium (*Figure 5.3.4 B*). However, when exposed to E4-conditioned medium, there was a marked increase in phosphorylation at this site (*Figure 5.3.4 C*). This was first detectable in the lysate prepared at 5 min post-exposure and still present at 10 min, with some reduction at 30 min. By 60 min, the site had returned to its basal level. The signal at 30 min post-exposure with apoE4 (*Figure 5.3.4 C*) has been compromised by the presence of an artefact on the film, which partially obscures the band of interest. At present, it is not conclusive as to whether phosphorylation of Ser473 is actually retained at this time-point. However, despite this, there is a clear isoform differential effect revealed at this site: apoE4 stimulating phosphorylation of Ser473 of PKB/Akt, whilst apoE3 had no effect.

Phosphorylation changes at PKB/Akt-Thr308 were less well defined (*Figure 5.3.5*). Despite loading equivalent amounts of protein in each well, the intensity of bands seems variable, with the apparent degree of phosphorylation increasing and decreasing between points across the time-course, even in the presence of control-conditioned medium (*Figure 5.3.5 A*). Exposure to E3-conditioned medium (*Figure 5.3.5 B*) and E4-conditioned medium (*Figure 5.3.5 C*) produced a similarly inconsistent pattern of expression and is difficult to analyse in a suitably qualitative manner. This experiment was repeated several times: for some experiments, new lysates were prepared by culturing SH-SY5Y cells and treating with the conditioned media, and other instances the Western blotting was attempted with either immunoprecipitated samples or 'neat' lysates. However, results remained unclear. Furthermore, stripping these nitrocellulose

membranes and reprobing with α-Akt antibody revealed that the band being detected was PKB/Akt. However, the intensity of the band, which by inference is equivalent to the amount of the protein in question being present in the lysate, was inconsistent across the film. The variation in band intensity may be a reflection of the limitations of the Bradford assay, as this was the method for preparing lysates for loading on the gel: based on the results of this assay, they were diluted in distilled water to give an equivalent concentration (1 μg/μl) of each sample. Although relatively accurate, the possibility for variance and errors to be introduced at this stage should be appreciated with this protein concentration measurement technique. As such, with the data currently available, the activity at the Thr308 site of PKB/Akt in the given conditions remains inconclusive.

### 5.3.3 Detection of NOS3 and its phosphorylated form

The presence of NOS3 protein in SH-SY5Y cells was investigated by Western blotting, as shown in *Figure 5.3.6.* This shows an immunoblot for a time course from 1 min to 6 h post-exposure to control- (*Figure 5.3.6 A*), E3- (*Figure 5.3.6 B*) and E4- (*Figure 5.3.6 C*) conditioned medium. The presence of NOS3 was detectable, although the lysates treated with E4-conditioned medium were much more defined. The reason for this difference is unclear at present.

To investigate the phosphorylation status of this protein, immunoprecipitation was performed using α-NOS3 to enrich the lysates followed by immunoblotting with α-NOS3-pSer1177 antibody. Despite repeated attempts at this experiment, the blots did not detect phosphorylation at this site being phospho-modified, although Coomassie blue staining (see *Section 2.4.3.5*) revealed the presence of protein in the gel following electrophoresis, whilst Ponceau S staining of the nitrocellulose membrane (see *Section 2.4.4.2*) showed sample transfer had occurred and sample loading was relatively consistent across the gel. A more robust confirmation of this was achieved by stripping blots that had been probed with α-NOS3-pSer1177, then reprobing with α-NOS3, as shown in *Figure 5.3.7.* This demonstrated that both E3-conditioned medium (*Figure 5.3.7 A*) and E4-conditioned medium (*Figure 5.3.7 B*) immunoprecipitates were loaded equally and, although pSer1177 form of NOS3 was not detected, the non-phosphorylated form was present in the immunoprecipitate. Although it is disappointing that phosphorylation of NOS3 was not observed, this does provide evidence suggesting the sensitivity of the α-NOS3-pSer1177. Also of note is that E4-conditioned medium samples appear marginally more intense, as was observed in *Figure 5.3.6.*

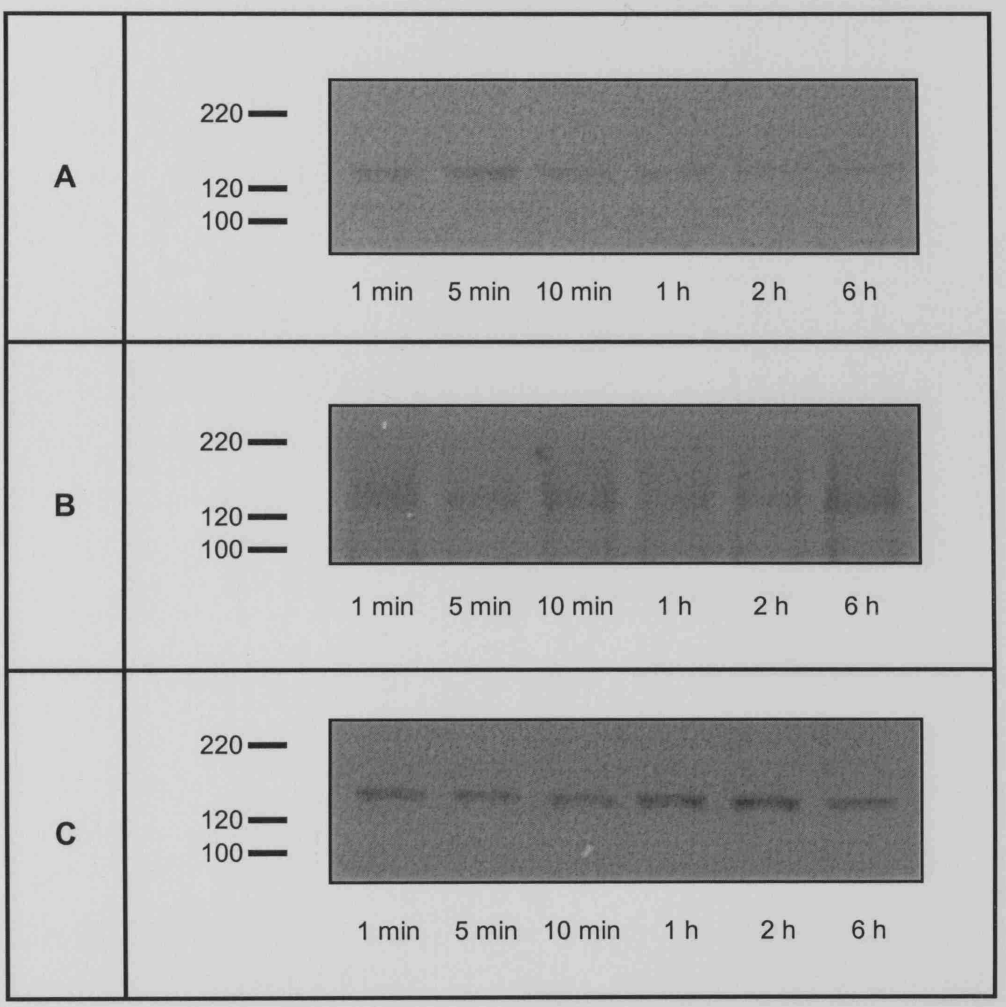


**Figure 5.3.6 Exposure of SH-SY5Y cells to E3- and E4-conditioned medium does not affect expression of NOS3 as assessed by Western blot**

*Cultured SH-SY5Y cells were exposed to CHO-conditioned medium for 1, 5 and 10 min, then 1, 2 and 6 h. Expression of NOS3 was assessed by immunoblotting with α-NOS3 antibody. Marker on the left hand edge represents molecular weight size markers (kDa); NOS3 ≡ 140 kDa.*

*(A) CHOdhfr-; (B) CHO-E3; and (C) CHO-E4 treatment medium.*

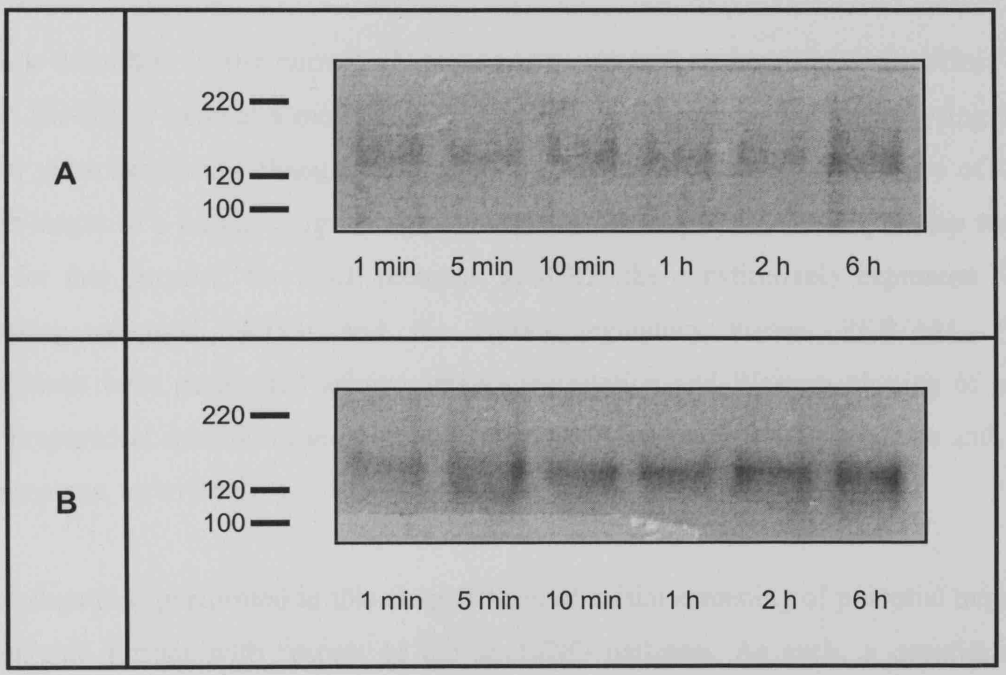


**Figure 5.3.7 Reprobing of blots with α-NOS3 following an initial immunoblot of immunoprecipitates with α-NOS3-pSer1177**

*Cultured SH-SY5Y cells were exposed to CHO-conditioned medium for 1, 5 and 10 min, then 1, 2 and 6 h. Following this, samples were immunoprecipitated with α-NOS3 to enrich lysates, then assayed by Western blot for the presence of pSer1177 NOS3. Figures above represent stripping of this blot, then reprobing with α-NOS3 to confirm the presence of NOS3 on the membrane, despite no pSer1177 being detected. Marker on the left hand edge represents molecular weight size markers (kDa); NOS3 ≡ 140 kDa.*
*(A) CHO-E3; and (B) CHO-E4 treatment medium.*

## 5.4 DISCUSSION

The foundational work described in *Chapter 3* established the presence of relevant apoE receptors and components of the NO biosynthesis pathway in human neuronal cell lines, with particular reference to the neuroblastoma cell line, SH-SY5Y. With this as a basis, it was hoped that the release of NO as a response to apoE-conditioned medium could be assayed with this cell line, and was investigated in *Chapter 4*. However, the findings from that study proved inconclusive and could not be fully resolved with the assay methods available.

The work described in the current chapter was an attempt to investigate the effect of apoE on SH-SY5Y cells at a more discreet stratum. This was achieved by analysing the potential phosphorylation changes to a panel of proteins that are representative of the different stages of a putative signalling pathway mediated by apoE. Three proteins were chosen for this purpose: the apoE receptor, apoER2; the constitutively expressed NO synthesising enzyme, NOS3; and the NOS3 regulatory kinase, PKB/Akt. The investigations were performed using immunoprecipitation and Western blotting of cell lysates prepared at specific time-points ranging from 1 min to 6 h post-exposure and, in some instances, up to 24 h.

The investigations performed in this chapter form an initial screening of potential targets to investigate further with respect to the apoE/NO pathway. As such, a quantitative analysis of changes in phosphorylation over time (if indeed a change had occurred) has not been undertaken. Instead, the focus has been far more on a qualitative differentiation of effects that exposure to an exogenous apoE source can have on these neuroblastoma cells, and whether these are detectable, as opposed to measurable. Following on, if time permitted, experimental conditions could have been fully rationalised and optimised to allow an accurate measure of change in phosphorylation state of the different proteins investigated against their basal characteristic.

The presence of all three proteins, which had been detected at the mRNA-level in *Chapter 3*, was confirmed at the protein-level by Western blotting. Exposure of cells to E3-conditioned medium did not appear to affect the phosphorylation state of any of the proteins investigated, and was similar to the effect of control-conditioned medium. However, treating with E4-conditioned medium appeared to increase phosphorylation at Ser473 of PKB/Akt, and also tyrosine phosphorylation of apoER2. In both instances, a

peak level of phosphorylation was detected at 5 min post-exposure to apoE4, with a gradual decrease over the remainder of the time-course. Conversely, as already noted for E3-conditioned medium, apoE4 had no effect on NOS3 phosphorylation at the Ser1177 site; nor was any discernible effect observed at the Thr308 site of PKB/Akt. These results do seem to indicate an apoE isoform differential effect with respect to PKB/Akt and apoER2 signalling events, validating to some extent the hypothesis that apoE4 can modify cellular functions in neuronal cells. Unfortunately, the lack of any phosphorylation change in NOS3 was disappointing. However, this does support the findings presented in *Chapter 4*, whereby changes in NO release were not apparently different from basal levels when SH-SY5Y cells were exposed to apoE-conditioned medium. Moreover, the stripping and reprobing of these blots to check for the presence of NOS3 on the membrane revealed bands at the correct molecular weight, indicating that this immunoblotting assay was sensitive.

The effect of apoE-conditioned medium on apoER2 was not unexpected, as apoE is a ligand for this receptor. Currently, much interest in this receptor stems from its interaction with the very-low-density lipoprotein receptor (VLDL-r): in concert, they are a ligand for Reelin, and have been shown to play important roles in neuronal migration and positioning in the cerebral cortex and cerebellum in mice [319,320]. However, whether apoE-laden lipoprotein particles actually utilise apoER2 for receptor-mediated endocytosis of these particles is unclear. Studies in mice have demonstrated that the binding efficiency of apoER2 for β-VLDL particles is threefold lower than the LDL-receptor [150]. Furthermore, the foundational study by Yamamoto's group, who first identified apoER2, revealed that the receptor had very poor affinity for LDL and VLDL, but would bind with high affinity to apoE-rich β-VLDL particles [226]. More recently, Bu and colleagues investigated the endocytic rates of a panel of apoE receptors, including apoER2, LRP, VLDL-r and LDL-r. They discovered that whilst LRP had an extremely rapid and efficient rate of endocytosis, apoER2 and VLDL-r were significantly less effective at this process [321]. Our group has demonstrated that apoER2 (but, notably, not LDL-r) is located in caveolae, the same subcellular region that numerous other signalling components – such as NOS3, PSD-95 and Src – could potentially be located, which gave credence to apoER2's role in signalling events [322], and there is further evidence that strongly indicates that apoER2 does not have a primary role in lipoprotein endocytosis at all, but rather influencing signalling events such as those described above [323].

Although structurally very similar to the LDL-r and VLDL-r, apoER2 has the distinction of featuring a 59 amino acid insert present in its cytoplasmic tail, which contains 3 proline-rich PxxP motifs [226,324]. As discussed in *Chapter 1, Section 1.4.5*, these motifs are potential Src homology 3 (SH3) binding domains [325]. Many proteins that contain SH3 domains are involved in signal transduction pathways [326,327]. Furthermore, apoER2 (but not VLDL-r) can interact with the adaptor protein c-Jun N-terminal kinase (JNK) interacting protein (JIP) [328]. This can promote PKB/Akt activation as well as interacting with anterograde molecular motor kinesin, which could allow it to putatively act as a scaffold for transporting signalling molecules such as Dab-1 along microtubules [329,229].

The apoE4 induced tyrosine phosphorylation of apoER2 observed in the present study is supported by the concomitant phosphorylation of Akt at Ser473. It is likely that the two events are linked, as apoER2 is a known upstream propagator for PI3K and, in-turn, PKB/Akt activation. However, one problematic aspect of this conclusion is the time taken for phosphorylation at these sites to return to their basal level. For apoER2, the initial tyrosine phosphorylation is detected at 5 min post-treatment, which persists for at least 10 min, and even seems to be present to some extent after 1 h (*Figure 5.3.2 C*). In the case of PKB/Akt phosphorylation at Ser473 (presented in *Figure 5.3.4*), the change is initially detectable 10 min post-treatment and persists for at least 30 min, although by 1 h it returned to its basal level (though no intermediate time-points were assayed). Previous investigations of apoER2 tyrosine phosphorylation in EA.hy926 endothelial cells by our group has demonstrated that in response to apoE2-conditioned media, a peak level of phosphorylation could be observed at 2.5 min post-exposure; this was completely diminished by 10 min when it had returned to its resting state [211]. However, D'Mello's group investigated PKB/Akt in rat cerebellar granule cells in response to a range of neuronal survival factors such as insulin-like growth factor (IGF-1) and cyclic-AMP [330]. Their study revealed that exposure to IGF-1 resulted in sustained phosphorylation at both Ser473 and Thr308, which started 2 min post-treatment and had not diminished by the end-point of 1 h, a finding that has been observed in other studies [331,332].

The observed phosphorylation changes of PKB/Akt are significant and represent an apoE isoform differential effect. It could be argued that this is of more significance than the apoER2 response, as this is a downstream effect of protein phosphorylation; there must

be an initiating event upstream of Akt phosphorylation at Ser473, which has propagated to this kinase. Most probably this pathway involves the action of PI3K; this could be confirmed by the use of a PI3K inhibitor such as wortmannin or LY294002, the presence of which should abolish this phosphorylation change. Once phosphorylated and active, there are a range of signalling events that could be potentiated by PKB/Akt [314], including activation of NOS3 and glycogen synthase kinase-3 (GSK-3) [333]. The phosphorylation sites at Ser473 and Thr308 act synergistically to generate a high level of PKB/Akt activity [334]. Initial activation is thought to occur through Thr308, which is then followed by phosphorylation of Ser473, putatively though the action of PDK1, which is an established as a mechanism for Thr308 phosphorylation. Furthermore, it was thought that phosphorylation of Ser473 could not occur without the prior activity of Thr308. However, in 2000, Alessi's group investigated this activity in mouse embryonic stem cells where the both copies of the PDK1 gene were knocked-out [335]. Most surprisingly, these cells were viable and did not undergo premature apoptosis. Exposure to IGF-1 did not result in phosphorylation at Thr308, implicating PDK1 as an essential modifier of phosphorylation state of this residue. However, Ser473 was phosphorylated, even in the absence of stimulatory factors; in the presence of IGF-1, a two-fold increase was observed. Moreover, phosphorylation of GSK-3 was also abolished in these cells, indicating that Thr308 plays a vital role in downstream activation events. There is now an emerging view that indicates Ser473 phosphorylation (either through PKB/Akt autophosphorylation or by the action of PDK1) actually precedes events at Thr308 [241,336,337]

Ultimately, both Ser473 and Thr308 require phosphorylation if PKB/Akt is to be an effective activator of downstream signalling events. This may be a reason for NOS3 not undergoing any phospho-modification in this particular system. The data presented in *Chapter 4* indicated that exposure to apoE-conditioned media was having some effect on SH-SY5Y cells, but this effect could not reproducibly quantified using the assay methods available. It was hoped that observing molecular changes of NOS3 could elucidate some of the events occurring within this signalling pathway. The influence of PKB/Akt on NOS3 is well characterised [188,187,183], whilst the phosphorylation at Ser1177 of NOS3 is a well-established activation event for nitric oxide biosynthesis. However, there is the possibility that NOS3 responds to phosphorylation changes in PKB/Akt in a similar manner to GSK-3, namely that activation of PKB/Akt must occur at both Thr308 and Ser473 before the signal can be propagated to NOS3, which activates this enzyme and

synthesises NO. An interesting aside to this investigation would have been to assay any phosphorylation changes that may occur to GSK-3 in the lysates that were prepared.

The present study has demonstrated that exposure of SH-SY5Y cells to apoE-conditioned medium does indeed result in detectable intracellular changes over the specified time-course. Furthermore, these changes were isoform specific, with apoE4 delivering elevated phosphorylation of PKB/Akt at Ser473 and tyrosine phosphorylation of apoER2. Physiologically, with respect to NO release, no change has been detectable in these cells, which was further supported by the lack of activation of NOS3 at the biochemical level. However, a wide range of signalling events can be instigated by PKB/Akt, so there is a potential for other intracellular events to have been modified by the action of apoE exposure.

# Chapter 6

# GENERAL DISCUSSION

# 6.0 GENERAL DISCUSSION

## 6.1 THE EXISTING INFORMATION

As outlined in *Chapter 1*, Alzheimer's disease represents a significant healthcare issue for Western societies. By the middle of this century, an estimated 25% of the population in the West will be over the age of 65; approximately one-third of these are likely to be affected by AD. The legacy of this disease can be measured by two distinct indices: the progressive effects on a patient's quality of life; and the cost of long-term care and treatment for those affected.

Though our understanding of AD pathology and disease progression has advanced over the last few decades, establishing a complete natural history for the disease's genesis and advancement through to cognitive dysfunction still eludes. The twin events of abnormal amyloid precursor protein processing and the hyperphosphorylation of microtubule-associated tau are widely regarded as the instigatory factors that lead to, respectively, amyloid-rich neuritic plaques and paired-helical filaments (PHFs), the two classic hallmarks of AD pathology [1]. Genetic linkage analysis has identified highly penetrant missense mutations in three genes in familial forms of AD, the amyloid precursor protein (APP), presenilin-1 (PS-1) and presenilin-2 (PS-2) [12,93,8]. Despite this, 90-95% of AD cases are late-onset, occurring sporadically with no observable mutation in the APP or presenilin genes [165,98].

Understanding the molecular basis of AD was given a significant boost over 10 years ago by the discovery that the ε4 allele of apoE was genetically linked to late-onset AD, representing a key susceptibility gene in the development of the disease [102,101]. However, despite numerous efforts, the precise contribution of apoE4 to disease pathogenesis remains unclear, although a range of investigations have studied its effects on neurobiology and physiology with respect to AD. These include: its co-localisation with amyloid-rich neuritic plaques in AD brains as well as its accumulation in regions of damaged or regenerating nerves [338,339], where it may function as a scavenger to retain cholesterol to be utilised in the axonal regeneration process [129]; binding and stabilising microtubules to inhibit hyperphosphorylation of tau [229,131,130]; isoform differential promotion of neurite extension [133,134]; and enhancement of fibrillisation of Aβ peptides to generate neuritic plaques [340].

## 6.2 ApoE-MEDIATED SIGNALLING THROUGH RECEPTORS

This present study has investigated a particular physiological function that could be susceptible to the different apoE isoforms, namely the biosynthesis of nitric oxide, a ubiquitous intercellular messenger that can modulate cerebral blood flow, thrombosis and neurotransmitter release as well as contributing to morphogenesis and synaptic plasticity [240,167]. The effect of exposure of neuronal cells to apoE was investigated and a number of approaches were taken in the course of this research with the eventual goal being to effectively assay this response. In the first instance, a survey was performed to determine suitable cell line(s) that could be utilised for investigation. Quantitative reverse-transcriptase-PCR was employed for this, and a panel of 38 human cell lines was investigated, 12 from neuronal sources, on a 96-well plate. This investigation revealed that in the 12 brain-derived cell lines there was relatively good expression of LDL-r, VLDL-r, LRP, apoER2 and scavenger receptors SR-BI and SR-BII; all cell-surface receptors known to bind apoE.

Significantly, expression of the VLDL-r was consistently strong in neuronal cell lines (although, the highest expression of this receptor was in cell lines derived from smooth muscle cells), and the expression of apoER2 supported existing studies that have implicated it as being predominantly expressed in the brain [226]. In fact, apoER2, in concert with VLDL-r, is widely accepted to function as a cellular receptor on the surface of post-mitotic neurons for the signalling factor, Reelin; thus ensures correct positional migration of these cells during brain development [148]. There is evidence to suggest that apoER2, unlike certain other apoE receptors, does not have a primary function as an endocytosing agent of apoE-laden lipoproteins for lipid uptake, but rather functions as a signalling receptor. This is further espoused by the observation that the cytoplasmic tail of apoER2 has a series of proline-rich residues that can recruit SH3 signalling motif-containing proteins, which raises the prospect of it initiating or transducing a signal from the cell-surface to downstream targets. Following on from the identification of enhanced apoER2 expression in brain-derived cell lines, the effect of exposure to apoE-conditioned medium on phosphorylation of the receptor was investigated in *Chapter 5*. In this case, exposure to apoE4-conditioned medium resulted in an increase in tyrosine phosphorylation approximately 5 min post-treatment, which was not seen in the presence of E3- or control-conditioned medium.

The proline-rich domains of the cytoplasmic intracellular region of apoER2 are a distinct feature that has also been identified in the cytoplasmic tail of SR-BII, the splice variant of SR-BI, which was shown herein to be expressed preferentially in many brain derived cell lines. This may be a significant finding, as the tail sequence of SR-BII could function in a similar manner to apoER2 by instigating signalling pathways that could have profound downstream effects. Furthermore, scavenger receptors are known to have an affinity for Aβ [341], as well as strong expression in astrocytes [342,343,344]. A recent study investigated the effect of mouse SR-BI overexpression in HepG2 cells [345]. These recombinant cells were found to preferentially take up HDL particles over LDL. Moreover, exposure to HDL resulted in a 10-fold increase in phosphorylation of NOS3 at the Ser1177 residue, at a similar level at both 5 min and 30 min post-exposure to HDL. Concomitantly, there was a 2-fold increase in the conversion of [$^{14}$C]-arginine to [$^{14}$C]-citrulline in these cells, indicating enhanced NO biosynthesis. Other studies have attested to similar findings in both human endothelial and CHO cells [160,346,347], in addition to identifying both PKB/Akt and mitogen activated protein (MAP) kinase (MAPK) as downstream propagators of a signal that originates from the interaction of SR-BI with PI3K and eventually activates NOS3 [161].

This evidence strongly supports the contention that SR-BI is a significant contributory factor in the release of NO, at least in the cardiovascular system. The most likely pathway involves the C-terminal PDZ[9] domain and its interaction with the PDZ-domain containing adaptor protein, PDZK1 [348,239]. At present there are no data directly supporting the theory that NO biosynthesis can be mediated via SR-BI in neuronal cells. However, the C-terminal region of SR-BII is completely dissimilar to that of SR-BI, and is distinguished by the presence of SH3 motifs, as described above [164]. Potentially, therefore, SR-BII has the capability of propagating a signal from the cell surface through to NOS activation, or some other downstream effect.

Unfortunately, the putative effects of these distinct signalling regions of SR-BII may not be as obvious as their very presence would imply. Silver's group investigated the effect of HDL exposure to COS-M6 kidney cell lines overexpressing either SR-BI or SR-BII [349]. In both transfected cell-lines, HDL binding and cholesterol flux was similar, which reflects the fact that apart from the C-terminal, both SR-BI and SR-BII are identical, including their ligand binding region. Although, with regard to this finding, of

[9] postsynaptic density protein (PSD-95)/*Drosophila* discs-large (dlg)/tight-junction protein (ZO1)

note is a study by van der Westhuyzen and colleagues (who first identified the presence of the SR-BII splice variant), which revealed SR-BII influencing cholesterol trafficking differently to SR-BI [350]. Moreover, Silver's investigation reported that SR-BII did not appear to phosphorylate NOS3, which was supported by the absence of HDL-stimulated NO release in this recombinant cell line [349]. To investigate the significance of the PDK1-binding domain in SR-BI, the activity of a cell line mutant that lacked this domain was assayed, wherein phosphorylation of NOS3 and concomitant activation was abolished. These findings indicate that the PDK1-binding domain is a key contributory element of NOS3 activation by SR-BI, whereas there is no apparent influence of SR-BII on these events. At present, this remains the only study to explore the putative abilities of SR-BII to mediate the activity of NOS3. The findings in this thesis revealed preferential expression of SR-BII in several neuronal cell lines, which could also be investigated with respect to this putative functionality. Clearly there must be a rationale for this prevalence, although this is not immediately apparent with the existing data. Certainly the presence of unique C-terminal signalling elements on SR-BII is not doubted. However, in this thesis, the functional repercussions of this were not explored beyond mRNA copy numbers.

Most recently, Carlsson and colleagues have reported the identification of a third form of scavenger receptor class B [351]. This form, identified as SR-BIII, arises from an alternate splice acceptor site on exon 11 (in much the same way as that which occurs in the generation of SR-BII), but with an additional frame-shift such that a region upstream of exon 12 (which in SR-BI is used in its entirety) now enters the reading frame and the stop codon occurs within the middle of this exon; the authors refer to this as exon 12 B. This novel splice variant was found in both macrophages and atherosclerotic plaques. As with SR-BII, the tail of SR-BIII is distinct, and is much longer at 55 amino-acids, although notably there are both SH2 and SH3 binding motifs in addition to a protein kinase C binding motif. This seems to implicate potential signalling functions, although this was not investigated. At present, this remains a novel finding, and has not been studied in any other groups.

## 6.3 ASSAYING NITRIC OXIDE RELEASE UPON apoE EXPOSURE

Surveying expression of apoE receptors and NO biosynthesis components in neuronal cell lines in *Chapter 3* identified SH-SY5Y neuroblastoma cells as a suitable cell line for investigating the response of exposure to apoE with respect to NO release. Although this

cell line was never the highest expressing neuronal cell line with respect to any individual apoE receptor, it did demonstrate relatively consistent expression of all the numerous receptors, as presented in *Figures 3.3* and *3.4*. Moreover, expression of the three NOS isoenzymes was also uniformly high in SH-SY5Y cells, especially relative to the other brain-derived cell lines that were assessed. Overall, the cumulative information from this analysis of neuronal cell lines appeared to indicate SH-SY5Y as a suitably diverse cellular model in so far as gene expression of relevant components of the putative apoE/NO release pathway were concerned. Furthermore, this cell line is easy to culture and has been utilised in numerous previous studies and are, therefore, relatively well characterised.

However, before exploring this pathway could be commenced, it was necessary to accurately measure the apoE content of conditioned medium prior to treating cells. An enzyme-linked immunosorbent assay (ELISA) technique was described in *Chapter 2 Section 2.5*, which led to the establishment of a robust and accurate sandwich ELISA for this purpose. This was utilised in the investigations described in *Chapter 4*, where SH-SY5Y cells were exposed to apoE3-, E4-, E2- and control- conditioned medium. A number of assay methods were studied, the most successful of which was the cyclic-GMP radioimmunoassay, which represented an indirect measure of NO biosynthesis. This indicated that the three apoE isoforms did indeed differentially modulate cGMP production such that E3-conditioned medium was the strongest, followed by E2 and then E4; relative to the control-conditioned medium, exposure to exposure to E4 gave a 6 % decrease in radioactivity counts, whilst E3 medium resulted in a 12 % decrease in radioactivity. However, this was a questionable result as these changes in radioactivity were only marginally distinct from what could be considered as null responses. Furthermore, due to the non-linear relationship between radioactivity count and cGMP concentration, this change in dpm is actually equivalent to an even smaller change in intracellular cGMP: the response with E3-conditioned medium of 12 % dpm change is equivalent to an approximately 1 % change in cGMP concentration. The inability to generate a substantial decrease in radioactive counts from the baseline level may well reflect the choice of cell line in this investigation.

With respect to NOS3 expression in neuronal cell lines, the highest expressing cell line was in fact the activated derivative of IMR-32 cells, which had a more neuron-like morphology, achieved by a 7 day exposure to retinoic acid prior to analysis. This cell line

had a 3-fold higher mRNA copy number of NOS3 expression relative to SH-SY5Y cells, and could have been more suitable for investigating the release of NO in response to apoE. Unfortunately, attempts at culturing the cells (before any attempts at treating it with retinoic acid) proved unsuccessful and it was not possible to establish a thriving culture. An alternative to trying to culture these IMR-32 cells could have been to transfect SH-SY5Y cells, which were very easy to culture, and have them overexpress NOS3. Establishing such a cell line would have proven a powerful tool for investigating the apoE/NO pathway.

Extending this further, SH-SY5Y cells could have been transfected to give recombinant cell lines overexpressing one or more apoE receptors, such as apoER2, SR-BI/SR-BII or LRP. This could have been an elegant demonstration of the effects of exposure to apoE-conditioned medium in the manner of the investigations described earlier in endothelial cells, where overexpression of SR-BI could be used to demonstrate its contribution to NOS3 phosphorylation and concomitant NO release [345]. The obvious criticism of such an approach is that it artificially exaggerates the cell surface chemistry of this cell line. However, such a study would have provided a proof-of-principle aim and would undoubtedly have enhanced the findings presented in *Chapter 4*.

A similar argument could be put forward with regard to the data presented in *Chapter 5*, where exposure to E3- and E4-conditioned medium gave isoform differential effects with respect to apoER2 tyrosine phosphorylation and phosphorylation at the Ser473 residue of PKB/Akt. In both instances, E4-conditioned medium gave an increased level of phosphorylation, initially detected at 5 min post-exposure and sustained for at least 30 min. However, there was no discernible activation of NOS3 at the Ser1177 residue with either apoE treatment, implying that there would be no associated increase in nitric oxide release. This calls into question once again the putative conclusion in *Chapter 4*, where a change in cGMP was inferred by the minor shifts in radioactive counts when exposed to apoE-conditioned medium relative to control-conditioned medium. It was suggested that the decrease in radioactivity might indicate NO biosynthesis (as is implicated by increased cGMP production), while cautioning that this might simply be the baseline activity of the cells in these conditions. The failure to detect NOS3 phosphorylation would support the latter.

## 6.4 FINAL THOUGHTS – A ROBUST HYPOTHESIS?

The principal hypothesis in this thesis was that exposure of human brain-derived cells to apoE will result in a change in NO release, and that this will show an isoform differential effect. The investigation presented in *Chapter 5* seems to support the presence of an isoform differential effect, with a putative signalling pathway that involves phosphorylation changes to apoER2 and PKB/Akt, most probably coupled by PI3K. Significantly, though, this did not propagate to NOS3 as was postulated. At a more functional level, an attempt to demonstrate this isoform differential effect by either directly measuring NO release through the DAF fluorescent assay or indirectly through the cGMP radioimmunoassay, did appear to support the existence of a isoform differential effect. However, these results were flawed somewhat by the lack of sensitivity when attempting to measure what seemed to be very subtle changes in NO biosynthesis in response to apoE.

The genetic linkage of the ε4 allele of apoE to AD is well-established; as has been discussed in *Chapter 1*, the reasons for this are yet to be fully elucidated despite investigations over more than a decade. The ability of apoE to regulate NO release has been previously demonstrated in endothelial cells and platelets by our group [352,211,353,354], and extending this apoE-NO link to neuronal cells as a putative contributory factor to AD is logical and sensible. Insofar as combining the different components of this study – apoE, nitric oxide and Alzheimer's disease – there is significant support from a study by Colton's group, where the release of NO was measured in monocyte-derived macrophages taken from patients diagnosed with AD and compared with non-AD controls [355]. This study demonstrated that AD patients genotyped as ε4 homozygous produced a significantly higher NO release (as measured by nitrite levels) in response to immune activation by interferon-γ (IFN-γ) compared to both ε3 homozygous AD and non-AD patients.

However, the investigations presented in this thesis are an attempt to rationalise the NO response to apoE directly in human brain-derived neuronal cells rather than blood-monocyte macrophages. Nitric oxide is well-established as an intercellular messenger in the brain, with numerous downstream functions. The potential for apoE to affect this physiological balance is apparent, although the evidence presented in this thesis has not been conclusive. How significantly the different apoE isoforms contribute to fluxes in NO biosynthesis in the brain is yet to be fully explored. Although there is no completely

conclusive biochemical evidence that fully explains the genetic linkage of apoE4 to AD, there is likely to be a multitude of functions that apoE can impact upon within both the normal brain and in AD progression. As such, it is most likely to have an indirect effect by modulating the brain's metabolic functions in a multifactorial manner.

In the decade since the identification of the ε4 allele of apoE as a major susceptibility factor for developing AD, investigations have studied a range of hypotheses regarding its contribution to disease onset. The relationship between NO and apoE is certainly a component of AD pathophysiology where progress is being made and could ultimately prove to be a critical component in concert with other established mechanisms linked to apoE4. These future findings will be awaited, therefore, with great interest.

# BIBLIOGRAPHY


1. Nussbaum RL,Ellis CE. (2003). Alzheimer's disease and Parkinson's disease. *N.Engl.J.Med.* **348**: 1356-64.

2. Hebert LE, Scherr PA, Bienias JL, Bennett DA,Evans DA. (2003). Alzheimer disease in the US population: prevalence estimates using the 2000 census. *Arch.Neurol.* **60**: 1119-22.

3. Feldman H, Gauthier S, Hecker J, Vellas B, Hux M, Xu Y, Schwam EM, Shah S,Mastey V. (2004). Economic evaluation of donepezil in moderate to severe Alzheimer disease. *Neurology.* **63**: 644-50.

4. Rodgers A B. (2005). 2004-2005 progress report on Alzheimer's disease (http://www.alzheimers.org/pr04-05/index.asp). 1-88.

5. Gasparini L, Racchi M, Binetti G, Trabucchi M, Solerte SB, Alkon D, Etcheberrigaray R, Gibson G, Blass J, Paoletti R,Govoni S. (1998). Peripheral markers in testing pathophysiological hypotheses and diagnosing Alzheimer's disease. *FASEB J.* **12**: 17-34.

6. Ganguli M, Dodge HH, Shen C, Pandav RS,DeKosky ST. (2005). Alzheimer disease and mortality: a 15-year epidemiological study. *Arch.Neurol.* **62**: 779-84.

7. Carlson GA. (2003). A welcoming environment for amyloid plaques. *Nat.Neurosci.* **6**: 328-30.

8. Suh YH,Checler F. (2002). Amyloid precursor protein, presenilins, and alpha-synuclein: molecular pathogenesis and pharmacological applications in Alzheimer's disease. *Pharmacol.Rev.* **54**: 469-525.

9. Racchi M,Govoni S. (2003). The pharmacology of amyloid precursor protein processing. *Exp.Gerontol.* **38**: 145-57.

10. Checler F,Vincent B. (2002). Alzheimer's and prion diseases: distinct pathologies, common proteolytic denominators. *Trends Neurosci.* **25**: 616-20.

11. Esler WP,Wolfe MS. (2001). A portrait of Alzheimer secretases--new features and familiar faces. *Science.* **293**: 1449-54.

12. Li YJ, Scott WK, Hedges DJ, Zhang F, Gaskell PC, Nance MA, Watts RL, Hubble JP, Koller WC, Pahwa R, Stern MB, Hiner BC, Jankovic J, Allen FA, Jr., Goetz CG, Mastaglia F, Stajich JM, Gibson RA, Middleton LT, Saunders AM, Scott BL, Small GW, Nicodemus KK, Reed AD, Schmechel DE, Welsh-Bohmer KA, Conneally PM, Roses AD, Gilbert JR, Vance JM, Haines JL,Pericak-Vance MA. (2002). Age at onset in two common neurodegenerative diseases is genetically controlled. *Am.J.Hum.Genet.* **70**: 985-93.

13. Campion D, Dumanchin C, Hannequin D, Dubois B, Belliard S, Puel M, Thomas-Anterion C, Michon A, Martin C, Charbonnier F, Raux G, Camuzat A, Penet C, Mesnage V, Martinez M, Clerget-Darpoux F, Brice A,Frebourg T. (1999). Early-onset autosomal dominant Alzheimer disease: prevalence, genetic heterogeneity, and mutation spectrum. *Am.J.Hum.Genet.* **65**: 664-70.

14. Maurer K, Volk S,Gerbaldo H. (1997). Auguste D and Alzheimer's disease. *Lancet.* **349**: 1546-49.

15. O'Brien C. (1996). Auguste D. and Alzheimer's disease. *Science.* **273**: 28.

16. Graeber MB, Kosel S, Egensperger R, Banati RB, Muller U, Bise K, Hoff P, Moller HJ, Fujisawa K,Mehraein P. (1997). Rediscovery of the case described by Alois Alzheimer in 1911: historical, histological and molecular genetic analysis. *Neurogenetics.* **1**: 73-80.

17. Alzheimer A, Stelzmann RA, Schnitzlein HN,Murtagh FR. (1995). An English translation of Alzheimer's 1907 paper, "Uber eine eigenartige Erkankung der Hirnrinde". *Clin.Anat.* **8**: 429-31.

18. Blessed G, Tomlinson BE,Roth M. (1968). The association between quantitative measures of dementia and of senile change in the cerebral grey matter of elderly subjects. *Br.J.Psychiatry.* **114**: 797-811.

19. Mesulam M. (2004). The cholinergic lesion of Alzheimer's disease: pivotal factor or side show? *Learn.Mem.* **11**: 43-49.

20. Gauthier S, Panisset M, Nalbantoglu J,Poirier J. (1997). Alzheimer's disease: current knowledge, management and research. *CMAJ.* **157**: 1047-52.

21. Cummings JL. (2004). Alzheimer's disease. *N.Engl.J.Med.* **351**: 56-67.

22. Kurt MA, Davies DC,Kidd M. (1999). beta-Amyloid immunoreactivity in astrocytes in Alzheimer's disease brain biopsies: an electron microscope study. *Exp.Neurol.* **158**: 221-28.

23. Kurt MA, Davies DC,Kidd M. (1997). Paired helical filament morphology varies with intracellular location in Alzheimer's disease brain. *Neurosci.Lett.* **239**: 41-44.

24. Davies P,Maloney AJ. (1976). Selective loss of central cholinergic neurons in Alzheimer's disease. *Lancet.* **2**: 1403.

25. Bowen DM, White P, Flack RH, Smith CB,Davison AN. (1974). Brain-decarboxylase activities as indices of pathological change in senile dementia. *Lancet.* **1**: 1247-49.

26. Perry EK, Perry RH, Blessed G,Tomlinson BE. (1978). Changes in brain cholinesterases in senile dementia of Alzheimer type. *Neuropathol.Appl.Neurobiol.* **4**: 273-77.

27. Perry EK, Tomlinson BE, Blessed G, Bergmann K, Gibson PH,Perry RH. (1978). Correlation of cholinergic abnormalities with senile plaques and mental test scores in senile dementia. *Br.Med.J.* **2**: 1457-59.

28. Terry AV, Jr.,Buccafusco JJ. (2003). The cholinergic hypothesis of age and Alzheimer's disease-related cognitive deficits: recent challenges and their implications for novel drug development. *J.Pharmacol.Exp.Ther.* **306**: 821-27.

29. Scarpini E, Scheltens P,Feldman H. (2003). Treatment of Alzheimer's disease: current status and new perspectives. *Lancet Neurol.* **2**: 539-47.

30. Reisberg B, Doody R, Stoffler A, Schmitt F, Ferris S,Mobius HJ. (2003). Memantine in moderate-to-severe Alzheimer's disease. *N.Engl.J.Med.* **348**: 1333-41.

31. Lipton SA,Rosenberg PA. (1994). Excitatory amino acids as a final common pathway for neurologic disorders. *N.Engl.J.Med.* **330**: 613-22.

32. Tariot PN, Farlow MR, Grossberg GT, Graham SM, McDonald S,Gergel I. (2004). Memantine treatment in patients with moderate to severe Alzheimer disease already receiving donepezil: a randomized controlled trial. *JAMA.* **291**: 317-24.

33. Lemere CA, Blusztajn JK, Yamaguchi H, Wisniewski T, Saido TC,Selkoe DJ. (1996). Sequence of deposition of heterogeneous amyloid beta-peptides and APO E in Down syndrome: implications for initial events in amyloid plaque formation. *Neurobiol.Dis.* **3**: 16-32.

34. Braak H,Braak E. (1997). Frequency of stages of Alzheimer-related lesions in different age categories. *Neurobiol.Aging.* **18**: 351-57.

35. Egensperger R, Kosel S, von EU,Graeber MB. (1998). Microglial activation in Alzheimer disease: Association with APOE genotype. *Brain Pathol.* **8**: 439-47.

36. Iwatsubo T, Odaka A, Suzuki N, Mizusawa H, Nukina N,Ihara Y. (1994). Visualization of A beta 42(43) and A beta 40 in senile plaques with end-specific A beta monoclonals: evidence that an initially deposited species is A beta 42(43). *Neuron.* **13**: 45-53.

37. Klafki HW, Wiltfang J,Staufenbiel M. (1996). Electrophoretic separation of betaA4 peptides (1-40) and (1-42). *Anal.Biochem.* **237**: 24-29.

38. Morgan C, Colombres M, Nunez MT,Inestrosa NC. (2004). Structure and function of amyloid in Alzheimer's disease. *Prog.Neurobiol.* **74**: 323-49.

39. Czasch S, Paul S,Baumgartner W. (2005). A comparison of immunohistochemical and silver staining methods for the detection of diffuse plaques in the aged canine brain. *Neurobiol.Aging.*

40. Walsh DM, Hartley DM, Kusumoto Y, Fezoui Y, Condron MM, Lomakin A, Benedek GB, Selkoe DJ,Teplow DB. (1999). Amyloid beta-protein fibrillogenesis. Structure and biological activity of protofibrillar intermediates. *J.Biol.Chem.* **274**: 25945-52.

41. Joachim CL, Morris JH,Selkoe DJ. (1989). Diffuse senile plaques occur commonly in the cerebellum in Alzheimer's disease. *Am.J.Pathol.* **135**: 309-19.

42. Akiyama H, Mori H, Saido T, Kondo H, Ikeda K,McGeer PL. (1999). Occurrence of the diffuse amyloid beta-protein (Abeta) deposits with numerous Abeta-containing glial cells in the cerebral cortex of patients with Alzheimer's disease. *Glia.* **25**: 324-31.

43. Wang HY, D'Andrea MR,Nagele RG. (2002). Cerebellar diffuse amyloid plaques are derived from dendritic Abeta42 accumulations in Purkinje cells. *Neurobiol.Aging.* **23**: 213-23.

44. Schmidt ML, Schuck T, Sheridan S, Kung MP, Kung H, Zhuang ZP, Bergeron C, Lamarche JS, Skovronsky D, Giasson BI, Lee VM,Trojanowski JQ. (2001). The fluorescent Congo red derivative, (trans, trans)-1-bromo-2,5-bis-(3-hydroxycarbonyl-4-hydroxy)styrylbenzene (BSB), labels diverse beta-pleated sheet structures in postmortem human neurodegenerative disease brains. *Am.J.Pathol.* **159**: 937-43.

45. Gyure KA, Durham R, Stewart WF, Smialek JE,Troncoso JC. (2001). Intraneuronal abeta-amyloid precedes development of amyloid plaques in Down syndrome. *Arch.Pathol.Lab Med.* **125**: 489-92.

46. Mehta PD, Dalton AJ, Mehta SP, Kim KS, Sersen EA,Wisniewski HM. (1998). Increased plasma amyloid beta protein 1-42 levels in Down syndrome. *Neurosci.Lett.* **241**: 13-16.

47. Dewji NN, Shelton ER, Adler MJ, Chan HW, Seegmiller JE,Coronel C. (1990). Processing of Alzheimer's disease-associated beta-amyloid precursor protein. *J.Mol.Neurosci.* **2**: 19-27.

48. Wolfe MS. (2002). Therapeutic strategies for Alzheimer's disease. *Nat.Rev.Drug Discov.* **1**: 859-66.

49. Hartmann T, Bergsdorf C, Sandbrink R, Tienari PJ, Multhaup G, Ida N, Bieger S, Dyrks T, Weidemann A, Masters CL,Beyreuther K. (1996). Alzheimer's disease betaA4 protein release and amyloid precursor protein sorting are regulated by alternative splicing. *J.Biol.Chem.* **271**: 13208-14.

50. Konig G, Monning U, Czech C, Prior R, Banati R, Schreiter-Gasser U, Bauer J, Masters CL,Beyreuther K. (1992). Identification and differential expression of a novel alternative splice isoform of the beta A4 amyloid precursor protein (APP) mRNA in leukocytes and brain microglial cells. *J.Biol.Chem.* **267**: 10804-9.

51. Golde TE, Estus S, Usiak M, Younkin LH,Younkin SG. (1990). Expression of beta amyloid protein precursor mRNAs: recognition of a novel alternatively spliced form and quantitation in Alzheimer's disease using PCR. *Neuron.* **4**: 253-67.

52. Tanzi RE, McClatchey AI, Lamperti ED, Villa-Komaroff L, Gusella JF,Neve RL. (1988). Protease inhibitor domain encoded by an amyloid protein precursor mRNA associated with Alzheimer's disease. *Nature.* **331**: 528-30.

53. Smith RP, Higuchi DA,Broze GJ, Jr. (1990). Platelet coagulation factor XIa-inhibitor, a form of Alzheimer amyloid precursor protein. *Science.* **248**: 1126-28.

54. Oltersdorf T, Ward PJ, Henriksson T, Beattie EC, Neve R, Lieberburg I,Fritz LC. (1990). The Alzheimer amyloid precursor protein. Identification of a stable intermediate in the biosynthetic/degradative pathway. *J.Biol.Chem.* **265**: 4492-97.

55. Hooper NM,Turner AJ. (2002). The search for alpha-secretase and its potential as a therapeutic approach to Alzheimer s disease. *Curr.Med.Chem.* **9**: 1107-19.

56. Weidemann A, Konig G, Bunke D, Fischer P, Salbaum JM, Masters CL,Beyreuther K. (1989). Identification, biogenesis, and localization of precursors of Alzheimer's disease A4 amyloid protein. *Cell.* **57**: 115-26.

57. Wolf D, Quon D, Wang Y,Cordell B. (1990). Identification and characterization of C-terminal fragments of the beta-amyloid precursor produced in cell culture. *EMBO J.* **9**: 2079-84.

58. Haass C,Selkoe DJ. (1993). Cellular processing of beta-amyloid precursor protein and the genesis of amyloid beta-peptide. *Cell.* **75**: 1039-42.

59. Naslund J, Jensen M, Tjernberg LO, Thyberg J, Terenius L,Nordstedt C. (1994). The metabolic pathway generating p3, an A beta-peptide fragment, is probably non-amyloidogenic. *Biochem.Biophys.Res.Commun.* **204**: 780-787.

60. Hussain I, Powell D, Howlett DR, Tew DG, Meek TD, Chapman C, Gloger IS, Murphy KE, Southan CD, Ryan DM, Smith TS, Simmons DL, Walsh FS, Dingwall C,Christie G. (1999). Identification of a novel aspartic protease (Asp 2) as beta-secretase. *Mol.Cell Neurosci.* **14**: 419-27.

61. Vassar R, Bennett BD, Babu-Khan S, Kahn S, Mendiaz EA, Denis P, Teplow DB, Ross S, Amarante P, Loeloff R, Luo Y, Fisher S, Fuller J, Edenson S, Lile J, Jarosinski MA, Biere AL, Curran E, Burgess T, Louis JC, Collins F, Treanor J, Rogers G,Citron M. (1999). Beta-secretase cleavage of Alzheimer's amyloid precursor protein by the transmembrane aspartic protease BACE. *Science.* **286**: 735-41.

62. Yan R, Bienkowski MJ, Shuck ME, Miao H, Tory MC, Pauley AM, Brashier JR, Stratman NC, Mathews WR, Buhl AE, Carter DB, Tomasselli AG, Parodi LA, Heinrikson RL,Gurney ME. (1999). Membrane-anchored aspartyl protease with Alzheimer's disease beta-secretase activity. *Nature.* **402**: 533-37.

63. Sinha S, Anderson JP, Barbour R, Basi GS, Caccavello R, Davis D, Doan M, Dovey HF, Frigon N, Hong J, Jacobson-Croak K, Jewett N, Keim P, Knops J, Lieberburg I, Power M, Tan H, Tatsuno G, Tung J, Schenk D, Seubert P, Suomensaari SM, Wang S, Walker D, Zhao J, McConlogue L,John V. (1999). Purification and cloning of amyloid precursor protein beta-secretase from human brain. *Nature.* **402**: 537-40.

64. Acquati F, Accarino M, Nucci C, Fumagalli P, Jovine L, Ottolenghi S,Taramelli R. (2000). The gene encoding DRAP (BACE2), a glycosylated transmembrane protein of the aspartic protease family, maps to the down critical region. *FEBS Lett.* **468**: 59-64.

65. Bennett BD, Babu-Khan S, Loeloff R, Louis JC, Curran E, Citron M,Vassar R. (2000). Expression analysis of BACE2 in brain and peripheral tissues. *J.Biol.Chem.* **275**: 20647-51.

66. Yan R, Munzner JB, Shuck ME,Bienkowski MJ. (2001). BACE2 functions as an alternative alpha-secretase in cells. *J.Biol.Chem.* **276**: 34019-27.

67. Bouillot C, Prochiantz A, Rougon G,Allinquant B. (1996). Axonal amyloid precursor protein expressed by neurons in vitro is present in a membrane fraction with caveolae-like properties. *J.Biol.Chem.* **271**: 7640-7644.

68. Marquez-Sterling NR, Lo AC, Sisodia SS,Koo EH. (1997). Trafficking of cell-surface beta-amyloid precursor protein: evidence that a sorting intermediate participates in synaptic vesicle recycling. *J.Neurosci.* **17**: 140-151.

69. Bendotti C, Forloni GL, Morgan RA, O'Hara BF, Oster-Granite ML, Reeves RH, Gearhart JD,Coyle JT. (1988). Neuroanatomical localization and quantification of amyloid precursor protein mRNA by in situ hybridization in the brains of normal, aneuploid, and lesioned mice. *Proc.Natl.Acad.Sci.U.S.A.* **85**: 3628-32.

70. Citron M, Vigo-Pelfrey C, Teplow DB, Miller C, Schenk D, Johnston J, Winblad B, Venizelos N, Lannfelt L,Selkoe DJ. (1994). Excessive production of amyloid beta-protein by peripheral cells of symptomatic and presymptomatic patients carrying the Swedish familial Alzheimer disease mutation. *Proc.Natl.Acad.Sci.U.S.A.* **91**: 11993-97.

71. Sisodia SS, Koo EH, Hoffman PN, Perry G,Price DL. (1993). Identification and transport of full-length amyloid precursor proteins in rat peripheral nervous system. *J.Neurosci.* **13**: 3136-42.

72. Chyung JH,Selkoe DJ. (2003). Inhibition of receptor-mediated endocytosis demonstrates generation of amyloid beta-protein at the cell surface. *J.Biol.Chem.* **278**: 51035-43.

73. Kang J, Lemaire HG, Unterbeck A, Salbaum JM, Masters CL, Grzeschik KH, Multhaup G, Beyreuther K,Muller-Hill B. (1987). The precursor of Alzheimer's disease amyloid A4 protein resembles a cell-surface receptor. *Nature.* **325**: 733-36.

74. Rossjohn J, Cappai R, Feil SC, Henry A, McKinstry WJ, Galatis D, Hesse L, Multhaup G, Beyreuther K, Masters CL,Parker MW. (1999). Crystal structure of the N-terminal, growth factor-like domain of Alzheimer amyloid precursor protein. *Nat.Struct.Biol.* **6**: 327-31.

75. Quast T, Wehner S, Kirfel G, Jaeger K, De Luca M,Herzog V. (2003). sAPP as a regulator of dendrite motility and melanin release in epidermal melanocytes and melanoma cells. *FASEB J.* **17**: 1739-41.

76. Sinha S, Dovey HF, Seubert P, Ward PJ, Blacher RW, Blaber M, Bradshaw RA, Arici M, Mobley WC,Lieberburg I. (1990). The protease inhibitory properties of the Alzheimer's beta-amyloid precursor protein. *J.Biol.Chem.* **265**: 8983-85.

77. Schmaier AH, Dahl LD, Hasan AA, Cines DB, Bauer KA,Van Nostrand WE. (1995). Factor IXa inhibition by protease nexin-2/amyloid beta-protein precursor on phospholipid vesicles and cell membranes. *Biochemistry.* **34**: 1171-78.

78. Borchelt DR, Ratovitski T, van Lare J, Lee MK, Gonzales V, Jenkins NA, Copeland NG, Price DL,Sisodia SS. (1997). Accelerated amyloid deposition in the brains of transgenic mice coexpressing mutant presenilin 1 and amyloid precursor proteins. *Neuron.* **19**: 939-45.

79. Howland DS, Trusko SP, Savage MJ, Reaume AG, Lang DM, Hirsch JD, Maeda N, Siman R, Greenberg BD, Scott RW,Flood DG. (1998). Modulation of secreted beta-amyloid precursor protein and amyloid beta-peptide in brain by cholesterol. *J.Biol.Chem.* **273**: 16576-82.

80. Citron M, Oltersdorf T, Haass C, McConlogue L, Hung AY, Seubert P, Vigo-Pelfrey C, Lieberburg I,Selkoe DJ. (1992). Mutation of the beta-amyloid precursor protein in familial Alzheimer's disease increases beta-protein production. *Nature.* **360**: 672-74.

81. Cai XD, Golde TE,Younkin SG. (1993). Release of excess amyloid beta protein from a mutant amyloid beta protein precursor. *Science.* **259**: 514-16.

82. Kidd M. (1963). Paired helical filaments in electron microscopy of Alzheimer's disease. *Nature.* **197**: 192-93.

83. Wisniewski HM, Narang HK,Terry RD. (1976). Neurofibrillary tangles of paired helical filaments. *J.Neurol.Sci.* **27**: 173-81.

84. De Boni U,Crapper DR. (1978). Paired helical filaments of the Alzheimer type in cultured neurones. *Nature.* **271**: 566-68.

85. Kosik KS, Joachim CL,Selkoe DJ. (1986). Microtubule-associated protein tau (tau) is a major antigenic component of paired helical filaments in Alzheimer disease. *Proc.Natl.Acad.Sci.U.S.A.* **83**: 4044-48.

86. Grundke-Iqbal I, Iqbal K, Quinlan M, Tung YC, Zaidi MS,Wisniewski HM. (1986). Microtubule-associated protein tau. A component of Alzheimer paired helical filaments. *J.Biol.Chem.* **261**: 6084-89.

87. Roher AE, Palmer KC, Chau V,Ball MJ. (1988). Isolation and chemical characterization of Alzheimer's disease paired helical filament cytoskeletons: differentiation from amyloid plaque core protein. *J.Cell Biol.* **107**: 2703-16.

88. Grundke-Iqbal I, Iqbal K, Tung YC, Quinlan M, Wisniewski HM,Binder LI. (1986). Abnormal phosphorylation of the microtubule-associated protein tau (tau) in Alzheimer cytoskeletal pathology. *Proc.Natl.Acad.Sci.U.S.A.* **83**: 4913-17.

89. Anderton BH, Betts J, Blackstock WP, Brion JP, Chapman S, Connell J, Dayanandan R, Gallo JM, Gibb G, Hanger DP, Hutton M, Kardalinou E, Leroy K, Lovestone S, Mack T, Reynolds CH,Van Slegtenhorst M. (2001). Sites of phosphorylation in tau and factors affecting their regulation. *Biochem.Soc.Symp.* 73-80.

90. Hamdane M, Sambo AV, Delobel P, Begard S, Violleau A, Delacourte A, Bertrand P, Benavides J,Buee L. (2003). Mitotic-like tau phosphorylation by p25-Cdk5 kinase complex. *J.Biol.Chem.* **278**: 34026-34.

91. Lee G, Thangavel R, Sharma VM, Litersky JM, Bhaskar K, Fang SM, Do LH, Andreadis A, Van Hoesen G,Ksiezak-Reding H. (2004). Phosphorylation of tau by fyn: implications for Alzheimer's disease. *J.Neurosci.* **24**: 2304-12.

92. Shelton SB, Krishnamurthy P,Johnson GV. (2004). Effects of cyclin-dependent kinase-5 activity on apoptosis and tau phosphorylation in immortalized mouse brain cortical cells. *J.Neurosci.Res.* **76**: 110-120.

93. Myers AJ,Goate AM. (2001). The genetics of late-onset Alzheimer's disease. *Curr.Opin.Neurol.* **14**: 433-40.

94. De Strooper B, Saftig P, Craessaerts K, Vanderstichele H, Guhde G, Annaert W, Von Figura K,Van Leuven F. (1998). Deficiency of presenilin-1 inhibits the normal cleavage of amyloid precursor protein. *Nature.* **391**: 387-90.

95. Wolfe MS, Xia W, Ostaszewski BL, Diehl TS, Kimberly WT,Selkoe DJ. (1999). Two transmembrane aspartates in presenilin-1 required for presenilin endoproteolysis and gamma-secretase activity. *Nature.* **398**: 513-17.

96. Mehta ND, Refolo LM, Eckman C, Sanders S, Yager D, Perez-Tur J, Younkin S, Duff K, Hardy J,Hutton M. (1998). Increased Abeta42(43) from cell lines expressing presenilin 1 mutations. *Ann.Neurol.* **43**: 256-58.

97. Murayama O, Tomita T, Nihonmatsu N, Murayama M, Sun X, Honda T, Iwatsubo T,Takashima A. (1999). Enhancement of amyloid beta 42 secretion by 28 different presenilin 1 mutations of familial Alzheimer's disease. *Neurosci.Lett.* **265**: 61-63.

98. Ritchie K,Lovestone S. (2002). The dementias. *Lancet.* **360**: 1759-66.

99. Saunders AM, Strittmatter WJ, Schmechel D, George-Hyslop PH, Pericak-Vance MA, Joo SH, Rosi BL, Gusella JF, Crapper-MacLachlan DR, Alberts MJ,. (1993). Association of apolipoprotein E allele epsilon 4 with late-onset familial and sporadic Alzheimer's disease. *Neurology.* **43**: 1467-72.

100. Strittmatter WJ, Saunders AM, Schmechel D, Pericak-Vance M, Enghild J, Salvesen GS,Roses AD. (1993). Apolipoprotein E: high-avidity binding to beta-amyloid and increased frequency of type 4 allele in late-onset familial Alzheimer disease. *Proc.Natl.Acad.Sci.U.S.A.* **90**: 1977-81.

101. Corder EH, Saunders AM, Strittmatter WJ, Schmechel DE, Gaskell PC, Small GW, Roses AD, Haines JL,Pericak-Vance MA. (1993). Gene dose of apolipoprotein E type 4 allele and the risk of Alzheimer's disease in late onset families. *Science.* **261**: 921-23.

102. Corder EH, Lannfelt L, Bogdanovic N, Fratiglioni L,Mori H. (1998). The role of APOE polymorphisms in late-onset dementias. *Cell Mol.Life Sci.* **54**: 928-34.

103. Tanzi RE. (1999). A genetic dichotomy model for the inheritance of Alzheimer's disease and common age-related disorders. *J.Clin.Invest.* **104**: 1175-79.

104. Corder EH, Saunders AM, Risch NJ, Strittmatter WJ, Schmechel DE, Gaskell PC, Jr., Rimmler JB, Locke PA, Conneally PM, Schmader KE,. (1994). Protective effect of apolipoprotein E type 2 allele for late onset Alzheimer disease. *Nat.Genet.* **7**: 180-184.

105. Pedersen WA, Chan SL,Mattson MP. (2000). A mechanism for the neuroprotective effect of apolipoprotein E: isoform-specific modification by the lipid peroxidation product 4-hydroxynonenal. *J.Neurochem.* **74**: 1426-33.

106. Tanzi RE,Bertram L. (2001). New frontiers in Alzheimer's disease genetics. *Neuron.* **32**: 181-84.

107. Weisgraber KH. (1994). Apolipoprotein E: structure-function relationships. *Adv.Protein Chem.* **45**: 249-302.

108. Ho YY, Deckelbaum RJ, Chen Y, Vogel T,Talmage DA. (2001). Apolipoprotein E inhibits serum-stimulated cell proliferation and enhances serum-independent cell proliferation. *J.Biol.Chem.* **276**: 43455-62.

109. Laffont I, Takahashi M, Shibukawa Y, Honke K, Shuvaev VV, Siest G, Visvikis S,Taniguchi N. (2002). Apolipoprotein E activates Akt pathway in neuro-2a in an isoform-specific manner. *Biochem.Biophys.Res.Commun.* **292**: 83-87.

110. Shore VG,Shore B. (1973). Heterogeneity of human plasma very low density lipoproteins. Separation of species differing in protein components. *Biochemistry.* **12**: 502-7.

111. Ordovas JM,Mooser V. (2002). The APOE locus and the pharmacogenetics of lipid response. *Curr.Opin.Lipidol.* **13**: 113-17.

112. Aleshkov SB, Li X, Lavrentiadou SN,Zannis VI. (1999). Contribution of cysteine 158, the glycosylation site threonine 194, the amino- and carboxy-terminal domains of apolipoprotein E in the binding to amyloid peptide beta (1-40). *Biochemistry.* **38**: 8918-25.

113. Utermann G, Hees M,Steinmetz A. (1977). Polymorphism of apolipoprotein E and occurrence of dysbetalipoproteinaemia in man. *Nature.* **269**: 604-7.

114. Mahley RW,Huang Y. (1999). Apolipoprotein E: from atherosclerosis to Alzheimer's disease and beyond. *Curr.Opin.Lipidol.* **10**: 207-17.

115. Mahley RW,Ji ZS. (1999). Remnant lipoprotein metabolism: key pathways involving cell-surface heparan sulfate proteoglycans and apolipoprotein E. *J.Lipid Res.* **40**: 1-16.

116. Wilson C, Wardell MR, Weisgraber KH, Mahley RW,Agard DA. (1991). Three-dimensional structure of the LDL receptor-binding domain of human apolipoprotein E. *Science.* **252**: 1817-22.

117. Segall ML, Dhanasekaran P, Baldwin F, Anantharamaiah GM, Weisgraber KH, Phillips MC,Lund-Katz S. (2002). Influence of apoE domain structure and polymorphism on the kinetics of phospholipid vesicle solubilization. *J.Lipid Res.* **43**: 1688-700.

118. Morrow JA, Segall ML, Lund-Katz S, Phillips MC, Knapp M, Rupp B,Weisgraber KH. (2000). Differences in stability among the human apolipoprotein E isoforms determined by the amino-terminal domain. *Biochemistry.* **39**: 11657-66.

119. Raffai RL, Dong LM, Farese RV, Jr.,Weisgraber KH. (2001). Introduction of human apolipoprotein E4 "domain interaction" into mouse apolipoprotein E. *Proc.Natl.Acad.Sci.U.S.A.* **98**: 11587-91.

120. Laws SM, Hone E, Gandy S,Martins RN. (2003). Expanding the association between the APOE gene and the risk of Alzheimer's disease: possible roles for APOE promoter polymorphisms and alterations in APOE transcription. *J.Neurochem.* **84**: 1215-36.

121. Strittmatter WJ,Bova HC. (2002). Molecular biology of apolipoprotein E. *Curr.Opin.Lipidol.* **13**: 119-23.

122. LaDu MJ, Gilligan SM, Lukens JR, Cabana VG, Reardon CA, Van Eldik LJ,Holtzman DM. (1998). Nascent astrocyte particles differ from lipoproteins in CSF. *J.Neurochem.* **70**: 2070-2081.

123. Petegnief V, Saura J, Gregorio-Rocasolano N,Paul SM. (2001). Neuronal injury-induced expression and release of apolipoprotein E in mixed neuron/glia co-cultures: nuclear factor kappaB inhibitors reduce basal and lesion-induced secretion of apolipoprotein E. *Neuroscience.* **104**: 223-34.

124. Schmechel DE, Saunders AM, Strittmatter WJ, Crain BJ, Hulette CM, Joo SH, Pericak-Vance MA, Goldgaber D,Roses AD. (1993). Increased amyloid beta-peptide deposition in cerebral cortex as a consequence of apolipoprotein E genotype in late-onset Alzheimer disease. *Proc.Natl.Acad.Sci.U.S.A.* **90**: 9649-53.

125. Roses AD. (1995). Apolipoprotein E genotyping in the differential diagnosis, not prediction, of Alzheimer's disease. *Ann.Neurol.* **38**: 6-14.

126. Strittmatter WJ, Weisgraber KH, Huang DY, Dong LM, Salvesen GS, Pericak-Vance M, Schmechel D, Saunders AM, Goldgaber D,Roses AD. (1993). Binding of human apolipoprotein E to synthetic amyloid beta peptide: isoform-specific effects and implications for late-onset Alzheimer disease. *Proc.Natl.Acad.Sci.U.S.A.* **90**: 8098-102.

127. Strittmatter WJ,Roses AD. (1995). Apolipoprotein E and Alzheimer disease. *Proc.Natl.Acad.Sci.U.S.A.* **92**: 4725-27.

128. Raber J, Huang Y,Ashford JW. (2004). ApoE genotype accounts for the vast majority of AD risk and AD pathology. *Neurobiol.Aging.* **25**: 641-50.

129. Vancea JE, Campenotb RB,Vancec DE. (2000). The synthesis and transport of lipids for axonal growth and nerve regeneration. *Biochim.Biophys.Acta.* **1486**: 84-96.

130. Strittmatter WJ, Saunders AM, Goedert M, Weisgraber KH, Dong LM, Jakes R, Huang DY, Pericak-Vance M, Schmechel D,Roses AD. (1994). Isoform-specific interactions of apolipoprotein E with microtubule-associated protein tau: implications for Alzheimer disease. *Proc.Natl.Acad.Sci.U.S.A.* **91**: 11183-86.

131. Scott BL, Welch K, deSerrano V, Moss NC, Roses AD,Strittmatter WJ. (1998). Human apolipoprotein E accelerates microtubule polymerization in vitro. *Neurosci.Lett.* **245**: 105-8.

132. Beffert U, Danik M, Krzywkowski P, Ramassamy C, Berrada F,Poirier J. (1998). The neurobiology of apolipoproteins and their receptors in the CNS and Alzheimer's disease. *Brain Res.Brain Res.Rev.* **27**: 119-42.

133. Bellosta S, Nathan BP, Orth M, Dong LM, Mahley RW,Pitas RE. (1995). Stable expression and secretion of apolipoproteins E3 and E4 in mouse neuroblastoma cells produces differential effects on neurite outgrowth. *J.Biol.Chem.* **270**: 27063-71.

134. Teter B, Xu PT, Gilbert JR, Roses AD, Galasko D,Cole GM. (2002). Defective neuronal sprouting by human apolipoprotein E4 is a gain-of-negative function. *J.Neurosci.Res.* **68**: 331-36.

135. Goldstein JL,Brown MS. (1974). Binding and degradation of low density lipoproteins by cultured human fibroblasts. Comparison of cells from a normal subject and from a patient with homozygous familial hypercholesterolemia. *J.Biol.Chem.* **249**: 5153-62.

136. Krieger M. (1998). The "best" of cholesterols, the "worst" of cholesterols: a tale of two receptors. *Proc.Natl.Acad.Sci.U.S.A.* **95**: 4077-80.

137. Herz J,Bock HH. (2002). Lipoprotein receptors in the nervous system. *Annu.Rev.Biochem.* **71**: 405-34.

138. Nimpf J,Schneider WJ. (2000). From cholesterol transport to signal transduction: low density lipoprotein receptor, very low density lipoprotein receptor, and apolipoprotein E receptor-2. *Biochim.Biophys.Acta.* **1529**: 287-98.

139. Wolozin B, Kellman W, Ruosseau P, Celesia GG,Siegel G. (2000). Decreased prevalence of Alzheimer disease associated with 3-hydroxy-3-methyglutaryl coenzyme A reductase inhibitors. *Arch.Neurol.* **57**: 1439-43.

140. Herz J,Strickland DK. (2001). LRP: a multifunctional scavenger and signaling receptor. *J.Clin.Invest.* **108**: 779-84.

141. Trommsdorff M, Borg JP, Margolis B,Herz J. (1998). Interaction of cytosolic adaptor proteins with neuronal apolipoprotein E receptors and the amyloid precursor protein. *J.Biol.Chem.* **273**: 33556-60.

142. Tissir F,Goffinet AM. (2003). Reelin and brain development. *Nat.Rev.Neurosci.* **4**: 496-505.

143. Fiore F, Zambrano N, Minopoli G, Donini V, Duilio A,Russo T. (1995). The regions of the Fe65 protein homologous to the phosphotyrosine interaction/phosphotyrosine binding domain of Shc bind the intracellular domain of the Alzheimer's amyloid precursor protein. *J.Biol.Chem.* **270**: 30853-56.

144. Tanahashi H,Tabira T. (2002). Characterization of an amyloid precursor protein-binding protein Fe65L2 and its novel isoforms lacking phosphotyrosine-interaction domains. *Biochem.J.* **367**: 687-95.

145. Rebeck GW, Moir RD, Mui S, Strickland DK, Tanzi RE,Hyman BT. (2001). Association of membrane-bound amyloid precursor protein APP with the apolipoprotein E receptor LRP. *Brain Res.Mol.Brain Res.* **87**: 238-45.

146. van der GP. (2002). Phosphorylation of LRP1: regulation of transport and signal transduction. *Trends Cardiovasc.Med.* **12**: 160-165.

147. Howell BW,Herz J. (2001). The LDL receptor gene family: signaling functions during development. *Curr.Opin.Neurobiol.* **11**: 74-81.

148. Trommsdorff M, Gotthardt M, Hiesberger T, Shelton J, Stockinger W, Nimpf J, Hammer RE, Richardson JA,Herz J. (1999). Reeler/Disabled-like disruption of neuronal migration in knockout mice lacking the VLDL receptor and ApoE receptor 2. *Cell.* **97**: 689-701.

149. Helbecque N,Amouyel P. (2000). Very low density lipoprotein receptor in Alzheimer disease. *Microsc.Res.Tech.* **50**: 273-77.

150. Sun XM,Soutar AK. (1999). Expression in vitro of alternatively spliced variants of the messenger RNA for human apolipoprotein E receptor-2 identified in human tissues by ribonuclease protection assays. *Eur.J.Biochem.* **262**: 230-239.

151. Riddell DR, Vinogradov DV, Stannard AK, Chadwick N,Owen JS. (1999). Identification and characterization of LRP8 (apoER2) in human blood platelets. *J.Lipid Res.* **40**: 1925-30.

152. Acton S, Rigotti A, Landschulz KT, Xu S, Hobbs HH,Krieger M. (1996). Identification of scavenger receptor SR-BI as a high density lipoprotein receptor. *Science.* **271**: 518-20.

153. Landschulz KT, Pathak RK, Rigotti A, Krieger M,Hobbs HH. (1996). Regulation of scavenger receptor, class B, type I, a high density lipoprotein receptor, in liver and steroidogenic tissues of the rat. *J.Clin.Invest.* **98**: 984-95.

154. Hatzopoulos AK, Rigotti A, Rosenberg RD,Krieger M. (1998). Temporal and spatial pattern of expression of the HDL receptor SR-BI during murine embryogenesis. *J.Lipid Res.* **39**: 495-508.

155. Temel RE, Trigatti B, DeMattos RB, Azhar S, Krieger M,Williams DL. (1997). Scavenger receptor class B, type I (SR-BI) is the major route for the delivery of high density lipoprotein cholesterol to the steroidogenic pathway in cultured mouse adrenocortical cells. *Proc.Natl.Acad.Sci.U.S.A.* **94**: 13600-13605.

156. Kozarsky KF, Donahee MH, Rigotti A, Iqbal SN, Edelman ER,Krieger M. (1997). Overexpression of the HDL receptor SR-BI alters plasma HDL and bile cholesterol levels. *Nature.* **387**: 414-17.

157. Rigotti A, Trigatti BL, Penman M, Rayburn H, Herz J,Krieger M. (1997). A targeted mutation in the murine gene encoding the high density lipoprotein (HDL) receptor scavenger receptor class B type I reveals its key role in HDL metabolism. *Proc.Natl.Acad.Sci.U.S.A.* **94**: 12610-12615.

158. Varban ML, Rinninger F, Wang N, Fairchild-Huntress V, Dunmore JH, Fang Q, Gosselin ML, Dixon KL, Deeds JD, Acton SL, Tall AR,Huszar D. (1998). Targeted mutation reveals a central role for SR-BI in hepatic selective uptake of high density lipoprotein cholesterol. *Proc.Natl.Acad.Sci.U.S.A.* **95**: 4619-24.

159. Babitt J, Trigatti B, Rigotti A, Smart EJ, Anderson RG, Xu S,Krieger M. (1997). Murine SR-BI, a high density lipoprotein receptor that mediates selective lipid uptake, is N-glycosylated and fatty acylated and colocalizes with plasma membrane caveolae. *J.Biol.Chem.* **272**: 13242-49.

160. Li XA, Titlow WB, Jackson BA, Giltiay N, Nikolova-Karakashian M, Uittenbogaard A,Smart EJ. (2002). High density lipoprotein binding to scavenger receptor, Class B, type I activates endothelial nitric-oxide synthase in a ceramide-dependent manner. *J.Biol.Chem.* **277**: 11058-63.

161. Mineo C, Yuhanna IS, Quon MJ,Shaul PW. (2003). High density lipoprotein-induced endothelial nitric-oxide synthase activation is mediated by Akt and MAP kinases. *J.Biol.Chem.* **278**: 9142-49.

162. Ikemoto M, Arai H, Feng D, Tanaka K, Aoki J, Dohmae N, Takio K, Adachi H, Tsujimoto M,Inoue K. (2000). Identification of a PDZ-domain-containing protein that interacts with the scavenger receptor class B type I. *Proc.Natl.Acad.Sci.U.S.A.* **97**: 6538-43.

163. Webb NR, de Villiers WJ, Connell PM, de Beer FC,van der Westhuyzen DR. (1997). Alternative forms of the scavenger receptor BI (SR-BI). *J.Lipid Res.* **38**: 1490-1495.

164. Webb NR, Connell PM, Graf GA, Smart EJ, de Villiers WJ, de Beer FC,van der Westhuyzen DR. (1998). SR-BII, an isoform of the scavenger receptor BI containing an alternate cytoplasmic tail, mediates lipid transfer between high density lipoprotein and cells. *J.Biol.Chem.* **273**: 15241-48.

165. Mulcahy JV, Riddell DR,Owen JS. (2004). Human scavenger receptor class B type II (SR-BII) and cellular cholesterol efflux. *Biochem.J.* **377**: 741-47.

166. Graf GA, Roswell KL,Smart EJ. (2001). 17beta-Estradiol promotes the up-regulation of SR-BII in HepG2 cells and in rat livers. *J.Lipid Res.* **42**: 1444-49.

167. Murphy S. (2000). Production of nitric oxide by glial cells: regulation and potential roles in the CNS. *Glia.* **29**: 1-13.

168. Law A, Gauthier S,Quirion R. (2001). Say NO to Alzheimer's disease: the putative links between nitric oxide and dementia of the Alzheimer's type. *Brain Res.Brain Res.Rev.* **35**: 73-96.

169. Jesko H, Chalimoniuk M,Strosznajder JB. (2003). Activation of constitutive nitric oxide synthase(s) and absence of inducible isoform in aged rat brain. *Neurochem.Int.* **42**: 315-22.

170. Ortega MA,Amaya Aleixandre dA. (2000). Nitric oxide reactivity and mechanisms involved in its biological effects. *Pharmacol.Res.* **42**: 421-27.

171. Brown GC. (1999). Nitric oxide and mitochondrial respiration. *Biochim.Biophys.Acta.* **1411**: 351-69.

172. Wiesinger H. (2001). Arginine metabolism and the synthesis of nitric oxide in the nervous system. *Prog.Neurobiol.* **64**: 365-91.

173. Andrew PJ,Mayer B. (1999). Enzymatic function of nitric oxide synthases. *Cardiovasc.Res.* **43**: 521-31.

174. Michel T,Feron O. (1997). Nitric oxide synthases: which, where, how, and why? *J.Clin.Invest.* **100**: 2146-52.

175. Ruan J, Xie Q, Hutchinson N, Cho H, Wolfe GC,Nathan C. (1996). Inducible nitric oxide synthase requires both the canonical calmodulin-binding domain and additional sequences in order to bind calmodulin and produce nitric oxide in the absence of free Ca2+. *J.Biol.Chem.* **271**: 22679-86.

176. Brenman JE, Chao DS, Gee SH, McGee AW, Craven SE, Santillano DR, Wu Z, Huang F, Xia H, Peters MF, Froehner SC,Bredt DS. (1996). Interaction of nitric oxide synthase with the postsynaptic density protein PSD-95 and alpha1-syntrophin mediated by PDZ domains. *Cell.* **84**: 757-67.

177. Sabio G, Reuver S, Feijoo C, Hasegawa M, Thomas GM, Centeno F, Kuhlendahl S, Leal-Ortiz S, Goedert M, Garner C,Cuenda A. (2004). Stress- and mitogen-induced phosphorylation of the synapse-associated protein SAP90/PSD-95 by activation of SAPK3/p38gamma and ERK1/ERK2. *Biochem.J.* **380**: 19-30.

178. Liu J, Hughes TE,Sessa WC. (1997). The first 35 amino acids and fatty acylation sites determine the molecular targeting of endothelial nitric oxide synthase into the Golgi region of cells: a green fluorescent protein study. *J.Cell Biol.* **137**: 1525-35.

179. Sessa WC. (2004). eNOS at a glance. *J.Cell Sci.* **117**: 2427-29.

180. Garcia-Cardena G, Fan R, Stern DF, Liu J,Sessa WC. (1996). Endothelial nitric oxide synthase is regulated by tyrosine phosphorylation and interacts with caveolin-1. *J.Biol.Chem.* **271**: 27237-40.

181. Goligorsky MS, Li H, Brodsky S,Chen J. (2002). Relationships between caveolae and eNOS: everything in proximity and the proximity of everything. *Am.J.Physiol Renal Physiol.* **283**: F1-10.

182. Fleming I,Busse R. (2003). Molecular mechanisms involved in the regulation of the endothelial nitric oxide synthase. *Am.J.Physiol Regul.Integr.Comp Physiol.* **284**: R1-12.

183. Gallis B, Corthals GL, Goodlett DR, Ueba H, Kim F, Presnell SR, Figeys D, Harrison DG, Berk BC, Aebersold R,Corson MA. (1999). Identification of flow-dependent endothelial nitric-oxide synthase phosphorylation sites by mass spectrometry and regulation of phosphorylation and nitric oxide production by the phosphatidylinositol 3-kinase inhibitor LY294002. *J.Biol.Chem.* **274**: 30101-8.

184. Cantrell DA. (2001). Phosphoinositide 3-kinase signalling pathways. *J.Cell Sci.* **114**: 1439-45.

185. Lawlor MA,Alessi DR. (2001). PKB/Akt: a key mediator of cell proliferation, survival and insulin responses? *J.Cell Sci.* **114**: 2903-10.

186. Boo YC, Sorescu G, Boyd N, Shiojima I, Walsh K, Du J,Jo H. (2002). Shear stress stimulates phosphorylation of endothelial nitric-oxide synthase at Ser1179 by Akt-independent mechanisms: role of protein kinase A. *J.Biol.Chem.* **277**: 3388-96.

187. Dimmeler S, Fleming I, Fisslthaler B, Hermann C, Busse R,Zeiher AM. (1999). Activation of nitric oxide synthase in endothelial cells by Akt-dependent phosphorylation. *Nature.* **399**: 601-5.

188. Fulton D, Gratton JP, McCabe TJ, Fontana J, Fujio Y, Walsh K, Franke TF, Papapetropoulos A,Sessa WC. (1999). Regulation of endothelium-derived nitric oxide production by the protein kinase Akt. *Nature.* **399**: 597-601.

189. Chen ZP, Mitchelhill KI, Michell BJ, Stapleton D, Rodriguez-Crespo I, Witters LA, Power DA, Ortiz de Montellano PR,Kemp BE. (1999). AMP-activated protein kinase phosphorylation of endothelial NO synthase. *FEBS Lett.* **443**: 285-89.

190. Urushitani M, Nakamizo T, Inoue R, Sawada H, Kihara T, Honda K, Akaike A,Shimohama S. (2001). N-methyl-D-aspartate receptor-mediated mitochondrial Ca(2+) overload in acute excitotoxic motor neuron death: a mechanism distinct from chronic neurotoxicity after Ca(2+) influx. *J.Neurosci.Res.* **63**: 377-87.

191. Perry G, Nunomura A, Hirai K, Zhu X, Perez M, Avila J, Castellani RJ, Atwood CS, Aliev G, Sayre LM, Takeda A,Smith MA. (2002). Is oxidative damage the fundamental pathogenic mechanism of Alzheimer's and other neurodegenerative diseases? *Free Radic.Biol.Med.* **33**: 1475-79.

192. Ishii K, Muelhauser F, Liebl U, Picard M, Kuhl S, Penke B, Bayer T, Wiessler M, Hennerici M, Beyreuther K, Hartmann T,Fassbender K. (2000). Subacute NO generation induced by Alzheimer's beta-amyloid in the living brain: reversal by inhibition of the inducible NO synthase. *FASEB J.* **14**: 1485-89.

193. van Oost BA, Edgell CJ, Hay CW,MacGillivray RT. (1986). Isolation of a human von Willebrand factor cDNA from the hybrid endothelial cell line EA.hy926. *Biochem.Cell Biol.* **64**: 699-705.

194. Schnell JR, Dyson HJ,Wright PE. (2004). Structure, dynamics, and catalytic function of dihydrofolate reductase. *Annu.Rev.Biophys.Biomol.Struct.* **33**: 119-40.

195. Tagalakis AD, Graham IR, Riddell DR, Dickson JG,Owen JS. (2001). Gene correction of the apolipoprotein (Apo) E2 phenotype to wild-type ApoE3 by in situ chimeraplasty. *J.Biol.Chem.* **276**: 13226-30.

196. Mullis KB,Faloona FA. (1987). Specific synthesis of DNA in vitro via a polymerase-catalyzed chain reaction. *Methods Enzymol.* **155**: 335-50.

197. Mullis K, Faloona F, Scharf S, Saiki R, Horn G,Erlich H. (1986). Specific enzymatic amplification of DNA in vitro: the polymerase chain reaction. *Cold Spring Harb.Symp.Quant.Biol.* **51 Pt 1**: 263-73.

198. Bustin SA. (2000). Absolute quantification of mRNA using real-time reverse transcription polymerase chain reaction assays. *J.Mol.Endocrinol.* **25**: 169-93.

199. Bustin SA. (2002). Quantification of mRNA using real-time reverse transcription PCR (RT-PCR): trends and problems. *J.Mol.Endocrinol.* **29**: 23-39.

200. Ginzinger DG. (2002). Gene quantification using real-time quantitative PCR: an emerging technology hits the mainstream. *Exp.Hematol.* **30**: 503-12.

201. Higuchi R, Fockler C, Dollinger G,Watson R. (1993). Kinetic PCR analysis: real-time monitoring of DNA amplification reactions. *Biotechnology (N.Y.).* **11**: 1026-30.

202. Tan W, Fang X, Li J,Liu X. (2000). Molecular beacons: a novel DNA probe for nucleic acid and protein studies. *Chemistry.* **6**: 1107-11.

203. Bradford MM. (1976). A rapid and sensitive method for the quantitation of microgram quantities of protein utilizing the principle of protein-dye binding. *Anal.Biochem.* **72**: 248-54.

204. Spector T. (1978). Refinement of the coomassie blue method of protein quantitation. A simple and linear spectrophotometric assay for less than or equal to 0.5 to 50 microgram of protein. *Anal.Biochem.* **86**: 142-46.

205. Blum CB, Aron L,Sciacca R. (1980). Radioimmunoassay studies of human apolipoprotein E. *J.Clin.Invest.* **66**: 1240-1250.

206. Olin KL, Potter-Perigo S, Barrett PH, Wight TN,Chait A. (2001). Biglycan, a vascular proteoglycan, binds differently to HDL2 and HDL3: role of apoE. *Arterioscler.Thromb.Vasc.Biol.* **21**: 129-35.

207. Rosseneu M, Vercaemst R, Vinaimont N, Van Tornout P, Henderson LO,Herbert PN. (1981). Quantitative determination of human plasma apolipoprotein A-I by laser immunonephelometry. *Clin.Chem.* **27**: 856-59.

208. Uchida Y, Ito S,Nukina N. (2000). Sandwich ELISA for the measurement of Apo-E4 levels in serum and the estimation of the allelic status of Apo-E4 isoforms. *J.Clin.Lab Anal.* **14**: 260-264.

209. Tozuka M, Yoshida Y, Tanigami J, Miyachi M, Katsuyama T,Kanai M. (1991). Development of an enzyme-linked immunosorbent assay of apolipoprotein E-AII complex in plasma. *Clin.Chem.* **37**: 1645-48.

210. Gracia V, Fiol C, Hurtado I, Pinto X, Argimon JM,Castineiras MJ. (1994). An enzyme-linked immunosorbent assay method to measure human apolipoprotein E levels using commercially available reagents: effect of apolipoprotein E polymorphism on serum apolipoprotein E concentration. *Anal.Biochem.* **223**: 212-17.

211. Sacre SM, Stannard AK,Owen JS. (2003). Apolipoprotein E (apoE) isoforms differentially induce nitric oxide production in endothelial cells. *FEBS Lett.* **540**: 181-87.

212. Harris JD, Schepelmann S, Athanasopoulos T, Graham IR, Stannard AK, Mohri Z, Hill V, Hassall DG, Owen JS,Dickson G. (2002). Inhibition of atherosclerosis in apolipoprotein-E-deficient mice following muscle transduction with adeno-associated virus vectors encoding human apolipoprotein-E. *Gene Ther.* **9**: 21-29.

213. Harris JD, Graham IR, Schepelmann S, Stannard AK, Roberts ML, Hodges BL, Hill V, Amalfitano A, Hassall DG, Owen JS,Dickson G. (2002). Acute regression of advanced and retardation of early aortic atheroma in immunocompetent apolipoprotein-E (apoE) deficient mice by administration of a second generation [E1(-), E3(-), polymerase(-)] adenovirus vector expressing human apoE. *Hum.Mol.Genet.* **11**: 43-58.

214. Ferré F, Pezzoli P,Buxton E. (1996). Quantitation of RNA transcripts using RT-PCR. 175-90.

215. Piatak Jr M, Wages Jr J, Luk K,Lifson JD. (1996). Quantification of RNA by competitive RT-PCR: theoretical consideration and practical advice. 191-221.

216. Ikeda T, Murakami M,Funaba M. (2004). Reliability of RT-PCR methods for measuring relative gene expression in mast cells. *Vet.Immunol.Immunopathol.* **100**: 1-5.

217. Moore DJ, Chambers JK, Murdock PR,Emson PC. (2002). Human Ntera-2/D1 neuronal progenitor cells endogenously express a functional P2Y1 receptor. *Neuropharmacology.* **43**: 966-78.

218. Moore DJ, Chambers JK, Wahlin JP, Tan KB, Moore GB, Jenkins O, Emson PC,Murdock PR. (2001). Expression pattern of human P2Y receptor subtypes: a quantitative reverse transcription-polymerase chain reaction study. *Biochim.Biophys.Acta.* **1521**: 107-19.

219. Komatsu N, Yamamoto M, Fujita H, Miwa A, Hatake K, Endo T, Okano H, Katsube T, Fukumaki Y,Sassa S. (1993). Establishment and characterization of an erythropoietin-dependent subline, UT-7/Epo, derived from human leukemia cell line, UT-7. *Blood.* **82**: 456-64.

220. Goldring MB, Birkhead JR, Suen LF, Yamin R, Mizuno S, Glowacki J, Arbiser JL,Apperley JF. (1994). Interleukin-1 beta-modulated gene expression in immortalized human chondrocytes. *J.Clin.Invest.* **94**: 2307-16.

221. Guyton JR, Miller SE, Martin ME, Khan WA, Roses AD,Strittmatter WJ. (1998). Novel large apolipoprotein E-containing lipoproteins of density 1.006-1.060 g/ml in human cerebrospinal fluid. *J.Neurochem.* **70**: 1235-40.

222. Li X, Kypreos K, Zanni EE,Zannis V. (2003). Domains of apoE required for binding to apoE receptor 2 and to phospholipids: implications for the functions of apoE in the brain. *Biochemistry.* **42**: 10406-17.

223. Takahashi S, Oida K, Ookubo M, Suzuki J, Kohno M, Murase T, Yamamoto T,Nakai T. (1996). Very low density lipoprotein receptor binds apolipoprotein E2/2 as well as apolipoprotein E3/3. *FEBS Lett.* **386**: 197-200.

224. Strickland DK, Gonias SL,Argraves WS. (2002). Diverse roles for the LDL receptor family. *Trends Endocrinol.Metab.* **13**: 66-74.

225. Webb JC, Patel DD, Jones MD, Knight BL,Soutar AK. (1994). Characterization and tissue-specific expression of the human 'very low density lipoprotein (VLDL) receptor' mRNA. *Hum.Mol.Genet.* **3**: 531-37.

226. Kim DH, Iijima H, Goto K, Sakai J, Ishii H, Kim HJ, Suzuki H, Kondo H, Saeki S,Yamamoto T. (1996). Human apolipoprotein E receptor 2. A novel lipoprotein receptor of the low density lipoprotein receptor family predominantly expressed in brain. *J.Biol.Chem.* **271**: 8373-80.

227. Okuizumi K, Onodera O, Namba Y, Ikeda K, Yamamoto T, Seki K, Ueki A, Nanko S, Tanaka H,Takahashi H. (1995). Genetic association of the very low density lipoprotein (VLDL) receptor gene with sporadic Alzheimer's disease. *Nat.Genet.* **11**: 207-9.

228. Weiss KH, Johanssen C, Tielsch A, Herz J, Deller T, Frotscher M,Forster E. (2003). Malformation of the radial glial scaffold in the dentate gyrus of reeler mice, scrambler mice, and ApoER2/VLDLR-deficient mice. *J.Comp Neurol.* **460**: 56-65.

229. Beffert U, Stolt PC,Herz J. (2004). Functions of lipoprotein receptors in neurons. *J.Lipid Res.* **45**: 403-9.

230. Benhayon D, Magdaleno S,Curran T. (2003). Binding of purified Reelin to ApoER2 and VLDLR mediates tyrosine phosphorylation of Disabled-1. *Brain Res.Mol.Brain Res.* **112**: 33-45.

231. Li Y, Marzolo MP, van Kerkhof P, Strous GJ,Bu G. (2000). The YXXL motif, but not the two NPXY motifs, serves as the dominant endocytosis signal for low density lipoprotein receptor-related protein. *J.Biol.Chem.* **275**: 17187-94.

232. Schneider WJ,Nimpf J. (2003). LDL receptor relatives at the crossroad of endocytosis and signaling. *Cell Mol.Life Sci.* **60**: 892-903.

233. Sanchez-Guerra M, Combarros O, Infante J, Llorca J, Berciano J, Fontalba A, Fernandez-Luna JL, Pena N,Fernandez-Viadero C. (2001). Case-control study and meta-analysis of low density lipoprotein receptor-related protein gene exon 3 polymorphism in Alzheimer's disease. *Neurosci.Lett.* **316**: 17-20.

234. Kang DE, Pietrzik CU, Baum L, Chevallier N, Merriam DE, Kounnas MZ, Wagner SL, Troncoso JC, Kawas CH, Katzman R,Koo EH. (2000). Modulation of amyloid beta-protein clearance and Alzheimer's disease susceptibility by the LDL receptor-related protein pathway. *J.Clin.Invest.* **106**: 1159-66.

235. Ulery PG,Strickland DK. (2000). LRP in Alzheimer's disease: friend or foe? *J.Clin.Invest.* **106**: 1077-79.

236. Causevic M, Ramoz N, Haroutunian V, Davis KL,Buxbaum JD. (2003). Lack of association between the levels of the low-density lipoprotein receptor-related protein (LRP) and either Alzheimer dementia or LRP exon 3 genotype. *J.Neuropathol.Exp.Neurol.* **62**: 999-1005.

237. Ma SL, Ng HK, Baum L, Pang JC, Chiu HF, Woo J, Tang NL,Lam LC. (2002). Low-density lipoprotein receptor-related protein 8 (apolipoprotein E receptor 2) gene polymorphisms in Alzheimer's disease. *Neurosci.Lett.* **332**: 216-18.

238. Bultel-Brienne S, Lestavel S, Pilon A, Laffont I, Tailleux A, Fruchart JC, Siest G,Clavey V. (2002). Lipid free apolipoprotein E binds to the class B Type I scavenger receptor I (SR-BI) and enhances cholesteryl ester uptake from lipoproteins. *J.Biol.Chem.* **277**: 36092-99.

239. Silver DL. (2002). A carboxyl-terminal PDZ-interacting domain of scavenger receptor B, type I is essential for cell surface expression in liver. *J.Biol.Chem.* **277**: 34042-47.

240. Kone BC, Kuncewicz T, Zhang W,Yu ZY. (2003). Protein interactions with nitric oxide synthases: controlling the right time, the right place, and the right amount of nitric oxide. *Am.J.Physiol Renal Physiol.* **285**: F178-F190.

241. Scheid MP,Woodgett JR. (2003). Unravelling the activation mechanisms of protein kinase B/Akt. *FEBS Lett.* **546**: 108-12.

242. Krul ES,Tang J. (1992). Secretion of apolipoprotein E by an astrocytoma cell line. *J.Neurosci.Res.* **32**: 227-38.

243. Starck M, Bertrand P, Pepin S, Schiele F, Siest G,Galteau MM. (2000). Effects of pro-inflammatory cytokines on apolipoprotein E secretion by a human astrocytoma cell line (CCF-STTG1). *Cell Biochem.Funct.* **18**: 9-16.

244. Murakami M, Ushio Y, Morino Y, Ohta T,Matsukado Y. (1988). Immunohistochemical localization of apolipoprotein E in human glial neoplasms. *J.Clin.Invest.* **82**: 177-88.

245. Moncada S, Palmer RM,Higgs EA. (1991). Nitric oxide: physiology, pathophysiology, and pharmacology. *Pharmacol.Rev.* **43**: 109-42.

246. Archer S. (1993). Measurement of nitric oxide in biological models. *FASEB J.* **7**: 349-60.

247. Nagano T. (1999). Practical methods for detection of nitric oxide. *Luminescence.* **14**: 283-90.

248. Lincoln J, Hoyle CHV,Burnstock G. (1997). Measurement of nitric oxide. 197-214.

249. Liu X, Liu Q, Gupta E, Zorko N, Brownlee E,Zweier JL. (2005). Quantitative measurements of NO reaction kinetics with a Clark-type electrode. *Nitric.Oxide.* **13**: 68-77.

250. Alderton WK, Cooper CE,Knowles RG. (2001). Nitric oxide synthases: structure, function and inhibition. *Biochem.J.* **357**: 593-615.

251. Lincoln J, Hoyle CHV,Burnstock G. (1997). Measurement of nitric oxide synthase activity. 215-30.

252. Nieves C, Jr.,Langkamp-Henken B. (2002). Arginine and immunity: a unique perspective. *Biomed.Pharmacother.* **56**: 471-82.

253. Yu JG, Ishine T, Kimura T, O'Brien WE,Lee TJ. (1997). L-citrulline conversion to L-arginine in sphenopalatine ganglia and cerebral perivascular nerves in the pig. *Am.J.Physiol.* **273**: H2192-H2199.

254. Kojima H, Nakatsubo N, Kikuchi K, Urano Y, Higuchi T, Tanaka J, Kudo Y,Nagano T. (1998). Direct evidence of NO production in rat hippocampus and cortex using a new fluorescent indicator: DAF-2 DA. *Neuroreport.* **9**: 3345-48.

255. Kojima H, Nakatsubo N, Kikuchi K, Kawahara S, Kirino Y, Nagoshi H, Hirata Y,Nagano T. (1998). Detection and imaging of nitric oxide with novel fluorescent indicators: diaminofluoresceins. *Anal.Chem.* **70**: 2446-53.

256. Kojima H, Sakurai K, Kikuchi K, Kawahara S, Kirino Y, Nagoshi H, Hirata Y,Nagano T. (1998). Development of a fluorescent indicator for nitric oxide based on the fluorescein chromophore. *Chem.Pharm.Bull.(Tokyo).* **46**: 373-75.

257. Denninger JW,Marletta MA. (1999). Guanylate cyclase and the .NO/cGMP signaling pathway. *Biochim.Biophys.Acta.* **1411**: 334-50.

258. Simonds WF. (1999). G protein regulation of adenylate cyclase. *Trends Pharmacol.Sci.* **20**: 66-73.

259. Klein C. (2002). Nitric oxide and the other cyclic nucleotide. *Cell Signal.* **14**: 493-98.

260. Blaise GA, Gauvin D, Gangal M,Authier S. (2005). Nitric oxide, cell signaling and cell death. *Toxicology.* **208**: 177-92.

261. Linder JU,Schultz JE. (2003). The class III adenylyl cyclases: multi-purpose signalling modules. *Cell Signal.* **15**: 1081-89.

262. Silberbach M,Roberts CT, Jr. (2001). Natriuretic peptide signalling: molecular and cellular pathways to growth regulation. *Cell Signal.* **13**: 221-31.

263. Kobialka M,Gorczyca WA. (2000). Particulate guanylyl cyclases: multiple mechanisms of activation. *Acta Biochim.Pol.* **47**: 517-28.

264. Hamad AM, Clayton A, Islam B,Knox AJ. (2003). Guanylyl cyclases, nitric oxide, natriuretic peptides, and airway smooth muscle function. *Am.J.Physiol Lung Cell Mol.Physiol.* **285**: L973-L983.

265. Wedel B,Garbers D. (2001). The guanylyl cyclase family at Y2K. *Annu.Rev.Physiol.* **63**: 215-33.

266. Sardon T, Baltrons MA,Garcia A. (2004). Nitric oxide-dependent and independent down-regulation of NO-sensitive guanylyl cyclase in neural cells. *Toxicol.Lett.* **149**: 75-83.

267. Friebe A,Koesling D. (2003). Regulation of nitric oxide-sensitive guanylyl cyclase. *Circ.Res.* **93**: 96-105.

268. Lucas KA, Pitari GM, Kazerounian S, Ruiz-Stewart I, Park J, Schulz S, Chepenik KP,Waldman SA. (2000). Guanylyl cyclases and signaling by cyclic GMP. *Pharmacol.Rev.* **52**: 375-414.

269. Hanafy KA, Krumenacker JS,Murad F. (2001). NO, nitrotyrosine, and cyclic GMP in signal transduction. *Med.Sci.Monit.* **7**: 801-19.

270. Bellamy TC, Wood J,Garthwaite J. (2002). On the activation of soluble guanylyl cyclase by nitric oxide. *Proc.Natl.Acad.Sci.U.S.A.* **99**: 507-10.

271. Bellamy TC,Garthwaite J. (2002). The receptor-like properties of nitric oxide-activated soluble guanylyl cyclase in intact cells. *Mol.Cell Biochem.* **230**: 165-76.

272. Russwurm M,Koesling D. (2004). NO activation of guanylyl cyclase. *EMBO J.* **23**: 4443-50.

273. Russwurm M,Koesling D. (2004). Guanylyl cyclase: NO hits its target. *Biochem.Soc.Symp.* 51-63.

274. Russwurm M, Behrends S, Harteneck C,Koesling D. (1998). Functional properties of a naturally occurring isoform of soluble guanylyl cyclase. *Biochem.J.* **335 ( Pt 1)**: 125-30.

275. Budworth J, Meillerais S, Charles I,Powell K. (1999). Tissue distribution of the human soluble guanylate cyclases. *Biochem.Biophys.Res.Commun.* **263**: 696-701.

276. Gibb BJ,Garthwaite J. (2001). Subunits of the nitric oxide receptor, soluble guanylyl cyclase, expressed in rat brain. *Eur.J.Neurosci.* **13**: 539-44.

277. Mergia E, Russwurm M, Zoidl G,Koesling D. (2003). Major occurrence of the new alpha2beta1 isoform of NO-sensitive guanylyl cyclase in brain. *Cell Signal.* **15**: 189-95.

278. Russwurm M, Wittau N,Koesling D. (2001). Guanylyl cyclase/PSD-95 interaction: targeting of the nitric oxide-sensitive alpha2beta1 guanylyl cyclase to synaptic membranes. *J.Biol.Chem.* **276**: 44647-52.

279. Ledo A, Frade J, Barbosa RM,Laranjinha J. (2004). Nitric oxide in brain: diffusion, targets and concentration dynamics in hippocampal subregions. *Mol.Aspects Med.* **25**: 75-89.

280. Krumenacker JS, Hanafy KA,Murad F. (2004). Regulation of nitric oxide and soluble guanylyl cyclase. *Brain Res.Bull.* **62**: 505-15.

281. Fiscus RR. (2002). Involvement of cyclic GMP and protein kinase G in the regulation of apoptosis and survival in neural cells. *Neurosignals.* **11**: 175-90.

282. Lohmann SM, Vaandrager AB, Smolenski A, Walter U,De Jonge HR. (1997). Distinct and specific functions of cGMP-dependent protein kinases. *Trends Biochem.Sci.* **22**: 307-12.

283. Endo S, Suzuki M, Sumi M, Nairn AC, Morita R, Yamakawa K, Greengard P,Ito M. (1999). Molecular identification of human G-substrate, a possible downstream component of the cGMP-dependent protein kinase cascade in cerebellar Purkinje cells. *Proc.Natl.Acad.Sci.U.S.A.* **96**: 2467-72.

284. Essayan DM. (2001). Cyclic nucleotide phosphodiesterases. *J.Allergy Clin.Immunol.* **108**: 671-80.

285. Manallack DT, Hughes RA,Thompson PE. (2005). The next generation of phosphodiesterase inhibitors: structural clues to ligand and substrate selectivity of phosphodiesterases. *J.Med.Chem.* **48**: 3449-62.

286. Garthwaite J,Garthwaite G. (1987). Cellular origins of cyclic GMP responses to excitatory amino acid receptor agonists in rat cerebellum in vitro. *J.Neurochem.* **48**: 29-39.

287. Bellamy TC,Garthwaite J. (2001). "cAMP-specific" phosphodiesterase contributes to cGMP degradation in cerebellar cells exposed to nitric oxide. *Mol.Pharmacol.* **59**: 54-61.

288. Garthwaite G, Goodwin DA,Garthwaite J. (1999). Nitric oxide stimulates cGMP formation in rat optic nerve axons, providing a specific marker of axon viability. *Eur J Neurosci.* **11**: 4367-72.

289. Bellamy TC, Wood J, Goodwin DA,Garthwaite J. (2000). Rapid desensitization of the nitric oxide receptor, soluble guanylyl cyclase, underlies diversity of cellular cGMP responses. *Proc.Natl.Acad.Sci.U.S.A.* **97**: 2928-33.

290. Leikert JF, Rathel TR, Muller C, Vollmar AM,Dirsch VM. (2001). Reliable in vitro measurement of nitric oxide released from endothelial cells using low concentrations of the fluorescent probe 4,5-diaminofluorescein. *FEBS Lett.* **506**: 131-34.

291. Fitzhugh AL,Keefer LK. (2000). Diazeniumdiolates: pro- and antioxidant applications of the "NONOates". *Free Radic.Biol.Med.* **28**: 1463-69.

292. Neill D, Hughes D, Edwardson JA, Rima BK,Allsop D. (1994). Human IMR-32 neuroblastoma cells as a model cell line in Alzheimer's disease research. *J.Neurosci.Res.* **39**: 482-93.

293. Nakatsubo N, Kojima H, Kikuchi K, Nagoshi H, Hirata Y, Maeda D, Imai Y, Irimura T,Nagano T. (1998). Direct evidence of nitric oxide production from bovine aortic endothelial cells using new fluorescence indicators: diaminofluoresceins. *FEBS Lett.* **427**: 263-66.

294. Rathel TR, Leikert JJ, Vollmar AM,Dirsch VM. (2003). Application of 4,5-diaminofluorescein to reliably measure nitric oxide released from endothelial cells in vitro. *Biol.Proced.Online.* **5**: 136-42.

295. Broillet M, Randin O,Chatton J. (2001). Photoactivation and calcium sensitivity of the fluorescent NO indicator 4,5-diaminofluorescein (DAF-2): implications for cellular NO imaging. *FEBS Lett.* **491**: 227-32.

296. Lopez-Figueroa MO, Caamano C, Marin R, Guerra B, Alonso R, Morano MI, Akil H,Watson SJ. (2001). Characterization of basal nitric oxide production in living cells. *Biochim.Biophys.Acta.* **1540**: 253-64.

297. Pandey KN, Nguyen HT, Sharma GD, Shi SJ,Kriegel AM. (2002). Ligand-regulated internalization, trafficking, and down-regulation of guanylyl cyclase/atrial natriuretic peptide receptor-A in human embryonic kidney 293 cells. *J.Biol.Chem.* **277**: 4618-27.

298. Nahavandi M, Tavakkoli F, Wyche MQ, Perlin E, Winter WP,Castro O. (2002). Nitric oxide and cyclic GMP levels in sickle cell patients receiving hydroxyurea. *Br.J.Haematol.* **119**: 855-57.

299. Pozner RG, Negrotto S, D'Atri LP, Kotler ML, Lazzari MA, Gomez RM,Schattner M. (2005). Prostacyclin prevents nitric oxide-induced megakaryocyte apoptosis. *Br.J.Pharmacol.* **145**: 283-92.

300. Ishigami M, Swertfeger DK, Hui MS, Granholm NA,Hui DY. (2000). Apolipoprotein E inhibition of vascular smooth muscle cell proliferation but not the inhibition of migration is mediated through activation of inducible nitric oxide synthase. *Arterioscler.Thromb.Vasc.Biol.* **20**: 1020-1026.

301. Moore ZW,Hui DY. (2005). Apolipoprotein E inhibition of vascular hyperplasia and neointima formation requires inducible nitric oxide synthase. *J.Lipid Res.* **46**: 2083-90.

302. Brown CM, Wright E, Colton CA, Sullivan PM, Laskowitz DT,Vitek MP. (2002). Apolipoprotein E isoform mediated regulation of nitric oxide release. *Free Radic.Biol.Med.* **32**: 1071-75.

303. Vitek MP, Snell J, Dawson H,Colton CA. (1997). Modulation of nitric oxide production in human macrophages by apolipoprotein-E and amyloid-beta peptide. *Biochem.Biophys.Res.Commun.* **240**: 391-94.

304. Tsutsui M. (2004). Neuronal nitric oxide synthase as a novel anti-atherogenic factor. *J.Atheroscler.Thromb.* **11**: 41-48.

305. Panayotou G. (1997). Multiple roles for phosphoinositide 3-kinases in signal transduction. 189-204.

306. Fruman DA, Meyers RE,Cantley LC. (1998). Phosphoinositide kinases. *Annu.Rev.Biochem.* **67**: 481-507.

307. El Sheikh SS, Domin J, Tomtitchong P, Abel P, Stamp G,Lalani EN. (2003). Topographical expression of class IA and class II phosphoinositide 3-kinase enzymes in normal human tissues is consistent with a role in differentiation. *BMC.Clin.Pathol.* **3**: 4.

308. An WL, Cowburn RF, Li L, Braak H, Alafuzoff I, Iqbal K, Iqbal IG, Winblad B,Pei JJ. (2003). Up-regulation of phosphorylated/activated p70 S6 kinase and its relationship to neurofibrillary pathology in Alzheimer's disease. *Am.J.Pathol.* **163**: 591-607.

309. Katso R, Okkenhaug K, Ahmadi K, White S, Timms J,Waterfield MD. (2001). Cellular function of phosphoinositide 3-kinases: implications for development, homeostasis, and cancer. *Annu.Rev.Cell Dev.Biol.* **17**: 615-75.

310. Staal SP, Hartley JW,Rowe WP. (1977). Isolation of transforming murine leukemia viruses from mice with a high incidence of spontaneous lymphoma. *Proc.Natl.Acad.Sci.U.S.A.* **74**: 3065-67.

311. Staal SP,Hartley JW. (1988). Thymic lymphoma induction by the AKT8 murine retrovirus. *J.Exp.Med.* **167**: 1259-64.

312. Staal SP. (1987). Molecular cloning of the akt oncogene and its human homologues AKT1 and AKT2: amplification of AKT1 in a primary human gastric adenocarcinoma. *Proc.Natl.Acad.Sci.U.S.A.* **84**: 5034-37.

313. Jones PF, Jakubowicz T, Pitossi FJ, Maurer F,Hemmings BA. (1991). Molecular cloning and identification of a serine/threonine protein kinase of the second-messenger subfamily. *Proc.Natl.Acad.Sci.U.S.A.* **88**: 4171-75.

314. Song G, Ouyang G,Bao S. (2005). The activation of Akt/PKB signaling pathway and cell survival. *J.Cell Mol.Med.* **9**: 59-71.

315. Nakatani K, Sakaue H, Thompson DA, Weigel RJ,Roth RA. (1999). Identification of a human Akt3 (protein kinase B gamma) which contains the regulatory serine phosphorylation site. *Biochem.Biophys.Res.Commun.* **257**: 906-10.

316. Nicholson KM,Anderson NG. (2002). The protein kinase B/Akt signalling pathway in human malignancy. *Cell Signal.* **14**: 381-95.

317. Ferguson KM, Kavran JM, Sankaran VG, Fournier E, Isakoff SJ, Skolnik EY,Lemmon MA. (2000). Structural basis for discrimination of 3-phosphoinositides by pleckstrin homology domains. *Mol.Cell.* **6**: 373-84.

318. Alessi DR, James SR, Downes CP, Holmes AB, Gaffney PR, Reese CB,Cohen P. (1997). Characterization of a 3-phosphoinositide-dependent protein kinase which phosphorylates and activates protein kinase Balpha. *Curr.Biol.* **7**: 261-69.

319. D'Arcangelo G. (2005). Apoer2: a reelin receptor to remember. *Neuron.* **47**: 471-73.

320. Curran T,D'Arcangelo G. (1998). Role of reelin in the control of brain development. *Brain Res.Brain Res.Rev.* **26**: 285-94.

321. Li Y, Lu W, Marzolo MP,Bu G. (2001). Differential functions of members of the low density lipoprotein receptor family suggested by their distinct endocytosis rates. *J.Biol.Chem.* **276**: 18000-18006.

322. Riddell DR, Sun XM, Stannard AK, Soutar AK,Owen JS. (2001). Localization of apolipoprotein E receptor 2 to caveolae in the plasma membrane. *J.Lipid Res.* **42**: 998-1002.

323. Sun XM,Soutar AK. (2003). The transmembrane domain and PXXP motifs of ApoE receptor 2 exclude it from carrying out clathrin-mediated endocytosis. *J.Biol.Chem.* **278**: 19926-32.

324. Kim DH, Magoori K, Inoue TR, Mao CC, Kim HJ, Suzuki H, Fujita T, Endo Y, Saeki S,Yamamoto TT. (1997). Exon/intron organization, chromosome localization, alternative splicing, and transcription units of the human apolipoprotein E receptor 2 gene. *J.Biol.Chem.* **272**: 8498-504.

325. Alexandropoulos K, Cheng G,Baltimore D. (1995). Proline-rich sequences that bind to Src homology 3 domains with individual specificities. *Proc.Natl.Acad.Sci.U.S.A.* **92**: 3110-3114.

326. Boggon TJ,Eck MJ. (2004). Structure and regulation of Src family kinases. *Oncogene.* **23**: 7918-27.

327. Buday L. (1999). Membrane-targeting of signalling molecules by SH2/SH3 domain-containing adaptor proteins. *Biochim.Biophys.Acta.* **1422**: 187-204.

328. Hoe HS, Harris DC,Rebeck GW. (2005). Multiple pathways of apolipoprotein E signaling in primary neurons. *J.Neurochem.* **93**: 145-55.

329. Stockinger W, Brandes C, Fasching D, Hermann M, Gotthardt M, Herz J, Schneider WJ,Nimpf J. (2000). The reelin receptor ApoER2 recruits JNK-interacting proteins-1 and -2. *J.Biol.Chem.* **275**: 25625-32.

330. Kumari S, Liu X, Nguyen T, Zhang X,D'Mello SR. (2001). Distinct phosphorylation patterns underlie Akt activation by different survival factors in neurons. *Brain Res.Mol.Brain Res.* **96**: 157-62.

331. Dudek H, Datta SR, Franke TF, Birnbaum MJ, Yao R, Cooper GM, Segal RA, Kaplan DR,Greenberg ME. (1997). Regulation of neuronal survival by the serine-threonine protein kinase Akt. *Science.* **275**: 661-65.

332. Vestling M, Wiehager B, Tanii H,Cowburn RF. (2001). Akt activity in presenilin 1 wild-type and mutation transfected human SH-SY5Y neuroblastoma cells after serum deprivation and high glucose stress. *J.Neurosci.Res.* **66**: 448-56.

333. Woodgett JR. (2005). Recent advances in the protein kinase B signaling pathway. *Curr.Opin.Cell Biol.* **17**: 150-157.

334. Alessi DR, Andjelkovic M, Caudwell B, Cron P, Morrice N, Cohen P,Hemmings BA. (1996). Mechanism of activation of protein kinase B by insulin and IGF-1. *EMBO J.* **15**: 6541-51.

335. Williams MR, Arthur JS, Balendran A, van der KJ, Poli V, Cohen P,Alessi DR. (2000). The role of 3-phosphoinositide-dependent protein kinase 1 in activating AGC kinases defined in embryonic stem cells. *Curr.Biol.* **10**: 439-48.

336. Scheid MP, Marignani PA,Woodgett JR. (2002). Multiple phosphoinositide 3-kinase-dependent steps in activation of protein kinase B. *Mol.Cell Biol.* **22**: 6247-60.

337. Yang J, Cron P, Thompson V, Good VM, Hess D, Hemmings BA,Barford D. (2002). Molecular mechanism for the regulation of protein kinase B/Akt by hydrophobic motif phosphorylation. *Mol.Cell.* **9**: 1227-40.

338. Gearing M, Schneider JA, Robbins RS, Hollister RD, Mori H, Games D, Hyman BT,Mirra SS. (1995). Regional variation in the distribution of apolipoprotein E and A beta in Alzheimer's disease. *J.Neuropathol.Exp.Neurol.* **54**: 833-41.

339. Weisgraber KH,Mahley RW. (1996). Human apolipoprotein E: the Alzheimer's disease connection. *FASEB J.* **10**: 1485-94.

340. Bales KR, Dodart JC, DeMattos RB, Holtzman DM,Paul SM. (2002). Apolipoprotein E, amyloid, and Alzheimer disease. *Mol.Interv.* **2**: 363-75, 339.

341. Alarcon R, Fuenzalida C, Santibanez M,von Bernhardi R. (2005). Expression of scavenger receptors in glial cells. Comparing the adhesion of astrocytes and microglia from neonatal rats to surface-bound beta-amyloid. *J.Biol.Chem.* **280**: 30406-15.

342. Bechmann I,Nitsch R. (1997). Identification of phagocytic glial cells after lesion-induced anterograde degeneration using double-fluorescence labeling: combination of axonal tracing and lectin or immunostaining. *Histochem.Cell Biol.* **107**: 391-97.

343. Husemann J,Silverstein SC. (2001). Expression of scavenger receptor class B, type I, by astrocytes and vascular smooth muscle cells in normal adult mouse and human brain and in Alzheimer's disease brain. *Am.J.Pathol.* **158**: 825-32.

344. Husemann J, Loike JD, Anankov R, Febbraio M,Silverstein SC. (2002). Scavenger receptors in neurobiology and neuropathology: their role on microglia and other cells of the nervous system. *Glia.* **40**: 195-205.

345. Zhong S, Liu C, Haviland D, Doris PA,Teng BB. (2005). Simultaneous expression of apolipoprotein B mRNA editing enzyme and scavenger receptor BI mediated by a therapeutic gene expression system. *Atherosclerosis.*

346. Yuhanna IS, Zhu Y, Cox BE, Hahner LD, Osborne-Lawrence S, Lu P, Marcel YL, Anderson RG, Mendelsohn ME, Hobbs HH,Shaul PW. (2001). High-density lipoprotein binding to scavenger receptor-BI activates endothelial nitric oxide synthase. *Nat.Med.* **7**: 853-57.

347. Uittenbogaard A, Shaul PW, Yuhanna IS, Blair A,Smart EJ. (2000). High density lipoprotein prevents oxidized low density lipoprotein-induced inhibition of endothelial nitric-oxide synthase localization and activation in caveolae. *J.Biol.Chem.* **275**: 11278-83.

348. Yesilaltay A, Kocher O, Rigotti A,Krieger M. (2005). Regulation of SR-BI-mediated high-density lipoprotein metabolism by the tissue-specific adaptor protein PDZK1. *Curr.Opin.Lipidol.* **16**: 147-52.

349. Assanasen C, Mineo C, Seetharam D, Yuhanna IS, Marcel YL, Connelly MA, Williams DL, Llera-Moya M, Shaul PW,Silver DL. (2005). Cholesterol binding, efflux, and a PDZ-interacting domain of scavenger receptor-BI mediate HDL-initiated signaling. *J.Clin.Invest.* **115**: 969-77.

350. Eckhardt ER, Cai L, Sun B, Webb NR,van der Westhuyzen DR. (2004). High density lipoprotein uptake by scavenger receptor SR-BII. *J.Biol.Chem.* **279**: 14372-81.

351. Svensson PA, Englund MC, Snackestrand MS, Hagg DA, Ohlsson BG, Stemme V, Mattsson-Hulten L, Thelle DS, Fagerberg B, Wiklund O, Carlsson LM,Carlsson B. (2005). Regulation and splicing of scavenger receptor class B type I in human macrophages and atherosclerotic plaques. *BMC.Cardiovasc.Disord.* **5**: 25.

352. Stannard AK, Riddell DR, Sacre SM, Tagalakis AD, Langer C, von Eckardstein A, Cullen P, Athanasopoulos T, Dickson G,Owen JS. (2001). Cell-derived apolipoprotein E (ApoE) particles inhibit vascular cell adhesion molecule-1 (VCAM-1) expression in human endothelial cells. *J.Biol.Chem.* **276**: 46011-16.

353. Riddell DR,Owen JS. (1999). Nitric oxide and platelet aggregation. *Vitam.Horm.* **57**: 25-48.

354. Riddell DR, Graham A,Owen JS. (1997). Apolipoprotein E inhibits platelet aggregation through the L-arginine:nitric oxide pathway. Implications for vascular disease. *J.Biol.Chem.* **272**: 89-95.

355. Colton CA, Needham LK, Brown C, Cook D, Rasheed K, Burke JR, Strittmatter WJ, Schmechel DE,Vitek MP. (2004). APOE genotype-specific differences in human and mouse macrophage nitric oxide production. *J.Neuroimmunol.* **147**: 62-67.

# PUBLICATIONS